Microwave Synthesis of Novel Methacrylate Monomers Designed to Reduce Biofilm Formation to Surfaces

Adam Alastair Dundas Msci



University of Nottingham
UK | CHINA | MALAYSIA

Thesis submitted to the University of Nottingham for the degree of Doctor of Philosophy

March 2018

Abstract

Rational design of biomaterials is hindered by the lack of quantitative structure-activity relationships (QSAR). Here we report the use of a QSAR to guide experimentation into a new chemical space; we predict and synthesize molecular structures for novel monomers that will reduce biofilm formation, and so identifying the lowest biofilm attachment polymer discovered to date. Cyclododecyl methacrylate was shown to reduce the formation of *P. aeruginosa* and *P. mirabilis* biofilms by up to 96 % and 97 % respectively compared to commercially available catheters. We believe that this is the first instance of a biomaterials screening program extending beyond the domain covered by the initial screen to predict a novel chemical entity with improved properties. This validates the QSAR approach for identifying polymers that resist biofilm formation beyond its chemical training domain.

High throughput discovery of the non-commercially available material space is hindered by the ability to synthesize large numbers of materials in a controlled reaction process to keep up with supply demands. In this thesis we also present the production of a microwave single-well reactor capable of synthesizing novel methacrylate monomers using a transesterification process, where the design of the reactor has shown to outperform both conventional and standard microwave heating techniques. Powers as low as 40 W have been used to achieve reaction temperatures of 160 $^{\circ}$C, showing great scale-out potential. With the approach of using QSAR for identifying potential biomaterials, monomer libraries can be judiciously chosen and then synthesised to enable high

throughput discovery programs to have unprecedented access to the non-commercially available space.

Acknowledgements

It has been my absolute pleasure and honour to work on such a diverse multi-disciplinary project which has only helped my scientific understanding. I would firstly like to thank my supervisors, Professor Morgan Alexander, Professor Derek Irvine, Dr Andrew Hook and Dr Georgios Dimitrakis for their wealth of advice and support. Their encouragement and patience has truly made this PhD an enjoyable project and allowed me to develop both professionally and personally. I would like to give special mentions to those who helped me in the laboratory. Dr Kevin Adlington and Dr George Hargreaves for their support in getting me started in a chemistry working environment. I would also like to thank Olutoba Sanni who performed the biological attachment assays during my work and who without this project would not have been as successful. I would also like to thank Dr Andrew Hook for acquiring the ToF-SIMS data for this project.

For both helping stimulate new ideas and providing a great source of humour and sanity I would like to thank the members of D20 (TJ, Sunny, Vicky, Rob, Stephen, Yasin, Toba, Leigh-Anne and Mike). I would also like to acknowledge members of the LBSA (now-AMHT) and Microwave Group for all their assistance and advice.

Last but by no means least I would like to appreciate all the love and support of my friends and family. Especially my parents Lynne and Alastair and sister Katie who have been a great support. I would also like to thank Vickie, who has had to deal with my moaning and groaning throughout my challenging, but enjoyable studies.

Published Articles

During this project, data acquired has been used to publish articles including:

Paulius M, Hook A.L, Dundas A.A, Irvine D.J, Sanni O, Anderson D.G, Langer R, Alexander M.R, Williams P and Winkler D.A, 'Prediction of Broad-spectrum Pathogen Attachment to Coating Materials for Biomedical Devices', ACS Applied Materials & Interfaces, 2017

Contents

1 Introduction 1

1.1 Aims and Objectives 3

Literature Review 4

1.2 Medical device associated bacterial infections 4
1.2.1 Biofilm formation on medical devices 4
1.2.2 Current strategies for reducing medical-device associated bacterial infections 7

1.3 Production of novel biomaterials using high throughput experimentation 11
1.3.1 Rational design of biomaterials 12
1.3.2 Discovery of novel biomaterials using polymer microarrays .. 15

1.4 Quantitative structure activity relationship models for targeted library development 19

1.5 Review of current material library synthesis 22

1.6 Benefits of using microwaves for organic synthesis 25
1.6.1 Thermal and non-thermal effects of microwave irradiation.... 26
1.6.2 Single mode vs multi-mode cavities..... 28
1.6.3 Use of monopole antennas to focus microwave irradiation 30

1.7 Developing microwave cavities using FDTD simulations 33
1.7.1 Optimising simulation conditions 33
1.7.2 Applications of FDTD simulations..... 34

2 Materials and Methods 36

2.1 Chemical Synthesis 36
2.1.1 Materials..... 36
2.1.2 Transesterification Reactions 37
2.1.3 Nitrogen gas sparging..... 39
2.1.4 Microwave Reactions 40
2.1.5 Free-radical polymerisation reactions..... 43

2.2 NMR..... 45

2.3 Polymer microarray Printing 47
2.3.1 Materials..... 47
2.3.2 Printing substrate preparation..... 47
2.3.3 Microarray Printing 48

2.4 ToF-SIMS..... 51

2.5 Bacterial Strains 54

2.6 Fluorescence imaging 55
2.6.1 Fluorescence microscopy..... 55
2.6.2 Confocal microscopy 56

2.7 Finite difference time domain simulations 58

2.8 Micro-well fabrication and experimentation 61
2.8.1 Materials..... 61
2.8.2 Microwave Safety 61
2.8.3 Impedance matching 61

3 Synthesis of Novel Methacrylate Monomers Using Microwaves and Nitrogen Sparging 63

3.1 Introduction 63
3.1.1 Aims and Objectives 66

3.2 Experimental methods 67
3.2.1 Conventional heating 67
3.2.2 Microwave heating 68
3.2.3 Nitrogen sparging 70
3.2.4 Nuclear magnetic resonance imaging 71

3.3 Results 72
3.3.1 Choice of fundamental reagent monomer 72
3.3.2 Effect of apparatus/glassware design on conversion 75
3.3.3 Comparison of conventional and microwave heating methods 76
3.3.4 Use of nitrogen sparging to overcome mass transfer limitations 81
3.3.5 Synthesis of novel methacrylate library 88

3.4 Discussion 93
3.4.1 Effect of reaction stability using both methyl and butyl methacrylate 93
3.4.2 Effect of glassware on reaction mass-transfer properties 95
3.4.3 Comparison of conventional and microwave heating methods 96
3.4.4 Library synthesis of novel methacrylate monomers 100

3.5 Conclusion 104

4 Identification of materials resistant to bacterial attachment using high throughput screening and computational models 105

4.1 Introduction 105
4.1.1 Aims and Objectives 109

4.2 Experimental Methods 110
4.2.1 Computational Predictions 110
4.2.2 Polymer Microarray Production 110
4.2.3 Bright Field Microscopy 114
4.2.4 ToF-SIMS 114
4.2.5 Bacterial Attachment Studies on Polymer Microarray 115
4.2.6 Toxicity Studies of Polymers and Contaminations 117
4.2.7 CyDMA Work up and polymerisation 118
4.2.8 Catheter Dip-Coating 119
4.2.9 Bacterial Attachment Studies on Catheter Sections 120

4.3 Results 122
4.3.1 Alpha Predictions of Monomers Resistant to Bacterial Attachment 122
4.3.2 Production of Polymer Microarrays (IMSTAR + ToF-SIMS) .. 123
4.3.3 Primary screening of novel methacrylate monomers 128
4.3.4 Toxicity Studies of Synthesis Polymers 131
4.3.5 Toxicity Studies of Transesterification Synthesis Contaminants 132
4.3.6 Scale up of CyDMA hit material for coating medical devices 134
4.3.7 Bacterial Attachment of CyDMA to Urinary Catheters 138

4.4 Discussion 141
4.4.1 Monomers predicted to reduce bacterial attachment 141
4.4.2 Effect of contaminants of bacterial growth 148

4.4.3 Printing of polymer microarray and characterisation of surface chemistry 142
4.4.4 Extrapolating *alpha* parameter to discover novel hit materials 143
4.4.5 Performance of hit materials to resist bacterial adhesion to medical devices 146

4.5 Conclusion 148

5 Design, Manufacture and Testing of Multi-Platform Microwave Reactor 151

5.1 Introduction 151
5.1.1 Aims and objectives 155

5.2 Experimental Methods 156
5.2.1 FDTD Simulations 156
5.2.2 Micro-well Manufacture 160
5.2.3 Safety Experiments 161
5.2.4 Transesterification Experiments 162

5.3 Results 165
5.3.1 Optimised design of Micro-well reactor 165
5.3.2 Safety simulations of optimised reactor 171
5.3.3 Micro-well commissioning 173
5.3.4 Effect of input power on reaction temperature 175
5.3.5 Synthesis of novel methacrylate monomers using micro-well reactor 176

5.4 Discussion 180
5.4.1 Effect of reactor radius on power density distribution 180
5.4.2 Effect of antenna shape on power density distribution 181
5.4.3 Effect of antenna length on observed power density distribution 182
5.4.4 Safe design of microwave reactors to prevent exposure to microwaves 184
5.4.5 Commissioning of Micro-well reactor for safe working practice 185
5.4.6 Feasibility of creating multi-well microwave reactor 187
5.4.7 Comparison of Micro-well, conventional and microwave heating methods on reaction conversion 188

5.5 Conclusion 191

6 Conclusions 192

6.1 Summary 192

6.2 Recommendations for future work 195

6.3 Concluding Remarks 197

References 199

List of Figures

Figure 1.1: Biofilm formation depicted on catheter. Process shows progress from first contact of planktonic bacteria through a maturation process before dispersing more planktonic bacteria to repeat the process and form a layer of biofilm 7
Figure 1.2: Formation of polymer microarrays; where monomer solutions are transferred by either contact or ink-jet printing pins and UV polymerised. [44] 12
Figure 1.3: Polymer microarray containing 576 materials printed in triplicate used for identifying key materials for reducing bacterial attachment[57] 16
Figure 1.4: hMSC cells grown on a polymer microarray (comprised of 24 different polymers mixed pairwise at ratios of 1:0,9:1 and 7:3 to give 1152 combinations) with a fluorescent stain to characterise cell adhesion to polymeric surfaces[41] 16
Figure 1.5: Flow diagram showing work flow to find suitable materials for preventing bacterial attachment to medical devices. The results from previous assessments of bacteria-material interactions can be used to predict and then synthesise novel monomers. The newly produced materials can be tested to further refine the model, leading to the discovery of the next generation of biomaterials. 21
Figure 1.6: Inhomogeneity of heating shown by use of a polypropylene 96-Well plate in domestic multi-mode microwave oven[68] 23
Figure 1.7: Efficiency of microwave heating demonstrated by showing (a) how microwaves directly heat reaction contents compared to (b) conventional conduction heating which initially heats vessel walls prior to reaction contents 27
Figure 1.8: Schematic showing the difference between (a) single mode cavity and (b) multimode cavity 30
Figure 2.1: Figure showing alcohols used for synthesis experiments performed in this project 37
Figure 2.2: Reaction sequence showing general reaction conditions used for transesterification experiments 37
Figure 2.3:Reaction mechanism for transesterification reactions, showing how functionalised alcohol group (R') can replace functionality of an ester group (R'') where LA is lewis-acid which typically was titanium butoxide. 38
Figure 2.4: Schematic showing different glassware used for synthesis experiments (a) 50 ml long necked vessel used with microwave reactions to

comply with safety choke design and also used for conventional experiments for direct comparison to microwave experiments (neck length 145 mm) (b) standard 50 ml flask used for optimised conventional reactions (neck length 43 mm) 39
Figure 2.5: (a) Alignment of molecules with dipoles in static external electric field (b) alignment of molecules in an oscillating external magnetic field . 41
Figure 2.6: Free-radical polymerisation mechanism showing the use of AIBN to polymerise functionalised methacrylate monomers 44
Figure 2.7: Figure showing calculation of conversion of product from alcohol by comparing shift of the same proton in different chemical environment 46
Figure 2.8: Figure showing commercial monomers used throughout this project 47
Figure 2.9: Schematic of pins typically used during contact microarray printing showing a solid pin and a quilled pin with reservoir for printing multiple microarrays in a single application 49
Figure 2.10: Schematic showing process of printing polymer microarray from (a) uptake of monomer solution from source plate using 946MP6B Arrayit quilled metal pins (b) transfer of monomer solution to pHEMA substrate surface where each spot was printed in triplicate (c) photopolymerisation of monomer solution under UV light (d) completed polymer microarray after 7 day drying period under high vacuum..... 50
Figure 2.11: Schematic showing operation of ToF-SIMS instrument from primary ion dosing to production of mass spectrum through flight path.[133] 51
Figure 2.12: Illustration of primary ion beam bombarding sample surface. Ionised and non-ionised fragments are ejected from sample surface 52
Figure 2.13: Excitation of electrons into higher energy states (blue) which then undergo vibrational or internal conversion emission (green) before emitted fluorescence to return to ground energy state (red) 55
Figure 2.14: Schematic of confocal microscope showing how different planes are brought into focus to allow for fluorescence imaging over a 3D object.[137] 56
Figure 2.15: Schematic demonstrating how a slug-tuner works, by manual movement of the two slugs up and down the length of the tuner, impedance of the tuner changes and allows for matching between power source and material load 62
Figure 3.1:Conventional heating set-up showing condensation equipment with water used as a coolant. Stopper is placed in top of distillation head and

thermocouple was used for a temperature feedback loop. Stirring was applied at 250 rpm to ensure a homogeneous mix was obtained..... 67
Figure 3.2: Schematic showing transesterification reaction conditions for using (a) methyl methacrylate and (b) butyl methacrylate 68
Figure 3.3: Schematic showing set-up of Miniflow 200SS with waveguide for transesterification experiments showing (a) Miniflow 200SS solid state generator (b) fine stub tuner (c) metal choke to prevent microwave leakage and (d) course sliding tuner 69
Figure 3.4: Reaction set-up of reaction utilising sparging technique. N_2 gas was passed through a 2 ml pipette, which was put through a stopper at the top of the distillation head. Thermocouple/fibre optic cable was also placed through the top of the distillation head for conventional/microwave heating respectively. Stirring was performed at 250 rpm to ensure a homogeneous mix was obtained..... 70
Figure 3.5:Reaction kinetics showing difference between using BMA at 160 °C and MMA at 100 °C 73
Figure 3.6: Transesterification experiment using MMA at 100 °C, showing a 19 % polymerisation of MMA (encircled in red) 74
Figure 3.7: Different 50-ml reaction vessels used throughout this project where (a) had to be used for microwave experiments due to safety restrictions (neck length of 145 mm) and (b) reaction vessel used for conventional heating experiments (neck length of 43 mm)..... 75
Figure 3.8: Difference in conversion by changing from short-necked reaction vessel to a long-necked reaction vessel 76
Figure 3.9: Reaction scheme showing the synthesis protocol for cyclododecyl methacrylate..... 77
Figure 3.10: Graph showing the change in conversion over-time for cyclododecyl methacrylate for both conventional and microwave heating methods 78
Figure 3.11: Reaction scheme showing the synthesis protocol for 5-methyl-2-(1-methylethyl) cyclohexyl methacrylate (LMMA), 4-methyl-2-pentyl methacrylate and 3-phenyl-2-propenyl methacrylate (CiMA) respectively 79
Figure 3.12: Series of graphs showing comparison of conventional and microwave heating methods for (a) 5-methyl-2-(1-methylethyl) cyclohexyl methacrylate (LMMA) (b) 4-Methyl-2-pentyl Methacrylate (MpMA) (c) 3-phenyl-2-propenyl methacrylate (CiMA)..... 80

Figure 3.13: Graph showing the comparison between conventional heating and conventional heating with nitrogen sparging applied after 15 minutes of heating for cyclododecyl methacrylate. Reactions were heated to 160 ˚C 82
Figure 3.14: ^{1}H Spectra of conventionally synthesised cyclododecyl methacrylate with nitrogen sparging after 4 hours of heating at 160 ˚C. BMA content has dropped to 7 % of the remaining cyclododecanol content. ... 83
Figure 3.15: ^{1}H spectrum of reaction condensate showing mixture of 57 % butanol and 43 % BMA after a 4 hour nitrogen sparging experiment. 84
Figure 3.16: Figure showing the difference in conversion when the starting ratio of BMA: alcohol is altered from 7:5 (blue circles) to 8:5 (green triangles) and compared against a 7:5 ratio with delayed sparging (red circles) 85
Figure 3.17: Comparison between conventional sparging technique and microwave sparging technique when sparging has been delayed by 45 minutes. Microwave power was set to 150 W input power. 86
Figure 3.18:^{1}H NMR spectrum of CyDMA synthesised using microwaves under N_2 sparging. Enlarged section of spectrum shows polymerisation in red circles that occurred during the reaction..... 87
Figure 3.19: Structures of synthesised monomers using optimised conventionally heated sparging method 90
Figure 3.20: Conversion of LMMA shown of a 50-hour period. Reaction conditions carried out at 150 ˚C and vacuum pump applied at 300 mbar for 30 minutes after 24 hours..... 91
Figure 3.21: Reaction sequence showing the attempted synthesis of 2-methyl-3-butyn-2-methacrylate. Reaction was performed at 160 ˚C, 140 ˚C and 100 ˚C..... 92
Figure 4.1: Flow diagram showing work flow to find suitable materials for preventing bacterial attachment to medical devices. The results from previous assessments of bacteria-material interactions can be used to predict and then synthesise novel monomers. The newly produced materials can be tested to further refine the model, leading to the discovery of the next generation of biomaterials. 107
Figure 4.2: Holmarc dip coating unit used for coating epoxy coated slides with pHEMA solution..... 111
Figure 4.3: a) Conversion rates of synthesised monomers and predictive bacterial adhesion value based upon alpha-predictive value. (*) Signifies commercially obtained monomer. b) Reaction scheme for the transesterification reaction at 160 ˚C with titanium butoxide (TNBT)

catalyst. c) Library of 12 materials used, with linear, cylcic aromatic, zwitterionic and cyclic pendant groups. NpMA and MEdMSPNH were mixed with tBCHA at ratios of 1:0 and 1:1, whilst nine other materials were mixed sequentially with tBCHA at ratios 1:0, 5:1, 2:1 and 1:1. 122
Figure 4.4: Phase contrast microscopy image of polymer microarray, used to identify if polymer spots have been successfully deposited onto the pHEMA surface 124
Figure 4.5: Ion map image showing the C2H5O+ ion associated to pHEMA, the substrate material upon which the polymers are printed..... 125
Figure 4.6: Series of diagrams showing mixing of copolymer series where ■ designates ion associated to tBCHA (C4H9+) and ○ designates an ion associated to a) CyDMa b) HPhOPA c) PhMA d) EGPhEA e) LMMA f) GeMA g) DdMA h) CHMA i) BnMA or j) NpMA. Copolymer series which had poor mixing were not compared with *alpha* in copolymer data..... 127
Figure 4.7: Bacterial fluorescence relationship for a) *P. aeruginosa* homopolymer relationship (R^2 = 0.62) and b) *P. mirabilis* relationship (R^2 = 0.45) with N = 3 technical repeats 129
Figure 4.8: Copolymer data showing correlation between *alpha* and (a) Copolymers incubated in *P aeruginosa* and (b) Copolymers incubated in *P. mirabilis*. *P. aeruginosa* data shows a strong trend (R^2 = 0.80) over the reported range of *alpha* as reported by Sanni et al. Each measurement has N = 3 repeats..... 130
Figure 4.9: Use of TECAN plate reader to monitor the growth of *P. aeruginosa* through measuring the optical density. Range of different synthesised polymers were observed along with commercially available materials and controls which included only LB media and LB media with bacteria but no polymer. 131
Figure 4.10: Figures showing the growth of *P. aeruginosa* with the presence of contaminations found from transesterification experiments at varying concentrations. (a) Butyl methacrylate (b) n-butanol (c) dodecanol (d) lauryl methacrylate. Each result was comprised of N = 3 samples..... 133
Figure 4.11: ^{1}H NMR of purified CyDMA. Summation of peaks totals a proton number of 28, corresponding to CyDMA structure expected..... 135
Figure 4.12: DEPT 135 spectrum showing assigned carbon numbers to CyDMA structure. Only two peaks for CH and CH_3 were observed, which correspond to the carbon next to the ester group in the cyclic ring structure and the end methyl group. 136

Figure 4.13: DEPT 90 NMR spectra showing the single CH peak in the CyDMA structure, which refers to the carbon next to the ester group in the cyclic structure, which is also the carbon that changes the chemical environment under transesterification synthesis experiments. 137
Figure 4.14: NMR of crude polymerisation mixture of CyDMA, showing a conversion of 61 % 138
Figure 4.15: Confocal microscopy data of attachment of *P. aeruginosa* and *P. mirabilis* to sections of coated catheters. CyDMA showed to reduce attachment of both bacterial species compared to other identified hit materials and commercial controls. Each measurement was comprised of N = 6 measurements with 2 biological repeats 139
Figure 5.1: Coaxial cable simulated during FDTD simulations showing aluminium outer conductor (r = 4 mm), PTFE dielectric (r = 3.5 mm) and aluminium inner conductor (r = 1.5 mm). Electromagnetic wave travels through the dielectric material and is then propagated into differing reactor designs..... 157
Figure 5.2: FDTD reactor design after applying mesh-grid format for simulations. Each individual cell is then calculated individually and summed across the entire structure to visualise the propagation of electromagnetic waves through a structure. 158
Figure 5.3: Structure showing exterior air interface with a port on the outside (red) face. Leaked microwaves could then be measured at this interface and compared against the microwave dosage limit..... 160
Figure 5.4: Manufactured Micro-well reactor showing (a) whole reactor including 40 mm coaxial section and 50 mm cylindrical reaction vessel (b) N-type connector used for connecting to high-power coaxial cable (c) top-view showing protruding antenna and PTFE sheath covering inside of the reactor 161
Figure 5.5: Experimental set-up of Micro-well showing (a) Miniflow 200SS (b) Coaxial cable (c) Sliding coaxial tuner and (d) Micro-well reactor.... 163
Figure 5.6: Figure showing the effect of changing the reactor size on power density distribution with a, b and c showing the XY = 10 mm power density for reactor sizes of 8.13, 15 and 20 mm respectively. Figures d, e and f show the XZ = 2.8 mm power density distribution for reactor sizes of 8.13, 15 and 20 mm respectively. All geometries were performed with a cylindrical antenna with length equal to 10 mm. For the 8.13 mm radius well, geometry comprised of 200,000 cells, the 15 mm radius geometry contained 650,000

cells and the 15 mm radius geometry contained 1.8 million cells. All geometries were performed for 30,000 iterations. 166
Figure 5.7: Range of antennas shapes simulated during the project showing (a) cylindrical antenna (b) pointed antenna (c) inverted cone antenna and (d) tapered cylindrical antenna. 167
Figure 5.8: Power density distributions for antenna designs showing an XY slice at 10 mm on the left (figures a, b, c and d) and an XZ slice at 2.6 mm on the right (figures e, f, g and h). Designs shown in figure a and e represent simulations performed with a cylindrical antenna. Designs shown in figure b and f represent simulations performed with a pointed antenna. Designs shown in figures c and g represent simulations performed with an inverted cone antenna. Designs shown in figures d and h represent simulations performed with a tapered cylindrical antenna design. Simulations were performed with a mesh containing 650,000 cells and performed for 30,000 iterations. 168
Figure 5.9: Power density distributions for different length antenna designs showing an XY slice at 10 mm on the left (figures a, b, c and d) and an XZ slice at 2.6 mm on the right (figures e, f, g and h). Designs shown in figure a and e represent simulations performed with no antenna. Designs shown in figure b and f represent simulations performed with a cylindrical antenna of length 5 mm. Designs shown in figures c and g represent simulations performed with a cylindrical antenna of length 10 mm. Designs shown in figures d and h represent simulations performed with a cylindrical antenna of length 15 mm. Simulations were performed with a mesh containing 650,000 cells and performed for 30,000 iterations. 170
Figure 5.10: Graph showing the leaking of microwaves from optimised Micro-well reactor, showing a peak in power density around 2.6 GHz, however this power density is still negligible compared to current microwave reactor standards 172
Figure 5.11: Micro-well reactor vessel shown with additional PTFE sheath around the circumference of the reactor wall. 173
Figure 5.12: Figure showing the comparison of coupling between unmatched and matched BMA and methanol. Measurements were made using a Rohde & Schwarz ZVL network analyser 174
Figure 5.13: Graph showing the heating times of different input powers. Observed that at 20 W it was not possible to achieve heat up times within the time period of the reaction 175

Figure 5.14: Monomers synthesised using the Micro-well reactor using 60 W input power over 150 minutes 176
Figure 5.15: ^{1}H Spectra showing the reduction of BMA compared to cyclododecanol after 150 minutes of heating in the Micro-well reactor. NMR showed reaction mixture only containing 31 % BMA compared to the remaining cyclododecanol, with an overall conversion of 78 % 178
Figure 5.16: ^{1}H proton spectra showing synthesis of CyDMA in Micro-well in a 8:5 starting ratio of BMA:Cyclododecanol, showing an improved conversion of 81 % with 116% BMA leftover compared to the remaining cyclododecanol 179

List of Tables

Table 1.1: Bacterial infection rates in hospital with associated costs and fatalities in intensive-care units across the US. [15] 5
Table 1.2: Characteristics of microwave and conventional heating[77] 26
Table 2.1: Dielectric constants and loss tangents for a range of different solvents[74] 43
Table 2.2: Description of bacterial strains used throughout this project .. 54
Table 3.1: Table showing the remaining amount of BMA left in reaction vessel at comparable conversions of approximately 80 % when comparing to amount of reagent alcohol left in vessel 86
Table 3.2: Table showing monomers synthesised using the optimised conventionally heated sparging method 89
Table 4.1: Table of ions identified by ToF-SIMS for associated monomer materials to identify how the feed ratios compared to the actual monomer ratios 126
Table 5.1: Table showing the cut-off frequency of the TE_{11} mode for air, BMA and butanol at different reactor sizes 171
Table 5.2: Transesterification synthesis comparison using conventional, microwave and micro-well prototype methodologies. Materials synthesised include [a] Cyclododododecyl Methacrylate (CyDMA), [b] 3-phenyl-2-propenyl Methacrylate (CiMA), [c] 4-Methyl-2-pentyl methacrylate (MpMA) and [d] 5-methyl-2-(1-methylethyl) cyclohexyl methacrylate 177

1 Introduction

The concept of a post-antibiotic era, where patients contract bacterial infections that are resistant to the last line of antibiotic defence due to the development of antimicrobial resistance (AMR) and a lack of new antibiotics is becoming a reality.[1,2] Therefore, the prevention of bacterial infections has become an utmost priority in order to reduce mortality and morbidity in clinical settings. Medical devices have been shown to cause an unacceptably high amount of bacterial infections as they provide sites for the formation of bacterial biofilms in the body.[3] Materials scientists and medical device engineers have suggested various means to reduce device-associated infection, including killing methods such as the incorporation of antibiotics and non-killing methodologies including using polymer coatings to prevent bacterial adhesion to the surface.[4,5] The discovery of anti-attachment polymer coatings utilised a materials discovery program which often make use of a non-biased material library to screen a wide chemical space. However, the development of quantitative structure-activity relationships (QSAR) has enabled a more systematic exploration of available materials to enable material libraries to be judiciously chosen.[6] A large chemical space has largely been left unexplored with non-commercially available materials, but this can be changed by using QSAR to systematically select non-commercially available materials that can then be synthesised with confidence of obtaining a material that can reduce attachment of bacteria to surfaces. Current library synthesis methods involve the non-specific heating of individual reactions by placing a multi-well vessel either into an incubator or heating block, resulting in poor reaction control.[7,8] Microwaves have been shown to selectively heat reactions to give higher reaction and make use

of volumetric heating to rapidly increase reaction temperatures.[9] The heating of multiple reactions simultaneously (combinatorial synthesis) using microwaves has currently been limited to either using a multi-mode source to irradiate samples simultaneously, but with poor reaction control, or to use a single mode source to heat an individual reaction with high control, but this vastly reduces the throughput when attempting to synthesis an entire materials library.[10]

The work described in this thesis utilises current QSAR computational models to develop a monomer library from which polymers can be formed in a microarray for high throughput assessment of biofilm formation. These monomers will be assessed to find a polymer that can reduce bacterial adhesion to medical devices. Simultaneously, a microwave reactor capable of synthesising novel methacrylate monomers will be designed and produced to develop a system which can efficiently produce novel monomers for high throughput discovery programs. This will require a reactor capable of synthesising monomers with a low power input (< 100 W) to make a combinatorial synthesis reactor feasible when scaled up such that a low total power is required to heat multiple vessels simultaneously.

1.1 Aims and Objectives

Aims outlined for the work herein can be shown below with corresponding objectives:

1. Develop monomer library based upon QSAR to identify polymers for medical devices with reduced bacterial adhesion and biofilm formation
    a. Use a current QSAR computational model to identify possible hit materials
    b. Synthesise materials that are not commercially available
    c. Print monomer library and photocure to form a polymer microarray with which to test predictive QSAR model
    d. Scale up hit materials identified to coat sections of silicone catheter for in vitro studies
2. Produce working single-mode microwave reactor for development of high throughput combinatorial synthesis system capable of producing novel methacrylate monomers
    a. Perform finite-difference time domain (FDTD) simulations to identify optimum reactor design with high power density distribution and ensure design operate within current exposure limits
    b. Manufacture designed microwave reactor and perform commissioning experiments to ensure design is safe
    c. Use developed microwave reactor to synthesise novel methacrylate monomers
    d. Perform viability studies to test whether produced microwave reactor can be scaled to work in high throughput

1.2 Medical device associated bacterial infections

Medical devices such as catheters and endotracheal tubes have revolutionised modern medicine and allowed for increased patient care throughout current healthcare systems. Commonly used devices such as catheters provide a range of essential tasks from carrying patient waste to providing ports to facilitate breathing/ventilation of unconscious patients, administer medicine, nutrition, and sample blood. However, despite providing a lifeline to patients throughout hospitals, medical devices have been shown to be susceptible to complications including bacterial infections (biofilms) and blood clots.[11–13] A report by O'Neill has also suggested that healthcare associated bacterial infections (HAIs) will cause more deaths than cancer by 2050.[14]

1.2.1 Biofilm formation on medical devices

Despite being a crucial part of healthcare, medical devices often cause complications which most prevalently include infections. Research that investigated the frequency and cost per infection in the US is shown in Table 1.1.

Table 1.1: Bacterial infection rates in hospital with associated costs and fatalities in intensive-care units across the US. [15]

Infection Type	Annual Infection (n)	Mean hospital cost per infection (US$)	Mean deaths per year
Surgical-site infection	290,485	25,546	13,088
Ventilator-associated pneumonia	250,205	9,966	35,967
Central-line associated bloodstream infection	248,678	36,441	30,655
Catheter-associated urinary tract infection	561,677	1,006	8,205

Table 1.1 shows not only the associated cost per infection but the high mortality rates that are associated to medical-device associated bacterial infections, with in some cases fatality rates exceeding 10 % of initial infection rates.

Biofilm formation in clinical settings usually originate from the patient themselves or a healthcare professional and can migrate from the surface of skin to a catheter port which then infect the device.[16] The common microorganisms that cause bacterial infections include gram-positive bacteria such as *Staphylococcus aureus* and *Staphylococcus epidermidis* as well as gram-negative bacteria such as *Pseudomonas aeruginosa, Proteus mirabilis* and *Escherichia coli*.[16,17] Microorganisms can form biofilms on a wide range of surfaces including medical devices, living tissues and water system piping.[18] Biofilm formation is a multi-stage process and can be divided into the following steps: (1) Reversible attachment of planktonic bacterial species to the surface with weak interactions such as Van der Waals. (2) Irreversible attachment of planktonic bacteria to the surface with interactions to deposited proteins on the surface, or with pili from the surface of the bacteria. Pili are hair-like extensions from the surface of the bacteria which can interact with surfaces. (3) Cell to cell adhesion and proliferation of bacterial colonies on the surface. (4) Maturation of the bacteria colonies into biofilms containing a extracellular polymeric substance (EPS) which protects the bacteria from surrounding environment.[19] (5) Detachment of bacteria cells from biofilm which go on to colonise further areas of the surface. [20,21] The biofilm formation process can be shown in Figure 1.1. Biofilms have been shown to be particularly resistant

to treatment through use of antibiotics, even in the absence of antibiotic resistance genes.[22–24]

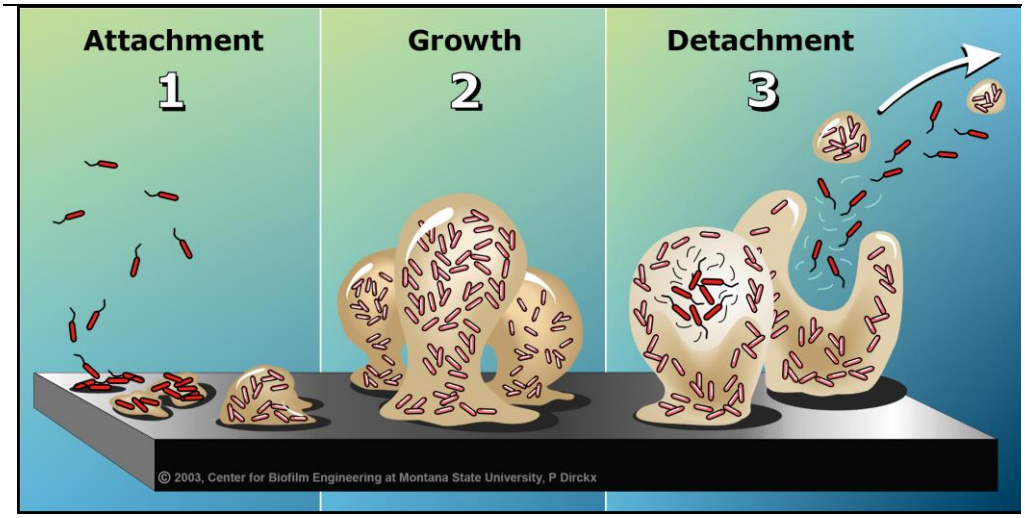


Figure 1.1: Biofilm formation depicted on substrate. Process shows progress from first contact of planktonic bacteria through a maturation process before dispersing more planktonic bacteria to repeat the process and form a layer of biofilm[25]

1.2.2 Current strategies for reducing medical-device associated bacterial infections

There is currently no widely accepted method to prevent the adhesion of bacteria to medical devices to prevent bacterial infections. The costly and painful procedure of replacing infected devices is the only way to effectively treat infected medical devices.[26] There are numerous preventative measures in place to try and stop bacterial infections which include the use of best hygiene practice, antibiotics and device coatings such as silver oxides/alloys,[4,27,28] however these have failed to prevent high infection rates as shown previously in Table 1.1.

A key preventative measure currently used to prevent surgical site infections is the implementation of good hand hygiene practices.[29] Despite this being of crucial importance, observational studies have shown that whilst pre-procedure hand hygiene is overall high (95 %), postoperative hand hygiene is not as routinely followed with only 80 % of nurses following correct hand hygiene procedure.[27] This shows that

despite best hygiene practice, health-care associated infections (HAIs) can be caused by human error, and hence an alternative solution is required to prevent infections in clinical settings.

Another widely used preventative measure includes the use of antibiotics to treat infections, which as well as combating blood infections such as sepsis, [30] have been used to combat medical device infections by using antibiotic lock solutions.[31] Antibiotic lock therapy involves using highly concentrated antibiotic solutions in the lumen of catheters to treat catheter-related bloodstream infections to avoid the need to remove and replace the existing catheter.[28,32] A key parameter of using lock-solutions is to ensure an appropriate antibiotic is used, and numerous different solutions have been successfully applied,[33,34] however the use has been restricted due to the rapid increase in antibiotic resistance.

Antibiotics have begun to also be incorporated into medical device coatings to prevent biofilm formation. Rifampicin, Trimethoprim and Triclosan have been used by Bayston *et al* when dissolved in chloroform to form a antimicrobial coating on peritoneal catheters[4]. Tests were performed to examine the activity of the antimicrobial, which showed up to 50 days protective ability[4]. The time taken to kill 100 % of bacteria by counting remaining bacteria was observed after 72 hours. It was discovered that a >98.9% reduction was achieved compared to controls with a multi-antimicrobial agent coating[4]. Studies showed that bacterial strains became resistant when exposed to a single antimicrobial agent coating. Again, a large concern with using anti-microbial coatings is that the antibiotic resistance of bacteria could be increased and cause the need

for further antibiotics to be developed. Another problem occurs when highly resistant microbes attach to a catheter with antibiotics, as the coating would be rendered inert by the resistance of the new microbes.

Another approach that was utilised by Heard *et al* was the use of chlorhexidine and silver sulfadiazine as coatings for central venous catheters.[35] This was shown to be successful in reducing the colonisation of *Staphylococcus aureus* over a 25 day time period in vitro, but the coating was only able to prevent colonisation of *Enterococcus* for 4 days in vitro. However, no difference in efficacy was observed in human trials, were 151 patients were inserted with a coated catheter and 157 were inserted with a triple-lumen catheter. An additional problem to this approach other than the potential to increase antibiotic resistance in bacteria is the use of both chlorohexidine and silver sulfadiazine, which can cause anaphylactic shock and hence cannot be widely applied to every patient.[36,37]

A current strategy employed to reduce the medical device associated bacterial infects is the coating of medical devices with silver oxides and alloys to reduce biofilm formation. Silver oxide coatings were shown to not statistically reduce the formation of biofilms in clinical settings,[38] however the incorporation of silver alloys into coatings has shown to potentially reduce bacterial adhesion though the findings of these products have been largely inconclusive.[39,40]

Despite best efforts, current strategies to prevent biofilm attachment to medical devices are not currently working. Furthermore, the increased overuse of antibiotic treatments

that these solutions offer would only work short-term until bacteria become resistant to the antibiotics used. Hence a new outlook on the prevention of biofilm is required, ideally one that avoids the use of antibiotics and that prevents the build-up of antibiotic resistance.

1.3 Production of novel biomaterials using high throughput experimentation

High throughput methodologies have been used to advance the field of materials discovery through a combinatorial approach that enables thousands of experiments to be performed in a single iterative process. This approach originates from Thomas Edison in 1878, who realized there was a limitation to his own predictions and hence increased the amount of experiments performed, testing over 3000 materials for the use as filament in an incandescent lamp.[41] Similarly, the interaction of biological systems with materials is a poorly understood process and would benefit from non-biased high throughput screening.[42] High throughput methodologies have developed a way to circumvent this knowledge gap by allowing novel materials to be discovered through the screening of thousands of materials, an area which was previously lacking for the discovery of novel biomaterials.[43] High throughput methodologies have had a large amount of success in the form of polymer microarrays by the groups of Anderson,[44] Alexander[45] and Bradley.[46] Polymer microarrays are formed by the deposition of a range of monomer solutions onto a substrate, which are then UV-polymerised. This then leaves in place thousands of polymer spots, which can be screened to analyse biological, chemical and physical properties in a high throughput regime.[47]

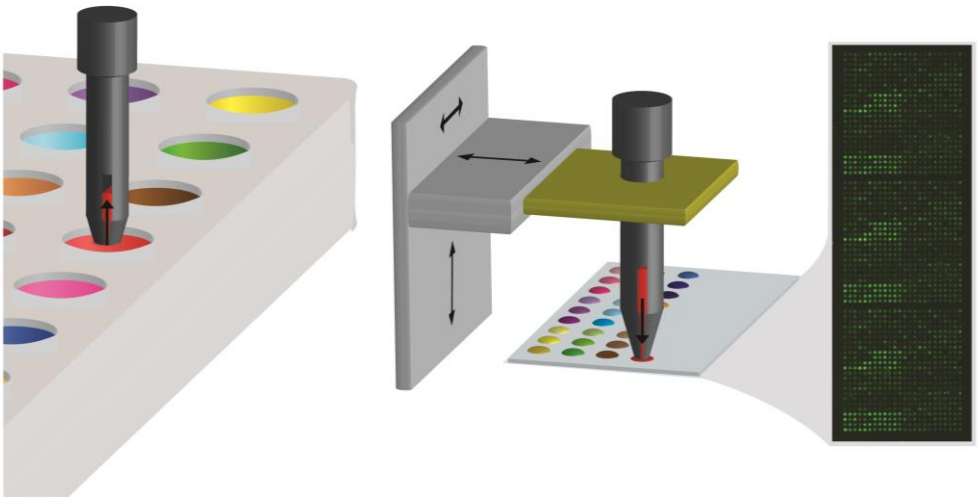


Figure 1.2: Formation of polymer microarrays; where monomer solutions can be transferred by either contact or ink-jet printing pins and UV polymerised. [48,49]

1.3.1 Rational design of biomaterials

Medical devices have been shown to increase patient welfare in clinical settings by offering treatment that otherwise would not be possible such as carrying patient waste, providing nutrition and facilitate breathing for unconscious patients. Current medical devices have been manufactured using biomaterials such as silicone that are retrofitted from previous applications due to beneficial mechanical properties and inert nature.[50] Whilst these properties are useful for a vast range of applications, the tendency to promote biofilm formation was not considered when used for medical devices and have been shown to be wholly inadequate when regarding bacterial adhesion.[38,51]

Research into polymethacrylates as biomaterials can be traced to an observation made when pilots of warplanes sustained eye injuries containing plastic from the plane canopy. It was noted that these shards remained inert within body tissue.[52] This led

to the development of intraocular lenses that have improved the quality of life of millions of cataract suffering patients worldwide. This early pioneering led to large multi-disciplinary collaborations to formalise design principles for novel biomaterials, particularly of the idea that leeching of toxic material from biomaterials will adversely affect healing. This started the understanding of biocompatibility of different materials within the human body.[53]

The design of biomaterials has led to a gathering of fundamental physico-chemical knowledge surrounding the cell-surface interaction. Decuzzi *et al*. developed a theoretical model that investigated the binding of a thin biolayer across a surface where receptor and ligand molecules were distributed across the surface of the substrate and biolayer respectively.[54] The surface energy was theoretically calculated by summing the contributions of chemical energy, the elastic energy and the energy associated with the generation of non-specific interfacial interactions, which could be altered to give surfaces with small, intermediate and high surface energies.[54] It was discovered that for small surface energies, an increase in surface roughness was detrimental to cellular adhesion, for an intermediate surface energy surface roughness was found not to effect cellular attachment and for high surface energies, an optimal roughness can be identified to maximise cellular adhesion. It is also widely accepted that surface chemistry impacts upon both cellular adhesion and proliferation with examples of research showing how surface chemistry effects mesenchymal cell adhesion and differentiation.[55,56]

The knowledge of bacteria-surface interactions is more poorly understood.[57] Studies have shown that bacterial adhesion is strongly affected by physico-chemical properties of both the bacteria and surface including interactions with bacteria structural features such as flagella and pili.[57,58] An interesting report by Mitik-Dineva *et al* demonstrated that a smooth glass surface had higher bacterial adhesion for 3 bacterial species (*E.Coli*, *Pseudomonas aeruginosa* and *Staphylococcus aureus*) compared to a nano-rough glass surface.[59] This demonstrated a dependence on bacterial adhesion on surface topography. The interaction between pili and flagella and the surface has also been reported to be heavily dependent on surface chemistry, either promoting or preventing bacterial adhesion.

A large amount of publications have gathered information regarding either cell or bacterial interactions with surfaces, but it has rarely been used in conjunction with one another. However, it has been reported that the use of nanostructures can be used to promote attachment of osteoblasts whilst reducing attachment of *Staphylococcus epidermidis* or *E.coli,* by Colon *et al* and Ploux *et al* respectively.[60,61] This shows the useful application of both cell and bacteria-surface knowledge to develop a system which could promote the attachment of cells whilst reducing the chance of bacterial infections for bone implant fabrication processes.

Despite progress, the development of novel biomaterials through rational design is still difficult, as cell-surface relationships (such as bacterial attachment and biofilm formation) are often poorly defined.[50] An alternate solution is required to allow for more relationships and observations to be

made for surface-cell/bacteria relationships such as using high throughput material discovery methodologies.

1.3.2 Discovery of novel biomaterials using polymer microarrays

High throughput discovery programmes (HTDP) have allowed for an alternative to rational design of materials when processes such as the bacteria-surface interaction are poorly understood.[50] HTDP offer an opportunity to screen a wide diverse of materials to discover potential new hit biomaterials. One such HTDP platform is the use of polymer microarrays to gain information of cellular adhesion to polymeric surfaces. A polymer microarray is an array where a large monomer library has been deposited onto a substrate, (usually pHEMA), and polymerised on slide to form an array containing hundreds of polymers on a single slide (Figure 1.3).



Figure 1.3: Polymer microarray containing 576 materials printed in triplicate used for identifying key materials for reducing biofilm formation[62]

This provides a platform for high throughput experimentation and characterisation to take place. This technology was first demonstrated by Anderson *et al* to observe adhesion of stem cells to polymeric surfaces.[48] Polymer microarrays were seeded with human mesenchymal stem cells (hMSC) and stained with a green fluorescent stain (Alexa 488) 48 hours after seeding so that cell attachment can be measured by observing fluorescence intensity (Figure 1.4).[44]

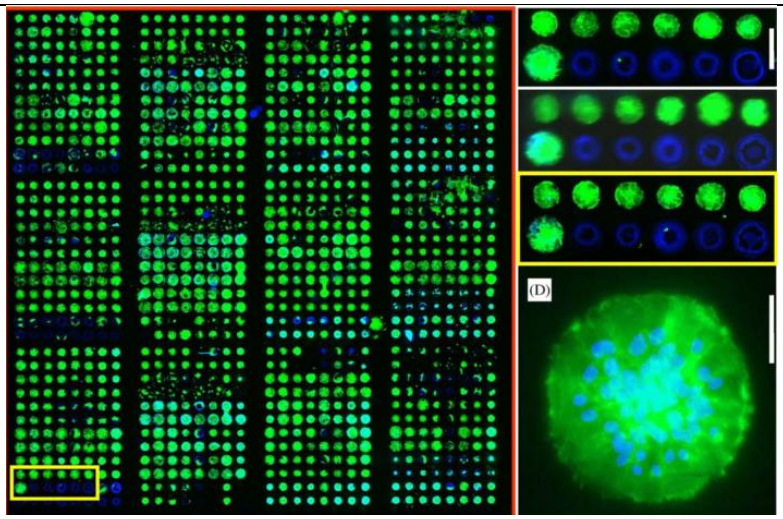


Figure 1.4: hMSC cells grown on a polymer microarray (comprised of 24 different polymers mixed pairwise at ratios of 1:0,9:1 and 7:3 to give 1152 combinations) with a fluorescent stain to characterise cell adhesion to polymeric surfaces[44]

The screening process of a large polymer library allowed for an unbiased screen of a large range of chemistries, effectively performing hundreds of experiments with a single iterative process. It was identified that most of the polymers that were tested promoted attachment of hMSC cells, however polymers with a large amount of poly(ethylene glycol) (PEG) inhibited cell attachment. This showed how a high throughput programme has developed understanding of a poorly understood process by

identifying key chemical moieties that prevent attachment of hMSC cells.

Polymer microarrays have been used to observe the interaction between polymeric surfaces and bacteria. This process discovered novel biomaterials which reduce biofilm formation to medical devices, to prevent bacterial infections in patients. Polymers were identified by Hook *et al.* to reduce biofilm formation on urinary catheters through the use of polymer microarrays as a high throughput materials discovery platform.[62] Polymer microarrays were used to analyse the surface chemistry of polymer spots using surface characterisation techniques such as time of flight secondary ion mass spectrometry (ToF-SIMS). This enabled key ions to be identified for controlling cellular response.[63] This process was repeated multiple times to screen large amounts of polymers to discover hit materials that could be scaled up and coat silicone catheters.[45] This led to the discovery of a material that reduced the attachment of *Pseudomonas aeruginosa*, *Staphylococcus aureus* and *Escherichia coli* by approximately an order of magnitude compared to current clinically used urinary catheters.[45] The mechanism of preventing bacteria adhering to the surface was shown to not be bactericidal, and hence this process will not contribute to the increase of antibiotic resistance, which has proven to be a major obstacle for other suggested solutions.

HTPD such as polymer microarrays have demonstrated the versatility for screening for hit materials for a range of applications in a large chemical space. However, for maximum discovery flexibility, the monomer building blocks for these

screening campaigns must be cheap and readily accessible (i.e. not requiring bespoke synthesis). This typically restricts researchers to monomers that are commercially available for which there are approximately 300 (meth)acrylates/(meth)acrylamides, thereby limiting the chemical diversity that can be screened. However, the number of monomers that can be synthesised is immeasurable, and hence HTDP are missing a vast range of materials in non-commercially available materials. A larger, more diverse monomer library will enable HTDP to make subtle changes to polymer functionalities to investigate specific surface-cell relationships. Equally, a more diverse library will enable a larger diversity of functionalities to be screened, increasing the likelihood of discovering a hit material.

The ability to create a 'super' library of potential hit target polymers would require computational models that could predict material properties prior to experimental investigation. This would allow bespoke libraries to be created and tailored to the targeted application.

1.4 Quantitative structure activity relationship models for targeted library development

Previous polymer microarray experimentation involved using a non-biased materials library to screen as wide a chemical space as possible. This is primarily due to the large knowledge-gap surrounding the bacteria-surface interaction.[42] To overcome this problem, quantitative structure activity relationship (QSAR) models have been developed with the capability to predict biomaterials with favourable properties.[6,64]

Anti-microbial and anti-fungal paint has been developed by Hoque *et al* and also preliminary structure-activity relationships were discussed.[65] A library of polymers with different structures, molecular weight and hydrophobicity based upon polyethylenimine was used to develop an anti-microbial surface. The surfaces were shown to be bactericidal, as the author intended, and was discovered that linear polymers were found to have a higher killing rate than branched polymers. [65]

Further QSAR work developed by Sanni *et al* showed a correlation between molecular descriptors and bacterial adhesion which showed that weakly amphiphilic rigid monomers resist bacterial adhesion.[6] The number of rotatable bonds (nRoTB) and the calculated partition coefficient (cLogP) was used to develop a model to predict the biofilm formation of monomers which can be shown in Equation 1 and was described as the *alpha* parameter [6].

$$\alpha = 0.44nRoTB - cLogP$$

Equation 1: *Alpha* parameter showing how bacterial adhesion of hydrocarbon polymers is related to the hydrophobicity and rigidity of material[6]

The parameter was developed by initially observing the adhesion of *P. aeruginosa* to a polymer microarray consisting of 24 copolymers made from tert-butyl cyclohexyl acrylate (tBCHA), cyclohexyl acrylate (CHMA), 4-tert-butyl acrylate (tBA) and 3,3,5-trimethylhexyl acrylate (TMHA).[6] The proposed *alpha* parameter showed a correlation of $R^2 = 0.83$, suggesting that low bacterial adhesion is seen on nonpolar rigid materials. To test the robustness of the model, the model was applied to previously acquired data which initially included fluorocarbon, amines, multiple glycol units and di/tri acrylates.[6] This showed a poor correlation due to the large amount of materials represented out of the original data set used to calculate *alpha*. However it was shown to be applied to a subset of 37 poly(meth)acrylates with hydrocarbon pendant groups and a correlation was seen between 32 of these materials showing that the model could be applied to 86% of the materials that were tested. [6] This research suggests that an effective materials discovery feedback loop can be formed by predicting the performance of materials before testing, and then using the results from resulting experiments of novel materials to make more accurate and robust computational models (Figure 1.5).

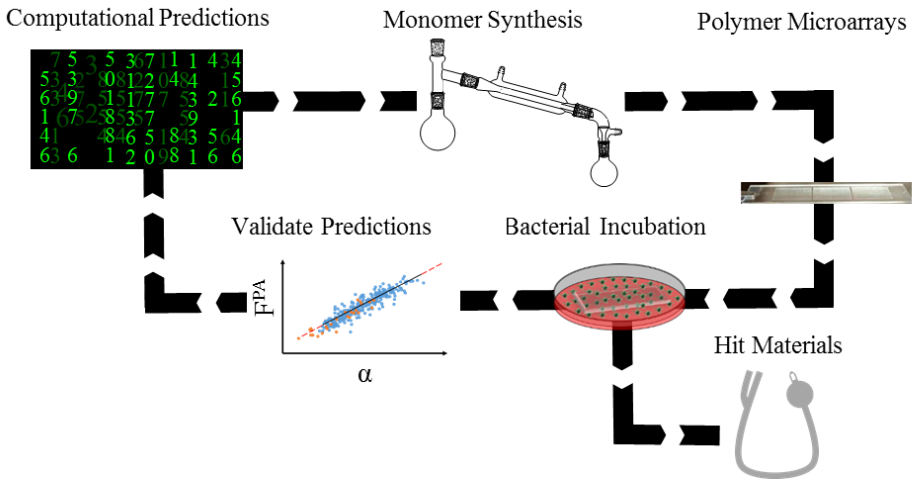


Figure 1.5: Flow diagram showing work flow to find suitable materials for preventing biofilm formation to medical devices. The results from previous assessments of bacteria-material interactions can be used to predict and then synthesise novel monomers. The newly produced materials can be tested to further refine the model, leading to the discovery of the next generation of biomaterials.

Furthermore, by being able to predict material performance, the large unexplored non-commercially available material space can be explored by predicting materials that can be synthesised to provide a library to either probe specific bacteria-structure relationships or to be judiciously chosen to increase the likelihood of obtaining a hit material fit for purpose. However, polymer microarrays can contain thousands of materials on a single glass slide,[47] and hence non-commercially available materials need to be able to be provided quickly enough to keep up with microarray production to make the exploration of non-commercially available materials a viable option. Hence, having access to a reactor capable of synthesising a range of different novel monomers in a single batch process would enable the largely unexplored non-commercially to be accessible for high throughput screening experiments.

1.5 Review of current material library synthesis

A major limitation of HTDP is the use of commercial materials to form a materials library for experimentation. This restricts the ability to search for novel hit materials for a targeted application. Combinatorial chemistry offers a solution to be able to synthesise a library with a wide range of diversity and there have been numerous combinatorial chemistry methods that have been used in previous publications.[7,66–69] An example of combinatorial chemistry to synthesise a wide range of polymers was demonstrated by Anderson *et al* where 2350 polymers were synthesised from a library consisting of 119 commercial monomers.[70] Monomers were transferred into a 96-well plate and incubated for 5 days at 56 °C with 1 ml of dimethyl sulfoxide (DMSO). Resulting polymers were then used to find hit materials for the transfection of the luciferase expressing plasmid, pCMV-luc into a monkey kidney fibroblast cell-line COS-7.[70] The top 50 polymers from the initial screen were then individually optimised for the transfection assay to ensure a correct polymer:DNA ratio was used. This shows how a combinatorial chemistry approach was used to choose a small subsection of a large library to take forward for further optimisation experiments and proves how essential combinatorial chemistry could be for HTDP. However, a few drawbacks of this approach are that there is a distinct lack of synthesis control by leaving a well plate in an incubator for 5 days. Each material will have different thermal conductivities and will heat unevenly, and so the temperature of each reaction is unlikely to be the same. Furthermore, the reaction time took 5 days to complete, which adds considerable time to an already long high throughput experimental process.

Another approach to combinatorial chemistry is to use microwaves to be able to synthesis a wide range of materials in a single batch process. This has been used extensively using domestic microwave ovens to heat a library of materials in a container such as a well plate to heat each individual reactions.[71,72] A common problem with utilising multi-mode microwaves is the change in temperature heating deriving from the distribution of microwaves within the cavity. This was demonstrated by *Glass et al* where a difference of 20 ˚C was observed in a 96-Well plate between the outside and centre of the plate for the formation of an 880 member compound library using solid-phase synthesis(Figure 1.6).[73]

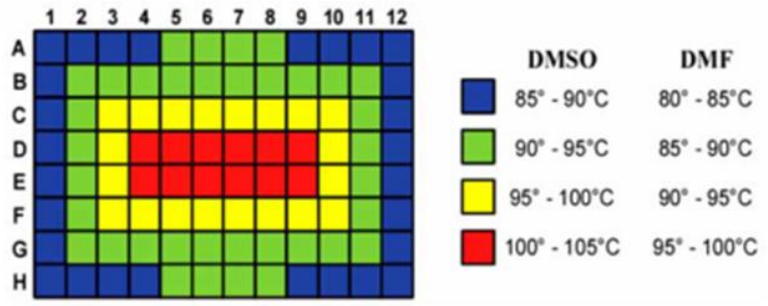


Figure 1.6: Inhomogeneity of heating shown by use of a polypropylene 96-Well plate in domestic multi-mode microwave oven[73]

Another example of a library synthesiser was described by Murray *et al* where a multimode microwave source was utilised to synthesise a peptide library in a 96-well plate system that was placed inside the microwave cavity. It was observed that whilst acceptable levels of purity were obtained, that levels of purity of the same material depended on where on the 96-well plate it was positioned, with purities ranging from 50 to 80 % depending on position.[71] This was described as an issue with agitation of the peptide mixture, but could also have arisen from the uneven heating distribution of multi-mode microwaves.

Another issue was that despite the authors being able to use a probe to measure temperature of a single reaction, largely the reaction temperatures were unmonitored and hence definitive conclusions on heating distribution cannot be answered but demonstrates a distinct lack of control of reaction conditions.

A final proposed system which has been suggested is to use a single-mode cavity to synthesise novel materials and link multiple systems together to provide a working microwave synthesiser capable of monitoring each reaction independently of one another. This has been used as a proof of concept design for the amplification of DNA for polymerase reactions. Kempitiya *et al* produced a single well working prototype to perform amplification of water for polymerase chain reactions which raised temperatures to 72 °C using only 400 mW of power in 6 minutes.[74] This was achieved by being able to ensure all microwave power was able to couple with the load material. An issue could arise from only using water as a model, as components such as phosphates and sugars could cause microwave specific heating which could be detrimental to impedance matching which would cause a reduction in microwave absorption. This would cause a change in reaction temperature and therefore polymerase activity. Temperature measurements were done using a fibre optic cable which offered a low uncertainty of measurements of 0.3 °C. The microfluidic microwave chamber also comprised of a ground plate with a small hole in which water was inserted, which prevented excess evaporation of water, showing in effect poor mass transfer ability. However, this was done for a very small reaction volume of 4.1 μL but demonstrates the ability to design an efficient mono-mode microwave reactor with large scale out potential.

1.6 Benefits of using microwaves for organic synthesis

Microwave assisted organic synthesis (MAOS) has gained traction since the reported use of microwaves to accelerate organic reactions. The first reported use of microwaves to heat organic chemical reactions in 1986 by Gedye *et al* and Giguere *et al*.[75,76] The development of MAOS has progressed from using domestic microwave ovens to dedicated optimised reactors with matched impedances. Microwaves are electromagnetic waves in the frequency range of 0.3 to 300 GHz. Industrial, scientific and medical (ISM) bands are radio bands specifically reserved for industrial, scientific and medical purposes such that they do not interfere with any telecommunication frequencies.[77] A large amount of microwave applicators are used at 2.45 GHz which is a worldwide acknowledged ISM allocation. Microwaves have been used to heat chemical reactions because they can transfer energy to polar materials without breaking chemical bonds, therefore the microwave irradiation itself cannot initiate chemical reactions.[77–79] However, the transfer of energy has shown to be incredibly effective at increasing reaction yields whilst reducing reaction times from hours to minutes per reaction. A comparison of microwave vs conventional heating methods is shown in Table 1.2, where crucially microwaves are shown to be a volumetric heating method compared to conventional conduction heating which is a superficial heating technique, and this leads to rapid heating times with greater control of reaction temperature compared to conventional methods.

Table 1.2: Characteristics of microwave and conventional heating[80]

Microwave Heating	Conventional Heating
Energetic coupling	Conduction/Convection
Volumetric Heating	Superficial heating
Selective	Non-Selective
Dependent on material properties	Less dependent
Rapid heating	Slow heating

This has led to a surge of publications using MAOS to optimise reactions that were previously time consuming and resulted in low yields.[81] Another benefit of microwaves is through green chemistry, where many publications have been able to synthesise novel materials using solvent-free chemistry using a reduced power input compared to conventional methods with minimal wastage.[82–84]

1.6.1 Thermal and non-thermal effects of microwave irradiation

The use of microwaves for organic synthesis has been shown to reduce reaction times from hours to minutes, reduce side reactions and increase reaction yields.[9] Microwave irradiation has been reported to induce a combination of thermal and alleged non-thermal effects in reaction mixtures.[85] A key thermal effect of microwave heating is dielectric heating, where polar molecules are rapidly heated by microwave irradiation, however non-polar molecules are incapable of absorbing microwave radiation and hence are not heated by microwaves.[86,87] This process is described in further detail in 2.1.4. Numerous alleged non-thermal effects have also been

described in literature including: 1) the superheating of solvents showing in some cases up to 20 °C increase in boiling temperature compared to conventional heating methods.[87] 2) The selective heating of highly microwave absorbent metal catalysts in a less polar reaction medium.[88,89] 3) formation of microwave induced hot-spots in homogenously mixed reaction mixture due to the coupling of microwaves to specific reagents.[90] 4) Elimination of wall effects caused by inverted temperature gradient, which also leads to quick initial heat-up times (Figure 1.7).[91] It is important to note that, whilst in literature these effects are termed non-purely thermal effects, in reality, these effects are still thermal effects (i.e. a rate enhancement is observed due to a temperature change), though experimentally these temperature changes cannot be measured.[9]

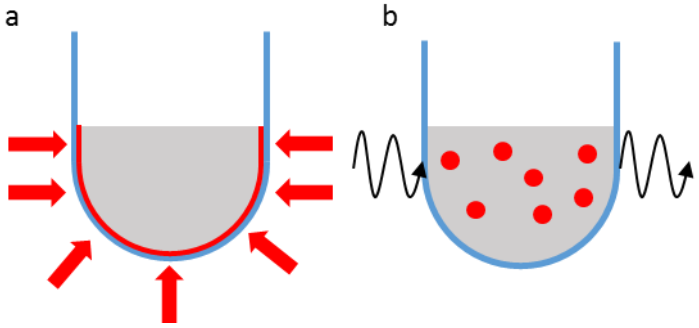


Figure 1.7: Efficiency of microwave heating demonstrated by showing (a) how microwaves directly heat reaction contents compared to (b) conventional conduction heating which initially heats vessel walls prior to reaction contents

A more controversial area of microwave heating is the effects of non-thermal or athermal effects. Historically this term was used to describe outcomes of microwave synthesis experiments that differed from conventional heating methods. Non-thermal effects have been described using Arrhenius' equation which shows the dependence of the rate constant of a reaction on the

absolute temperature, a pre-exponential factor and the activation energy for the reaction (Equation 2).

$$k = Ae^{\frac{-E_\alpha}{RT}}$$

Equation 2: Arrhenius's equation showing dependence of reaction rate constant on the pre-exponential factor A, activation energy E_α and the temperature T

The pre-exponential factor, A, represents the probability of favourable molecular impacts, and has been postulated by Binner *et al* to be affected by microwave irradiation by increasing molecular vibrations, which would increase the reaction rate, k.[92] Another effect has been proposed that arises from a reduction in the activation energy E_α, from the increase in change of entropy caused by uniform oscillation of polar molecules within an oscillating electric field, which was suggested by Lewis *et al* for imidization reactions using microwave irradiation.[93] This would suggest an increase in reaction rate that is not related to the temperature. These concepts have never been experimentally proved, only suggested as to reasons at which reactions have been accelerated. However, as previously mentioned, localized temperatures may be a lot higher than the bulk temperature and hence that reported chemical reactions could in fact be occurring at a higher temperature rather than microwave effecting the activation energy of reactions as these reports have suggested.

1.6.2 Single mode vs multi-mode cavities

Previous literature covers a wide range of MAOS applications ranging from transitional-metal catalysis to medicinal chemistry/drug discovery as well as experiments to investigate combinatorial and parallel processing through to industrial scale up processes.[72,94] However the method of which microwaves

are used in these applications varies. There are two main categories of microwave cavities, monomode and multimode cavities (Figure 1.8). A multimode applicator inputs radiation created by a magnetron directly into a cavity, where it is dispersed and forms multiple standing waves within the cavity, which then causes irregular power density distributions.[78] Multimode applicators benefit from being able to irradiate multiple samples simultaneously as multimode applicators can heat larger areas.[95] However a major limitation arises from the heating pattern caused by multiple modes within the cavity. This highly reduces the control over reactions due to high variations in microwave exposure from one area to another.

However, a monomode or single mode applicator will use a power source (magnetron or solid-state), to input a single mode of microwave radiation into a cavity. The radiation forms a singular standing wave pattern within the cavity with nodes and anti-nodes of microwave energy intensity.[96] The field uniformity allows for a high rate of heating and greater control over reaction conditions. However the design of these cavities mean that only small volumes can be processed at a time due to the size of the cavities, causing a large drawback when considering high throughput systems.[10] A major advantage of single mode cavities is the ability to match the input signal to the load, enabling majority if not all of the input power to be able to be absorbed by the load material.[97]

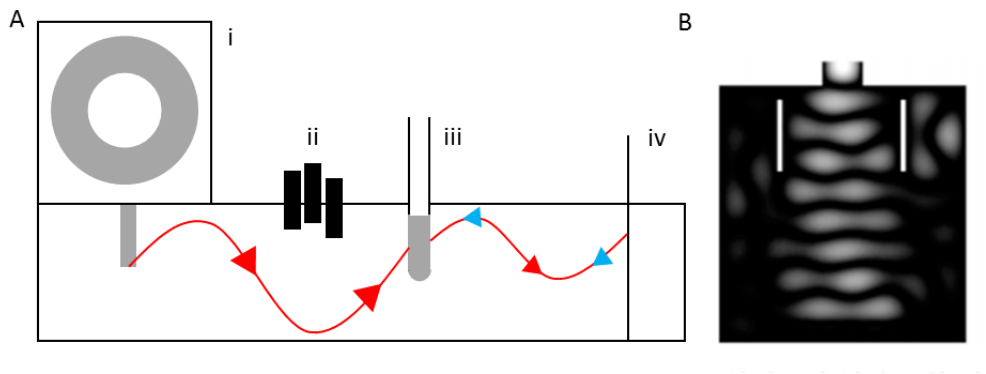


Figure 1.8: (a) Schematic of single mode cavity utilising (i) microwave power source which uses fine stub tuners (ii) and a coarse plate tuner (iv) to couple microwaves to the sample (iii). (b) Shows a diagram of a multimode cavity with irregular electric field patterns due to propagation of multiple electromagnetic modes[98]

The design of a microwave reactor ultimately depends on the application, and the choice of using a multi-mode or mono-mode is critical in how a reactor will perform. Additional critical design choices include reactor geometry and matching the input power to load material using antennas.

1.6.3 Use of monopole antennas to focus microwave irradiation

To operate a microwave cavity safely, chokes are often implemented to ensure that the system is working below the cut-off frequency and hence attenuate microwaves such that microwaves are not leaked into the laboratory and causing a safety issue. However, in some applications, microwaves need to be controlled in an open environment for a specific application such as tumour ablation or drill processing which requires microwaves to penetrate outside of a cavity.[99,100] Monopole antennas can be used to couple microwaves to material loads to offer a directionality to microwave heating. Hence by using antennas, it is possible to focus energy into a specific area that requires heating.

Different modifications can be made to antennas to make them fit for purpose, such as using a metal reflector to ensure microwaves only penetrate in one direction as used by McWilliams *et al*[100]. The antenna was first simulated and then tested on porcine tissue with the aim of ablating tissues next to critical structures such as nerves and organs. This demonstrated a simple and easy way to manipulate microwave energy to only irradiate a chosen area.

However, work carried out by Jerby *et al* works at changing the antenna geometry to also control the heating effects of microwaves. It was shown theoretically[101] and experimentally that by changing the antenna to a cone shape, it is possible to focus the microwave energy into a point in front of the antenna which allowed the author to perform dust-free drilling[102]. This shows that antennas can be designed to couple microwave energy to deliver microwaves to a desired load, which has been shown to be applied to the design of microwave reactor capable of monomer synthesis described within this work.

It has been shown how MAOS benefits chemical reactions by offering volumetric heating that can rapidly increase reaction temperatures with greater control compared to conventional heating methods. Monopole antenna cavity designs have then shown how a microwave source can be manipulated to heat specific areas for a range of different uses. However, most microwave applications require thorough theoretical model designs before experimental work can commence. The design of microwave reactors are too complex to be designed using numerical methods and therefore computational models that use approximations such as finite difference time domain

(FDTD) simulations are required to fully understand how electromagnetic waves will propagate through a proposed microwave reactor. This thesis focuses on the use of FDTD over other methodologies such as finite elements methods due to the decreased computational power associated with FDTD simulations.

1.7 Developing microwave cavities using FDTD simulations

Finite difference time domain (FDTD) simulations have been extensively used to effectively design electromagnetic applications before manufacture to reduce trial and error failures. The FDTD algorithm allows for designs to be divided into regular mesh-grids and simulates the time evolution of Maxwell's equations.[103,104] This process was used during this project to design and simulate geometrical designs such that designs would not only perform as required, but also be safe to operate.

1.7.1 Optimising simulation conditions

A critical design aspect of microwave reactor designs is ensuring the design is safe for laboratory users, and using the cut off frequency (Equation 3) allows for a reactor to be safely designed before being manufactured.[105]

$$f_{c_{nm}} = \frac{p'_{nm}}{2\pi a\sqrt{\mu\varepsilon}}$$

Equation 3: Cut off frequency for circular waveguide where a = radius, p'_{nm} = wave mode constant, μ = magnetic permeability and ε = relative permittivity[105]

After geometrical design, a regular mesh is applied so FDTD simulations can be performed. This mesh is applied such that Maxwell's equations can be calculated over each individual cell and summed together to illustrate how electromagnetic radiation varies over time.[103] A common problem with meshing in FDTD is staircasing.[106,107] Staircasing is where the cell units poorly fit the geometrical design, causing a breakdown of the FDTD algorithm due to a change in electromagnetic field over a cell. A simple solution to this is to increase the mesh size, which will improve simulation precision, but at the cost of increasing

simulation time. However, a reported solution involved using non-orthogonal meshing at curved boundaries between material interfaces. The reported method allows for higher precision simulations, but maintaining short simulation times by using orthogonal meshing for the bulk of the simulation.[107]

In order to compare different geometrical designs, it is important to consider the matching of each reactor, which allows for like for like comparison between different designs and also enables an efficient reactor to be designed that couples majority of input power to the material load.[108]

1.7.2 Applications of FDTD simulations

FDTD simulations have shown to be a powerful tool to create, efficient microwave reactors capable of a range of applications including biotelemetry, ablation therapies and dust-free drilling.[99,108,109] Jerby *et al* demonstrate the use of FDTD simulations to theoretically analyse desirable thermal-runaway effects within a material to allow for dust free drilling.[101] Theoretical analysis of the thermal runaway effect in mullite was able to show temperature rises of up to 1300 K in seconds and able to confine the microwaves to a 4 mm width hot spot. Biotelemetry offers useful in-situ feedback for medical applications and has used FDTD simulations to simulate short-range biomedical devices including pacemakers.[109]

An alternative application for FDTD has been reported by Zhao *et al* for the modelling of switched gradients of human bodies in MRI.[110] This has been used with the development of the FDTD method to be able to include the simulation of low frequencies, which historically has not been possible, which can now be applied to complex bioelectromagnetic problems.

A more direct medical application for FDTD simulations is used for microwave imaging, where a simulation is performed after acquiring MRI data of a patient who has suspected to have breast cancer. This is possible due to the contrast in dielectric properties between normal breast tissue and malignant tumours.[111] This technique been used to successfully identify breast cancer within patients using backscattered waveforms from an MRI scan, which could lead to the reduction of health checks required to successfully diagnose patients. [112]

FDTD simulations offer the opportunity to develop a microwave reactor in a thorough investigative manner, to explore the effect that a range of different parameters has on the power density distribution observed within the load material. This enables a first-time prototype to be designed with a high chance of functioning for the designed purpose, saving both time and costs.

2 Materials and Methods

2.1 Chemical Synthesis

2.1.1 Materials

Methyl methacrylate (MMA), butyl methacrylate and titanium butoxide used for all transesterification experiments were obtained from Sigma Aldrich and used as-received. A range of alcohols were used to synthesise novel methacrylate monomers: cyclododecanol, cetyl alcohol, 4-nitrobenzyl alcohol and 3-phenyl-2-propen-1-ol from VWR international and used as received. Further alcohols: dodecanol, l-menthol, geraniol, 2-methyl-3-butyn-2-ol, 4-methyl-2-pentanol and 2-ethyl-1-hexanol were purchased Sigma Aldrich and used as received. Finally, alcohols: 2 chlorobenzyl alcohol, 4 methylbenzyl alcohol, 4-isopropylbenzyl alcohol and piperonyl alcohol, were purchased from Fisher Scientific and used as received. 4-Methoxyphenol was purchased from Sigma Aldrich to be used as an inhibitor and was used as received. All alcohols used can be found in Figure 2.1. 2,2'-azobis(2-methylpropionitrile) (AIBN), a thermal free-radical initiator, was used for polymerisation experiments and acquired from Sigma-Aldrich.

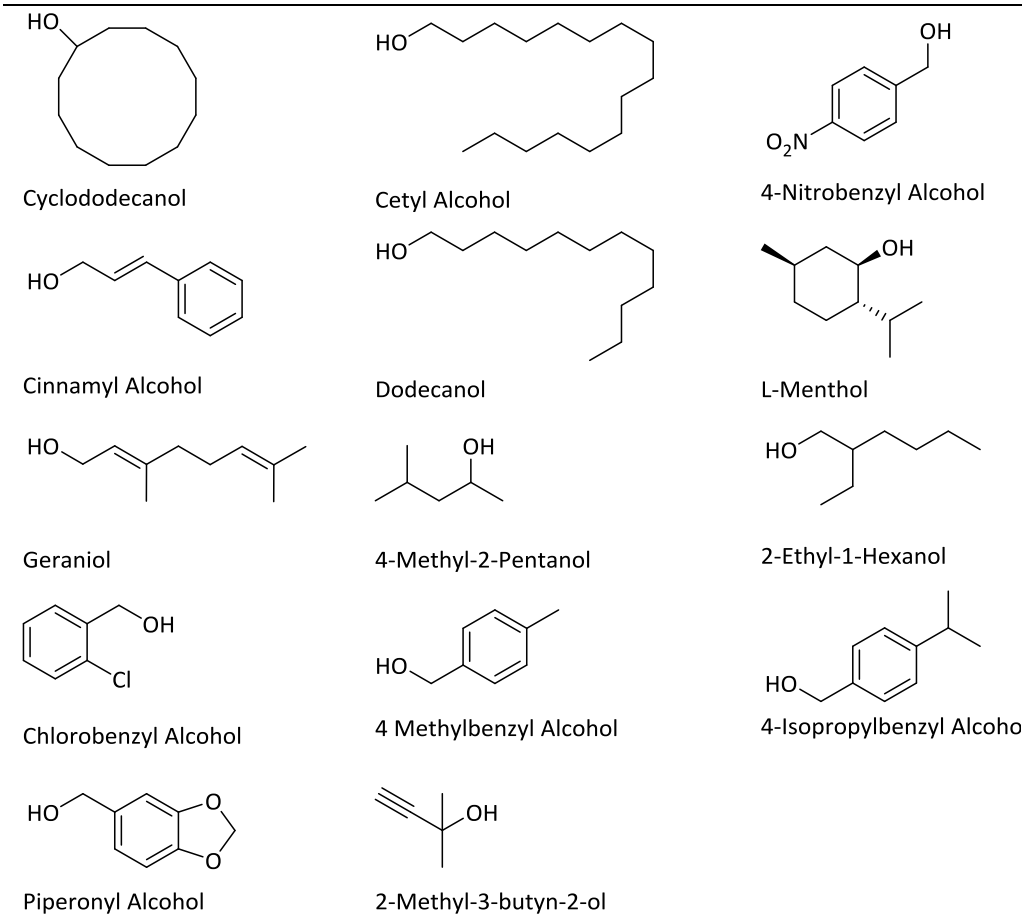


Figure 2.1: Figure showing alcohols used for synthesis experiments performed in this project

2.1.2 Transesterification Reactions

Transesterification experiments have been performed in the past for a range of applications including lipid synthesis and manufacture of biofuels.[113,114] The simplicity and reaction speed offered by transesterification mechanisms allow for a degree of flexibility to synthesise a vast range of novel methacrylate monomers. The reaction sequence can be shown in Figure 2.2.

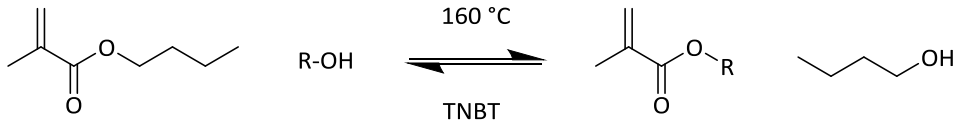


Figure 2.2: Reaction sequence showing general reaction conditions used for transesterification experiments

The reaction mechanism for transesterification reactions can be found in Figure 2.3. The mechanism shows how a fundamental ester can have the functionality changed by simply changing the alcohol used during the experiment.

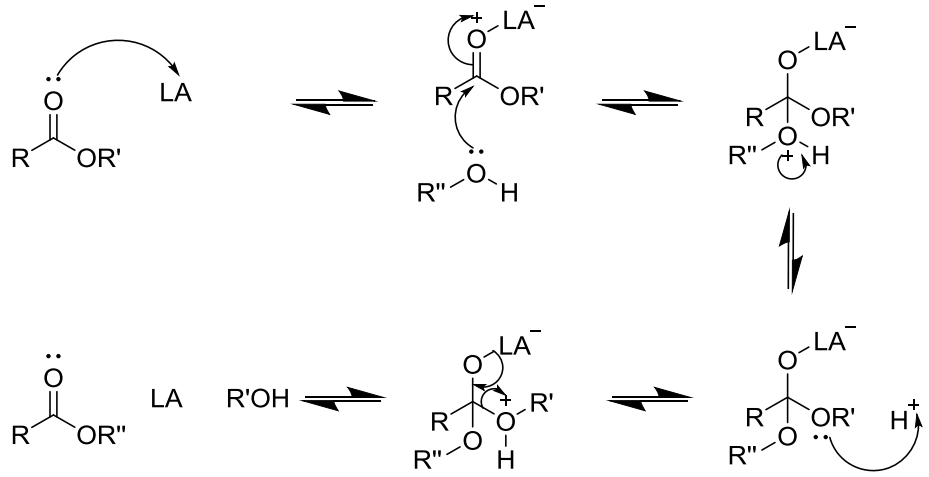


Figure 2.3:Reaction mechanism for transesterification reactions, showing how functionalised alcohol group (R') can replace functionality of an ester group (R'') where LA is lewis-acid which typically was titanium butoxide

As shown in Figure 2.2, the transesterification mechanism is a reversible process. Therefore, by using Le Chatelier's principle, adding an excess of one of the starting reagents will push the reaction towards the products and aid in the production of novel methacrylates to a higher conversion.[115] Therefore, for a majority of reactions a starting molar ratio of 7:5 was used of butyl methacrylate: alcohol respectively. All synthesis reactions used 1 % (molar ratio) catalyst which was titanium butoxide. Two reaction vessels were used which were either short or long neck vessels to either optimise reaction conditions or mimic microwave experiments respectively (Figure 2.4). Long neck-vessels had to be used for microwave reactions due to a metal choke used to prevent microwave leakage. Reactions were sampled and quenched in the freezer for analysis using NMR.

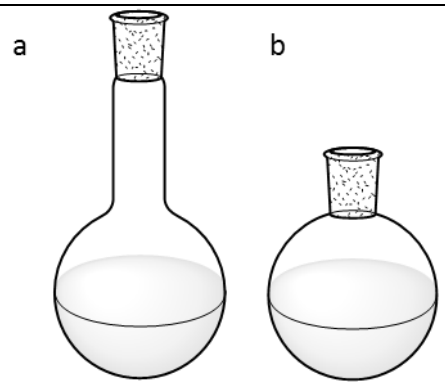


Figure 2.4: Schematic showing different glassware used for synthesis experiments (a) 50 ml long necked vessel used with microwave reactions to comply with safety choke design and also used for conventional experiments for direct comparison to microwave experiments (neck length 145 mm) (b) standard 50 ml flask used for optimised conventional reactions (neck length 43 mm)

2.1.3 Nitrogen gas sparging

Nitrogen gas sparging was used during this project and is a technique utilized to improve reaction yields.[116,117] Gas sparging involves blowing in gas directly into a reaction, which is then dispersed into the reaction media to take up a large surface area. Nitrogen gas sparging has been used before to aid the distillation of products or by-products to separate materials from liquid mixtures.[118] This was a desirable aspect of using gas sparging to help remove butanol by-products made by transesterification experiments in order to achieve higher conversions. The reaction yield of chemical reactions has been shown to be improved by two common mechanisms, one is that the inclusion of gas bubbles increases the surface area of the reaction.[119] Also, the implementation of gas sparging allowed for the removal of the by-product and aid to shift the dynamic equilibrium towards reaction completion.[119,120] Reactions that required gas sparging were connected to a gas manifold and sparging was commenced after 45 minutes. This was to allow for a build-up of butanol that required to be removed.

2.1.4 Microwave Reactions

Microwave-assisted chemistry has been shown to enhance reaction yields due to the ability of exciting molecular bonds, but not sufficient energy to be able to break bonds.[77–79] Microwaves are able to utilise volumetric heating to heat up an entire reaction mixture unlike conventional heating methods that heat via conduction of a hot plate or oil bath, and this allows for a rapid heat-up time and greater control of internal reaction temperatures[90]

Previous reports have described how microwaves selectively heat some materials more than others and this phenomenon is known as dielectric heating. Microwaves form part of the electromagnetic spectrum between 300 MHz and 300 GHz.[121] Electromagnetic waves can be can be separated into an electric and magnetic field component.[122] The electric field component has been shown to be responsible for dielectric heating and can be separated into two main heating mechanisms. The first heating mechanism can be described by the dipolar polarization experienced by molecules under exposure of microwaves.[123] For a material to be heated by microwaves, it is essential that a dielectric is present which in turn will try and align with an external electric field (Figure 2.5). A dielectric is a material that does not have a permanent magnetic dipole but can be polarized under an electromagnetic wave such that molecules align with an applied field.

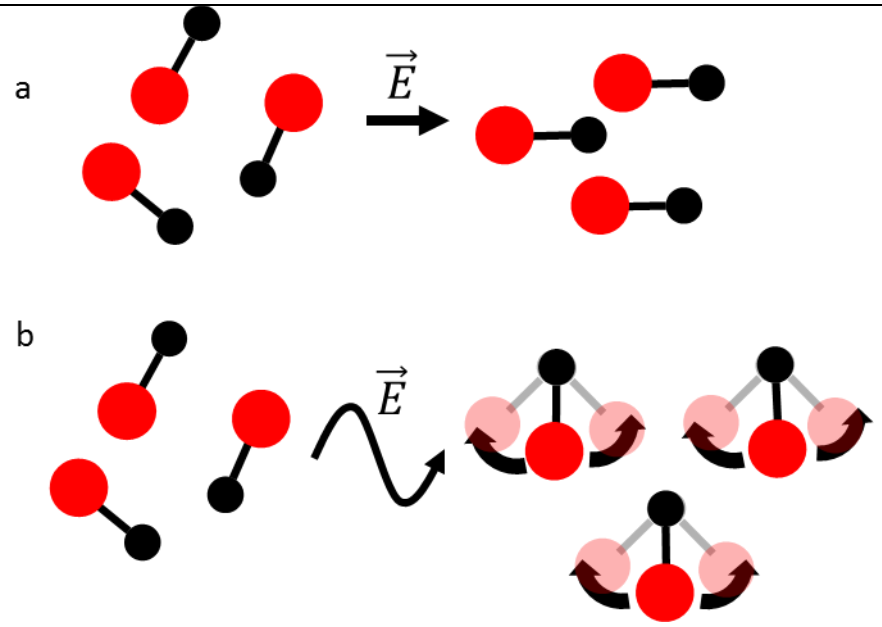


Figure 2.5: (a) Alignment of molecules with dipoles in static external electric field (b) alignment of molecules in an oscillating external magnetic field

However, when an oscillating external electric is applied, as is the case in the irradiation of microwaves, the dielectric will oscillate with the electric field. When the frequency is very small (<300 MHz) the dielectric will oscillate in time with the external field and little heating will occur. Likewise, if the frequency is too high (>300 GHz) the dielectric will not be able to respond quickly enough to the applied field and therefore no heating would occur.[91] When the frequency is between these limits, (in the microwave range), the dipoles rotate, but do not fully align with the electric field and this causes a phase mismatch between the dipoles and the external electric field, resulting in heat loss into the reaction mixture.[124]

This would suggest that the more polar a material, the larger the heating effects experienced due to the exposure of microwave irradiation. But it has been shown that this is not the case and that the dielectric constant can be split into a real and imaginary component (Equation 4).[125]

$$\varepsilon = \varepsilon' - i\varepsilon''$$

Equation 4: Absolute permittivity equation showing relationship between the dielectric constant ε′ and dielectric loss ε′′ components

Despite some materials having the same polarity it has been shown that ε′ only quantifies the ability of a material to store electrical potential energy under the influence of an electric field.[77] ε′′ defines a materials ability to convert the stored energy into heat.[77] A more appropriate parameter to define a materials ability to transfer energy into heat is the loss factor which is defined as described in Equation 5.[126]

$$tan\delta = \frac{\varepsilon''}{\varepsilon'}$$

Equation 5: Relationship between dielectric loss and dielectric constant showing materials ability to transfer energy into heat

This can be demonstrated in Table 2.1, where Lidström *et al*[77] showed a range of solvents with associated dielectric constant and loss tangent values. It was noted that solvents with high dielectric constant values did not scale with high loss tangent values.

Table 2.1: Dielectric constants and loss tangents for a range of different solvents[77]

Solvent	Dielectric Constant (ε_s)	Loss tangent (tan δ)
Acetic acid	6.1	0.091
Ethyl acetate	6.2	0.174
THF	7.6	0.059
Methylene chloride	9.1	0.047
Acetone	20.6	0.042
Ethanol	24.6	0.054
Methanol	32.7	0.941
Acetonitrile	36	0.659
Dimethylformamide	36.7	0.062
DMSO	47	0.161
Formic acid	58	0.722
Water	80.4	0.123

Another thermal heating effect from microwaves arises through the thermal conduction of selectively heated materials. An example of this is through heating of pure water and tap water. Due to the presence of ions in tap water solution, these ions are selectively heated by microwaves and cause a reaction mixture to heat up due to an increase in high kinetic collisions.[77] This is an effect that could cause more efficient heating of transesterification experiments from the ionisation of initial alcohol from the reaction.

2.1.5 Free-radical polymerisation reactions

To coat sections of catheters with identified hit polymers, a scale-up reaction was performed to provide enough polymer to coat small catheter sections. This was done by using a 1:1 (v/v %) ratio of monomer: toluene with a 1 % 2,2'-azobis(2-

methylpropionitrile) (AIBN) thermal initiator. The reaction mechanism for AIBN can be shown in Figure 2.6.

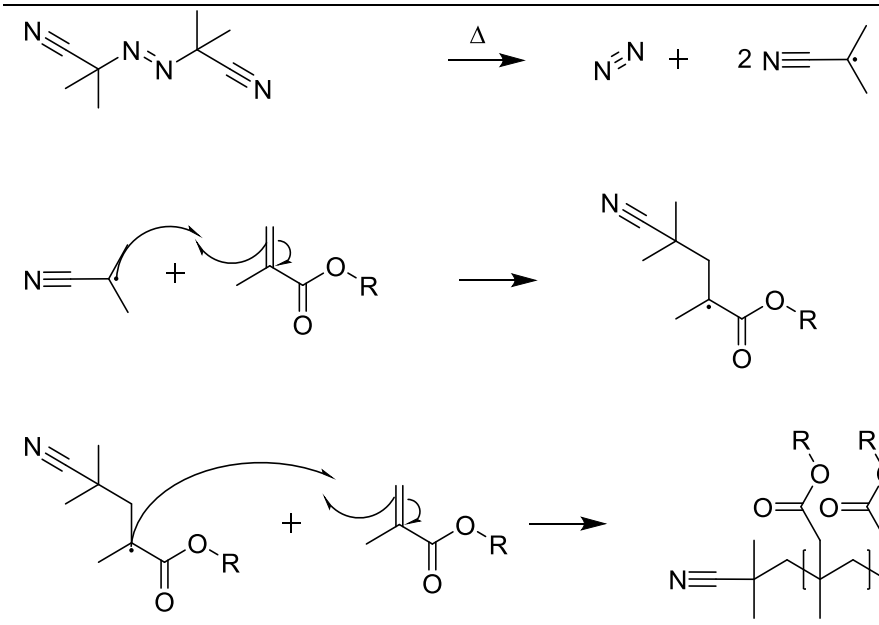


Figure 2.6: Free-radical polymerisation mechanism showing the use of AIBN to polymerise functionalised methacrylate monomers

Free-radical polymerisations are then terminated by two radical species reacting together to prevent the radical from propagating further through the chain.

2.2 NMR

Nuclear magnetic resonance spectroscopy is a commonly used technique for the analysis of the structure of organic molecules. A magnetic isotope is required to analyse a sample using NMR such as ^{1}H, ^{13}C, and ^{19}F.[127] A magnetic field applied such that majority of the magnetic isotopes are aligned in the 'alpha' orientation (aligned with magnetic field), with few isotopes aligned in the 'beta' positon (aligned against the magnetic field). A nuclear magnetic resonance spectrometer then pumps the isotopes into the higher energy beta position using electromagnetic radiation. When this radiation is removed, the isotopes relax back into their ground energy 'alpha' position. This fluctuation of magnetic field associated with the relaxation process can be detected and converted into peaks seen on NMR spectra.[128] Throughout this project, 1H NMR was used to calculate conversion levels for transesterification experiments and 13C NMR was used in conjunction with 1H NMR to characterise purified monomer. The main use of NMR was to determine the conversion of alcohol to the desired product. This was determined by comparing the shift in chemical environment experienced by one or more protons from the alcohol to the product. Separate NMR for individual reactants was performed to observe which peaks represented which reagent, and then the conversion was calculated as shown below in Figure 2.7.

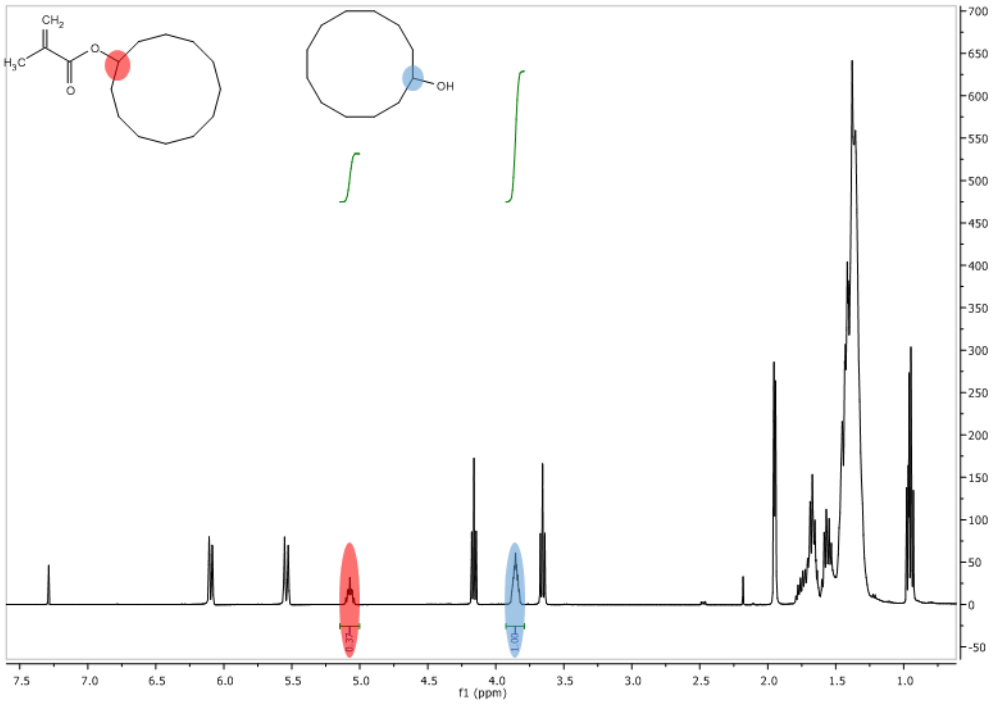


Figure 2.7: Figure showing calculation of conversion of product from alcohol by comparing shift of the same proton in different chemical environment

This process was used for a range of different experiments with different alcohols to assess how successful the synthesis experiment was, with a higher conversion in a shorter time being considered more successful.

2.3 Polymer microarray Printing

2.3.1 Materials

The commercially available monomers used throughout this project were purchased from Sigma Aldrich and used as received. All solvents used were acquired from fisher-scientific and used as received. Figure 2.8 shows the range of monomers used in conjunction with materials that were synthesised using the transesterification method.

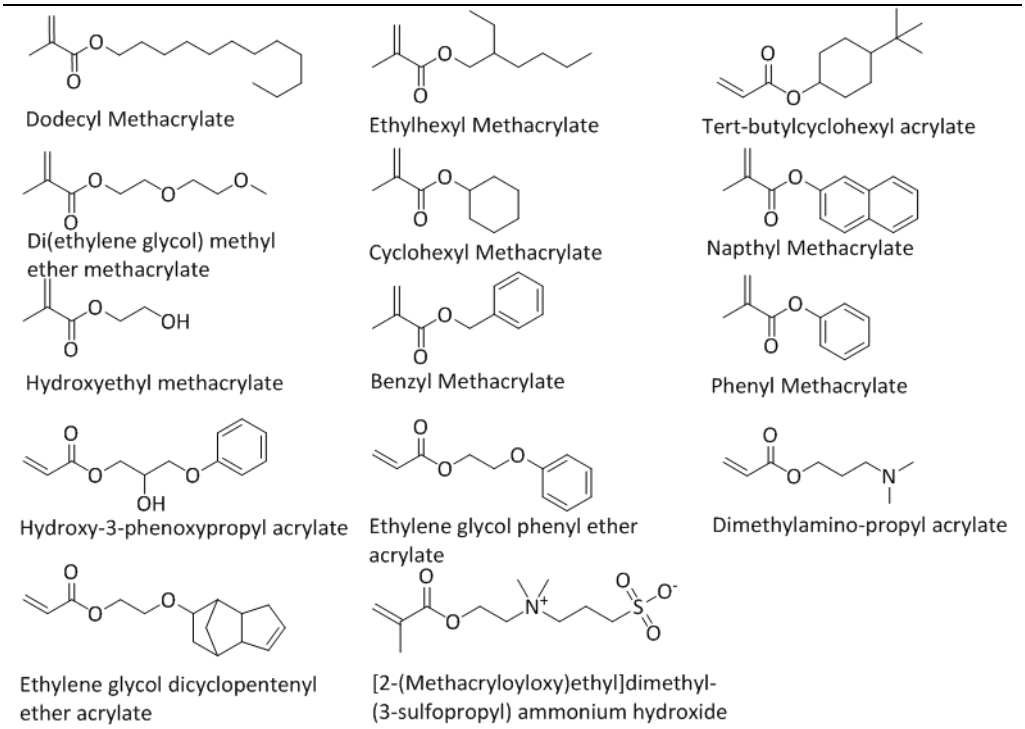


Figure 2.8: Commercial monomers used throughout this project

2.3.2 Printing substrate preparation

To successfully print a polymer microarray, a substrate that prevents spreading of monomer spots is essential to be able to distinguish individual polymers. pHEMA was chosen as a substrate which not only prevents spreading, but is also antifouling.[129] A 6 % w/v poly(2-hydroxyethyl methacrylate) (pHEMA) in 95%/5% v/v ethanol/water solution was used to coat functionalised glass slides. This was done using an

automated dip coater (Holmarc, India) to maintain control of insertion and extraction speeds. A relationship between retraction speed and coating thickness has been previously reported, and by using an automated dip-coater allows for greater control of coating thickness over a manual-dip method.[130]

2.3.3 Microarray Printing

Production of polymer microarrays has been previously performed using both contact[49,131] and non-contact[63,132,133] printing methodologies. Non-contact printing can be categorized into two main methodologies, piezoelectric inkjet printing and thermal inkjet printing.[63,134] Piezoelectric inkjet printing utilises a piezoelectric diaphragm which contracts and expands depending on an applied potential difference, which causes a pressure change to eject a droplet onto the substrate.[134,135] However contact printing, which was used throughout this project, utilised metal pins to transfer material from a source plate onto a printing substrate (Figure 2.9). An advantage of using quilled metal pins is the ability to store material within the pin to print multiple microarray slides in a single iteration, however a disadvantage is that these quills can become blocked if a material is too viscous.

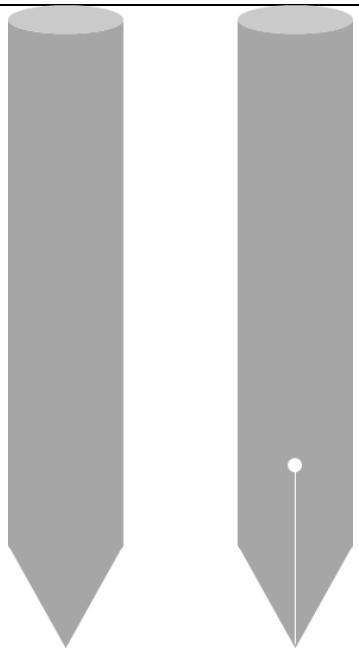


Figure 2.9: Schematic of pins typically used during contact microarray printing showing a solid pin and a quilled pin with reservoir for printing multiple microarrays in a single application

A typical printing process would wash and dry the pins before collecting monomer solution from the source plate, where the monomer mixture is uptaken through capillary action into quilled pins. The pins were then blotted onto glass slides to prevent spreading of excess monomer solution on the pHEMA substrate. The pins then transferred the monomer solution onto the microarray slides, where they were printed in triplicate on each slide before progressing to the next slide. This then allowed for 3 technical repeats of each material on a single slide, and then biological repeats could be obtaining by using multiple slides in an experiment. At the end of each iteration, the pins were washed and dried whilst a UV lamp was turned on to photo polymerise the monomer spots to fix them into place. At the end of the run, the UV lamp was turned on for an additional 10 minutes whilst under argon to ensure all monomers had been photo-polymerised. The slides were then removed and placed under high vacuum at ambient temperatures to remove any

excess solvent or unpolymerised material for 7 days. This process can be shown in Figure 2.10.

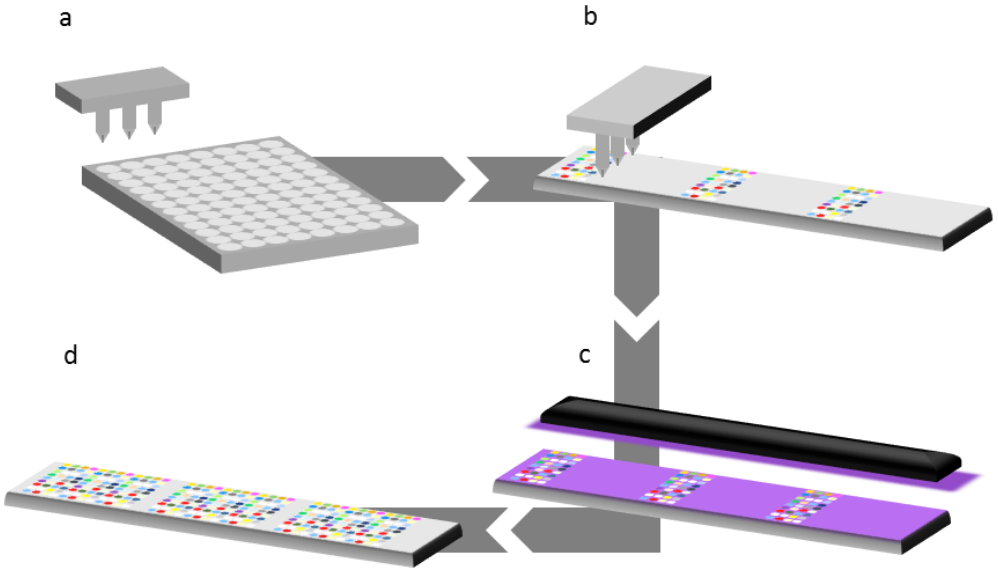


Figure 2.10: Schematic showing process of printing polymer microarray from (a) uptake of monomer solution from source plate using 946MP6B Arrayit quilled metal pins (b) transfer of monomer solution to pHEMA substrate surface where each spot was printed in triplicate (c) photopolymerisation of monomer solution under UV light (d) completed polymer microarray after 7 day drying period under high vacuum

After the drying process, the microarray was characterised using techniques including bright field microscopy and ToF-SIMS. Slides were then incubated with bacterial strains including *Pseudomonas aeruginosa* and *Proteus Mirabilis* to observe differences between bacterial adhesion on different polymeric surfaces.

2.4 ToF-SIMS

Time of flight secondary ion mass spectrometry (ToF-SIMS) is a surface sensitive mass spectrometry technique used to obtain detailed molecular information from the uppermost molecular layers of a sample.[136] In the case of polymer microarrays this enabled an automated surface chemistry analysis of a large polymer library. A schematic showing how a ToF-SIMS instrument functions is shown in Figure 2.11.

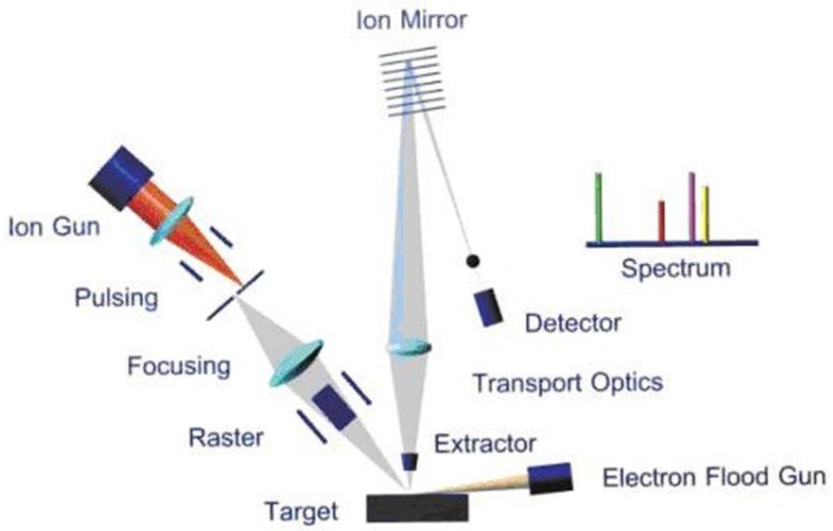


Figure 2.11: Schematic showing operation of ToF-SIMS instrument from primary ion dosing to production of mass spectrum through flight path.[137]

A primary ion beam (Bi_3^+) was used to bombard the sample with pulsed high energy, usually between 10 and 40 keV. Kinetic energy from the primary ion beam is transferred to the sample causing bond breakage and fragmentation of the surface chemistry leading to the emission of uncharged and charged fragment species from the sample surface (Figure 2.12). Only a small fraction of the ejected fragments are ionised (<1%). These ions can be mass analysed by being extracted into an analyser by a high voltage potential and mass is

determined by the time taken to travel from the sample to the detector.[138] Both negative and positive ions are present from the bombardment of primary ions, the instrument collects both negative and positive mode to obtain all possible data from samples. To account for the range of different kinetic energy on emission, an ion mirror as depicted in Figure 2.11 is used to correct them such that ions with higher energies travel further, and hence still arrive at the detector with ions of the same mass.

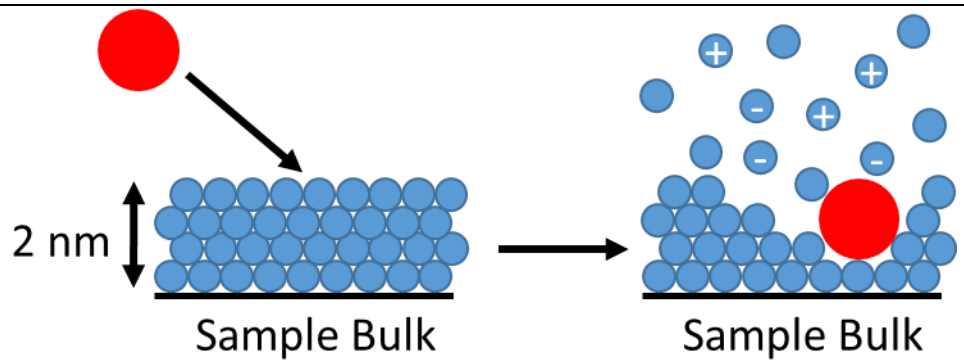


Figure 2.12: Illustration of primary ion beam bombarding sample surface. Ionised and non-ionised fragments are ejected from sample surface

As SIMS is inherently a destructive analytical technique, the primary ion dose is kept to less than 10^{13} ions/cm^2 such that the likelihood of primary ions bombarding sample already impacted and therefore damaged is minimal.[139,140] This involved using a pulsed primary ion source such that the sample is not continuously bombarded by the primary ion beam. To prevent the build-up of charge accumulating on the sample surface, an electron flood gun is used to neutralise the surface charge, as this can otherwise interfere with the dispersion of ions from the sample surface.

In addition to obtaining mass spectra, ToF-SIMS allows for the formation of chemical maps to assess chemical distribution of molecules of interest. Each individual pixel scanned in a ToF-SIMS image contains a full mass-spectra, hence the large visualisation of an entire data set can be used as a powerful analytical tool. However, ToF-SIMS has a few limitations in such that it is a vacuum-based technique, so any volatile materials cannot be analysed. Also, SIMS is a destructive technique, so samples used during ToF-SIMS analysis cannot be used for further characterisation or biological studies.

2.5 Bacterial Strains

P. aeruginosa and *P. mirabilis* strains used in this project are listed in Table 2.2.

Table 2.2: Description of bacterial strains used throughout this project

Bacterial Strain	Description	Origin
P. aeruginosa PAO1-N	Nottingham strain with plasmid pME6032ΔlacIQ::mCherry Tc resistant for constitutive expression of mCherry fluorescent tag	Hollway BW (1955) J Gen Microbiol 13:572-581
P. mirabilis	Nottingham strain with plasmid miniTn7-dsRedexpress	Dr. Jean Dubern's laboratory collection

Bacterial strains were transformed using plasmids described in Table 2.2 such that the fluorescence plasmids are amplified and expressed by the bacteria. This then allowed for the measurement of fluorescence intensity as a measure of bacterial adhesion to polymer surfaces.

2.6 Fluorescence imaging

To quantify bacterial adhesion to the surface of polymeric materials, bacteria were tagged with fluorescence genes such that by using fluorescence microscopy techniques, a light intensity can be measured and associated to bacterial adhesion.

2.6.1 Fluorescence microscopy

The measured fluorescence intensity of polymer microarrays was obtained using a Genepix 4000L, which enabled high throughput analysis using a laser scanning technique to measure the entire microarray in one iterative process. Fluorescence microscopy functions by exciting electrons into an excited energy state and measuring the emission frequency as the excited electrons return to the ground energy state. Electrons undergo internal conversion and/or vibrational relaxation before emitting fluorescence, which leads to differing peak excitation and emission frequencies. This process can be demonstrated in Figure 2.13.

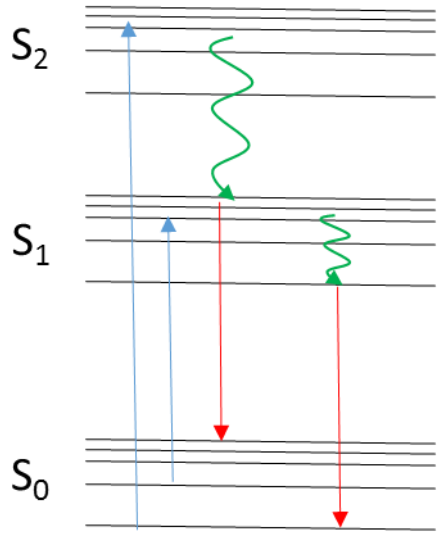


Figure 2.13: Excitation of electrons into higher energy states (blue) which then undergo vibrational or internal conversion

emission (green) before emitted fluorescence to return to ground energy state (red)

2.6.2 Confocal microscopy

When it is required to obtain fluorescence measurements from a 3D object, a confocal microscope was used to obtain bacterial fluorescence data, which allowed for multiple 2D images to be acquired over a specified z-range. A confocal microscope functions fundamentally in the same way as other fluorescence microscopy techniques but uses a dichroic mirror and confocal pin holes to only detect fluorescence from an image within the focal plane of an objective lens (Figure 2.14).

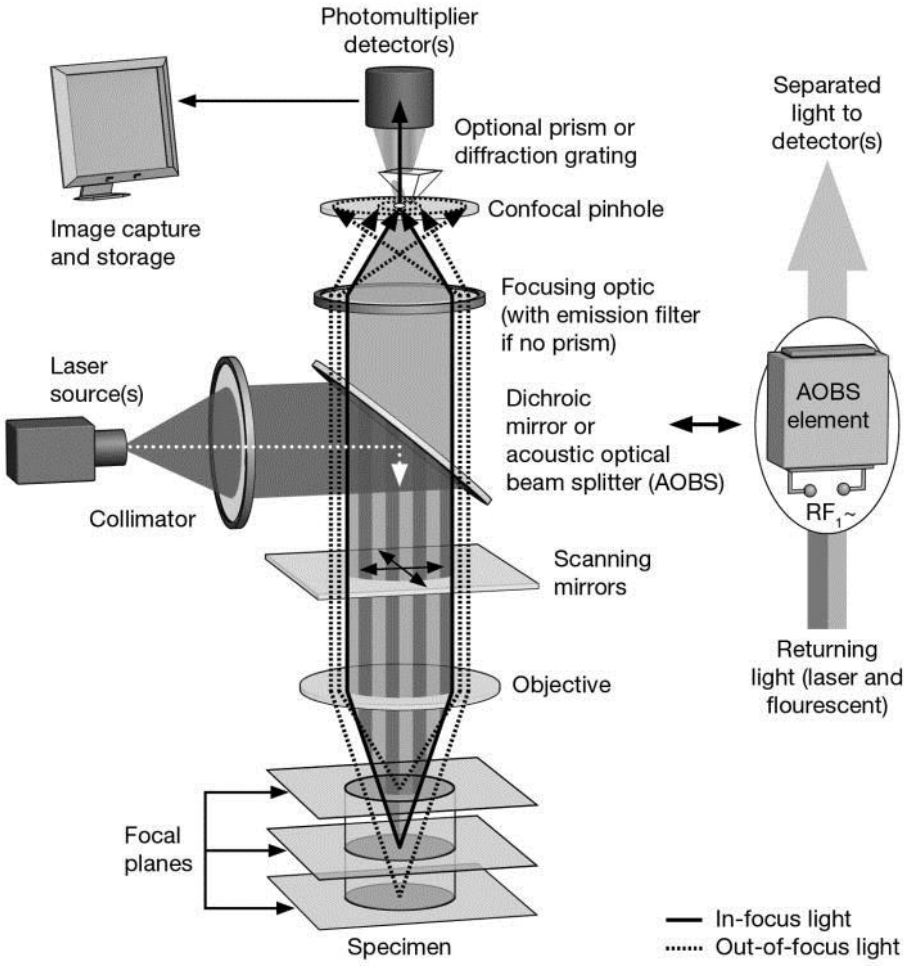


Figure 2.14: Schematic of confocal microscope showing how different planes are brought into focus to allow for fluorescence imaging over a 3D object.[141]

By adjusting the z-position of the objective lens or sample stage, it is possible to image different parts of the sample surface as each section comes into focus and passes fluorescence light through the confocal pinholes into the detector.

2.7 Finite difference time domain simulations

To prevent the need for an expensive trial and error system, FDTD simulations were performed in Vector Fields Concerto® to observe the propagation of microwaves through a range of different geometries. The optimised geometries were then used to produce a microwave reactor capable of synthesising novel methacrylate monomers. FDTD simulations were first proposed by Yee in 1966 by replacing differentials in Maxwell's equations with finite differences.[103] FDTD simulations start by observing the Maxwell's time dependent equations which are shown in Equation 6.

$$\nabla \times \vec{H} = \frac{\partial \vec{D}}{\partial t} + \vec{J}$$

$$\nabla \times \vec{E} = -\frac{\partial \vec{B}}{\partial t} - \vec{M}$$

$$\nabla . \overrightarrow{D} = \rho_e$$

$$\nabla . \overrightarrow{B} = \rho_m$$

Equation 6: Maxwell's time dependent equations where E is the electric field strength (Vm^{-1}), D is the electric displacement (Cm^{-2}), H is the magnetic field strength (Am^{-1}), B is the magnetic flux density (Wbm^{-2}), J is the electric current density (Am^{-2}), M is the magnetic current density (Vm^{-2}), ρ_e is the electric charge density (Cm^{-3}) and ρ_m is the magnetic charge density (Wbm^{-3})

For the development of FDTD simulations, only the first two Maxwell equations are required. By using alternative definitions for the electric displacement (D = εE) and magnetic flux density (B = μH), these equations can be rewritten to only depend on electromagnetic fields E and H as shown in Equation 7.

$$\nabla \times \vec{H} = \varepsilon \frac{\partial \vec{E}}{\partial t} + \sigma^e \vec{E} + \vec{J_\iota}$$

$$\nabla \times \vec{E} = -\mu \frac{\partial \vec{H}}{\partial t} - \sigma^m \vec{H} - \overrightarrow{M_\iota}$$

Equation 7: Alternative Maxwell's curl equations including definitions for the summed electric current density and summed magnetic current density

Both the electrical and magnetic current densities (J + M) are the sum of the conduction and impressed densities ($J = J_c + J_i$ and $M = M_c + M_i$ where $J_c = \sigma^e E$ and $M_c = \sigma^m E$). These equations contain constitutive relationships that allow for the input of properties for any linear isotropic material. These vector equations can then be broken down into 6 separate scalar equations associated to each direction (E_x, E_y, E_z, H_x, H_y and H_z) (Equation 8).[142]

$$\frac{\partial E_x}{\partial t} = \frac{1}{\varepsilon_x}\left(\frac{\partial H_z}{\partial y} - \frac{\partial H_y}{\partial z} - \sigma_x^e E_x - J_{ix}\right)$$
$$\frac{\partial E_y}{\partial t} = \frac{1}{\varepsilon_y}\left(\frac{\partial H_x}{\partial z} - \frac{\partial H_z}{\partial x} - \sigma_y^e E_y - J_{iy}\right)$$
$$\frac{\partial E_z}{\partial t} = \frac{1}{\varepsilon_z}\left(\frac{\partial H_y}{\partial x} - \frac{\partial H_x}{\partial y} - \sigma_z^e E_z - J_{iz}\right)$$
$$\frac{\partial H_x}{\partial t} = \frac{1}{\mu_x}\left(\frac{\partial E_y}{\partial z} - \frac{\partial E_z}{\partial y} - \sigma_x^m H_x - M_{ix}\right)$$
$$\frac{\partial H_y}{\partial t} = \frac{1}{\mu_y}\left(\frac{\partial E_z}{\partial x} - \frac{\partial E_x}{\partial z} - \sigma_y^m H_y - M_{iy}\right)$$
$$\frac{\partial H_z}{\partial t} = \frac{1}{\varepsilon_z}\left(\frac{\partial E_x}{\partial y} - \frac{\partial E_y}{\partial x} - \sigma_z^m H_z - M_{iz}\right)$$

Equation 8: Scalar Maxwell equations with constitutive parameters used for defining electric and magnetic fields used in FDTD simulations

These differential equations are then approximated by using finite differences to approximate the differential equations expressed in Equation 8. This can then be used to simulate the electrical and magnetic fields over a structure containing different isotropic materials over a defined time.

FDTD simulations were used within this project to design a microwave reactor capable of coupling of microwaves at a frequency of 2.45 GHz to heat a reaction mixture which utilised a transesterification process to develop novel methacrylate monomers.

2.8 Micro-well fabrication and experimentation

2.8.1 Materials

For the manufacture of the prototype, aluminium was used for the reactor and antenna, as it offered a cheap material that allowed the reactor to act as a cavity due to high reflectance properties of metals. For the dielectric and protective sheath components, Ertacetal® C was supplied by theplasticshop.co.uk and used as received.

2.8.2 Microwave Safety

Microwaves are a large health concern if exposed to a sufficiently high dosage, and hence a microwave dosage limit for microwave ovens has been determined as 5 mW/cm^2 at a range of 5 cm from the radiation source.[143] Human tissue has been shown to be particularly receptive to microwave irradiation, in the form of rapid heating.[144] It was then of critical importance that the microwave dosage limit was not exceeded by any reactor that is designed and built during this project. This was achieved primarily by using FDTD simulations as mentioned previously to simulate and measure microwave leakage, however once the reactor was built a HAZOP meeting and subsequent risk assessment were conducted to ensure a safe operation of the reactor.

2.8.3 Impedance matching

The inclusion of a Microlab/FXR SF-31N sliding tuner enabled power to be coupled between the microwave source and the material. The sliding tuner, which can be shown in Figure 2.15, operates by the movement of the reflective component, often referred to as a slug, to change the impedance of the tuner.

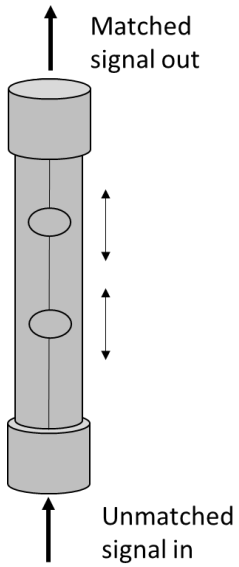


Figure 2.15: Schematic demonstrating how a slug-tuner works, by manual movement of the two slugs up and down the length of the tuner, impedance of the tuner changes and allows for matching between power source and material load

When the impedance of the tuner and the load material are matched, the coupling of microwaves to the material are at a maximum, allowing for efficient heating of the reaction mixture.

3 Synthesis of Novel Methacrylate Monomers Using Microwaves and Nitrogen Sparging

3.1 Introduction

The overall concept for this section of the study was to develop a high throughput synthesis route to novel methacrylate monomers, such that novel methacrylate monomer libraries could be efficiently synthesised to keep up with the demands from high throughput discovery programmes (HTDP). The strategy adopted involved the use of a simple one-step synthesis protocol that could be broadly applied to significant numbers of monomers to standardise the synthetic process. HTDP require the development of ready access to large diverse material libraries to increase the likelihood of discovering a hit material with desirable properties. Thus, it is typical that commercially available materials are frequently utilised to fill this requirement for a large material library at the outset of a study. However, only approximately 300 commercially available (meth)acrylates and acrylamides are currently available, which inherently restricts the materials that can be assessed within a materials library.

Transesterification is a chemical transformation that has been commonly been used for the production of biodiesel,[145,146] but have also been utilised for a one-step synthesis process to develop a range of ester materials including; different classes of lipids, higher (meth)acrylates and the cyclisation of oligocholates.[113,147–149] However, whilst this technique shows a high degree of freedom to create a range of different materials, a common limitation of transesterification experiments is that it

is difficult to obtain high conversions due to the mass transfer limit defined by Le Chatelier's principle.[115] Gas sparging has shown to improve mass transfer characteristics of reactions, enabling in the distillation of low-boiling materials that can then aid in reaction progression.[150] Hence, gas sparging has been used in conjunction with the transesterification process within this chapter to synthesis a novel monomer library.

A second important consideration for this section of the study is to develop an apparatus which can successfully synthesise materials in a high throughput process at the 10 – 30 ml scale. Conventional heating is not ideal for heating multiple reaction vessels simultaneously at these types of volumes. This is because typically in conventional methods of library synthesis, heat is applied to a range of different materials using an oven or by the heating of a large metal block.[70,151–153] These strategies can lead to poor heating distribution and so differing reaction temperatures/profiles being experienced by different reactions within the apparatus. These variations can be related to; (a) different thermal properties for each reaction mixture, (b) a mixtures position within the apparatus and/or (c) with time and hence can lead to differing and unpredicted reaction outcomes. Therefore, as well as confirming that the transesterification mechanism represents a viable option by which to synthesis a range of target monomers structures, microwave heating was used to volumetrically heat these transesterification reactions and the results compared to conventionally heated reactions which transfer heat via conduction/convection. Microwave heating has gained a large amount of interest in recent decades for organic/polymer synthesis due to the potential to achieve volumetric heating

(i.e. heat transfer directly to individual molecular species within the reaction mixture, and hence gives a much greater control over reaction temperature compared to conventional heating.[81,90,117] This chapter discusses the method development of a transesterification process to develop a range of novel methacrylate monomers and also how microwave heating, achieved by the application of the apparatus design discussed in Chapter 5, compares to conventional heating methods for the development purposes of a microwave reactor capable of synthesising novel methacrylate monomers.

3.1.1 Aims and Objectives

The aim of this chapter was to develop a one-step synthesis protocol that could be applied to develop a diverse monomer library for HTDP. The viability of applying this protocol to microwave irradiation was also examined to provide the basis of microwave reactor design which is later described in Chapter 5. This aim was achieved by completing the following objectives:

1. Obtaining a suitable fundamental monomer for transesterification experiments with an optimised starting ratio.
2. Optimising the synthesis protocol to obtain high conversions by overcoming mass transfer effects using nitrogen sparging.
3. Utilising the optimised method to develop a monomer library for use in subsequent downstream high throughput experimentation.
4. Comparing conventional and microwave heating methods to check feasibility of developing a high throughput synthesis reactor utilising by microwave energy.

3.2 Experimental methods

3.2.1 Conventional heating

Transesterification experiments were performed to synthesise novel methacrylate monomers using a condensation glassware set-up as shown in (Figure 3.1).

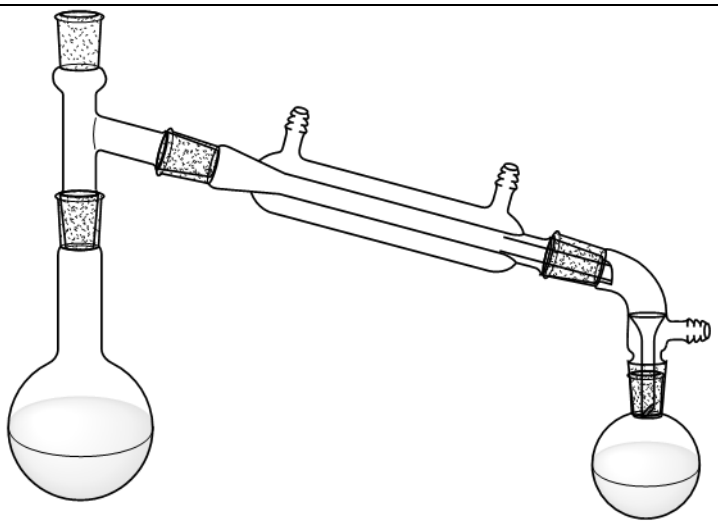


Figure 3.1:Conventional heating set-up showing condensation equipment with water used as a coolant. Stopper is placed in top of distillation head and thermocouple was used to monitor internal temperature. Stirring was applied at 250 rpm to ensure a homogeneous mix was obtained.

Reactions were typically prepared in a molar ratio of 7:5 of monomer:alcohol with 1 % molar ratio titanium butoxide (TNBT) catalyst. Reaction mixtures were heated to either 100/160 ˚C depending on if the monomer used was either MMA/Butyl methacrylate (BMA) respectively. Temperatures were measured using a thermocouple such that the internal reaction mixture temperature was measured and not that of the hot oil. Reaction equations for the transesterification process utilised during this project can be shown in Figure 3.2. A typical conventionally heated reaction contained 14.0 g of BMA (98.5 mmol), 12.9 g cyclododecanol (70.0 mmol) and 0.380 g of titanium butoxide catalyst (1.11 mmol).

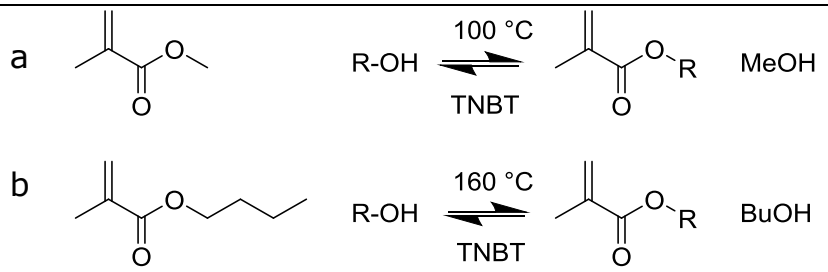


Figure 3.2: Schematic showing transesterification reaction conditions for using (a) methyl methacrylate and (b) butyl methacrylate

All reactions were performed in water-cooled distillation glassware to remove the by-product (methanol/butanol) from the reaction. Reactions were performed for a range of times from 2.5 to 48 hours. During the reactions at set times aliquots were taken and immediately quenched in a freezer to observe reaction kinetics using NMR.

3.2.2 Microwave heating

A series of transesterification experiments were performed using a Miniflow 200SS microwave reactor operating at 2.45 GHz which utilises a solid-state power generator. In a typical reaction, a sample reaction mixture was placed inside the microwave cavity and a metal choke was fitted to prevent microwave leakage to the surroundings. Prior to applying large powers to the test medium, the reaction integrity of the apparatus construction for each experiment was tested with an ETS-Lindgren EMF measurement detector. Reduced microwave power inputs (10 W) were applied to ensure that there was no any microwave leakage. Furthermore, whilst under low microwave powers, the input microwave power was also coupled to the load material by adjusting the cavity length and shape to reduce the reflected power to a minimum and hence improve coupling between the source and the load material. This was achieved by adjusting a sliding short that reduced the

length of the cavity and a fine stub tuner that pushed metal rods in and out of the cavity, where changing the cavity geometry is a common technique for matching the input power to the load material.[97,154] This procedure ensured that a single mode, standing wave was created within the cavity, so maximising the potential to deliver even energy transfer throughout the sample and so give the best opportunity to achieve volumetric heating of the bulk. After this procedure was complete, larger power inputs (>100 W) could be safely used. Reaction mixtures were heated to 100/160 °C depending on whether either MMA or BMA was the monomer reagent. The temperatures of the bulk mixtures were directly measured and recorded using a fibre-optic cable which was connected the Miniflow 200SS power source. As in the conventional case, aliquots were taken at fixed time periods and quenched to observe reaction kinetics. A diagram of an example of the experimental apparatus used is shown in Figure 3.3. A typical microwave heated reaction contained 14 g of BMA (98 mmol), 12.90 g cyclododecanol (70 mmol) and 0.38 g of titanium butoxide catalyst (1 mmol).

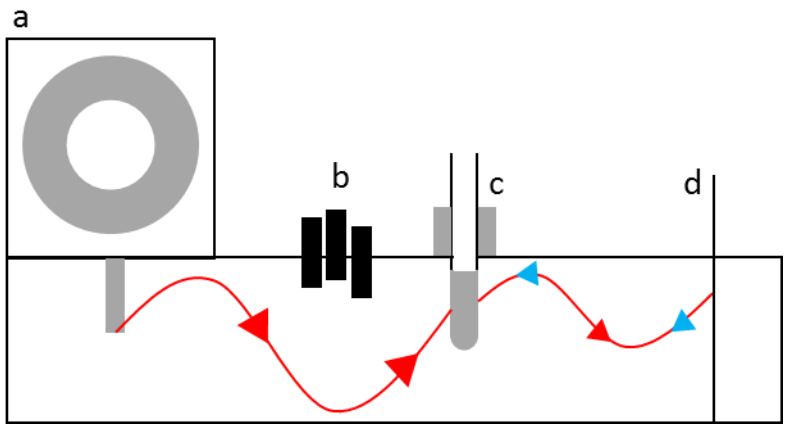


Figure 3.3: Schematic showing set-up of Miniflow 200SS with waveguide for transesterification experiments showing (a) Miniflow 200SS solid state generator (b) fine stub tuner (c) metal choke to prevent microwave leakage and (d) course sliding tuner

3.2.3 Nitrogen sparging

Nitrogen gas sparging was used with both microwave and conventional heating methods to observe the effect of flushing inert gas through the reaction mixture on the level of mass transfer achieved within the reaction system. The reaction set-up can be shown in Figure 3.4.

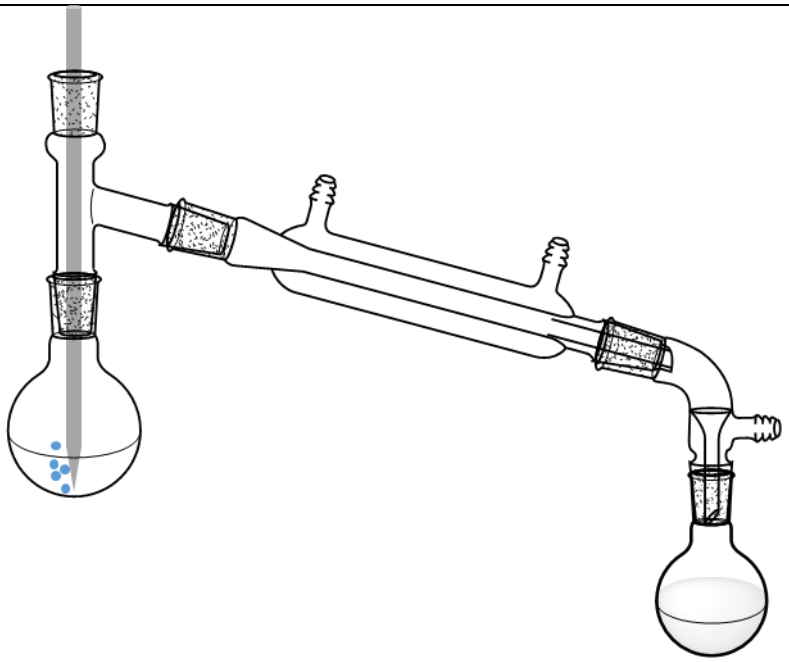


Figure 3.4: Reaction set-up of reaction utilising sparging technique. N_2 gas was passed through a 2 ml pipette, which was put through a stopper at the top of the distillation head. Thermocouple/fibre optic cable was also placed through the top of the distillation head for conventional/microwave heating respectively. Stirring was performed at 250 rpm to ensure a homogeneous mix was obtained.

The nitrogen gas was introduced *via* 2 ml glass pipette during the reaction, this method was chosen because it allowed the same 2ml glass pipette to be used in both the microwave and conventional heating method reaction. Sparging of the reaction mixture was started 15 minutes into the reaction. This was to prevent any loss of reagent alcohols, which were a solid (powdered) physical form, from the reaction medium which would alter the reaction stoichiometry. Typically, application of too stringent sparging too early was found to result in these

alcohols adhering to the sides of the reaction vessel above the reaction bulk.

3.2.4 Nuclear magnetic resonance imaging

To analyse progress of chemical reactions, a NMR 400 MHz Bruker machine was used. Samples were prepared using deuterated chloroform at an approximate ratio of 2 mg/ml for ^{1}H spectra and approximately 10 mg/ml for ^{13}C spectra. Spectra were then analysed using MestReNova software as described in Chapter 2.2.

3.3 Results

3.3.1 Choice of fundamental reagent monomer

As a starting point for performing these transesterification experiments, methyl methacrylate (MMA) was initially chosen as the starting monomer because this has successfully been used to manufacture functional methacrylates on an industrial basis.[149] Introducing different functional alcohols (i.e. containing the functional group of interest), novel methacrylate monomers can be synthesised at the multi-tonne scale. As the boiling point of MMA is 100 °C, the reaction temperature was kept at this temperature to prevent the excessive loss of the starting material by evaporation. Furthermore, an excess of methyl methacrylate was used such that the starting ratio of monomer: alcohol was a 7:5 molar ratio. This rationale was adopted for two reasons; (a) it would allow for some evaporative losses on MMA and (b) to shift the equilibrium of the reaction towards completion as defined by Le Chatelier's principle as described in Chapter 2.1.2.

Following this strategy, a series of conventionally heated transesterification experiments using cyclododecanol as the functional alcohol were performed to test the viability of using MMA as the fundamental monomer for the synthesis of a large monomer library. Cyclododecanol was chosen as the test alcohol, as it had a high boiling temperature which allowed for high reaction temperatures without distilling the reagent alcohol. Cyclododecyl methacrylate was also identified as a potential hit material for reducing the attachment of bacteria to surfaces, which is described in more detail in Chapter 4. Figure 3.5 shows the reaction conversion from MMA to cyclododecyl methacrylate over 48 hours.

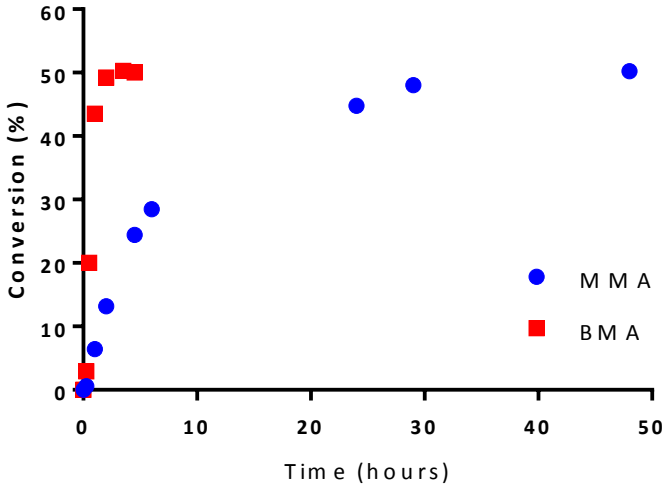


Figure 3.5:Reaction kinetics showing difference between using BMA at 160 °C and MMA at 100 °C, where both methods were limited to 50 % conversion by mass transfer effects.

Conversion was shown to reach a ceiling of 50 % after 48 hours of heating with MMA. This suggested that the reaction was mass transfer limited, i.e. the by-product condensate (methanol in the case of MMA) which needs to be removed to allow higher conversions to be reached as defined by Le Chatelier's principle was remaining in the medium. Due to this an alternative reaction solution was investigated in which BMA instead of MMA, which allowed for an increase of reaction temperature from 100 °C to 160 °C as a result in the change in boiling points of the respective monomers. It was proposed that this increase in temperature may improve the mass transfer within the system as it means that the medium is well above the boiling point of condensate in this system (in case of BMA butanol with a boiling point of 117 °C). This resulted in achieving 50 % conversion after 2 hours, a 24-fold increase in reaction rate compared to using MMA as the fundamental monomer as shown in Figure 3.5. However again conversion ceiling of 50% was observed. Another issue that was encountered during experiments

performed with MMA was the onset of polymerisation. Despite the addition of 4-methoxyphenol (MEHQ) as a radical inhibitor, polymerisation was often observed during experiments involving MMA. The presence of polymer in the final reaction mixture was observed by NMR analysis (Figure 3.6).

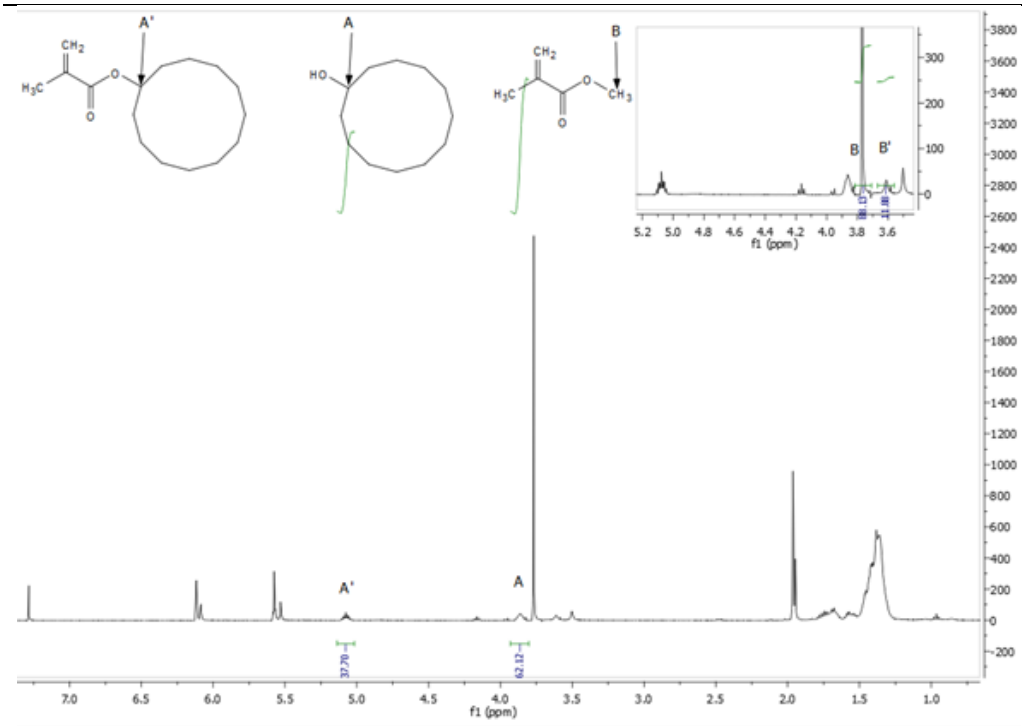


Figure 3.6: Transesterification experiment using MMA at 100 ˚C, showing a 12 % polymerisation of MMA by observing the peak broadening of the methyl group adjacent to the ester group (assignment B). Conversion of the experiment was shown to be 38 % comparing change in chemical environment of protons adjacent to the alcohol (A) to the product (A')

Meanwhile, no polymerisation was observed in the BMA experiments. This observation was attributed to either the lower reactivity of the BMA monomer because of steric effects introduced by the bulkier functional group and/or the much-reduced reaction time. For these reasons, BMA was chosen as the fundamental monomer for further transesterification experiments, this was because; (a) it allowed for comparable conversions in a much-reduced reaction time, (b) resulted in

no/minimal polymerisatioeing observed and (c) is low cost and readily available commercially.

3.3.2 Effect of apparatus/glassware design on conversion

When using the Miniflow 200SS for microwave heated experiments, it was a requirement to use a long-neck reaction vessel be used i.e. there was a significant length of glass between the top of the reactor and the distillation head (see Figure 3.7a). This was due to a metal choke which was placed on the condenser exit of the cavity to prevent the leaking of microwaves into the laboratory.

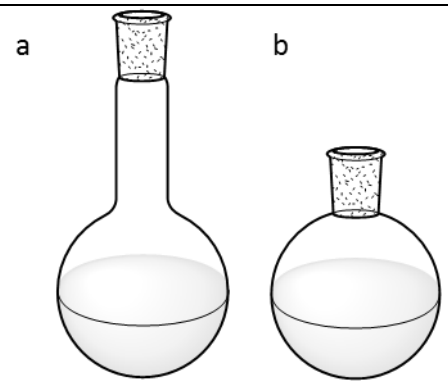


Figure 3.7: Different 50-ml reaction vessels used throughout this project where (a) had to be used for microwave experiments due to safety restrictions (neck length of 145 mm) and (b) reaction vessel used for conventional heating experiments (neck length of 43 mm)

Therefore, the investigation of the use of the application of a long and short neck design using only conventional heating methods was conducted (as a short neck vessel was not possible with microwave heating due to the large choke). The data from these experiments, (see Figure 3.8), demonstrated that by using a longer necked vessel, the mass-transfer properties of the system are altered in the later stages of the

reaction such that lower conversions were obtains from the long neck design.

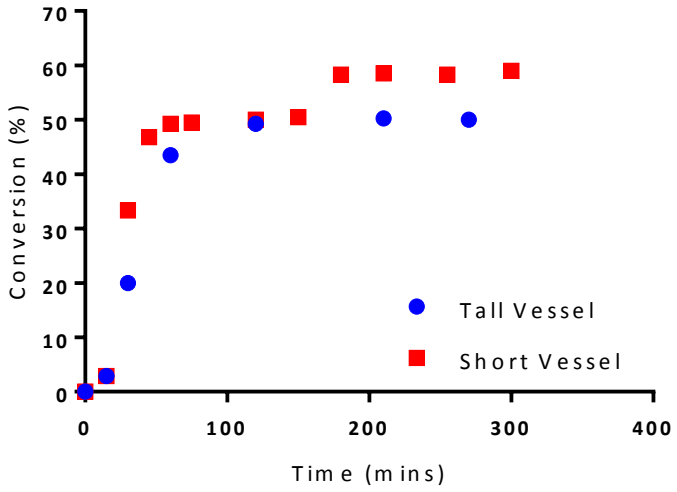


Figure 3.8: Difference in conversion by changing from short-necked reaction vessel to a long-necked reaction vessel

As shown by Figure 3.8, using a short-necked reaction vessel allowed for higher conversions to be obtained. This is due to the reduced headspace that any condensate must travel for the shorter reaction vessel. Hence, for fair comparison, microwave experiments were also conducted and compared to conventional heating experiments with a long-necked reaction vessel. However, this data showed the advantages of using a shorter vessel, and the research in Chapter 5 discusses the design of a microwave reactor vessel with a smaller headspace to improve mass-transfer properties.

3.3.3 Comparison of conventional and microwave heating methods

Having confirmed that the same glassware must be used for fair comparison of methods, comparisons between microwave and

conventional heating methods were performed in tall glassware (due to the inability to used short glassware in the microwave reactor for microwave leakage issues). Microwaves allow for reaction mixtures to be heated volumetrically, which offers more control over reaction temperatures compared to conventional heating methods.[81,90] Control over reaction temperature and the ability to easily control reactions independently is a large attraction for high throughout library synthesis, and this can be obtained by using microwave heating to volumetrically heat batch reactions in parallel. Prior to engaging in the design and build of a novel microwave reactor, the efficiency of microwaves to conduct the target transesterification were investigated and compared to conventional methods to define that the use of microwave heating was a feasible/desirable choice for heating transesterification reactions. Initial experiments were again performed with cyclododecanol, with the reaction scheme shown in Figure 3.9.

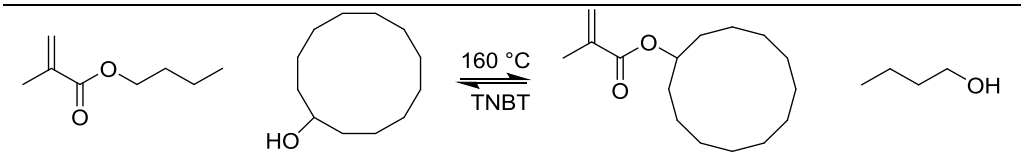


Figure 3.9: Reaction scheme showing the synthesis protocol for cyclododecyl methacrylate

Both conventional and microwave experiments were heated to 160 ˚C and aliquots were taken to observe the change in conversion from cyclododecanol to cyclododecyl methacrylate with this data shown in Figure 3.10.

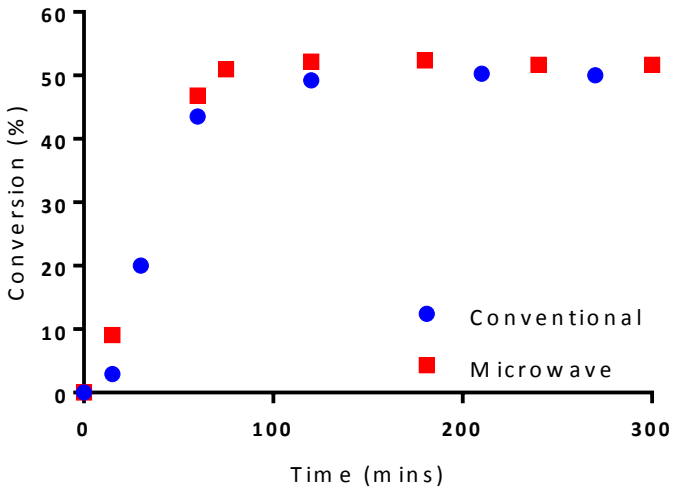


Figure 3.10: Graph showing the change in conversion over-time for cyclododecyl methacrylate for both conventional and microwave heating methods

This data showed that microwaves could achieve a 50 % conversion marginally more quickly than conventional heating (~75 mins for microwave heating (MWH) compared to 120 mins for conventional heating (CH)). However, it was also noted that for both heating mechanisms that: (a) neither could get past 50 % conversion and that (b) microwave heating obtained higher conversions after short time scales (15 minutes). This latter observation suggest that microwave volumetric heating may have it greatest effect in initially heating a chemical reaction and obtaining the desired reaction temperature in a shorter time scale.

This experimental procedure was then repeated with l-menthol, 4-methyl-2-pentanol and 3-phenyl-2-propen-1-ol (see reaction schemes in Figure 3.11) to observe the transesterification results obtained for different alcohols.

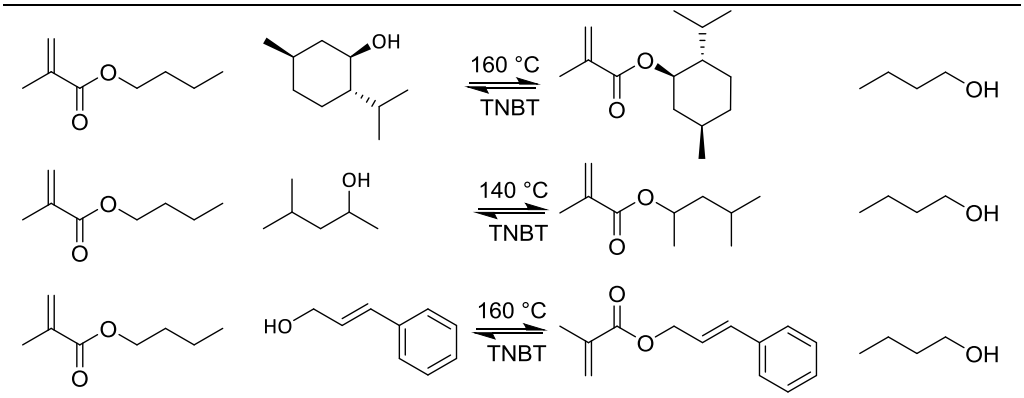


Figure 3.11: Reaction scheme showing the synthesis protocol for 5-methyl-2-(1-methylethyl) cyclohexyl methacrylate (LMMA), 4-methyl-2-pentyl methacrylate and 3-phenyl-2-propenyl methacrylate (CiMA) respectively

The reactions to synthesise LMMA and CiMA were performed at 160 ˚C, whilst MpMA was synthesised at a lower temperature of 140 ˚C due to a lower boiling point of the alcohol compared to the other alcohols used. The data from these experiments in shown in Figure 3.12.

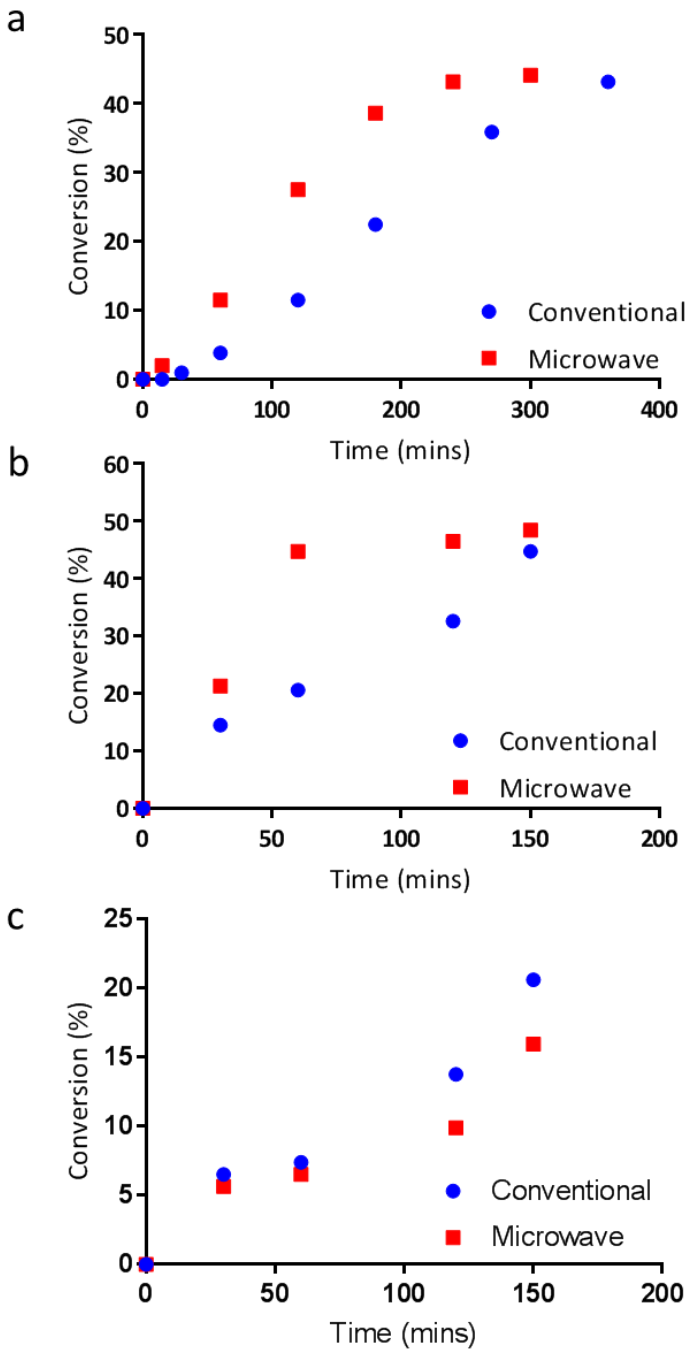


Figure 3.12: Series of graphs showing comparison of conventional and microwave heating methods for (a) 5-methyl-2-(1-methylethyl) cyclohexyl methacrylate (LMMA) (b) 4-methyl-2-pentyl methacrylate (MpMA) (c) 3-phenyl-2-propenyl methacrylate (CiMA)

Figure 3.12a and Figure 3.12b shows how microwave heating methods increased the reaction kinetics of the transesterification of LMMA and MpMA respectively, but also

demonstrated how these methods were limited to 50 %. This observation was confirmed by the lack of any condensate retrieved from reactions which indicated that these systems we highly likely to be mass transfer limited. However, the synthesis of CiMA, showed in Figure 3.12c, demonstrated that conventional heating obtained a higher conversion after 150 minutes compared to the microwave heating method.

3.3.4 Use of nitrogen sparging to overcome mass transfer limitations

To overcome the 50 % conversion barrier that has been shown to be a ceiling the reactions conducted up to this point, a nitrogen gas sparge was applied to reaction mixtures to aid in removing butanol condensate which was formed as a by-product of the transesterification reaction. Initially, nitrogen was applied to reaction mixtures after 15 minutes after heating was commenced, to allow for powdered alcohols to melt and create a homogeneous mix with other starting reagents. A conventionally heated transesterification experiment with cyclododecanol was the first reaction performed to observe how sparging effected the overall reaction conversion and compared to those of a standard, non-sparged conventionally heated experiment (see Figure 3.13).

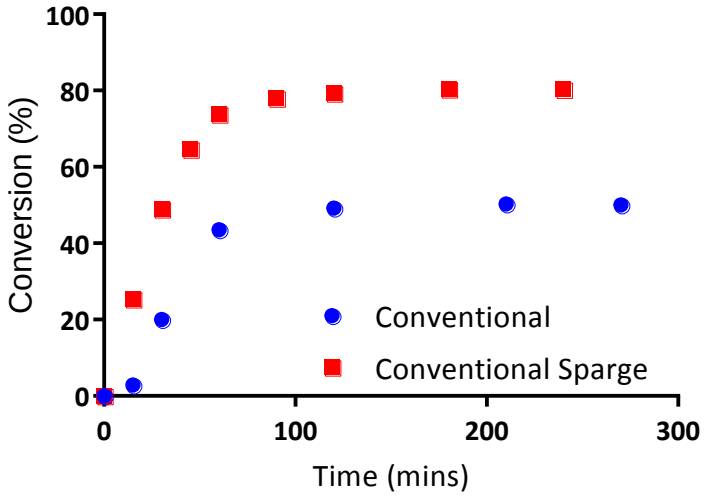


Figure 3.13: Graph showing the comparison between conventional heating and conventional heating with nitrogen sparging applied after 15 minutes of heating for cyclododecyl methacrylate. Reactions were heated to 160 ˚C

The data in Figure 3.13 showed that by the application of a nitrogen sparge, the reaction reached 80 % conversion in about 120 mins, and hence application of the gas overcoming previous mass transfer limitations. However, upon further examination, it was also discovered that the applied nitrogen sparge was also removing butyl methacrylate from the reaction mixture. This was detected from the NMR analysis, where an example spectrum shown in Figure 3.14, defined that the remaining BMA peak had dropped to 7 % of the total remaining reagent alcohol, (therefore the total net product was calculated to be 79 %). This meant that the reaction stoichiometry was changed as the reaction progressed.

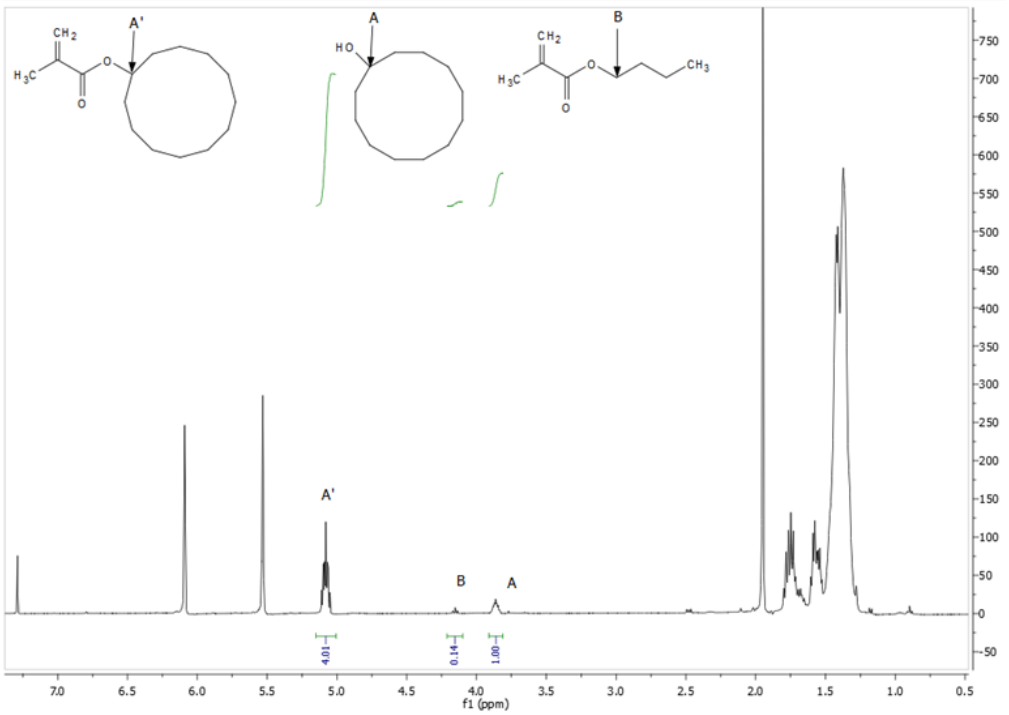


Figure 3.14: ^{1}H Spectra of conventionally synthesised cyclododecyl methacrylate with nitrogen sparging after 4 hours of heating at 160 ˚C. BMA content has dropped to 7 % of the remaining cyclododecanol content, shown by the reduction of protons next to ester group assigned B compared to the distinct alcohol peak assigned A. Conversion was shown to be 80 % by comparing change of chemical environment from A to A'.

This observation was supported by the analysis of the retrieved condensate from the reaction. It was shown in Figure 3.15 that the condensate mixture contained 57 % butanol and 43 % BMA. It was therefore concluded that, to obtain higher reaction conversions, this process loss of reagent methacrylate needed to be minimalised to leave as much BMA in the reaction vessel as possible.

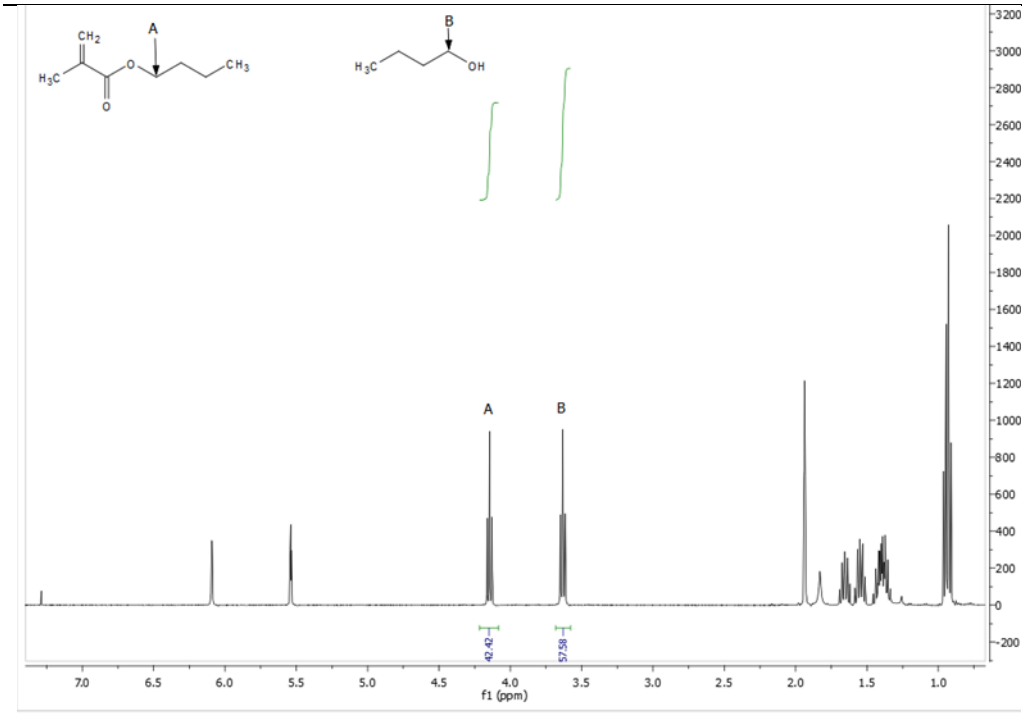


Figure 3.15: ^{1}H spectrum of reaction condensate showing mixture of 57 % butanol and 43 % BMA after a 4 hour nitrogen sparging experiment.

To prevent the evaporation of BMA from causing an overall reduction in potential end conversion, two options were explored to prevent this from happening. The starting ratio of BMA: alcohol was changed from 7:5 to 8:5 whilst keeping sparging start time at 15 minutes. Additionally, the starting ratio was kept at 7:5, but the sparging was delayed until 45 minutes during the reaction was also investigated to prevent the large removal of BMA. The data from these experiments is detailed in Figure 3.16.

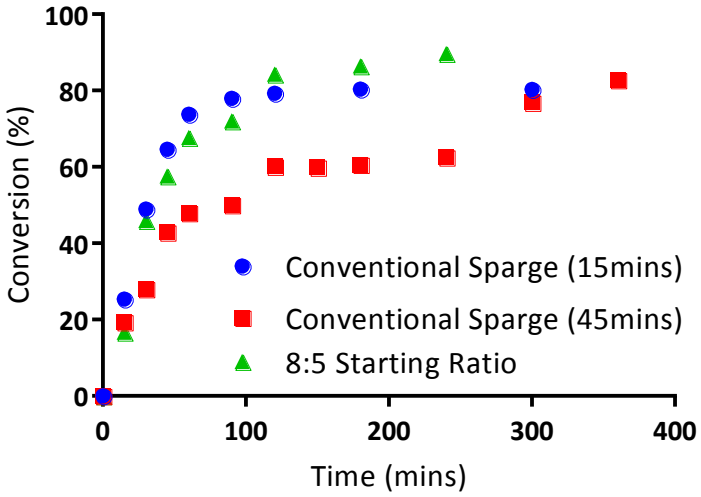


Figure 3.16: Figure showing the difference in conversion when the starting ratio of BMA: alcohol is altered from 7:5 (blue circles) to 8:5 (green triangles) and compared against a 7:5 ratio with delayed sparging (red circles)

Figure 3.16 showed that both methods of increasing BMA retention, i.e. including a larger amount of starting BMA and by delaying the start point of sparging, successfully enabled the reaction conversion to reach comparable final conversion levels. Additionally, delaying the onset of sparging also was noted to result in an extension of the reaction cycle time to reach this final conversion by an approximate factor of three. However, it was also observed that an increase in the BMA content also resulted in an increase in polymerisation. Therefore, the approach of delaying the sparge time was adopted as the optimised method for this project. The delaying of the sparging point decreased the apparent reaction rate that is associated to sparging experiments, but also allowed for the retention of BMA at later time points which can be shown in Table 3.1 by comparing the leftover reagent alcohol to the amount of remaining BMA.

Table 3.1: Table showing the remaining amount of BMA left in reaction vessel at comparable conversions of approximately 80 % when comparing to amount of reagent alcohol left in vessel. Reactions were carried out using butyl methacrylate and cyclododecanol at either a 7:5 or 8:5 ratio. Titanium butoxide was used as a catalyst at 1 % molecular weight and reactions were carried out at 160 °C.

Heating Method	Percentage of BMA remaining (%)
Conventional sparge (15mins)	7
Conventional sparge (45 mins)	150
8:5 Starting Ratio	115

With an optimised method for the synthesis of cyclododecyl methacrylate, a comparison was made with microwave and conventional heating to see how the use of nitrogen gas sparging effected the conversion of cyclododecyl methacrylate, this comparison data is shown in Figure 3.17.

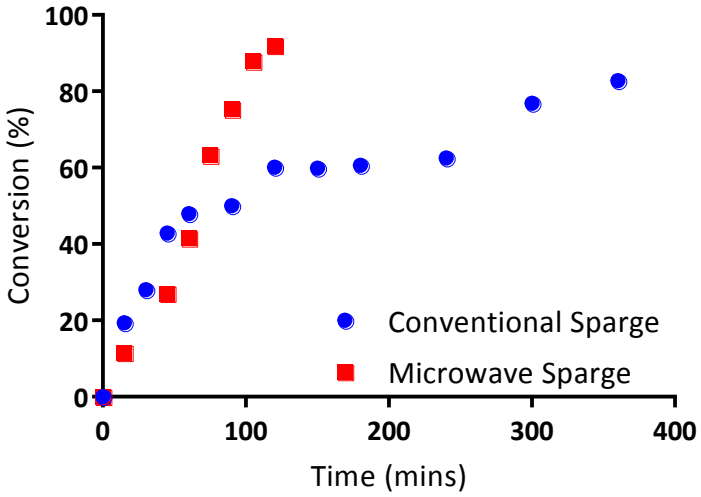


Figure 3.17: Comparison between conventional sparging technique and microwave sparging technique when sparging has been delayed by 45 minutes. Microwave power was set to 150 W input power.

Figure 3.17 shows how the use of microwave sparging enabled reaction conversions of more than 90 %. However, due to the

vessel required being a long-necked vessel, the nitrogen gas sparge required to remove the butanol by-product was introduced as a higher pressure. This change was also found in this experiment to cause the onset of some polymerisation during the reaction, which can be shown in Figure 3.18.

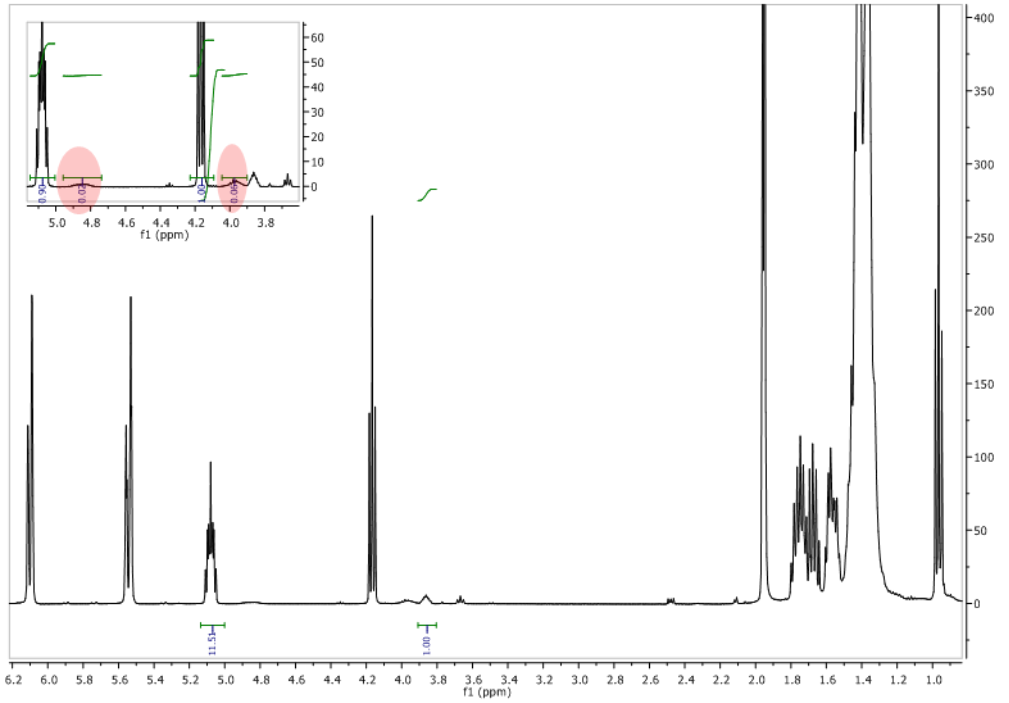


Figure 3.18: ^{1}H NMR spectrum of CyDMA synthesised using microwaves under N_2 sparging. Enlarged section of spectrum shows polymerisation in red circles that occurred during the reaction

However, the use of high microwave powers has also been identified to promote selective heating of radicals which could have caused small amounts of polymerisation at high temperatures.[155] Due to the slight polymerisation within the reaction mixture when microwave polymerisation was applied with sparging, the optimised method for creating a material library for HTDP was performed using conventional heating with sparging commencing after 45 minutes of heating with a short vessel. This process offered the best balance between obtaining high conversions and minimal polymerisation. A microwave

reactor is later developed using a method that promoted mass transfer, reduced the level of power required to drive the transesterification and removed the need of using nitrogen sparging, where the former is to promote cycle time reduction whilst the latter are to prevent polymerisation occurring. This reactor design work is discussed in Chapter 5.

3.3.5 Synthesis of novel methacrylate library

The optimised synthesis protocol allowed the synthesis of a monomer library which had a range of different moieties including linear, branched, aromatic and cyclic functionalities to be conducted. Alcohols with different chemistries, i.e. containing differing functional groups, for example the synthesis of nitrobenzyl methacrylate and chlorobenzyl methacrylate were able to be investigated. Table 3.2 shows the monomers that were synthesised during this study.

Table 3.2: Table showing monomers synthesised using the optimised conventionally heated sparging method.

Monomer	Conversion (%)
Cyclododecyl Methacrylate (CyDMA)	83
Dodecyl Methacrylate (DdMA)	90
5-methyl-2-(1-methylethyl) cyclohexyl Methacrylate (LMMA)	69
4-Methyl-2-pentyl Methacrylate (MpMA)	94
trans-3,7-Dimethyl-2,6-octadienyl Methacrylate (GeMA)	84
3-phenyl-2-propenyl Methacrylate (CiMA)	55
3,4-(Methylenedioxy)benzyl Methacrylate (PiMA)	82
2-Ethylhexyl Methacrylate (2EhMA)	81
Hexadecyl Methacrylate (CMA)	87
4-Isopropylbenzyl Methacrylate (IpbMA)	80
4-Methylbenzyl Methacrylate (MbMA)	93
2,6,6-Trimethylbicycloheptyl Methacrylate (αpMA)	81
4-Nitrobenzyl Methacrylate (NibMA)	81
2-Chlorobenzyl Methacrylate (ClbMA)	75
5-Isopropyl-2-methylphenyl Methacrylate (CaMA)	10

All reactions were performed at a ratio of (7:5) of butyl methacrylate:alcohol with a 1 % molecular weight of catalyst which was titanium butoxide. Reactions were left to progress for 45 minutes before nitrogen sparging was used to remove butanol by-product. All reactions were performed at 160 °C except for 4-methyl-2-pentyl methacrylate which was performed at 140 °C.

The associated structures for the monomers in Table 3.2 can be found in Figure 3.19. NMRs of these materials can be found in Appendices A - N. The target for reaction conversions was set to be 80 % based upon preliminary data which suggested that

polymers with up to 80 % conversion were shown to not affect the growth of *P. aeruginosa* and this is discussed Chapter 4. Hence by aiming for an 80 % conversion, the effect of BMA on the bacterial adhesion should be negligible.

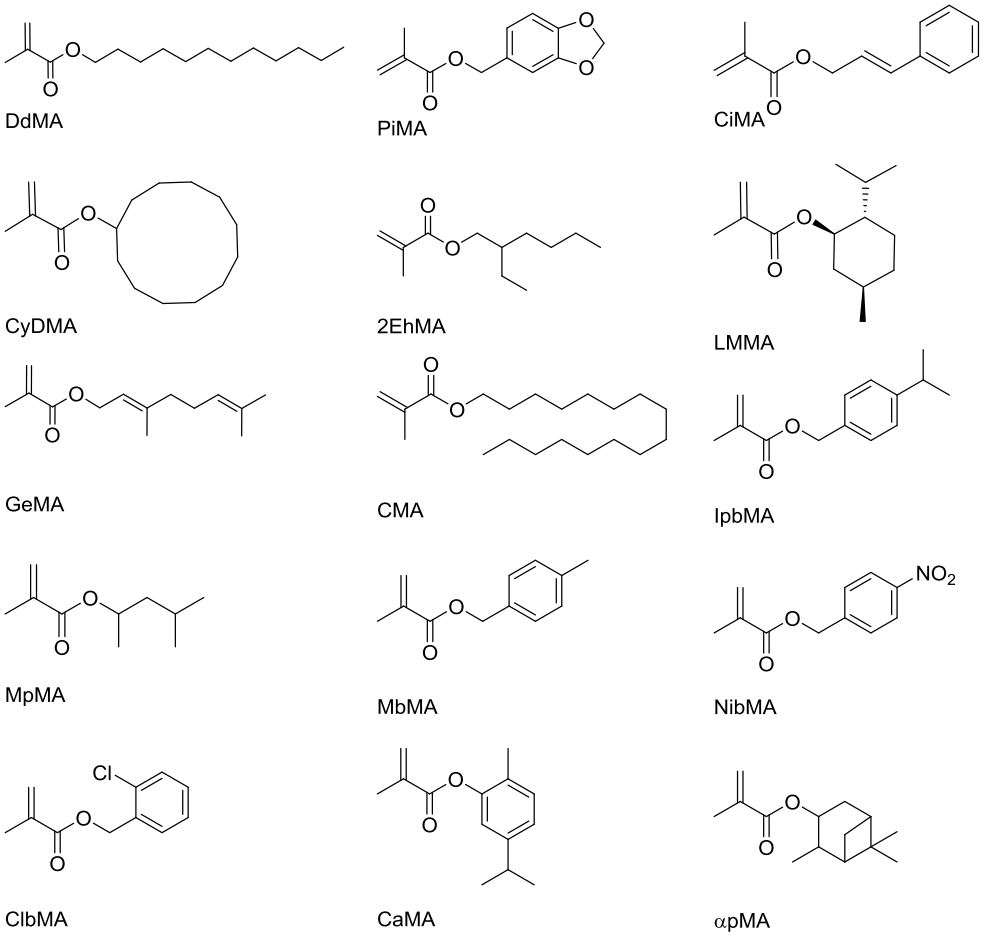


Figure 3.19: Structures of synthesised monomers using optimised conventionally heated sparging method

A high conversion (>80 %) was observed for most of the monomers synthesised apart from most notably: LMMA, CiMA and CaMA. Despite a poor conversion, it was noted that LMMA had a much higher conversion compared to CaMA despite having similar structures. However, CaMA was noted to contain an aromatic functionality as opposed to a cyclic aliphatic structure that is present in LMMA. This this may have some

bearing on either the electronic or steric environment of the reactive double bond and this result in differing conversion levels. To achieve a higher conversion for LMMA, a conventional heating experiment was performed with a vacuum which was applied after 24 hours to further extract butanol, however this was only able to achieve a conversion of 69 %, as shown in Figure 3.20. However, this procedure was not able to obtain high conversion for CaMA.

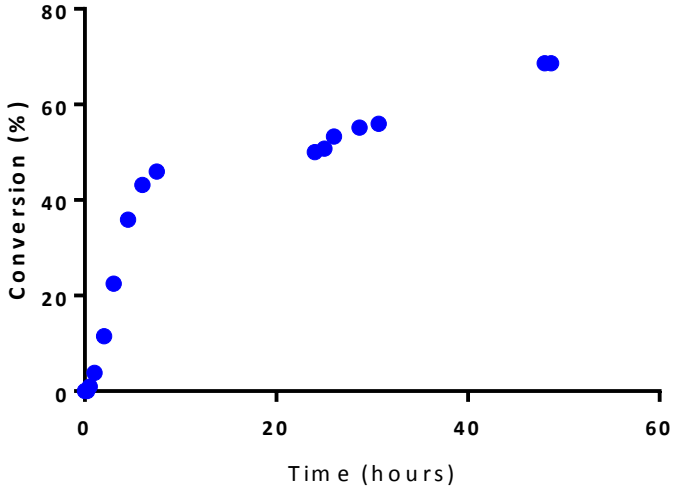


Figure 3.20: Conversion of LMMA shown of a 50-hour period. Reaction conditions carried out at 150 °C and vacuum pump applied at 300 mbar for 30 minutes after 24 hours.

Hence a higher conversion of LMMA was obtained for further use as a monomer in the material library for high throughput screening (discussed in Chapter 4), albeit without using the optimised synthesis method used to synthesise the rest of the methacrylate monomers as described in 3.3.4. The conversion of CiMA was later improved using the designed synthesis reactor described later in Chapter 5. Another monomer was attempted to be synthesised which was 2-methyl-3-butyn-2-methacrylate (Figure 3.21). However, the associated alcohol to this monomer has a boiling point of 104 °C, and hence using an optimised sparging method of 160 °C caused the alcohol to be

distilled, and by reducing the reaction temperature no conversion was observed.

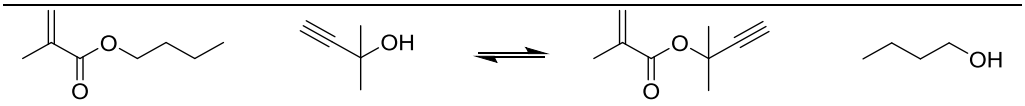


Figure 3.21: Reaction sequence showing the attempted synthesis of 2-methyl-3-butyn-2-methacrylate. Reaction was performed at 160 ˚C, 140 ˚C and 100 ˚C

3.4 Discussion

3.4.1 Effect of reaction stability using both methyl and butyl methacrylate

The synthesis of a wide-ranging library of novel methacrylate monomers requires a synthesis protocol that is cheap, simple, and most importantly capable of synthesising a large quantity of diverse novel monomers with differing monomer structures. This meant that a fundamental monomer that can be functionalised using simple chemical reaction type was required. Initially MMA was used, as it is a cheap and readily available material and by using the transesterification process a diverse library can be, theoretically, synthesised by accessing the vast number of commercially available alcohols to provide the desired molecular functionality to the monomer structure. Transesterifications form a by-product molecule which will be produced on an equimolar basis as the monomer is manufactured. This secondary product must be removed from such equilibrium-based process to achieve high yields of the desired molecule. The by-product of transesterification reactions using MMA was methanol, which has a boiling point of 64.7 °C.[156] This means that by having a reaction temperature of 100 °C, the temperature difference between processing temperature and the boiling point would be 35.3 °C, and so methanol should be able to be distilled from the reaction mixture by the use of condensation equipment. However, what was observed was that the removal of methanol from the reaction mixture proved difficult and the reaction was mass transfer limited and only achieve a maximum of 50% conversion. This led to the change of the choice of starting monomer to butyl methacrylate. An advantage of using butyl methacrylate was the higher boiling point (162 °C).[157] This led

to using a higher reaction temperature of 160 °C which ensured faster reaction kinetics for all experiments, which was shown in Figure 3.5, where BMA was able to achieve a mass-transfer limited conversion of 50 % at a 24-fold rate increase compared to MMA. As the by-product of reactions with BMA was butanol, which has a boiling point of 117.7 °C,[158] the mass transfer properties of the system were improved due to a higher temperature difference between reaction temperature and boiling point of butanol (42.3 °C). However, neither the MMA nor BMA based reactions were able to achieve higher than 50 % conversion when sparging was not applied due to the lack of condensate removal achieved and so the reaction was concluded to be mass transfer limited.

Furthermore, despite the addition of MEHQ as a radical inhibitor, MMA was noted to readily polymerise during reaction procedures as shown in Figure 3.6, whereas polymerisation was minimal when investigating experiments involving butyl methacrylate. This is likely due to increased steric effects introduced by the longer carbon chain associated with butyl methacrylate. Polymerisation during a reaction was even more prevalent when attempting to perform sparging experiments with MMA. This processing techniques was introduced to try to improve the mass transfer achieved in the reaction system, because sparging has been reported to improve reaction surface area which leads to higher reaction kinetics.[120]

The added benefits of being able to use BMA at higher reaction temperatures to increase the rate of reaction with also reduced observations of polymerisation made BMA the suitable fundamental monomer of choice for further transesterification

experiments with different alcohols to develop a range of novel methacrylate monomers.

3.4.2 Effect of glassware on reaction mass-transfer properties

To conduct fair comparisons between heating methods, an initial test was performed to observe the differences in mass-transfer properties between different glassware configurations typically used in each reaction type. Figure 3.8 showed the difference between using a tall and short reaction vessel for the synthesis of cyclododecyl methacrylate using conventional heating. This showed that by using a shorter reaction vessel, the conversion could be increased, showing that butanol had been removed from the reaction vessel more efficiently. For this reason, both conventional and microwave experiments were performed in long-necked vessels for comparison of the heating modes with this apparatus. The long neck apparatus had to be used for this comparison due to the need to use a choke in the microwave system on safety grounds. This highlighted a flaw in the design of the microwave system that due to the size requirement of the glassware, the mass transfer properties of the system were reduced. Thus, in the greater part of the project the latter techniques were used due to the benefit with mass-transfer whilst minimising any spurious polymerisation. This part of the study also highlighted the potential benefit that could be achieved by designing a novel microwave reactor concept that could use much less power to maximise the mass transfer benefits by using a much smaller choke but negate the onset of spurious polymerisation. This design study is described in Chapter 5.

3.4.3 Comparison of conventional and microwave heating methods

Microwaves throughout this project were primarily used due to the ease of controlling reaction conditions compared to conventional heating.[97] This would mean that for a high throughput synthesis reactor that the reaction temperature could be monitored and altered independently alongside other reactions in the same "batch" or array.

However, it was important to observe if using microwaves energy was a feasible option for driving the transesterification experiments when comparing to conventional heating. Since initial reports in 1986 of the first use of microwave-assisted organic synthesis (MAOS)[75], numerous publications have reported reduced reaction times and enhanced product purities.[159,160] Initial comparisons were made with the transesterification of cyclododecanol to cyclododecyl methacrylate and Figure 3.10 showed a small increase in reaction kinetics for the synthesis of CyDMA using microwaves compared to conventional heating methods. One possible reasons for this slight increase is due to volumetric heating. As also noted by Figure 3.10, the difference in conversion at 15 minutes is quite large, and this is likely due to the difference in heat-up times between the two methods. As microwave heating directly couples energy to the reaction mixture, samples that were irradiated using microwaves were able to reach the desired reaction temperatures much quicker than conventional heating methods, which could therefore explain the ability of microwaves to obtain a 50 % conversion quicker than conventional heating for the synthesis of CyDMA.

Figure 3.12a showed a larger difference between microwave and conventional heating methods, with microwave heating showing a much larger apparent reaction rate for the synthesis of LMMA. The synthesis of LMMA for both heating methods was shown to be a slow process, and this has been attributed to the steric hindrance associated to l-menthol, the corresponding alcohol for the transesterification reaction. It was shown again at short time period an increase in conversion using the microwave heating method compared to conventional heating which can be attributed to the fact that microwave heating is a volumetric heating effect whereas conventional heating relies on heat conduction for heating. The increase in reaction rate observed could also be associated to non-thermal effects by the increase of favourable collisions experienced under an oscillating electric field, which has also been previously reported, but not fundamentally proven.[87] For the MpMA simulation shown in Figure 3.12b, microwaves were also able to obtain a 50 % conversion quicker than conventional heating. Dielectric assessment of both MpMA and CiMA could offer further analysis potential for the reason microwave heating gave a higher conversion compared to conventional heating methods. However, Figure 3.12c showed the comparison of heating methods for the synthesis of CiMA. Whilst the final conversion was much lower albeit over a shorter reaction time compared to LMMA, the results suggested for this synthesis that conventional heating may be preferential over microwave heating. Very low conversions were observed for both conventional and microwave heating for CiMA, suggesting that conjugated materials do not allow for efficient reaction processes, which could be considered a limitation for the transesterification process.

A key feature for these reactions however is that by using both microwave and conventional condensation experiments, no experiment was observed to achieve more than a 50 % conversion, and this was confirmed when no condensate was collected from the receiving flask after the reaction process.

3.4.3.1 Effect of nitrogen sparging on synthesis of CyDMA

Due to the overall poor conversion observed for both conventional and microwave experiments, an addition nitrogen gas sparging step was added, and this was shown to remove butanol from the reaction vessel and hence drive the reaction towards completion. Figure 3.13 demonstrated the difference by utilising nitrogen gas sparging and showed an increase in conversion from 50 % to 80 %. This showed that by including a nitrogen sparge, the previously encountered conversion ceiling of 50 % was surpassed due to the increase mass transfer characteristics provided by the nitrogen sparging technique, which is a well-documented effect.[117,120]

Upon further analysis of the ^{1}H-NMR spectrum of the nitrogen sparged reaction, it was observed that the reason a higher conversion than 80 % was not obtained was because BMA as well as butanol had been removed from the reaction vessel and therefore preventing any further product from being formed, and this was confirmed by subsequent analysis of received condensate shown in Figure 3.15. The removal of BMA is due to the reaction temperature being close to the boiling point of BMA, and therefore the volatile BMA with the increased mass transfer characteristics from the sparged system causes a distillation of BMA.

Hence, to prevent the loss of BMA, further method development was required to enable a reliable synthesis method that could make a range of methacrylate monomers to a high conversion. First the starting ratio of BMA: alcohol was changed from a 7:5 molar ratio to 8:5 molar ratio. This enabled an equally high reaction rate, as the sparging was applied at the same time point of 15 minutes, however polymerisation was observed from this reaction process. The additional BMA increased the likelihood of generating free-radicals which caused polymerisation of the reagent methacrylate material.

A second variation to the method was to wait until 45 minutes instead of 15 minutes before starting with nitrogen sparging to remove butanol from the reaction. Whilst increasing the time for reactions to obtain a high conversion, it reduced the risk of distilling significant amounts of BMA. By delaying the starting point of sparging, the reaction progressed to 40 % before sparging was commenced, which then prevented the loss of any material (butanol or BMA) being removed from the reaction vessel in the first 45 minutes. Then by starting the sparging after 45 minutes, the mass transfer characteristics were improved with then removed butanol from the reaction vessel which allowed high conversions to be achieved.

The delayed sparging approach was then used to compare both microwave and conventional heating methods. Microwaves were able to achieve a higher conversion in a shorter time period (see Figure 3.17) where microwaves achieved a 90% conversion after 120 minutes compared to 60 % shown in conventional heating. However, with microwave heating a small amount of polymerisation was observed, which is possible due

to the application of nitrogen gas being too rigorous, and a balance must be achieved to distil the butanol by-product to obtain high purity materials and achieve minimal polymerisation.

However, this onset in observed polymerisation may not be because of the sparging pressure, it has been reported in that microwave heating can accelerate polymerisation by promoting propagation. Adlington et.al. have defined that a high temperature microwave polymerisation can result in 40% conversion within 3 minutes of commencing the reaction compared to only 4 % in a conventional equivalent over the same time.[155] This was also shown to result from the application of large power levels i.e.300 Watts and was attributed to the selective heating of the radical within the reaction medium. Thus, the BMA free radical polymerisation observed here may be because of this microwave selectively heating any radical that is formed at the high temperature and promoting polymerisation.

3.4.4 Library synthesis of novel methacrylate monomers

Non-commercially available materials offer a huge potential for HTMD programmes to discover a range of novel biomaterials that have largely been neglected due to excessive processing and costs required. Therefore, a key development throughout this study was to develop a simple synthesis protocol with the capability to develop a novel monomer library with a range of different chemical and structural moieties. This novel monomer synthesis was guided by quantitative structure activity relationship models which are discussed in Chapter 4, allowing

for guided synthesis into the non-commercially available chemical space.

A monomer library was synthesised using an optimised transesterification process with nitrogen gas sparging was shown in Figure 3.19. The nitrogen gas sparging was used to increase the mass transfer characteristics of the system to remove the by-product (butanol) from the system as explained in 3.4.3.1. Conventional sparging was used as a methodology due to the ability to use a short reaction vessel, whereas in the microwave system a tall reaction vessel is required due to the choke used to prevent microwave leakage. A large range of hydrocarbon structures were synthesised including linear, branched, aromatic and cyclic moieties. Chemical diversity was also incorporated into the monomer library with the synthesis of ClbMA, PiMA and NibMA. Isometric materials were synthesised including DdMA and CyDMA which were used to probe structure-activity relationships in Chapter 4. This showed the ability of using the transesterification mechanism to be able to produce a diverse range of materials, which has already been previously reported in literature with the range of lipids, methacrylates and oligocholates produced[113,147–149].

Table 3.2 shows how the transesterification mechanism was able to synthesise the diverse monomer library to a high conversion, which majority of materials showing higher than 80 % conversion. However, a few reactions were shown not to be suitable for the general reaction conditions (160 °C, 1 % molar ratio catalyst and nitrogen sparging). Some alcohols such as 2-methyl-3-butyn-2-ol which have a low boiling point (104 °C)[161] cannot be used in high temperature sparging experiments as it

causes a large amount of the reactant alcohol to be distilled under higher temperatures with sparging. This pushes the dynamic equilibrium of Le Chatelier's principle towards the reagents and prevents the reaction from progressing towards completion. One alternative was to reduce the reaction temperature to 100 °C such that the reagent alcohol was no longer being distilled, however it was noted that no conversion was obtained, despite rectifying Le Chatelier's principle so the reaction could progress in the forward direction. This is likely due to the use of BMA as the monomer reagent material, as BMA is more sterically hindered compared to other potential monomer reagents such as methyl methacrylate, and hence the temperature required to initiate the reaction for BMA could be higher than the reaction temperature required to retain the reagent alcohol. However, the synthesis of 4-methyl-2-pentanol into 4-methyl-2-pentyl methacrylate (MpMA) was performed at 140 °C and achieved a conversion of 94 % despite 4-methyl-2-pentanol having a lower boiling point of 132 °C.[162] This suggested that whilst a temperature of 100 °C was too little for 2-methyl-3-butyn-2-ol, 140 °C was enough to initiate a transesterification reaction and obtain MpMA with a high conversion.

Another limitation was with sterically hindered alcohols such as l-menthol and carvacrol which produced LMMA and CaMA at a relatively low conversion of 43 %/ 10 % respectively whilst using the sparging methodology.

The result of this study has shown that despite a few limitations, the transesterification mechanism has been shown to be a versatile process to develop a range of novel methacrylate

monomers in a single step process. For the further realisation of being useful for HTMD programmes, a reliable library synthesis reactor is required which is capable of simultaneously monitoring reaction conditions of different batch-process reactions, and this is discussed in detail in Chapter 5.

3.5 Conclusion

- BMA was chosen as the fundamental monomer for all transesterification experiments for this project, as higher temperatures allowed for quicker reaction rates and reduced polymerisation compared to MMA.
- Effect of reaction glassware was observed showing that vessels used for microwave reactions reduced the mass-transfer characteristics of system. Therefore, for fair comparison, microwave and conventional experiments were both performed in long-necked reaction vessels.
- Comparisons using CyDMA, LMMA, MpMA and CiMA reactions were used to show that microwaves for majority of cases either improved the reaction rate or showed comparable reaction rates to conventional methods, showing the suitability of using microwaves to synthesise monomers in this way.
- Nitrogen gas sparging was shown to increase the mass-transfer characteristics of transesterification experiments through the removal of the by-product butanol.
- By delaying the start point of nitrogen sparging, showed how not all BMA was distilled from the reaction showing potential to increase the overall conversion of reactions.
- Using the optimised synthesis protocol, 11 novel methacrylate monomers were produced with an overall conversion more than 80 %.

4 Identification of materials resistant to biofilm formation using high throughput screening and computational models

4.1 Introduction

The concept of a post antibiotic era is fast becoming a reality, with patients contracting bacterial infections that are becoming resistant to the last line of antibiotic treatments, whilst the development of antibiotics has stalled in the last decade and hence providing no alternative antibiotics for clinical use.[1,2] A report by the UK government (Lord Jim O'Neiil), has suggested that antimicrobial resistance will cause more fatalities than the current fatality rate of cancer by 2050.[14] Therefore, the prevention of bacterial infections in clinical settings has become an utmost priority to reduce mortality and morbidity. Medical device related infections have shown to occur due to the adhesion of planktonic bacteria to the device surface, which then produces a biofilm, which have shown to have increased resistance to antibiotic treatments.[3,4,16] These infections have largely been associated to the poor biological performance of material, usually silicone, which has desirable physical properties, but has been shown to promote the adhesion of planktonic bacteria.[50] A poor understanding of the surface-bacteria interaction has led to the utilization of high throughput material discovery (HTMD) campaigns in the search to discovery materials suitable for reducing biofilm formation.[5,47,134] Consequently, novel polymer coatings that reduce the adhesion of bacteria to surfaces have been discovered by HTMD methodologies, and this has been shown to be successful in in-vitro studies and pre-clinical animal

models.[45] Polymers discovered by Hook *et al* were shown to reduce biofilm formation on urinary catheters using polymer microarrays as a platform for high throughput screening.[62] HTMD programmes have so far been largely successful by using non-biased screening of large material libraries. This has allowed for polymer hit materials to be identified for a range of biological applications including the reduction of biofilm formation to medical devices, the expansion of pluripotent stem cells and providing bio-instructive implant materials.[5,131,163–165]

The non-commercially available material space is vast and therefore the number of possible polymers that can be synthesised is innumerable. Therefore, unguided material synthesis is not considered an effective use of time and resources compared to using commercially available materials. Utilising quantitative structure-activity relationships (QSAR) allows for the synthesis of novel materials to be directed to aid material discovery programmes. HTMD allow for rapid assessment of a large monomer library for discovery of a potential hit material for a desired application. For this reason, the monomers for the materials library must be readily accessible and relatively cheap, which traditionally limits research to commercially available monomers. Results shown in Chapter 3 have shown that a large chemical space can be accessed with a simple and repeatable synthesis protocol able to produce a range of different methacrylate monomers. Weakly amphiphilic monomers with reduced molecular flexibility have shown to produce polymers capable of resisting biofilm formation, and an analytical expression, *alpha*, has been derived which links the log of the calculated partition coefficient

(*clogP*) and the number of rotatable bonds (*nRotB*) to bacterial adhesion which can be shown in the equation below.

$$\alpha = 0.44nRoTB - cLogP$$

Equation 9: Alpha parameter showing how bacterial adhesion of hydrocarbon polymers is related to the hydrophobicity and rigidity of material[6]

Hence a*lpha* can be used to predict novel anti-bacterial attachment polymers for use in medical devices such as catheters. Therefore, with the simple transesterification process outlined in Chapter 3, an unprecedented access to non-commercially available monomers was used to develop polymeric surfaces that were predicted to reduce bacterial adhesion. The enabled the development of a feedback loop system that by using predicted materials to observe a biological response, which could then be used to improve the robustness of further computational models, which can therefore predict further materials to resist biofilm formation (Figure 4.1).

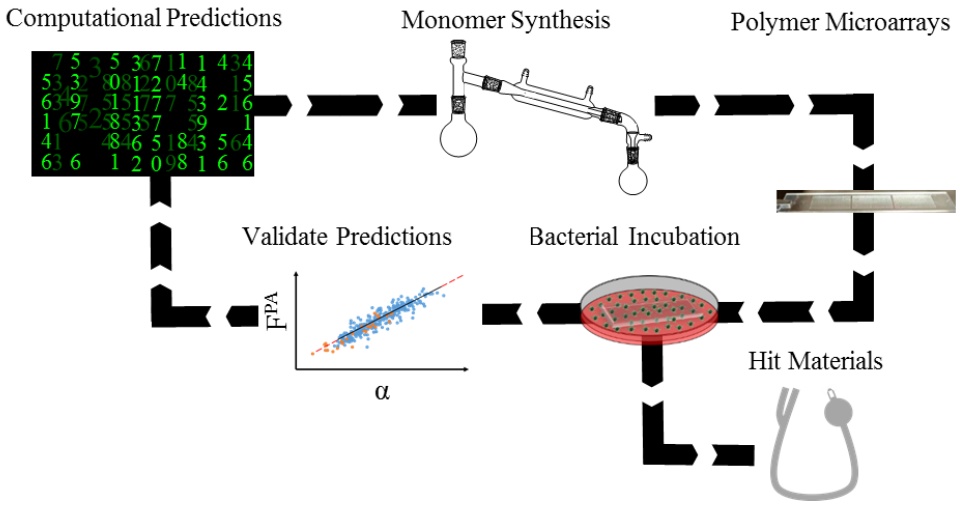


Figure 4.1: Flow diagram showing work flow to find suitable materials for preventing biofilm formation to medical devices. The results from previous assessments of bacteria-material interactions can be used to predict and then synthesise novel monomers. The newly produced materials can be tested to further refine the model, leading to the discovery of the next generation of biomaterials.

Synthesised monomers were compared against commercially available monomers in a polymer microarray, and the material that was predicted to have the lowest bacterial attachment, cyclododecyl methacrylate (CyDMA), was then also shown to have the lowest bacterial attachment experimentally for both *Pseudomonas aeruginosa* and *Proteus mirabilis*. CyDMA was then purified and scaled-up to coat sections of urinary catheter and compared to clinically used materials (Silicone and Bardex® I.C. Aquafil with a hydrogel and silver alloy coated catheter) as well as materials discovered within the group to already resist bacterial adhesion (EGDPEA:DEGMA (Ethylene glycol dicyclopentenyl acrylate: Di(ethylene glycol methyl ether methacrylate) and iBnA:triEGMA (Isobornyl acrylate: Tri(ethylene glycol methyl ether methacrylate)). This is the first instance of a biomaterials screening program extending beyond the domain covered by the initial screen to predict a novel chemical entity with improved properties. This validates the QSAR approach for identifying polymers that resist biofilm formation beyond its chemical training domain.

4.1.1 Aims and Objectives

The aim of this chapter was to use *alpha* to predict a range of novel methacrylate monomers predicted to reduce biofilm formation. These materials were then screened in a bacterial assay and hit materials were scaled up for coating sections of urinary catheter. This was achieved by the completing the following objectives:

1. Identify monomers predicted to resist attachment of bacteria using the *alpha* parameter.
2. Incorporate non-commercially available materials (as synthesised in Chapter 3) onto a polymer microarray for anti-bacterial attachment assays.
3. Analyse surface of polymer microarray to confirm copolymer mixing ratios for assessing copolymer material data.
4. Confirm the approach of using *alpha* parameter to predict biofilm formation for both *P. aeruginosa* and *P. mirabilis*
5. Scale-up of hit materials for coating sections of urinary catheter to test *in vitro* for reducing bacterial adhesion to medical devices.

4.2 Experimental Methods

4.2.1 Computational Predictions

A computational model published by Sanni *et al* was used to predict polymer materials that resist the attachment of *Pseudomonas aeruginosa*. The *alpha* value (α = 0.44nRoTB – clogP) was calculated using the clogP value and the number of rotatable bonds determined from the monomer structures.[6] For copolymer series a linearity was assumed between the two materials such that the *alpha* value for a 1:1 comprised of an average of the two-individual monomer *alpha* values. The *alpha* values were then plotted against subsequently obtained bacterial data to observe how the model performed with *alpha* values outside the published boundaries. The boundaries of the model were extrapolated by using materials with *alpha* values lower than the published limit, with the aim of identifying low attachment materials. The model was also extrapolated by observing the attachment of *Proteus mirabilis*, a bacteria species not covered by the initial model.

4.2.2 Polymer Microarray Production

4.2.2.1 Microarray Slide Preparation

To produce polymer microarrays, standard 75 x 25 mm glass slides coated with poly(2-hydroxyethyl methacrylate) (pHEMA) were used for the deposition of monomer solutions, which were then UV cured to form polymer microarrays. Epoxy silanised glass slides were used as the substrate for applying pHEMA, with the epoxy silane on the slide allowing for strong intermolecular interactions between the silane surface and the pHEMA. A 6 % w/v pHEMA in 95%/5% v/v ethanol/water solution was used to coat the functionalised glass slides using an automated dip-coating process. pHEMA was used as a

printing substrate as printed polymer spots have shown to adhere to the surface and not detach under culture conditions. Also, pHEMA is an example of a material which prevents biofilm formation, which allows for clear definition of spots when analysed.[166] This was done using an automated dip coater (Holmarc, India) to maintain control of insertion and extraction speeds (Figure 4.2). An insertion speed of 9 mm/s was used and an extraction speed of 1 mm/s, each slide was dipped 4 times, allowing for the solution to dry for 5 minutes before starting the next dip procedure. The slides were then left overnight at ambient conditions before being placed into a vacuum oven (0.325 mbar, room temperature (RT)) for 7 days before printing.



Figure 4.2: Holmarc dip coating unit used for coating epoxy coated slides with pHEMA solution

4.2.2.2 Array composition

Monomer solutions were prepared in a 50:50 % (v/v) mixture with a solvent which was comprised of a 50:50 (v/v) mixture of dimethylformamide (DMF) and toluene to account for the solubility of all polymers. A total of 4 synthesised monomers and 8 commercially available monomers were used for the

printing of the first polymer microarray (A1), leading to 61 polymers by sequential mixing of 9 monomers with tBCHA at ratios of 1:0, 5:1, 2:1 and 1:1 and 3 monomers were mixed with tBCHA at 1:0 and 1:1 only. Napthyl methacrylate (NpMA), benzyl methacrylate (BnMA) and [2-methacryloylamino)propyl)dimethyl[3-sulfopropyl)ammonium hydroxide (MEdMSPNH) were mixed sequentially with tBCHA at ratios of 1:0 and 1:1. CyDMA, trans-3,7-Dimethyl-2,6-octadienyl methacrylate (GeMA), 5-methyl-2-(1-methylethyl) cyclohexyl methacrylate (LMMA), dodecyl methacrylate (DdMA), ethylene glycol phenyl ether acrylate (EGPhEA), cyclohexyl methacrylate (CHMA), phenyl methacrylate (PhMA) and 2-hydroxy-3-phenoxypropyl acrylate (HPhOPA) were mixed sequentially with tBCHA at ratios of 1:0, 5:1, 2:1 and 1:1. A second polymer microarray (*A2*) included 13 synthesised monomers and 8 commercially available materials where 16 materials were mixed sequentially together to form a series of monomers mixed at either 1:0,2:1,1:2 or 0:1 ratios. The 16 monomers were then also combined with a further 5 commercial monomers in v/v ratios of 1:0, 3:1, 1:1,1:3 and 0:1. For each generation array a 384-well polypropylene source plate was prepared by filling each well with 18 µL of monomer mixture and 6 µL of a 4 % (w/v) solution of photoinitiator(2,2-Dimethoxy-2-phenylacetophenone (DMAP)):DMF. Due to printing errors and contaminations, A2 was not assessed with bacterial adhesion studies as shown by Appendix O and Appendix P.

4.2.2.3 Polymer Microarray Printing

Polymer microarrays were prepared on a XYZ3200 Biodot workstation. Quilled metal (946MP6B, Arrayit) pins were used

to produce polymer microarrays, where the quilled pins allowed up to 100 replicate prints of the same solution within one print cycle. The pins were cleaned in a sonicator water bath with toluene, methanol and DCM prior to being loaded into the printing workstation. The completed source plate and pHEMA coated slides were then loaded into the workstation which was then sealed and degassed with argon such that the O_2 levels were below 0.2 %, and a humidifier was used to maintain humidity at 30 %. Once these conditions were met, the printing script was started. A typical printing sequence began with a thorough cleaning of the pins, where pins were cleaned in a wash bath solution comprised of DMF and toluene in a 50:50 (v/v) ratio. After rinsing in the wash solution, the pins were transferred to a vacuum station to dry the pins. The washing and drying process was repeated twice before going to the source plate to collect monomer solution. After collection of the monomer solution, the pins transferred to a blotting stage where the pins were blotted to remove excess solution to prevent spreading of the monomer solution on the microarray substrate. Blotted steps were arranged with sufficient spacing such that no section of the blotting slide was blotted on twice with a separate material, to prevent any cross-contamination. After blotting, the pins were transferred to the pHEMA slides for printing. Each material was printed in triplicate on a single slide and a total of 10 slides were printed in total. After each iteration, the pins were transferred to the wash and vacuum stations to be rinsed and dried before collecting the next material and repeating the process. Whilst the pins were cleaning between iterations, a UV light source was turned on to initiate photopolymerising the monomer solution and fix it into place, as to prevent excess spreading of the monomer

solutions. At the end of the printing algorithm the UV light source was turned on for a further 10 minutes to fully polymerise the deposited monomer solutions. After the final UV polymerisation step, polymer microarrays were removed from the XYZ workstation and placed into a vacuum oven (0.325 mbar, RT) for 7 days to remove any excess monomer and solvent entrapped within the polymer spots.

4.2.3 Bright Field Microscopy

Prepared polymer microarrays were imaged using an Olympus IX51inverted automated (IMSTAR) microscope to obtain phase contrast and bright field images (x4 objective NA = 0.13) of the polymer microarrays. This gave an initial assessment of the printing process to see if the process was successful. The focal plane of the array was interpolated from 8 marker positions set manually prior to imaging.

4.2.4 ToF-SIMS

Acknowledgments are made to Dr Andrew Hook for acquiring ToF-SIMS data. To fully confirm that the polymer spots were printed successfully and not spreading across the pHEMA substrate, ToF-SIMS analysis was performed to observe the surface chemistry of the polymer microarray. A ToF-SIMS IV (IONTOF GmbH, Münster, Germany) instrument was used to acquire a 500 x 500 μm scan area in raster mode. A primary ion beam consisting of 25keV Bi_3^+ was used to generate ions from the sample surface which were analysed in the mass analyser. As the samples were non-conducting, charge compensation was applied with a low energy (20 eV) electron floodgun.[167] Negative spectra were calibrated using O^-, OH^-,

C_2H^-, C_2HO^-, $C_3H_3O^-$ and $C_3H_3O_2^-$ peaks whilst positive spectra were calibrated using CH_2^+, $C_2H_4^+$, $C_3H_6^+$ and $C_4H_8^+$ peaks.

4.2.5 Bacterial Attachment Studies on Polymer Microarray

Acknowledgements are made to Olutoba Sanni, who performed bacterial culture experiments on polymer microarrays and measured using fluorescence imaging

4.2.5.1 Polymer Microarray Incubation

Bacterial strains (mCherry tagged-*Pseudomonas aeruginosa* PA01-Nottingham (587/610 excitation/emission) and *Proteus mirabilis* DZM226637 DSRed (Nottingham collection) (587/610 excitation/emission) were streaked onto LB agar plates for the formation of colonies for bacterial culture experiments.[51] Overnight cultures were prepared by adding a single colony of bacteria using a sterile plastic loop to 10 ml of LB media, which was then placed in an incubator at 37 °C at 200 rpm overnight for approximately 18 hours. After the overnight culture, the culture was centrifuged at 10,000 rpm for 10 minutes and this was then resuspended in 10 ml of RPMI-1640 media, and this process was repeated to ensure all LB media had been removed from the culture. The optical density (OD) at 600 nm of the bacterial culture was determined by measuring 1 ml of pure RPMI-1640 as a blank against 100 µL of bacterial culture in 900 µL of RPMI-1640 media. The amount of bacterial culture to include in the polymer microarray incubation was determined by the optical density such that the concentration in a total of 15 ml of RPMI-1640 media was an OD_{600} of 0.01. Before adding the culture, the petri dish and polymer microarray were UV sterilised for 10 minutes to prevent external contamination

effecting the experiment. The 10-ml culture at an OD_{600} of 0.01 was then added to a petri dish which contained a single polymer microarray. In addition to the slide which contained bacteria, a control slide was also incubated which only contained 15 ml of RPMI-1640 media. The petri dishes were then sealed with parafilm and then incubated for 72 hours at 37 $^{\circ}$C on a moving platform rotated at 60 rpm.

4.2.5.2 Washing Protocol

After 72 hours of incubation, the polymer microarrays were removed from the incubator and rinsed to remove any non-attached bacteria from the surface and to remove salts that may have been deposited on the surface. The polymer microarrays were first placed into individual petri dishes with 15 ml of water and placed on a rocker platform at 30 rpm for 5 minutes. This was repeated a further time with distilled water and then a final time with Phosphate buffered saline (PBS). Both the control slide and the bacteria-incubated slide were washed with the same protocol for consistency. After the final rinse the slides were blotted on a piece of blue roll to remove as much moisture from the slide surface as possible.

4.2.5.3 Fluorescence Imaging

The slides were then placed into a Genepix 4000L which enabled high throughput scanning of the polymer microarrays. For the mcherry tagged *P. aeruginosa*, a 594 nm laser was used for exciting the fluorophore such that bacterial attachment could be measured, and a 594 nm laser was also used for DSred tagged *P. Mirabilis*. Once an image had been acquired, the data could be extracted using the Genepix Pro 6 software and analysed in Microsoft Excel.

4.2.6 Toxicity Studies of Polymers and Contaminations

The toxicity of polymerised materials and from any unreacted reagents present from the transesterification experiments were assessed. Bacterial cultures were prepared in the same way as described in Chapter 4.2.5.1 by preparing an overnight culture and resuspending in RPMI-1640 media. Acknowledgements are made to Olutoba Sanni who prepared and measured optical density of wells containing contaminants over a 24-hour period.

4.2.6.1 Polymer Toxicity Testing

For testing the toxicity of synthesised polymers, a black 96-well was filled with 20 µL of monomer with 1 % w/v photoinitiator (DMAP) to cover the bottom of the well-plate. Each monomer was deposited into three individual wells to give bacterial repeats. The source plate was then placed directly under a UV light source for 45 minutes in an argon environment to polymerise the deposited monomer. The well-plate was then placed into a vacuum oven for 7 days to simulate the same process as performed with polymer microarrays. After 7 days, the wells were filled with 200 µL of RPMI-1640 media that had been inoculated with *P. aeruginosa* which had been made to a concentration of OD_{600} = 0.01. Two controls were included during the experiment which included wells that only contained the bacteria in RPMI media as a positive control and wells that had only RPMI media as a negative control. The well-plate was then placed into a TECAN plate reader for 24 hours, where the optical density was measured every 30 minutes to monitor the growth of bacteria over a 24-hour period. Analysis of the data was performed in Microsoft Excel, where the average and standard deviation was plotted over the 24-hours and compared to the controls placed in the well-plate.

4.2.6.2 Toxicity of Transesterification Reagents

More toxicity experiments were performed to investigate the effect of any residual alcohol/methacrylate leftover from the synthesis process. Concentrations were determined based upon the concentrations that could be seen in an incubation of a polymer microarrays. As each polymer spot deposited was approximately 1 nL in volume, and a polymer microarray can consist of 2000 spots, assuming 0 % conversion, the concentration of the total incubated solution can be calculated to be 0.1 µL/ml, as each polymer microarray is incubated in 20 ml of RPMI-1640 media. The concentrations chosen were therefore 1 µL/ml, 0.5 µL/ml, 0.1 µL/ml, 0.05 µL/ml and 0.01 µL/ml. This allowed for the assessment of an order of magnitude above and below the worst-case scenario for monomer conversion. Each well was filled such that 200 µL of liquid was contained within the well, and each well was inoculated with *P. aeruginosa* (PA01) such that the OD_{600} was measured to be 0.01. Two controls were included during the experiment which included wells that only contained the bacteria in RPMI media as a positive control and wells that had only RPMI media as a negative control. The 96-well plate was then placed into the TECAN plate reader to measure the optical density at 600 nm every 30 minutes over a 24-hour period. Analysis of the data was performed in Microsoft Excel, where the average and standard deviation was plotted over the 24-hours and compared to the controls placed in the well-plate.

4.2.7 CyDMA Work up and polymerisation

After CyDMA had been identified on the polymer microarrays as a potential hit material, the monomer was purified using column chromatography, where a solvent system of 60:1 (hexane: ethyl acetate) was used to remove fractions. The fractions were

monitored using TLC (thin-layer chromatography) and fractions with pure CyDMA were collected and characterised using NMR spectroscopy. Once the monomer had been separated, a free-radical polymerisation was used by adding 500 mg of CyDMA and 500 µl of toluene with 1 % (w/v) AIBN as a thermal initiator. Prior to heating the reaction was degassed under argon for 30 minutes. The reaction was performed at 80 $^{\circ}$C for 4 hours, at which point the reaction was removed from heat and quenched in a freezer and the conversion of the reaction determined by NMR from the crude product by comparing the monomer and polymer peak integrals. The polymer was precipitated by dropwise addition to cold methanol. The molecular weight of the polymer was determined using a Polymer Laboratories GPC 50 instrument (gel-permeation chromatography). A calibration curve was made using polystyrene standards with a range of 443 000- 132 g mol^{-1} and data was analysed using Polymer Labs Cirrus 3.0 software.

4.2.8 Catheter Dip-Coating

Sections of silicone catheters were manually dipped into a silicone primer which was used to coat the surface of the catheter such that polymer solutions would adhere to the surface. After drying for 1 minute, the catheters were manually dipped into a 30 % w/v polymer solution in dichloromethane (DCM). The catheter sections were left to dry for 5 minutes before being dipped a further 2 times using the same drying protocol in-between dips. After the final drying procedure, catheters were left to dry at ambient conditions for 24 hours before placing into a vacuum oven (0.325 mbar,RT) to dry for a further 7 days before bacterial incubations were performed. Catheters were prepared with coatings of CyDMA, EGDPEA:DEGMA and iBnA:triEGMA using this manual dip-

coating procedure. Both iBnA and EGDPEA have been previously identified as hit materials for reducing bacterial attachment to urinary catheters.[6,45]

4.2.9 Bacterial Attachment Studies on Catheter Sections

Acknowledgements are made to Olutoba Sanni, who performed bacterial culture experiments on catheter sections and measured bacteria adhesion using confocal microscopy.

4.2.9.1 Bacterial incubation of catheter sections

Sections of CyDMA, EGDPEA:DEGMA, iBnA:triEGMA, Bardex® I.C. Aquafil with a hydrogel and silver alloy coated catheter and silicone catheters were incubated to observe the bacterial attachment of *P. aeruginosa* and *P. mirabilis*. For incubating the catheters in a bacterial culture of either *P. aeruginosa* or *P. mirabilis*, the same protocol was used as described in 4.2.5.1. However, the catheter sections were incorporated in the same petri dish for comparing between samples. Two biological repeats were performed for both *P. aeruginosa* and *P. mirabilis*.

4.2.9.2 Washing Protocol

The washing of the catheters was performed using the same methodology for the polymer microarrays outlined in 4.2.5.2.

4.2.9.3 Confocal microscopy of catheter samples

After the washing of the catheter sections, the samples were immediately imaged using a Zeiss AxioObserver Z1 confocal microscope. Samples were imaged using a x10 objective (NA = 0.3) with the wavelength of the Ar/Kr laser set at 555 nm. A laser power of 1 mW was used with a gain of 800 for imaging both mcherry-tagged *P. aeruginosa* and DSRed tagged *P. mirabilis*. The aperture size was defined as 1 AU which equates to 34.1 μm. Images were then processed through ZEN 2009 software, were the maximum intensity z-project images were

selected. Images were then processed in ImageJ were a threshold was used to remove sources of noise from the image. The percentage coverage was then calculated from these images and used as a measure to determine bacterial attachment to the catheter surface.

4.3 Results

4.3.1 Alpha Predictions of Monomers Resistant to Bacterial Attachment

4.3.1.1 *Alpha* model Predictions

A total of 4 synthesised monomers and 8 commercially available monomers were used for the printing of the *alpha* microarray, leading to 61 polymers by sequential mixing of 9 monomers with tBCHA at ratios of 1:0, 5:1, 2:1 and 1:1 and 3 monomers were mixed with tBCHA at 1:0 and 1:1 only.

a

Material (% Conversion)	Prediction
CyDMA (92)	-5.47
GMA (84)	-2.13
LMMA (69)	-3.51
DdMA (90)	-1.47
EGPhEA*	-0.07
BnMA*	-1.06
CHMA*	-2.09
PhMA*	-1.17
HPhOPA*	1.1
NpMAe*	-2.4
MEdMSPNH*	n/a
tBCHA*	-2.81

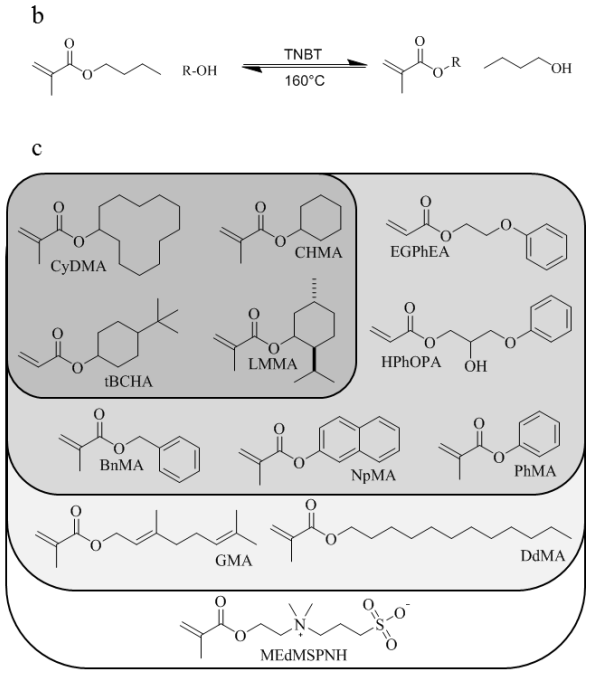


Figure 4.3: a) Conversion rates of synthesised monomers and predictive bacterial adhesion value based upon alpha-predictive value. (*) Signifies commercially obtained monomer. b) Reaction scheme for the transesterification reaction at 160 °C with titanium butoxide (TNBT) catalyst. c) Library of 12 materials used, with linear, cylcic aromatic, zwitterionic and cyclic pendant groups. NpMA and MEdMSPNH were mixed with tBCHA at ratios of 1:0 and 1:1, whilst nine other materials were mixed sequentially with tBCHA at ratios 1:0, 5:1, 2:1 and 1:1.

The *alpha* values of the monomers used and their associated chemical structures are shown in Figure 4.3. The monomers

were chosen to include a large range of *alpha* values that should give a large range of bacterial performances. HPhOPA had the largest *alpha* value of 1.1 whilst the lowest *alpha* value was -5.47 for CyDMA, which was synthesised using the transesterification process shown in Figure 4.3b and described in detail in Chapter 3. This meant that the range of bacterial attachment data was predicted to have the largest attachment on HPhOPA and the smallest attachment on CyDMA, with a large range of materials inbetween.

4.3.2 Production of Polymer Microarrays (IMSTAR + ToF-SIMS)

An initial imaging of polymer microarrays was performed to observe the polymer spots under bright field microscopy prior to being dried for 7 days. This allowed an initial check to observe if any obvious signs of misprinting/spreading occurred.

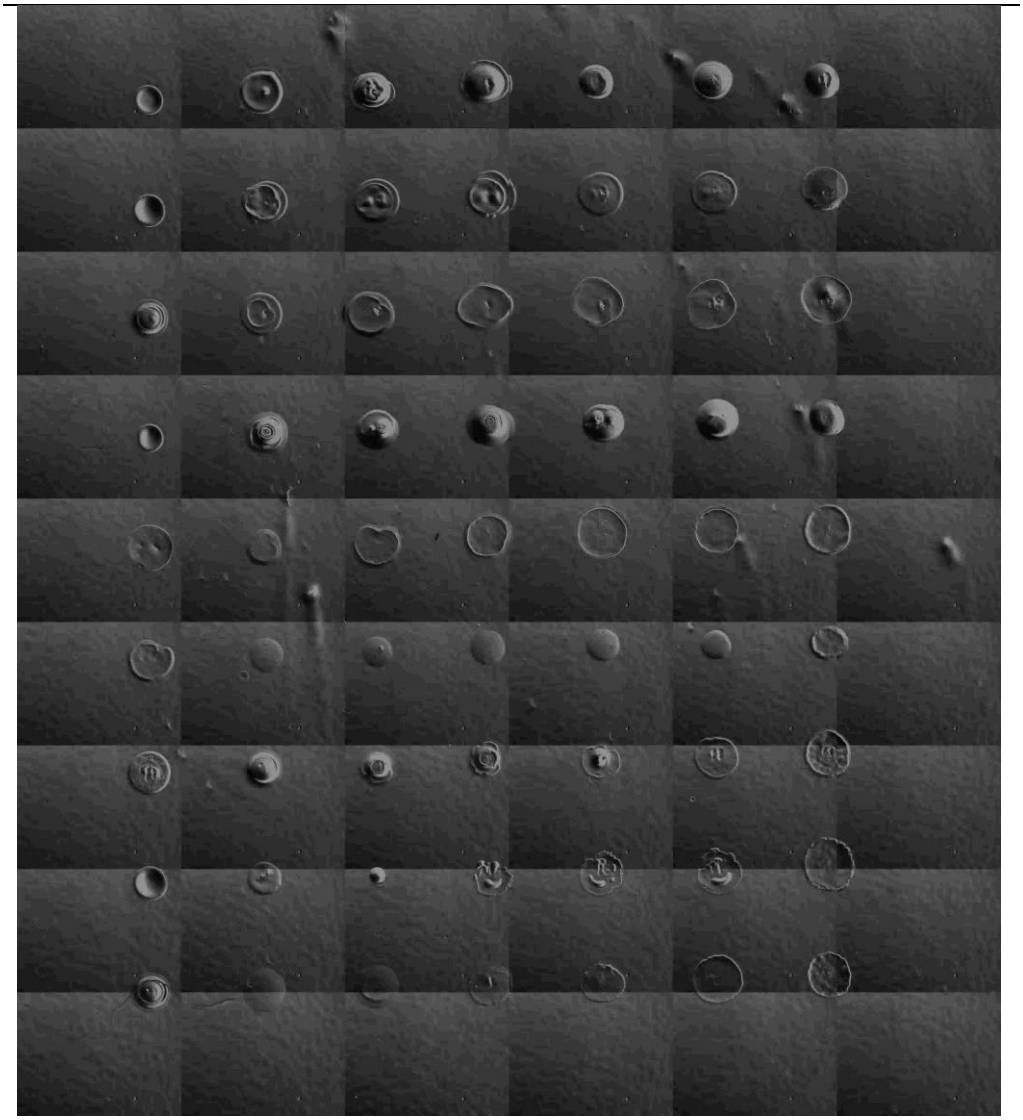


Figure 4.4: Phase contrast microscopy image of polymer microarray, used to identify if polymer spots have been successfully deposited onto the pHEMA surface

No obvious signs of polymer solutions spreading into one another were observed however there was signs of inconsistent printing by the varying size of the polymer spots Figure 4.4, but to confirm any possible spreading issues, a polymer microarray was placed into the ToF-SIMS, where characteristic ions could be detected to determine the surface chemistry of the polymer spots. Figure 4.5 shows a characteristic ion (45.04 u, $C_2H_5O^+$) associated to the pHEMA substrate material, which shows dark areas where the polymer spots were situated. In all cases

polymer spots were entirely surrounding by regions high in intensity for the ion $C_2H_5O^+$. This confirmed that polymer spots did not spread and remained distinct from each other.

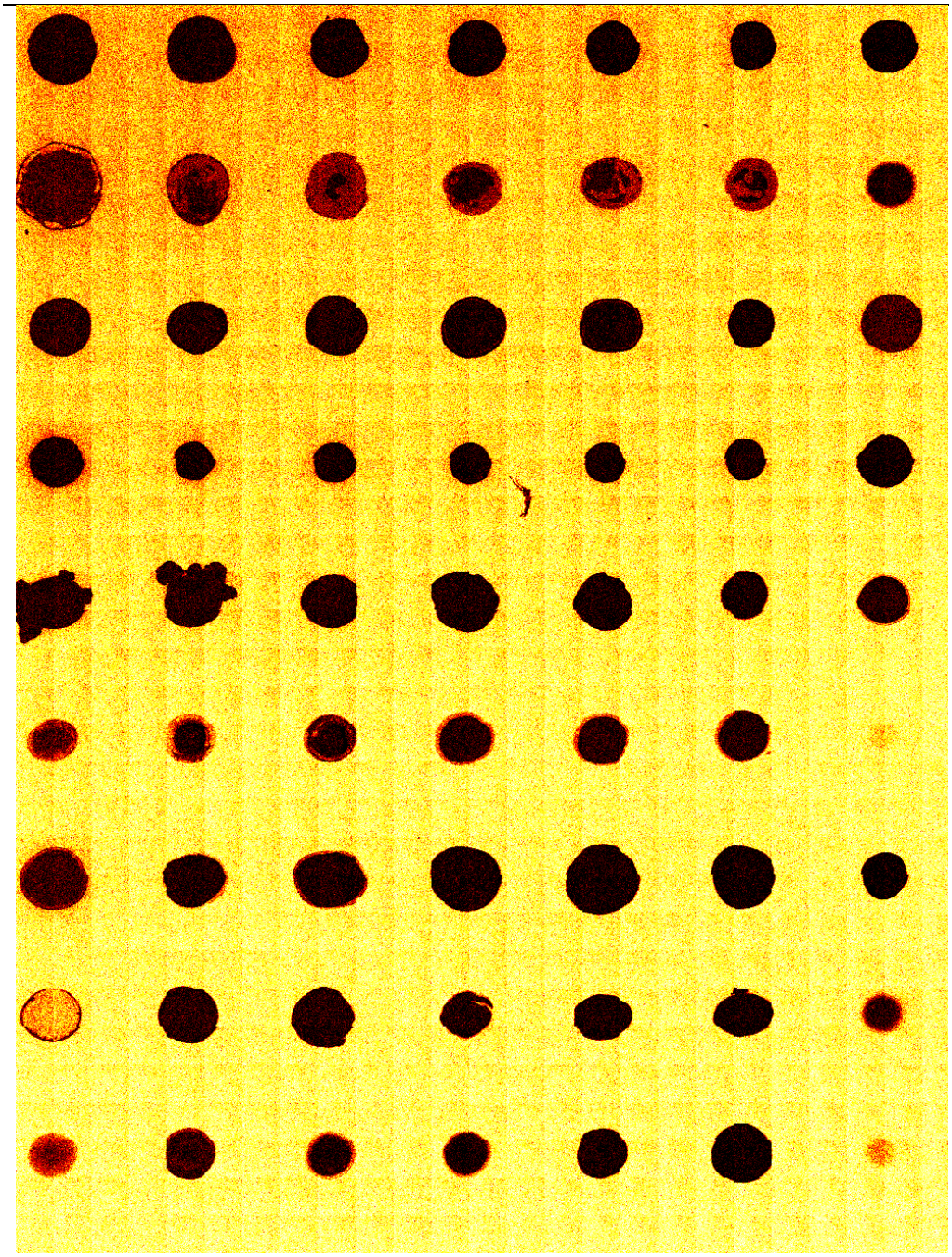


Figure 4.5: Ion map image showing the $C_2H_5O^+$ ion associated to pHEMA, the substrate material upon which the polymers are printed.

Following this, characteristic ions for each monomer was identified and used to compare the monomer feed ratio to the actual ratio of the monomer combination at the surface of the polymer. The ions used for identifying monomers are listed in Table 4.1.

Material	Unique Ion	Unique Ion (R^2)	tBCHA Ion	tBCHA Ion (R^2)
CyDMA:tBCHA	$C_{12}H_{23}O^-$	0.98	$C_4H_9^+$	0.85
HPhOPA:tBCHA	$C_6H_5O^-$	0.85	$C_4H_9^+$	0.89
PhMA:tBCHA	$C_7H_5O^+$	0.96	$C_4H_9^+$	0.74
EGPhEA:tBCHA	$C_6H_5O^-$	0.52	$C_4H_9^+$	0.74
LMMA:tBCHA			$C_4H_9^+$	0.92
GeMA:tBCHA			$C_4H_9^+$	0.63
BnMA:tBCHA	$C_7H_7O^-$	0.78	$C_4H_9^+$	0.94
DdMA:tBCHA	$C_{12}H_{23}O^-$	0.91	$C_4H_9^+$	0.79
DdMA-Commercial:tBCHA	$C_{12}H_{23}O^-$	0.77	$C_4H_9^+$	0.74
CHMA:tBCHA			$C_4H_9^+$	0.8
NpMA:tBCHA	$C_{10}H_7O^-$	0.92	$C_4H_9^+$	0.93

Table 4.1: Table of ions identified by ToF-SIMS for associated monomer materials to identify how the feed ratios compared to the actual monomer ratios

Using these ions, it was then possible to look at the linearity of the ion concentration with increase monomer feed ratio as shown in Figure 4.6.

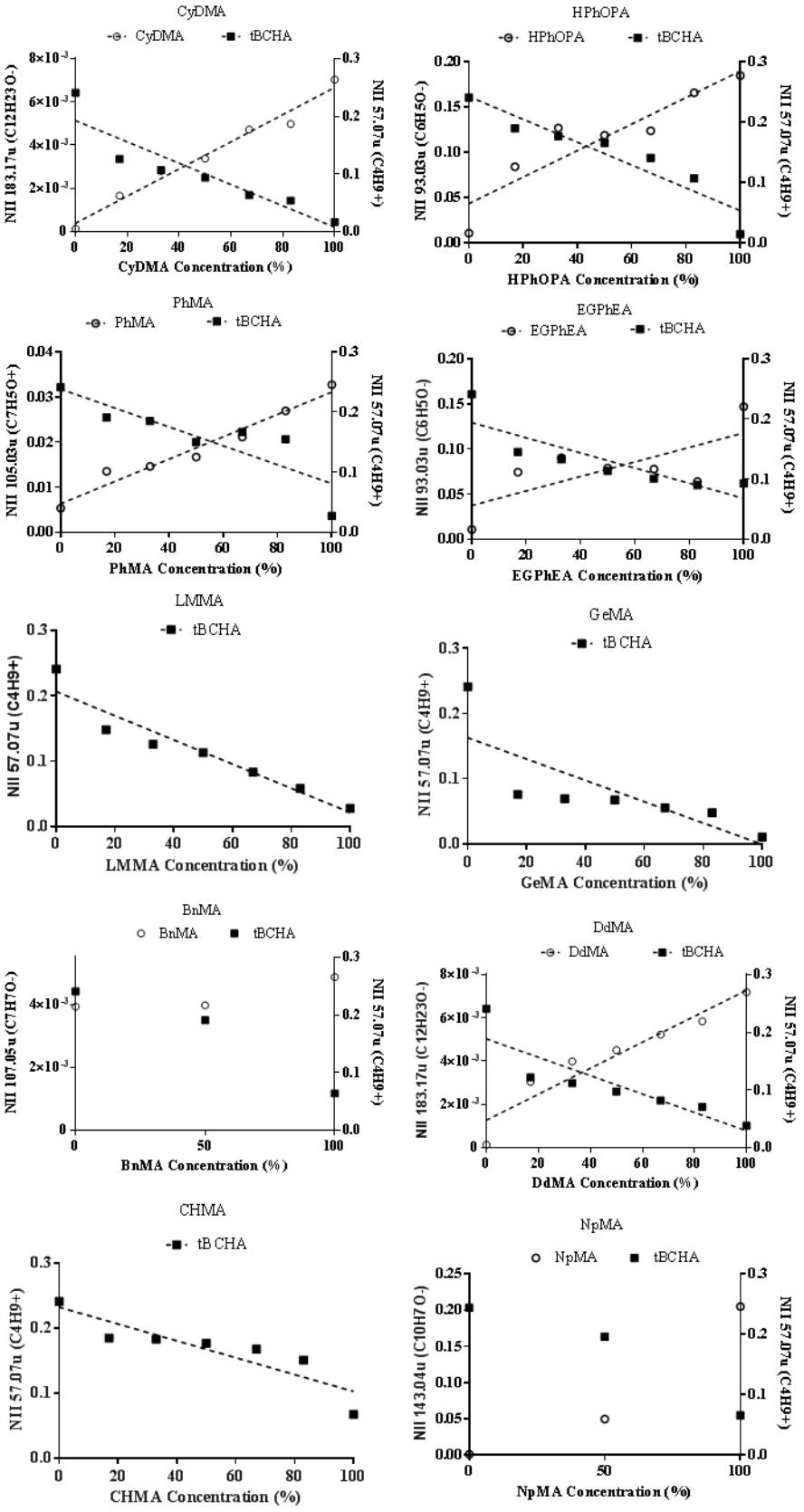


Figure 4.6: Series of diagrams showing mixing of copolymer series where ■ designates ion associated to tBCHA (C4H9+) and ○ designates an ion associated to a) CyDMa b) HPhOPA c) PhMA d) EGPhEA e) LMMA f) GeMA g) DdMA h) CHMA i) BnMA or j)

NpMA. Copolymer series which had poor mixing were not compared with *alpha* in copolymer data

Each copolymer series was analysed to observe the correlation between the feed monomer ratios and the observed monomer ratios under ToF-SIMS (Figure 4.6). Materials than had an average R^2 less than 0.8 (EGPhEA and GeMA) were excluded from co-polymer analysis for the *alpha* parameter. The lower R^2 values could be explained due to the matrix effect,[168] but as the chemical matrix is very similar and comprised of hydrocarbon chemical species, it is unlikely that the change of ion concentration across the copolymer series is entirely because of matrix effects. For this reason, a high R^2 threshold was used to slightly account for any possible matrix effects that could affect ion concentration being collected in the mass analyser. Due to the increased size of polymer microarray A2, there were problems with the printing runs where polymer arrays were not successfully printed (Appendix O) and also after ToF-SIMS analysis of a successfully printed array, there was a large source of fluorine contamination (Appendix P).

4.3.3 Primary screening of novel methacrylate monomers

After characterising the surface chemistry of the polymer microarrays, the slides were incubated in both *P. aeruginosa* and *P. mirabilis* and screened using the Genepix 4000L to determine the bacterial attachment to the polymer spots by observing the fluorescence associated with bacterial attachment and biofilm formation. Initial analysis involved observing the trend of the homopolymer library and seeing how they correlated with the *alpha* parameter (Figure 4.7).

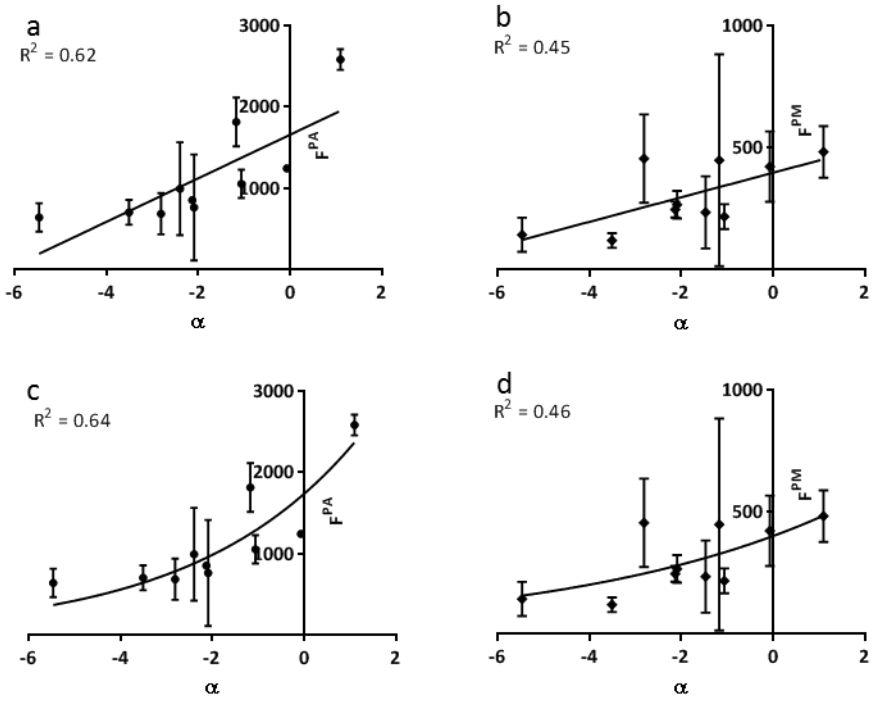


Figure 4.7: Bacterial fluorescence relationship for a) *P. aeruginosa* homopolymer relationship (R^2 = 0.62), b) *P. mirabilis* relationship (R^2 = 0.45) c) *P. aeruginosa* homopolymer relationship (R^2 = 0.64) with an exponential growth fit and d) *P. mirabilis* relationship (R^2 = 0.46) with an exponential growth fit. All experiments were conducted with N = 3 technical repeats

A linear correlation between the *alpha* parameter and bacterial adhesion was shown to be R^2 = 0.62 and R^2 = 0.45 for both *P. aeruginosa* and *P. mirabilis* respectively. The datasets were also analysed using an exponential growth fit (R^2 = 0.64 for *P. aeruginosa* and R^2 = 0.46 for *P. mirabilis* respectively), and this better represents the bacterial adhesion at lower *alpha* values, as it is impossible to obtain negative attachment as the linear model would suggest. The average coefficient of variance was calculated to be 27 %/39 % for each bacterial species data set respectively, suggesting that both models performed well considering the bacterial variance within the data. The correlation for *P. aeruginosa* identified a positive trend for *alpha*, with CyDMA being identified as a low attachment material. CyDMA was further identified as a hit material for

reducing the bacterial attachment of *P.* mirabilis, however the trend between bacterial adhesion and *alpha* was weaker, but still successfully identified materials that promoted/reduced bacterial attachment. To further test the *alpha* parameter, the copolymer bacterial data was analysed, shown in Figure 4.8.

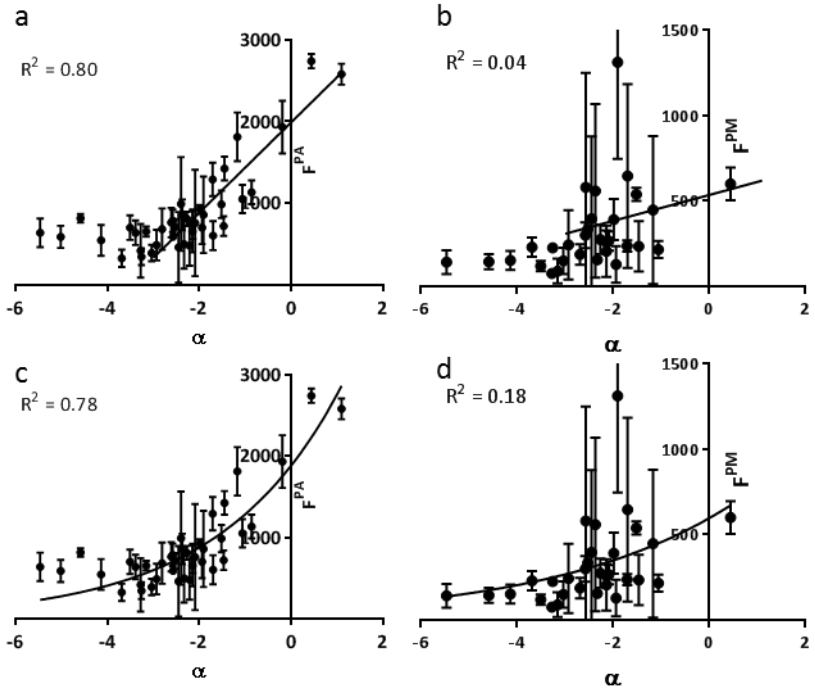


Figure 4.8: Copolymer data showing correlation between *alpha* and (a) Copolymers incubated in *P aeruginosa* and (b) Copolymers incubated in *P. mirabilis*. *P. aeruginosa* data shows a strong trend (R^2 = 0.80) over the reported range of *alpha* as reported by Sanni et al. c) *P. aeruginosa* copolymer relationship (R^2 = 0.78) with an exponential growth fit across whole dataset and d) *P. mirabilis* copolymer relationship (R^2 = 0.18) with an exponential growth fit across the whole dataset. All experiments were conducted with N = 3 technical repeats

A correlation of the known limits of the *alpha* parameter were included (from between -3 and 1.1 as reported by Sanni et al[6]), and the correlation shown for *P. aeruginosa* was shown to have good correlation with an R^2 = 0.80. Once the *alpha* value exceeded this point, the bacterial attachment plateaued, which could be either due to reaching the limit of detection of the experiment, or that no bacteria are now adhering to the sample

surface. A high correlation was shown with an exponential growth fit curve (R^2 = 0.78) between *alpha* and the adhesion of *P. aeruginosa* across the whole data set, which suggests that the bacterial fluorescence becomes non-linear as the fluorescence values approach zero. The screen for *P. mirabilis* however was shown to have no correlation across the same range with an R^2 = 0.04, and this was only marginally improved when using the exponential growth model (R^2 = 0.18). This suggests that *alpha* has a limit in not being able to successfully predict bacterial adhesion for *P. mirabilis.*

4.3.4 Bacterial Growth Studies of Synthesis Polymers

To test the toxicity of synthesised materials, materials were polymerised to the bottom of 96-well plates and the growth of *P. aeruginosa* was measured over 24 hours in LB media.

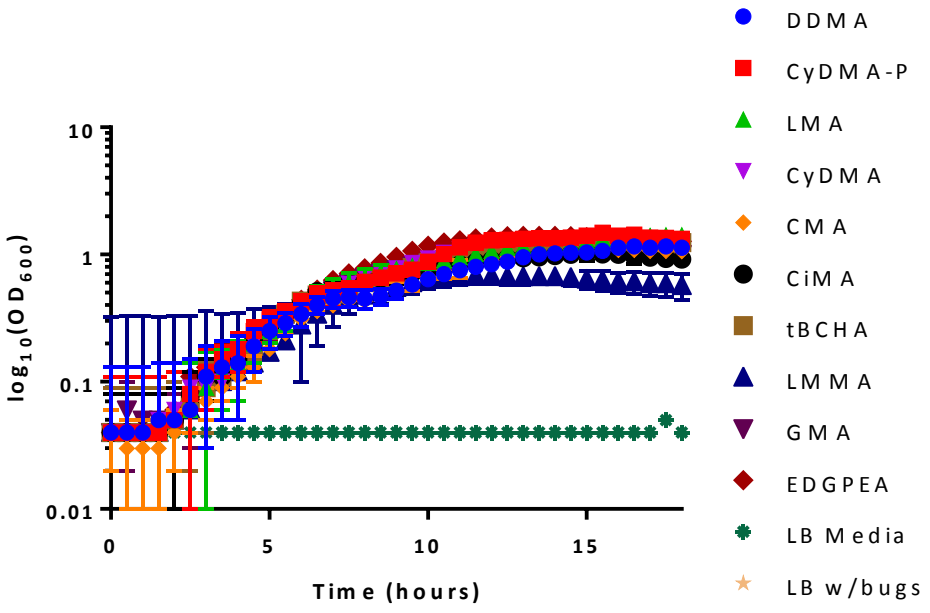


Figure 4.9: Use of TECAN plate reader to monitor the growth of *P. aeruginosa* through measuring the optical density. Range of different synthesised polymers were observed along with commercially available materials and controls which included only LB media and LB media with bacteria but no polymer.

Figure 4.9 showed how most of the polymers allowed for the growth on *P. aeruginosa* at the same rate as the control that included no polymer, as majority of materials were shown to be not significant when observing the growth after 24 hours using a 1-way ANOVA at the 95% confidence interval. The only exception to this was LMMA, which showed a slight decrease over time compared to the rest of the polymers, and this gave a p-value of 0.0003 when a t-test compared the bacteria control and LMMA after 24 hours showing a statistical difference. An example of purified CyDMA was also used and compared to the crude synthesised mixture which was used on the polymer microarray, and no effect to the bacteria was observed.

4.3.5 Bacterial Growth Studies of Transesterification Synthesis Reagents

A further test was conducted to observe the effects of possible contaminants arising from the transesterification synthesis protocol. A range of different reagents were tested including BMA (butyl methacrylate), BuOH (n-butanol), DdOH (Dodecanol) and LMA (lauryl methacrylate). The monomers were included in their unpolymerized form to test if any leftover residual monomers would influence the growth of the bacteria.

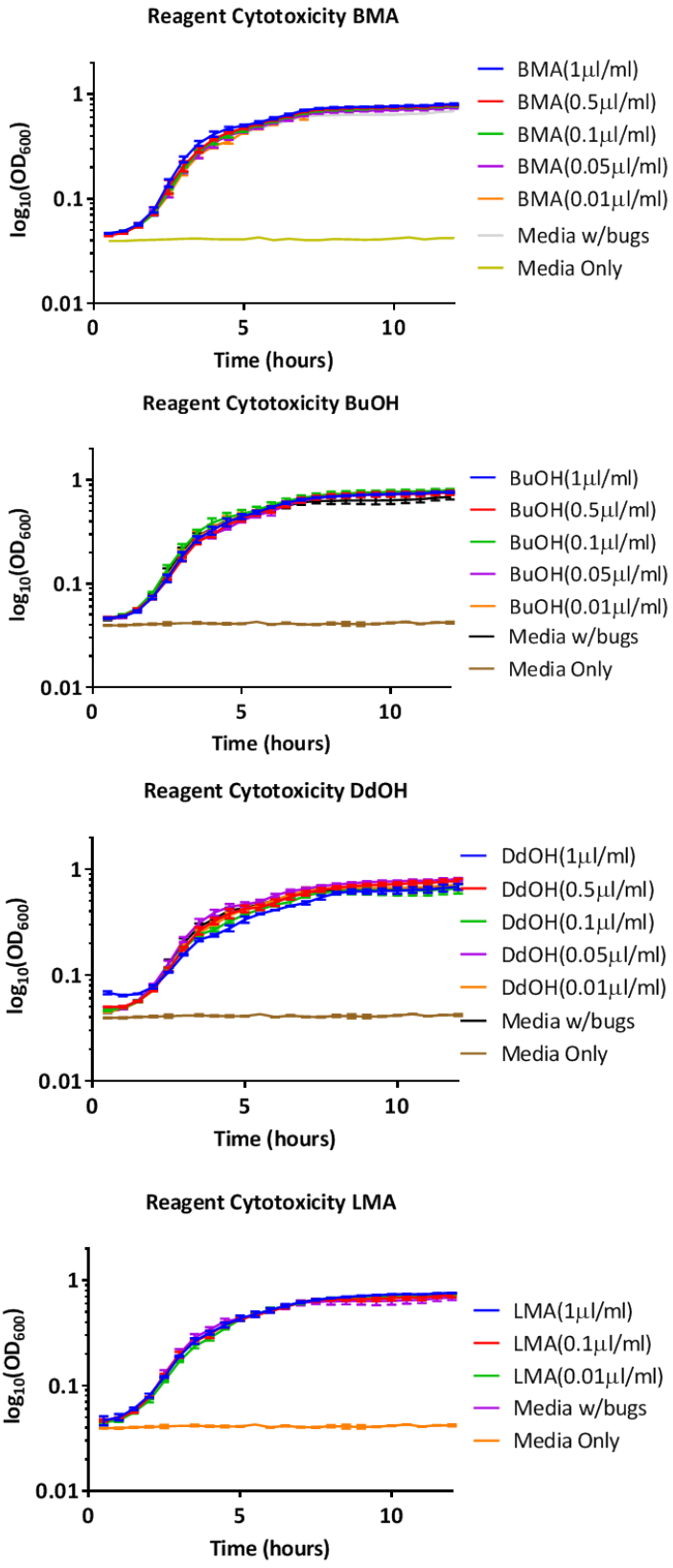


Figure 4.10: Figures showing the growth of *P. aeruginosa* with the presence of contaminations found from transesterification experiments at varying concentrations. (a) Butyl methacrylate

(b) n-butanol (c) dodecanol (d) lauryl methacrylate. Each result was comprised of N = 3 samples

As shown in Figure 4.10, the concentrations of unreacted reagents likely to be found in the incubation of polymer microarrays (0.1 µl/ml) was shown to not influence the growth of *P. aeruginosa*. The effect of DdOH (1 µl/ml) on bacterial growth showed the largest variance over the 24 hour incubation, but no statistical difference was found compared to the positive control with only bacteria (p-value = 0.8).

4.3.6 Scale up of CyDMA hit material for coating medical devices

To test CyDMA, which was identified as a hit material with the polymer microarray screen, the monomer was purified using column chromatography and analysed using NMR. Both ^{1}H and ^{13}C NMR was performed to identify the total number of protons within the monomer as well as making sure that the correct amount of CH and CH_3 peaks were observed.

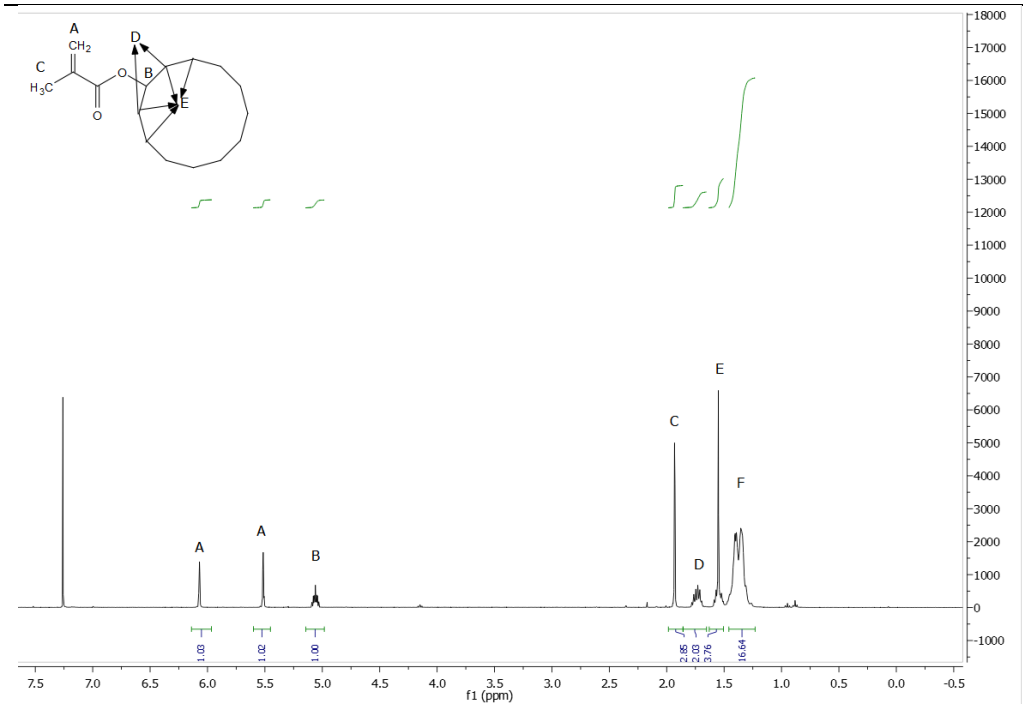


Figure 4.11: ^{1}H NMR of purified CyDMA. Summation of peaks totals a proton number of 28, corresponding to CyDMA structure expected. Assignment of peaks showing the (A) protons associated to C=C bond in methacrylate group (B) proton adjacent to ester group in ring structure (C) methyl group adjacent to acrylate group and (D,E,F) protons associated to carbons within the ring structure.

The NMR spectra identified protons in the expected areas of the spectrum, with methylene peaks and proton next to the ester group at high shifts with a large amount of smaller shifted protons. Figure 4.11 showed that the number of protons within the structure to be 28, which corresponds to the expected proton number from the structure of CyDMA. To further characterise the synthesised monomer, DEPT 45,90 and 135 spectrums were obtained to check that the expected carbon peaks were observed.

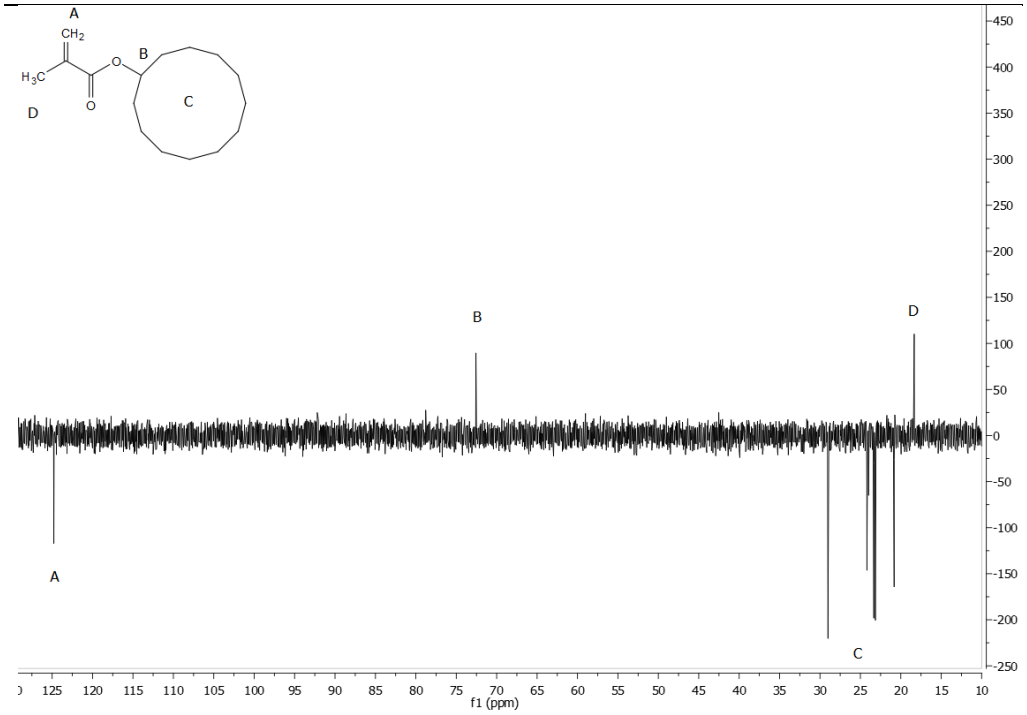


Figure 4.12: DEPT 135 spectrum showing assigned carbon numbers to CyDMA structure. Only two peaks for CH and CH_3 were observed, which correspond to the carbon next to the ester group in the cyclic ring structure (B) and the end methyl group (D). CH_2 peaks were identified which were associated to the C=C bond in the methacrylate group (A) and protons associated to the large ring structure (C)

The DEPT 135 spectrum (Figure 4.12) was obtained. Only one CH and one CH_3 group were detected (shown in the positive y-axis), which corresponds to the carbon next to the ester group in the cyclic structure and the end methyl group. The carbon next to the ether group in the cyclic structure would be expected to have a larger chemical shift compared to the CH_3 group and this was confirmed using a DEPT 90 spectra shown in Figure 4.13, with a peak at 72 ppm detected.

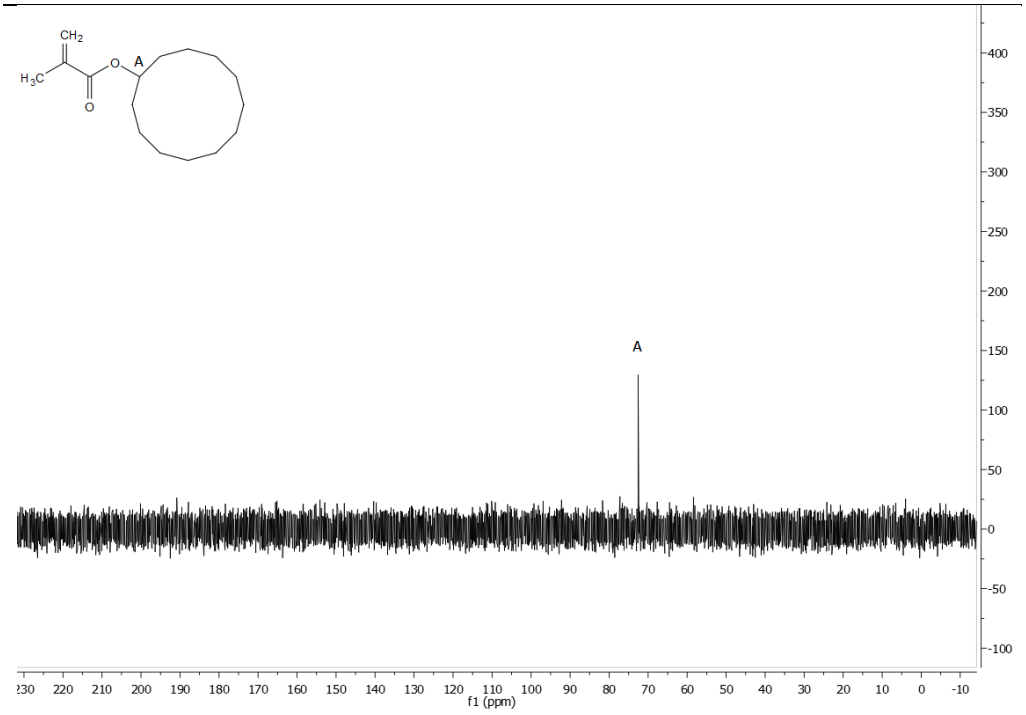


Figure 4.13: DEPT 90 NMR spectra showing the single CH peak in the CyDMA structure, which refers to the carbon next to the ester group in the cyclic structure, which is also the carbon that changes the chemical environment under transesterification synthesis experiments.

This was evidence that CyDMA had been successfully purified, as all peaks identified with the CyDMA structure and no unexplained peaks were found. After purifying CyDMA, the material was thermally polymerised using a free-radical polymerisation protocol and the crude mixture was again tested using NMR to identify the conversion of the synthesis process (Figure 4.14)

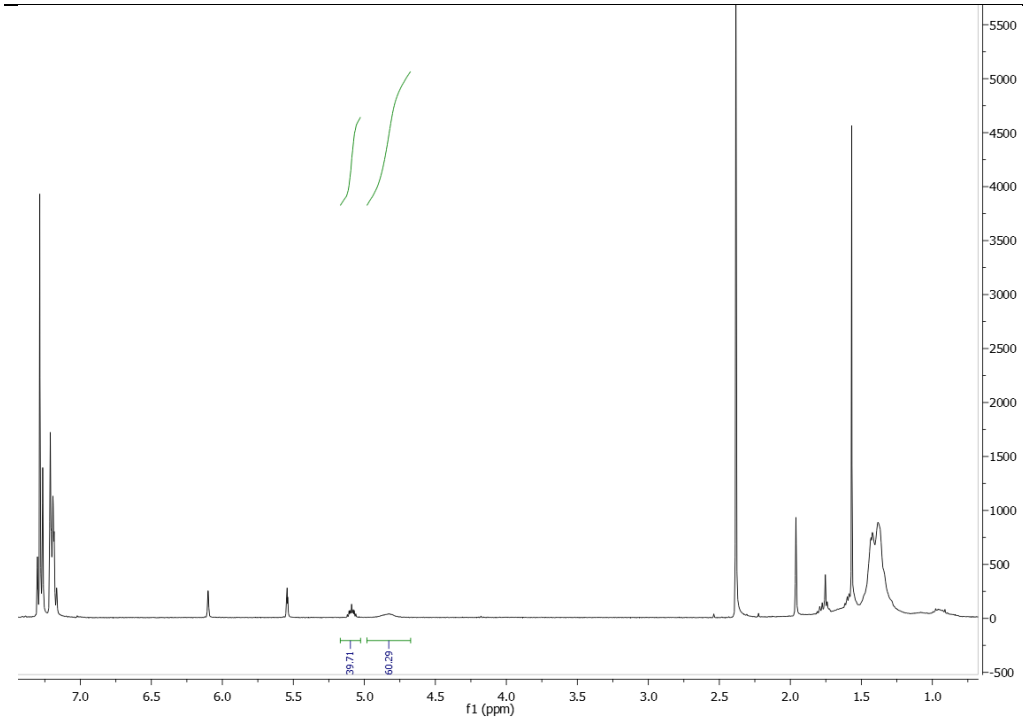


Figure 4.14: NMR of crude polymerisation mixture of CyDMA, showing a conversion of 60 %

The peak broadening associated to the polymerisation of CyDMA showed that the conversion of the polymerisation was 60 % when compared to the remaining unreacted monomer, and this mixture was then precipitated twice in cold methanol to separate the polymer from remaining monomer. GPC was used to characterise the polymer which was shown to have a M_n = 318 kDa and a polydispersity of 1.473. After drying in a vacuum oven, a 30 % polymer solution in DCM was made to coat catheter sections.

4.3.7 Bacterial Attachment of CyDMA to Urinary Catheters

Catheter sections were dip-coated with CyDMA and incubated in *P. aeruginosa* and *P. mirabilis* to observe the bacterial adhesion to the polymer coatings at a larger scale and compared against EGDPEA:DEGMA, iBnA:triEGMA, Bardex® I.C.

Aquafil with a hydrogel and silver alloy coated catheter and silicone catheter sections (Figure 4.15).

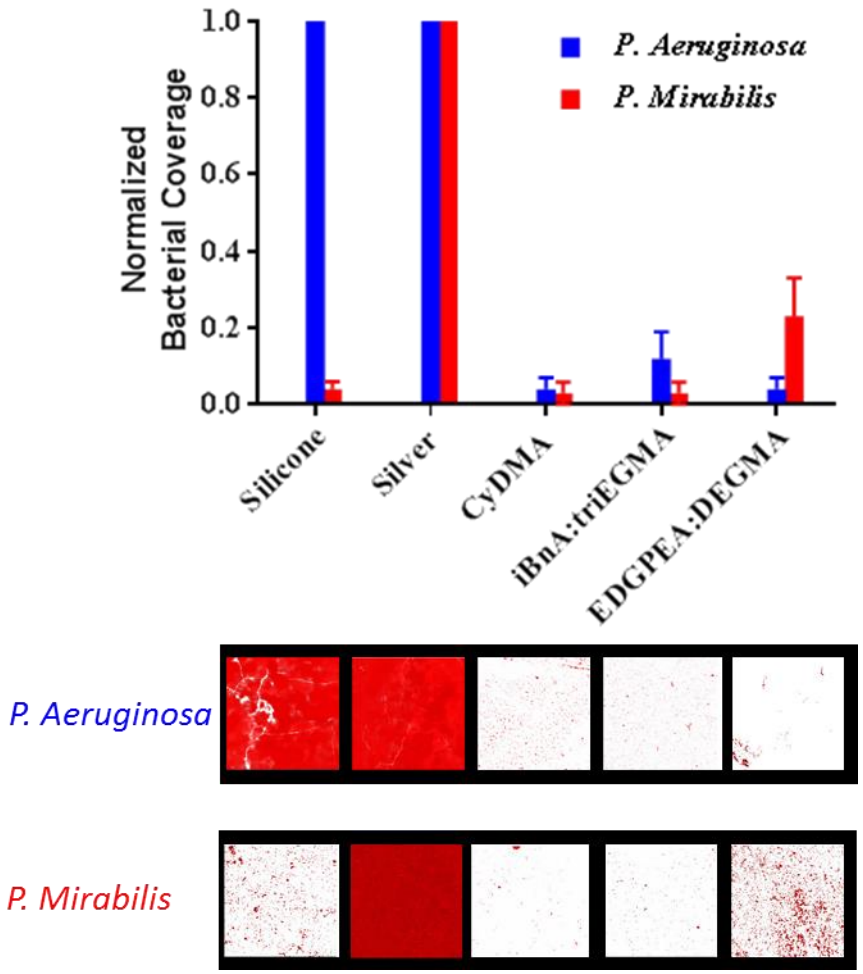


Figure 4.15: Confocal microscopy data of attachment of *P. aeruginosa* and *P. mirabilis* to sections of coated catheters. CyDMA showed to reduce attachment of both bacterial species compared to other identified hit materials and commercial controls. Each measurement was comprised of N = 6 measurements with 2 biological repeats

After incubation, the catheter sections were imaged using confocal microscopy. To allow comparison between different biological repeats the results were normalized against the Bardex® I.C. Aquafil with a hydrogel and silver alloy coated catheter control sample. The Bardex Aquafil section catheter showed high adhesion of both bacterial species. EGDPEA: DEGMA showed a normalized attachment of 0.04 ± 0.03, which

was the same as CyDMA for the attachment of *P. aeruginosa,* however CyDMA showed a high efficacy for also reducing the attachment of *P. mirabilis* (0.03 ± 0.03), which was comparable to silicone (0.04 ± 0.02) and iBnA:triEGMA (0.03 ± 0.03). Therefore, CyDMA was the only material that showed a high efficacy for reducing bacterial adhesion of both bacterial species to medical devices.

4.4 Discussion

4.4.1 Monomers predicted to reduce bacterial attachment

A key aspect of this project was to investigate the non-commercially available chemical space. As this is a vast space, a certain direction was required to be able to search for potential hit materials for reducing bacterial attachment in a productive manner. This was done by using the reported quantitative structure-activity relationship reported by Sanni et al, which correlated the molecular flexibility and hydrophobicity of a monomer to the ability of bacteria to adhere to the surface of the polymer using the parameter *alpha*. The bacterial attachment to a virtual library of polymers could then be predicted by calculating *alpha* from their structures, identifying candidate materials that experimental time and effort should be invested in. In this study, this approach was tested by first using alpha to select materials predicted to have a range of bacterial attachment performances (Figure 4.3). These materials were synthesised as described in Chapter 3. CyDMA was shown to be the material predicted to resist the attachment the most with an *alpha* value of -5.47, whereas HPhOPA (a commercial material), was shown to have an *alpha* value of 1.1 and therefore the material predicted to cause the highest attachment of bacteria. The simplicity of the *alpha* value allowed for a predictive hit material library to quickly be assembled. This promotes the approach of biased screening where specific materials can be tested for an application with confidence that a successful hit material will be discovered.

4.4.2 Printing of polymer microarray and characterisation of surface chemistry

Confirmation of successful microarray printing was performed in a couple of ways. An initial quick test was to use bright field microscopy to view that spots could be physically seen on the surface of the microarray and this was shown in Figure 4.4. However, it was not possible to see how well the spots formed and if the spots spread across the surface, as the microscopy image gives no chemical information of the surface. For this, it was necessary to use a technique which has chemical sensitivity to see if the materials have formed discrete spot formation instead of a mixture of materials on the surface of the microarray, and this was shown in Figure 4.5 by using ToF-SIMS. Figure 4.5 showed an ion map of the positive ion $C_2H_5O^+$ which is a characteristic ion of pHEMA which is the substrate material,[169] and not present in any of the other monomers used. This then showed how the dark regions of the microarray were contained into discrete areas and not overlapping with each other, showing how they were separated with regions of pHEMA and hence not spreading across the substrate surface. It was also seen that the spots were forming with different sizes relative to one another, which is likely due to the different hydrophobicity and viscosity properties of each polymer. This would cause materials to spread differently compared to one another and hence producing a range of diameter spots. The ToF-SIMS spectra were then used to identify key characteristic ions for each material which can be used to produce graphs to observe how the ratio of monomers over a co-polymer series varied when compared to the feed ratio. Due to effects such as phase separation[170] it was possible to observe some copolymer series where a non-linear trend was observed between the ion

intensities and the feed ratio, suggesting that one material was preferentially segregated to the surface compared to the other copolymer component. This would give us misleading results when observing the bacterial adhesion to the surface and correlating this to *alpha*, as the surface was no longer representative of the initial feed ratio. However, this non-linear relationship could be explained by matrix effects, however as the copolymer matrix was comprised of similar hydrocarbon structures,[168] it is unlikely that the ion concentration would be largely deviated because of this. Therefore, copolymers with an average R^2 value less than 0.8 were excluded from subsequent copolymer analysis, and this was shown in Figure 4.6.

4.4.3 Extrapolating *alpha* parameter to discover novel hit materials

The previous report by Sanni *et al*, which described the *alpha* parameter, described a parameter which worked for a range of materials from an *alpha* value of -3.5 and 1.1. Also, this was only performed for the bacterial attachment of *P. aeruginosa*. By using the model to predict materials that could prevent the attachment of *P. aeruginosa*, the range of the previous report could be extrapolated, which was done with the synthesis of CyDMA which had an *alpha* value of -5.47. The model was also extrapolated by incubating in *P. mirabilis* as well as *P. aeruginosa*. Figure 4.7 showed the attachment of both *P. aeruginosa* and *P. mirabilis* for the homopolymer materials on the microarray. A correlation between the *alpha* value and the fluorescence intensity for *P. aeruginosa* was observed, where the largest *alpha* value, HPhOPA, was also observed to show the highest fluorescence value and CyDMA, which had the lowest *alpha* value was shown to have the lowest fluorescence value. The R^2 of the correlation between *P. aeruginosa*

attachment and *alpha* graph was 0.62, suggesting that the *alpha* value was able to capture 62% of the variance within this data set. The average coefficient of variance was calculated to be 27 % and therefore the alpha model was shown to be working well when considering bacterial variance within the data. This is consistent with the previous work presented by Sanni et al.[6] Analysing the copolymer data for *P. aeruginosa* showed a poorer trend (R^2 = 0.57) across the entire range of data when correlating with *alpha*. However, when observing the data between -3 and 1.1, which was the range observed by Sanni et al[6], the correlation of the series increased to give an R^2 of 0.80, showing very good agreement with the structure-activity relationship. The plateauing of the bacterial adhesion at lower values of *alpha* could be explained by reaching an experimental sensitivity threshold. As the bacterial adhesion reduces, the sensitivity of the experiment will determine the minimum threshold that can be detected and trivially, the bacterial fluorescence cannot become negative, and therefore it is likely that the bacterial adhesion would tail off with decreasing *alpha* value, which is what can be shown by Figure 4.8a. Therefore, an exponential growth curve fit was applied to the data, and this was shown by Figure 4.8c and an R^2 = 0.78 was shown across the entire data set, showing that the *alpha* linear model is not suitable at lower bacterial fluorescence values. In a similar situation, if larger *alpha* values were to be included within the polymer microarray it would be expected an upper threshold would be reached at which point the polymer microarray spot was saturated with bacteria and further bacteria cannot physically adhere to the polymer surface. This would suggest that rather than a linear relationship between *alpha* and the attachment of *P. aeruginosa* would possibly be

better represented by a sigmoidal relationship, however this would need to be proven with further experimentation.

Further bacterial culture experiments were performed to investigate if alpha could be used to correlate bacterial attachment of a different bacterial species, *P. mirabilis*. The homopolymer correlation was shown to be less compared to the relationship between *P. mirabilis* with an R^2 = 0.45. However, taking the extremes of the graph, CyDMA was again shown to have high efficacy for reducing the adhesion of *P. Mirabilis* whilst HPhOPA again was shown to have one of the largest fluorescence values, and therefore *alpha* was shown to be able to have some predictive capability for a different bacterial species albeit with a reduction in the model robustness. The bacterial data set with *P. mirabilis* also had a much larger source of bacteria variance with an average coefficient of variance = 0.39, which could explain why the trend with *alpha* was lower than *P. aeruginosa*. Further repeats could help to clarify this, however both CyDMA and HPhOPA were observed to have relatively low percentage errors compared to other homopolymers and were both successful identified as low and high attachment respectively. When observing the *P. Mirabilis* attachment to the copolymer library, the model completely breaks down, with no feasible trend observed for either the full set of data or the restricted parameters defined by Sanni et al, suggesting that for the copolymer data that *alpha* poorly represents the attachment of *P. Mirabilis*. A reason for this could be due to the different properties of the bacterial species, with *P. mirabilis* containing much more flagella than *P. aeruginosa*, which could lend to differing attachment characteristics of the two different bacteria, despite both being examples of gram

negative bacterial species. This suggest that whilst *alpha* was used to successfully discover CyDMA as a material that prevents the attachment of *P. mirabilis*, the model is not robust enough to reliably predict novel polymers capable of preventing the attachment of *P. mirabilis*.

4.4.4 Performance of hit materials to resist bacterial adhesion to medical devices

After being identified by polymer microarray screenings as a potential hit material, CyDMA was scaled up to coat sections of urinary catheter for scale up bacterial adhesion experiments. CyDMA was compared against clinically used materials (silicone and Bardex® I.C. Aquafil with a hydrogel and silver alloy coated catheter) and was also compared against previously identified hit materials (EGDPEA:DEGMA and iBnA:triEGMA).[45]

The performance of these materials was first tested against *P. aeruginosa* and Figure 4.15 showed how CyDMA and EGDPEA:DEGMA showed the lowest bacterial adhesion (both 0.04 ± 0.03 AU) whilst the commercial controls (silicone and Bardex® I.C. Aquafil) were both significantly higher at 1 ± 0.05 and 1.04 ± 0.01 AU respectively. This demonstrated the significant advantage of novel polymer coatings over commercially available urinary catheters. The performance of the materials was then tested against *P.mirabilis* and again CyDMA was shown to be amongst the lowest attachment materials (0.03 ± 0.03 AU) along with silicone and iBnA:triEGMA (0.04 ± 0.02 and 0.03 ± 0.03 AU respectively). Silicone is still considered a healthcare risk as despite having comparable adhesion properties compared to the hit materials, silicone was still shown to support the attachment of *P. aeruginosa*. The Bardex® I.C. Aquafil catheter section was again

shown to be the worst performing material (1.00 ± 0 AU), highlighting the inappropriate use of this material as an anti-bacterial attachment medical device.

This process has demonstrated how a non-commercially available monomer was highlighted by a computational model and then again identified by a high throughput platform technology (polymer microarrays). CyDMA was then shown to outperform commercial and previously identified materials, showing how powerful a tool the combination of computational models and high throughput technologies can be to streamline material libraries for an application such as reducing bacterial adhesion. This work has the potential to pave the way for researchers to have access to the non-commercially available space by using computational models to allow a biased material selection process and to find materials that are fit for purpose.

4.4.5 Effect of contaminants of bacterial growth

To increase the throughput and feasibility of high throughput synthesis, synthesised materials were placed directly onto the polymer microarray screening platform without any purification steps. However, it was then important that any possible unreacted reagents were tested for bacterial toxicity to be confident that the polymer materials were not causing any bacterial growth/bactericidal effects that could give misleading results. Firstly, synthesised monomers were placed into a well-plate and UV polymerised to form a polymer film covering the entire of the base of the well, and then *P. aeruginosa* was incubated with LB media to observe how bacteria grew when exposed to impure polymers. Figure 4.9 showed that for many different polymers tested, the growth of the bacteria over 24 hours compared to a control with bacteria grown just in LB media with no polymer was unaltered. However, the bacteria were affected by LMMA, showing a reduction in the bacterial growth compared to the control. This suggested that a contamination/unreacted reagent present within LMMA could cause a reduction in bacterial growth and hence was a reason LMMA was not taken forward for further catheter coating experiments described in 4.3.7.

Further toxicity experiments involved using unreacted reagents at likely concentrations expected with the amount of polymer spots on a polymer microarray within the incubation volume used (2000 nL in 20 ml). Butanol, dodecanol, dodecyl methacrylate and butyl methacrylate were tested in concentrations ranging from 0.01 μL/ml to 1 μL/ml. Results were compared against a negative control to show that bacterial growth could be measured by using the optical density. All

variations of concentrations were shown to promote bacterial growth comparably to the positive control which contained no unreacted reagents and only *P. aeruginosa*, and this was proven with a 1-way ANOVA at the 95% confidence interval which showed no significance between data after 24 hours. This showed that in a worst-case scenario, when the monomer fails to cure during the photopolymerisation reaction, the unreacted products will not cause a reduction in bacterial growth rates and would therefore not be at a sufficient level to be toxic to the cells. This result provides confidence in the use of using non-purified monomer solutions whereby any residual alcohols or acrylates are unlikely to influence the bacterial attachment and biofilm formation on a given material.

4.5 Conclusion

- Previously published computational model (*alpha*) was used to identify potential hit materials able to reduce the attachment of *P. aeruginosa* where materials were synthesised as described in Chapter 3.
- Polymer microarrays were produced and incubated in both *P. aeruginosa* and *P. Mirabilis* to observe trends between *alpha* and bacterial adhesion.
- The surface chemistry of the polymer microarrays was characterised by ToF-SIMS to observe the monomer mixing ratios for copolymer series to see if they correlated to the feed ratios.
- *Alpha* was shown to correlate well with data obtained for *P.aeruginosa*, however the trend was poor for *P. Mirabilis*, but incubations identified CyDMA (α = -5.47) as a hit material and HPhOPA (α = 1.1) as a material that promoted bacterial attachment for both bacterial species.
- Scale-up and coating of catheter sections showed that CyDMA was identified as the material with the lowest bacterial attachment for both bacterial species, with a 96 %/97 % reduction when compared to the Bardex Aquafil catheter for *P. aeruginosa* and *P. mirabilis* respectively.
- The *alpha* model was used to predict materials, and materials outside commercially available space (CyDMA) was synthesised (Chapter 3) and shown to reduce bacterial adhesion of multiple bacterial species, showing the value of using computational models to explore the large unexplored non-commercially available chemical space.

5 Design, Manufacture and Testing of Multi-Platform Microwave Reactor

5.1 Introduction

Combinatorial synthesis has allowed for the development of large material libraries using a repetitive synthesis procedure which is applied to multiple reaction vessels in a single batch process.[171,172] This has been used to develop material libraries for a range of applications including anti-cancer drugs,[173] photosensitizers,[174] peptide synthesis,[175] solid-phase[176] and polymer synthesis[177] to name just a few. High throughput materials discovery (HTMD) programmes have been used to accelerate the identification of novel materials for specific applications, and these programs often use platform technologies such as polymer microarrays to screen thousands of materials in single iterative process. Polymer microarrays have been used to develop materials that reduce bacterial attachment to medical devices, expand pluripotent stem cells, increasing the maturity of cardiomyocytes and providing bio instructive implant materials.[45,163–165] HTMD programs typically require a large amount of different materials to be able to draw any significant conclusions and hence, commercially available materials are used to create a diverse chemical library as they offer a convenient source of a diverse range of materials. This can lead to two main issues: a) a large quantity of chemistries is left unexplored due to inability to access the wide chemical space available with non-commercially available materials b) by using commercial materials, it becomes difficult to probe finite changes in chemical moieties to assess specific structure-activity relationships. These problems can be resolved by using synthesised monomers in conjunction with predictive models to

produce a monomer library to probe designed scientific questions. However, a key issue that prevents the use of synthesised materials is the time required to synthesis a large amount of new chemical derivatives. Therefore, development of a system that allows reliable high throughput synthesis of novel monomers is essential to enable HTMD programs to utilize unprecedented access to a large chemical space.

Publications have reported instances of performing library synthesis reactions at room temperature where no heating is required and hence individual reaction temperature over each reaction mixture is not necessary. However, a large concern with these approaches arises when heating is required for the reaction to occur. Often processes utilise conventional heating methods whether that be in a temperature controlled oven or by using a large block-array arrangement where the heat delivered to all reaction mixtures is delivered by conduction of a container.[67,70] The lack of reaction control in these instances caused by using a single heating source can cause temperature gradients between reaction mixtures due to differing thermal properties.

Previous work by Kappe *et al* have discussed and developed microwave technologies to heat reactions for combinatorial library synthesis.[10,72,178,179] Work in this area currently utilises either multi-mode microwave ovens which can deliver microwaves to all reaction vessels however, like conventional heating this often leads to varying reaction temperatures due to the uneven distribution of microwaves throughout the microwave cavity.[73] Current library synthesisers also utilise single-mode microwave technology, by using robotics to

transport individual reaction vessels to a microwave cavity one at a time to exposure the reaction to a controlled single-mode microwave cavity.[178–180] Reaction temperature can then be monitored and controlled for each reaction mixture, but a cost of being able to heat reactions mixtures simultaneously as each reaction is transported to a microwave reactor, heated and then replaced with the next reaction. However, the inclusion of a single-mode microwave reactor capable of controlling and heating multiple reaction vessels has always proved difficult due the need to adjust impedance matching to each vessel to ensure adequate microwave coupling between load materials and microwave source. However, to start the development of a multiple vessel single mode synthesis reactor, this chapter focuses on the development of a single-well reactor which can be produced in larger numbers to work together in a modular format.

To prevent the requirement for vast and expensive trial and error experiments, computational simulations are often used to test a microwave reactor design before physical experimentation, and this results in a large saving of time and costings. A common methodology and the method used within this chapter is the use of finite-difference time domain simulations, were a range of applications have been designed through this method including biotelemetry, tissue ablation therapies and dust-free drilling.[102,108,109] FDTD simulations are quicker to perform compared to other methods such as finite elements methods, however FDTD simulations cannot perform simulations on finely detailed structures, and can often struggle with boundary conditions with curved boundaries. Work within this chapter concentrates on designing and developing a

microwave reactor using FDTD simulations with the view to develop a single-mode microwave reactor capable of synthesising novel methacrylate monomers for use within HTMD programmes as described in chapter 4. This reactor was then tested to ensure that it can be used in a safe working environment and then used to synthesise novel methacrylate monomers used the same process described in chapter 2.

5.1.1 Aims and objectives

The aim of this chapter was to design and develop a working single-well microwave reactor capable of synthesising novel methacrylate monomers in a safe working environment. This was achieved by the completing the following objectives:

1. Perform a range of FDTD experiments to create an optimised reactor geometry but observing changes in the reactor radius as well as the antenna shape and size
2. Perform FDTD simulations with optimised geometry to check if microwaves would leak from system by having external port to measure microwave leakage
3. Manufacture and perform preliminary tests of the reactor to check electrical connection between connectors and the antenna and that no significant leaks would occur (both physical and electromagnetic)
4. Perform experiments using the designed 'micro-well' reactor to synthesise novel methacrylate monomers using the same transesterification process as outlined in chapter 2

5.2 Experimental Methods

5.2.1 FDTD Simulations

Previously FDTD simulations have been used to develop a range of different antenna designs for applications such as dust-free drilling, tumour ablation and medical imaging.[99,100,181] All simulations were executed on a Lenovo ThinkPad (Intel core i5-4200U 1.6GHz processor and 8GB RAM) and performed in Vector Fields Concerto 7.5R3 software. Simulations were separated into two main objectives: achieving an optimised reactor geometry that can provide a high and uniform power density and then also testing the optimised geometry to ensure that there is no microwave leakage coming from the reactor that could pose a health risk for any laboratory users.

5.2.1.1 Optimising Microwave Reactor Design

The design of the Micro-well microwave reactor required optimising the reactor and antenna shape and size, applying material properties to relevant structures within the design. To simulate a power input, a coaxial cable was simulated as the power input source, with the electromagnetic wave travelling through the PTFE dielectric of the cable, and the design of this coaxial can be found in Figure 5.1. The coaxial cable had 3 parts, the inner and outer conductor which were simulated to be a perfect electrical conductor and the dielectric which was sandwiched between the inner and outer conductor which was set to be PTFE. The inner conductor had a radius of 1.5 mm and the radius of the dielectric was 3.5 mm such that the coaxial cable was a common commercially available cable when the

Micro-well was eventually fabricated. The inner conductor of the antenna was then extended into the microwave reactor to act as an antenna.

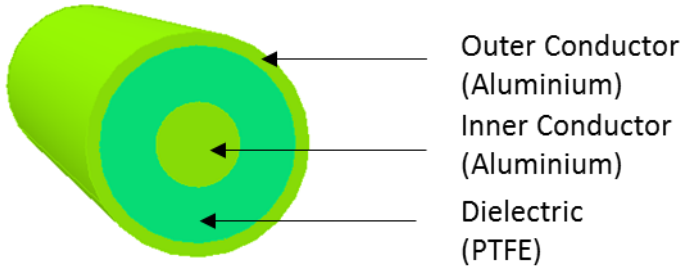


Figure 5.1: Coaxial cable simulated during FDTD simulations showing aluminium outer conductor (r = 4 mm), PTFE dielectric (r = 3.5 mm) and aluminium inner conductor (r = 1.5 mm). Electromagnetic wave travels through the dielectric material and is then propagated into differing reactor designs

Differing well radius were used including 8.13 mm (to simulate a 24-well plate), 15 mm and 40 mm. The design of the well was always kept cylindrical, and this was to maintain the TEM mode through the load material to try and obtain as uniform heating distribution as possible. The antenna was then modified in length (from 0 mm to 20 mm) and varied in shape including a pointed antenna, cylindrical antenna, inverted-cone antenna and a tapered antenna, to try and observe optimal conditions to achieve high power density distribution whilst maintaining field uniformity. Designs were simulated heating methanol such that large power densities could be observed which would potentially pose a problem with microwave leakage issues.

Once a geometry had been designed, an appropriate mesh network was applied. A large enough mesh ranging from 200,000 to 1.8 million cells (depending on the structure size) was applied such that there was no overlap between material

boundaries, as this would cause a poor modelling of microwaves within the geometry. This was done by increasing the number of cells such that the software could not identify any boundary issues where two materials were present in the same cell. An example of geometry with an applied mesh can be shown in Figure 5.2.

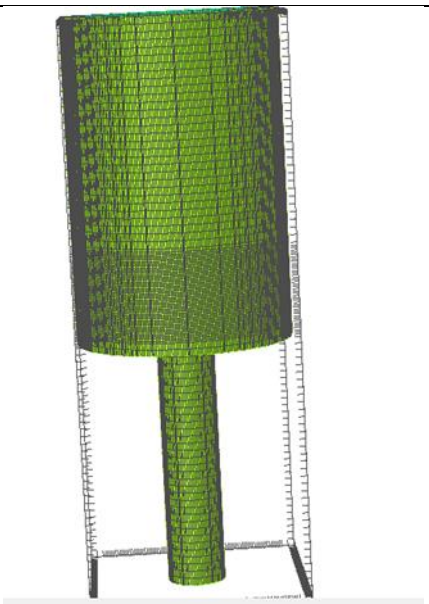


Figure 5.2: FDTD reactor design after applying mesh-grid format for simulations. Each individual cell is then calculated individually and summed across the entire structure to visualise the propagation of electromagnetic waves through a structure.

A limitation of simulations is primarily down to the capability of the computer used for the simulations, with a more powerful computer able to perform simulations with a finer mesh in a quicker time. However, the development of optimised simulation software has also allowed for meshing that accounts for curved boundaries, which can be used to achieve better mesh matching.[107]

The first simulations performed were reflected power (S_{11}) simulations which determine the matching between the power source and the material load. A swept frequency between 2 – 5

GHz was applied to determine the coupling over a frequency range that included the frequency of the Miniflow 200SS (2.45 GHz). A power input of 1 W was simulated to determine the matching between the material and the load. These simulations were done such that designs could be fairly compared against each other by ensuring that the same amount of microwave power was transmitted into the microwave reactor. Simulations could then be performed at single frequency 2.45 GHz at an input power such that 10 W of power is transmitted into the reaction mixture. Simulations were then performed with a mesh grid of approximately 850,000 cells for 50,000 iterations to observe the power density distribution from a range of different geometries. Geometries were then analysed using MATLAB to observe the power density distribution at the same point in XY (10 mm) and XZ (2.6 mm) directions. The objective of the simulations was to find a geometry that had as large a power density distribution as possible whilst maintaining a uniform distribution.

5.2.1.2 Safe Design of Microwave Reactor

Once an optimised microwave reactor geometry had been designed, it was important to check the safety aspect of the design before manufacturing the reactor. A separate interface was created outside the top of the reactor and set as an output port such that any microwaves of the fundamental TE_{11} mode were observed to leak out of the designed system. The simulation set-up can be shown in Figure 5.3.

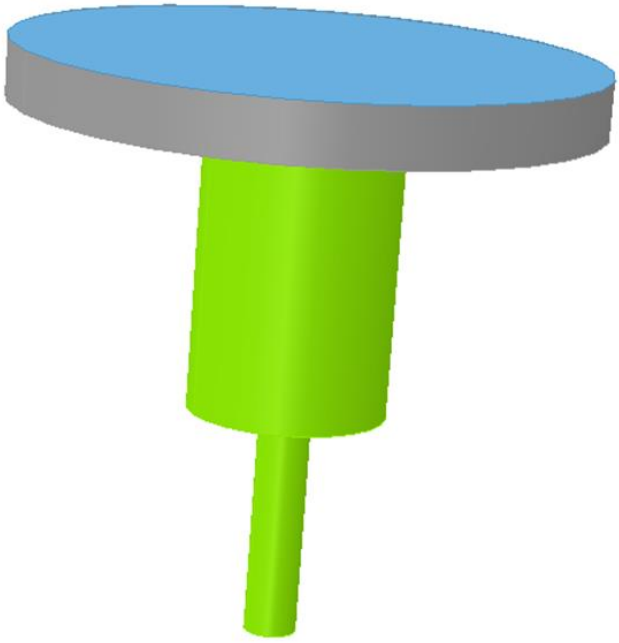


Figure 5.3: Structure showing exterior air interface with a port on the outside (red) face. Leaked microwaves could then be measured at this interface and compared against the microwave dosage limit

The simulated system was then exposed to 10 W of microwave energy, where the leaked microwaves were then compared against the microwave dosage limit to determine whether the reactor was deemed as safe and ready to be manufactured.

5.2.2 Micro-well Manufacture

The materials chosen for the micro-well prototype were aluminium and PTFE, due to the availability of the materials and the ability to work as a cavity wall and dielectric material respectively. The microwave reactor was assembled and soldered/welded together and connected to an N-type connector which was used to connect the reactor to a coaxial cable which was connected the Miniflow 200SS power source. To solder the aluminium antenna to the aluminium connector,

Multicore RA10 solder paste was used to connect the two pieces of aluminium together and maintain an electrical contact. A PTFE sheath was also placed over the antenna within the well and this was to protect the antenna from chemical erosion over time. An additional protective PTFE layer was added to the walls of the reactor to help prevent physical leaks. The finished prototype design can be shown in Figure 5.4.

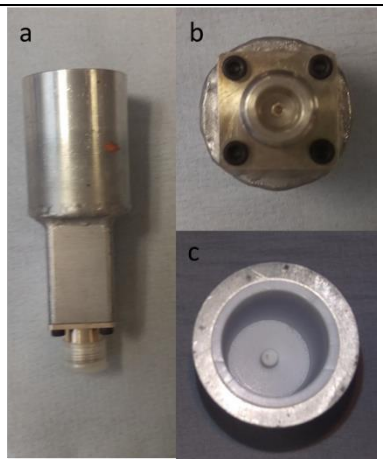


Figure 5.4: Manufactured Micro-well reactor showing (a) whole reactor including 40 mm coaxial section and 50 mm cylindrical reaction vessel (b) N-type connector used for connecting to high-power coaxial cable (c) top-view showing protruding antenna and PTFE sheath covering inside of the reactor

5.2.3 Safety Experiments

Once the Micro-well reactor had been received, a range of safety experiments were performed to commission the Micro-well before it could be used experimentally. Preliminary tests involved swell tests using PTFE to check that the integrity of the Micro-well will not be compromised over time. Swell tests involved measuring PTFE before and after a range of exposure tests with ambient and hot (160˚C) BMA and room temperature acetone.

Further safety tests involved both physical and electromagnetic tests to check that laboratory users will not suffer any exposure to hazardous materials or electromagnetic radiation. Physical leak tests involved filling the Micro-well with water and BMA separately and left for up to 5 hours to check no physical leak was observed. Before microwave power could be used with the Micro-well, the electric connections were tested using a multimeter, to ensure that microwaves could travel through the Micro-well reactor. Before large microwave powers were introduced into the reactor a Rohde & Schwarz ZVL Network analyser was used to observe the coupling of microwaves into different material loads. Before operation the analyser was calibrated using known responses including an air measurement, a short-circuited measurement and a 50 Ω impedance standard, all being measured at 2450 ± 50 MHz. After calibration, the network analyser was used to observe the S_{11} parameter showing the percentage power reflection from the load material. Electromagnetic leak tests were performed by inserting a lossy material, methanol, into the microwave and inserting microwave power in gradual steps and to attempt to measure any microwave leakage using an ETS-Lindgren EMF measurement kit**.** After no microwaves were observed to leak with methanol (above the allowed dosage limit of 5 mw/cm^2), the main reactant BMA was used to observe if any leaks could be observed with increasing microwave power. After this range of experiments the equipment was then declared fit for experimental use in a ventilated cupboard.

5.2.4 Transesterification Experiments

In addition to using the waveguide cavity, the Miniflow 200SS was also used in conjunction with the Micro-well design to

synthesise novel methacrylate monomers. The same safety procedure was followed for this protocol by testing for microwave leakages prior to using full power inputs using the ETS-Lindgren EMF measurement kit. However, to tune the cavity, a sliding cavity tuner (microlab SF-31N) was used and can be shown in the experimental set up in Figure 5.5. To tune the cavity, the stubs were moved up and down the tuner to couple the power source to the material load. Due to the experiment containing an open vessel, clamp-stands were used to secure the tuner and reactor vessel. An additional stamp was used to clamp to the already used clamp stand to provide additional stability.

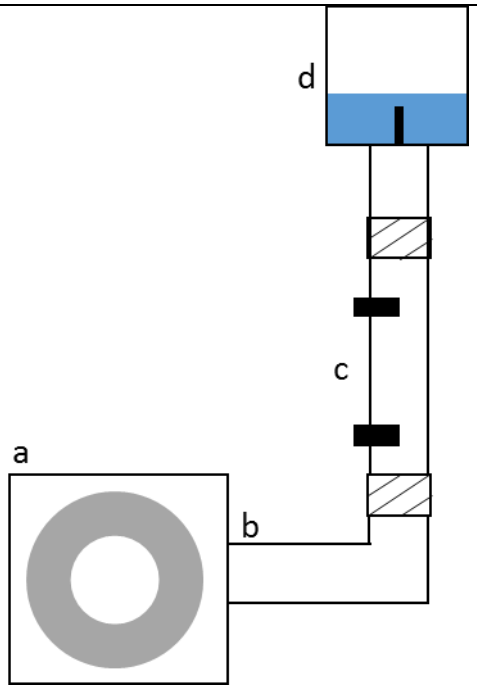


Figure 5.5: Experimental set-up of Micro-well showing (a) Miniflow 200SS (b) Coaxial cable (c) Sliding coaxial tuner and (d) Micro-well reactor

After the Micro-well was declared safe and an appropriate risk assessment had been completed, the Micro-well was tested to see if the design was fit for purpose. Initial tests included gradually increasing the input power to reach the desired reaction temperature of 160 ˚C, which was the desired reaction

temperature outlined in Chapter 2. Reactions were performed in the same way as outlined in Chapter 2, were a 1 % molar quantity of TNBT catalyst was used with a monomer:alcohol mixture which was in a 7:5 molar ratio. Reaction conversion was obtained by taking an aliquot from the final reaction mixture and using ^{1}H NMR to determine the conversion from the starting alcohol to final product.

5.3 Results

5.3.1 Optimised design of Micro-well reactor

5.3.1.1 Effect of reactor vessel radius on power density distribution

As a starting point for designing the microwave reactor geometry, the reactor size radius was optimised to achieve a uniform power density distribution whilst aiming for a high-power density as possible. Initial ideas including making a 24-well design with a reactor radius to match a single vessel from a 24-well reactor (r = 8.13 mm). This design was then compared against larger designs with a radius of 15 mm and a radius of 20 mm, and this can be shown in Figure 5.6.

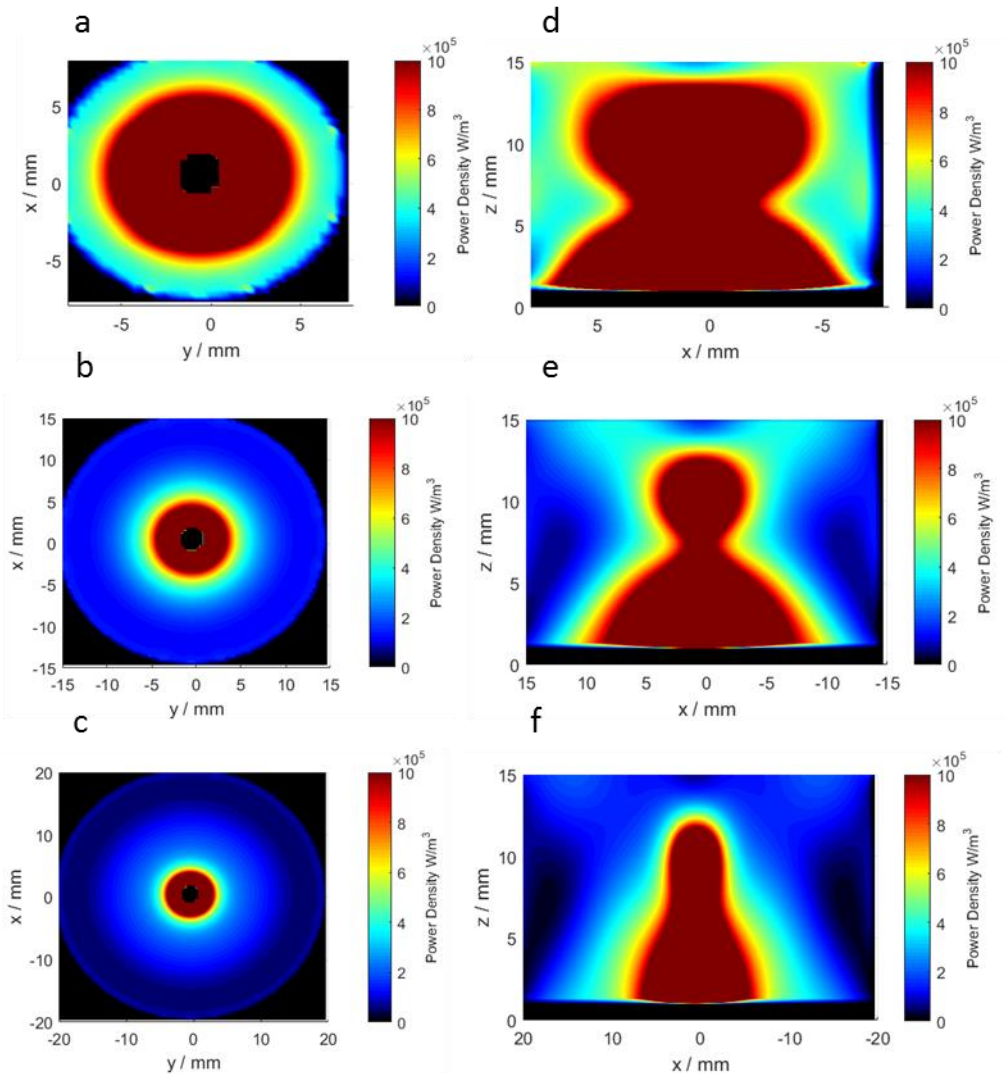


Figure 5.6: Effect of changing the reactor size on power density distribution with a, b and c showing the XY = 10 mm power density for reactor sizes of 8.13, 15 and 20 mm respectively. Figures d, e and f show the XZ = 2.8 mm power density distribution for reactor sizes of 8.13, 15 and 20 mm respectively. All geometries were performed with a cylindrical antenna with length equal to 10 mm. For the 8.13 mm radius well, geometry comprised of 200,000 cells, the 15 mm radius geometry contained 650,000 cells and the 15 mm radius geometry contained 1.8 million cells. All geometries were performed for 30,000 iterations.

As shown by Figure 5.6, as the reactor radius increases, the average power density distribution decreases. Specifically, as the radius increases the power density observed in the outer extremities of the design decreases.

5.3.1.2 Effect of antenna shape on power density distribution

After the size of the reactor had been optimised to 15 mm, the next parameter that was changed was the antenna shape, which included a flat cylindrical antenna, a pointed antenna, an inverted cone antenna and a tapered cylindrical antenna design, all of which are shown in Figure 5.7. The cylindrical antenna was chosen as an example of a simple geometry, whereas the pointed antenna seen in Figure 5.7b was chosen as an example of an antenna that could potentially achieve high power densities, but into a focused area as shown by Jerby *et al* for dust-free drilling.[99] The tapered and inverted cone antennas were used to observe how the change in width effected the observed power density distribution.

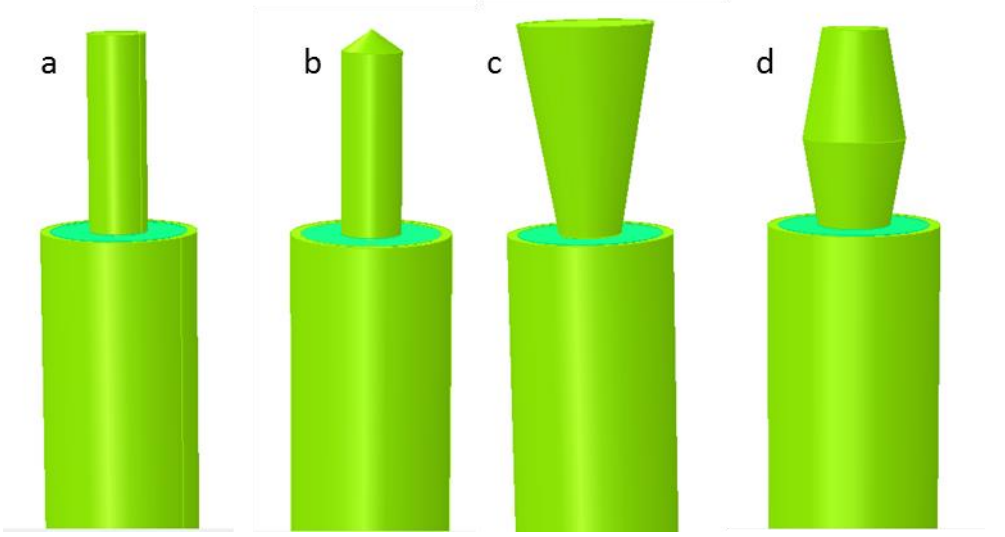


Figure 5.7: Range of antennas shapes simulated during the project showing (a) cylindrical antenna (b) pointed antenna (c) inverted cone antenna and (d) tapered cylindrical antenna.

These designs were then simulated such that 10 W of power was transmitted into the load material (methanol) to be able to compare the antenna shape designs fairly. The power density distributions can be shown in Figure 5.8.

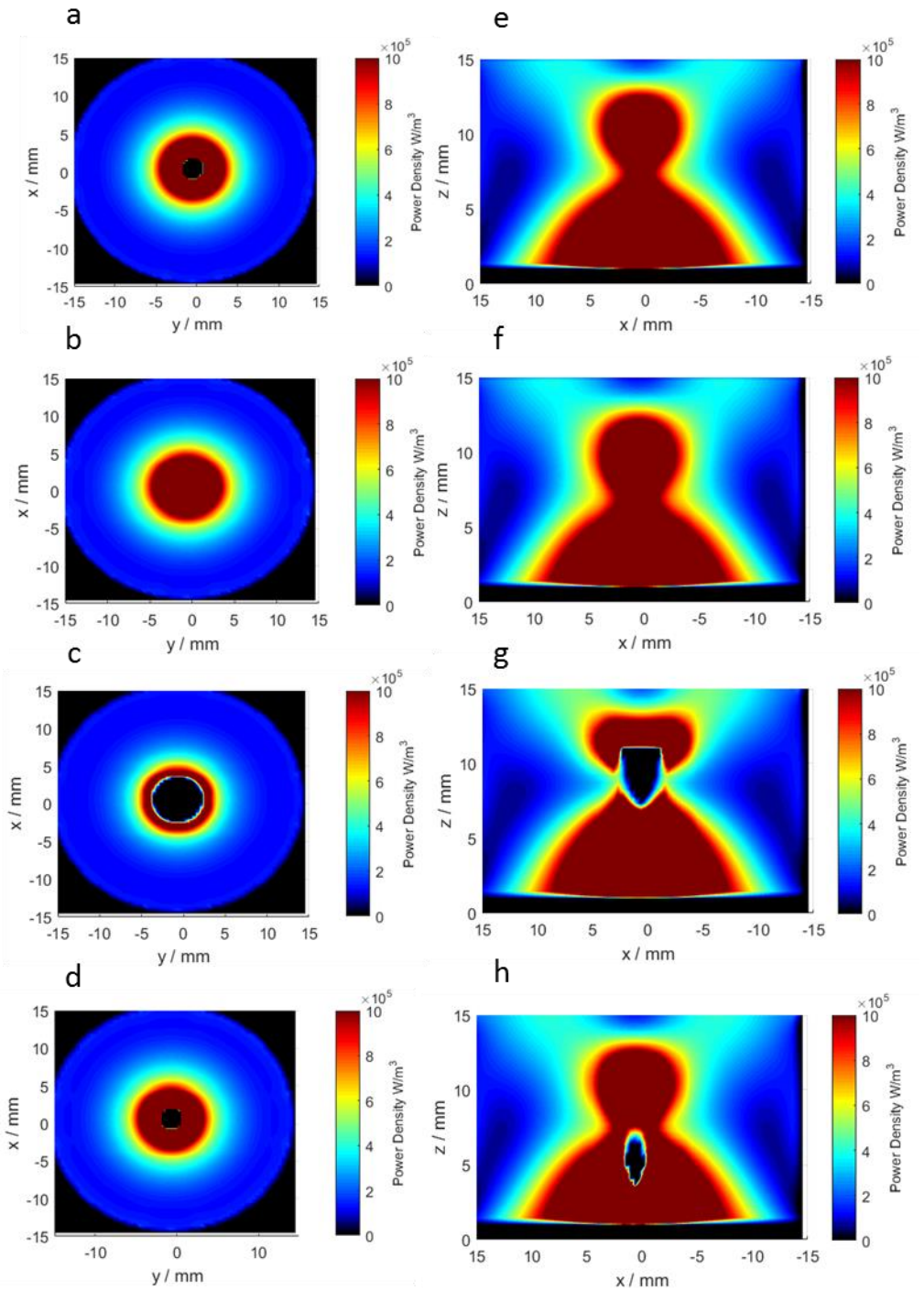


Figure 5.8: Power density distributions for antenna designs showing an XY slice at 10 mm on the left (figures a, b, c and d) and an XZ slice at 2.6 mm on the right (figures e, f, g and h). Designs shown in figure a and e represent simulations performed with a cylindrical antenna. Designs shown in figure b and f represent simulations performed with a pointed antenna. Designs shown in figures c and g represent simulations performed with an inverted cone antenna. Designs shown in figures d and h represent simulations performed with a tapered cylindrical antenna design. Simulations were performed with a mesh containing 650,000 cells and performed for 30,000 iterations.

As shown above in Figure 5.8, the power density distribution pattern for each design showed little difference between one another. Both the cylindrical design and the inverted cone design showed marginally better penetration compared to the tapered and the pointed conductors. All designs show the typical high coupling of microwaves to the antenna shown in red, and this dissipates further into the reaction mixture to lower power densities shown in blue. All simulations performed were done with a mesh grid containing 650,000 cells and performed for 30,000 iterations and displayed images show the power density distribution from 0 W/mm^3 shown in black to 10^6 W/mm^3 shown in red.

5.3.1.3 Effect of antenna length of power density distribution

A study was also performed to assess the effect of antenna length on the coupling capabilities of microwaves to the load material. This process along with the optimisation of reactor radius and antenna shape, allowed for the overall optimisation of a microwave reactor that can achieve as high, uniform power distributions as possible. This involved comparing cylindrical antennas in a 15 mm radius well at lengths of 0, 5, 10 and 20 mm. These comparisons can be found in Figure 5.9.

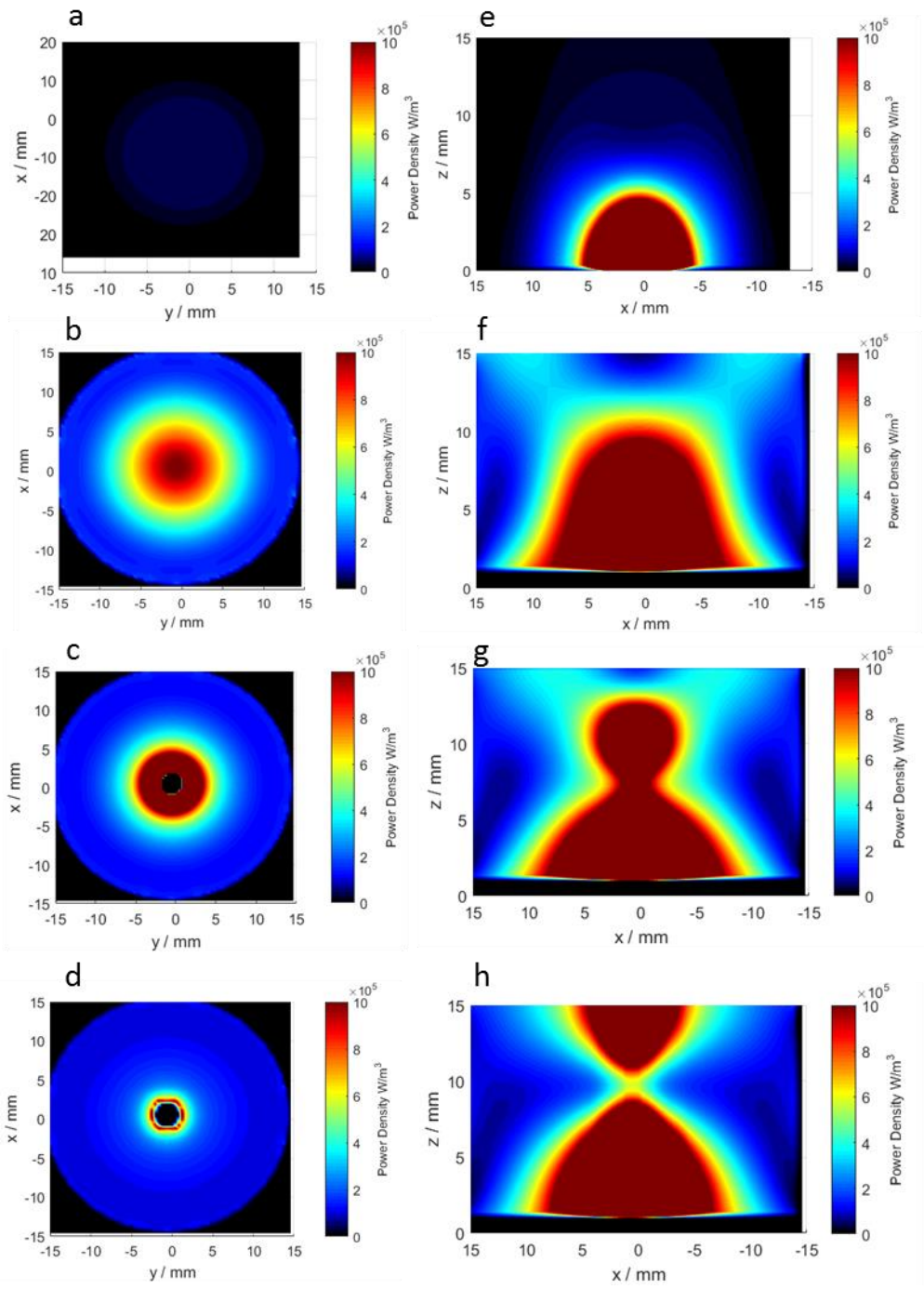


Figure 5.9: Power density distributions for different length antenna designs showing an XY slice at 10 mm on the left (figures a, b, c and d) and an XZ slice at 2.6 mm on the right (figures e, f, g and h). Designs shown in figure a and e represent simulations performed with no antenna. Designs shown in figure b and f represent simulations performed with a cylindrical antenna of length 5 mm. Designs shown in figures c and g represent simulations performed with a cylindrical antenna of length 10 mm. Designs shown in figures d and h represent simulations performed with a cylindrical antenna of length 15 mm. Simulations were performed with a mesh containing 650,000 cells and performed for 30,000 iterations.

Figure 5.9 shows how with increasing antenna length, the microwave coupling to the antenna also increases up to the limit of the load material. However, with longer antennas, the power density distribution is strongly coupled higher up in the reaction mixture, leaving areas of lower power density distribution beneath. All simulations performed were done with a mesh grid containing 650,000 cells and performed for 30,000 iterations and displayed images show the power density distribution from 0 W/mm^3 shown in black to 10^6 W/mm^3 shown in red.

5.3.2 Safety simulations of optimised reactor

Initial safety design was created by analysing the cut-off frequency of the designed system. The cut-off frequency can be shown in Equation 10.

$$f_{c_{nm}} = \frac{p'_{nm}}{2\pi a\sqrt{\mu\varepsilon}}$$

Equation 10: Cut off frequency for circular waveguide where a = radius, p'_{nm} = wave mode constant, μ = magnetic permeability and ε = relative permittivity[105]

Equation 10 describes that as the radius of the reactor decreases, the cut off frequency increases. Table 5.1 shows the cut-off frequency which was calculated for different reactor sizes and different load materials.

Table 5.1: Table showing the cut-off frequency of the TE_{11} mode for air, BMA and butanol at different reactor sizes

Radius (m)	Air f_c (GHz)	BMA f_c (GHz)	Butanol f_c (GHz)
0.008	36.6	16.3	8.7
0.015	19.5	8.7	4.7
0.02	14.6	6.5	3.5

As shown in Table 5.1, the operating frequency of the Micro-well (2.45 GHz) was below the cut-off frequency for all different

materials and radii of designs, and therefore leading to the prediction that these designs would not propagate microwaves without the use of an antenna to aid microwave coupling.

After an optimised microwave reactor had been designed, a simulation to observe the microwave leakage from the system was performed to ensure the reactor would be safe to use. An external interface was used to observe the coupling between an air interface at 5 mm from the reactor surface and the power source as shown in Figure 5.3. This lead to the observation of microwave leakage over a frequency range of 2 – 5 GHz which can be shown in Figure 5.10.

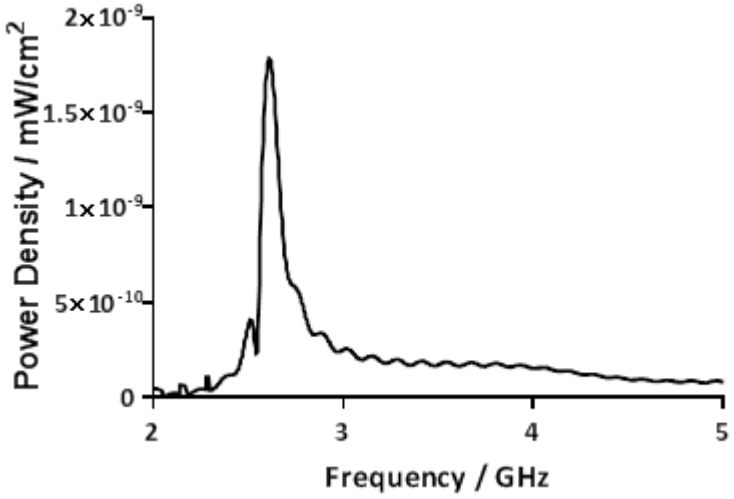


Figure 5.10: Graph showing the leaking of microwaves from optimised Micro-well reactor, showing a peak in power density around 2.6 GHz, however this power density is still negligible compared to current microwave reactor standards

Figure 5.10 shows the microwave leakage from the optimised Micro-well reactor, which shows a peak at 2.6 GHz, however due to operating below the cut-off frequency and having a large amount of head-space, the measured microwave leakage was shown to be well below the 5 mW/cm^2 limit for current

microwave reactors over the entire range of frequencies between 2 and 5 GHz.

5.3.3 Micro-well commissioning

To commission the Micro-well into the lab, the electrical contact was tested and confirmed to be intact by using a multimeter between the N-type connector and the aluminium antenna. Physical leak tests showed small leaking by using BMA and water at both room temperature and 160 °C, though consistent exposure to high temperature was not performed due to the inability to conventionally heat material inside the Micro-well. This was corrected by the addition of a sheath that ran around the circumference of the micro-well reactor which can be seen in Figure 5.11.

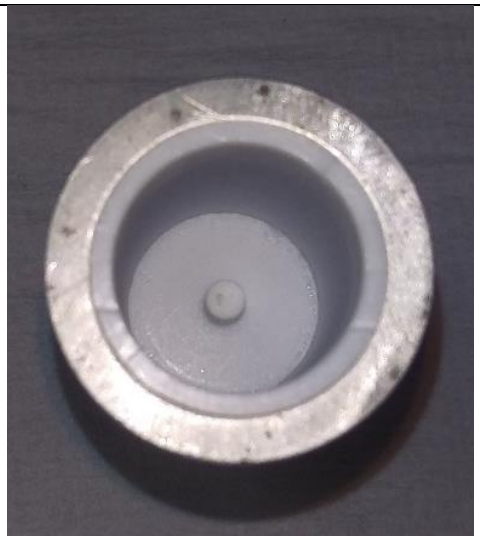


Figure 5.11: Micro-well reactor vessel shown with additional PTFE sheath around the circumference of the reactor wall.

The physical leaking of material was largely stopped by this addition, though small residues were still found after experimentation.

Swelling experiments were performed to check there was no compatibility issues between the PTFE sheath and chemicals

which were used for both synthesising new monomers and cleaning the Micro-well reactor. No effect was shown by leaving sections of PTFE for 3 hours in water, acetone and BMA at ambient temperature respectively. When the PTFE was exposed to BMA at reaction temperatures of 160 °C, no effect either was seen in swelling, however the material became much more pliable at higher temperatures, which was expected.

To test the coupling capabilities of the Micro-well reactor, a Rohde & Schwarz ZVL Network analyser was used to observe the coupling between the power source and different material loads including methanol and BMA. These results were then compared against the same materials but when using a microlab SF-31N sliding tuner, and this can be shown in Figure 5.12.

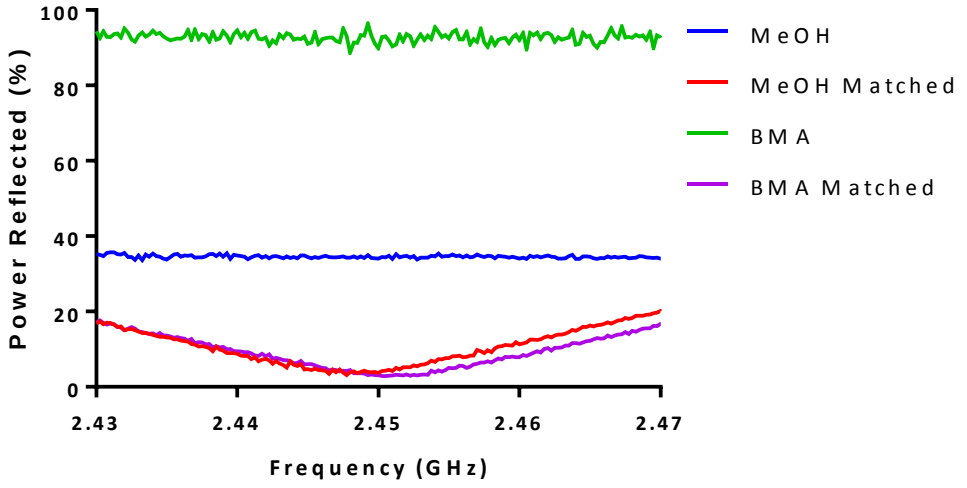


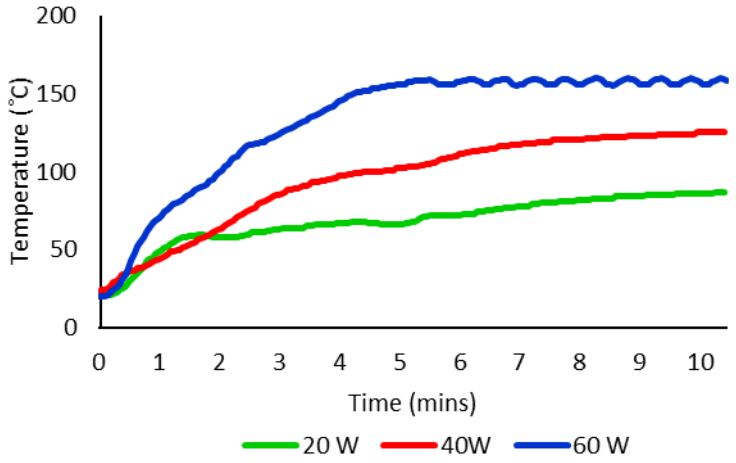
Figure 5.12: Figure showing the comparison of coupling between unmatched and matched BMA and methanol. Measurements were made using a Rohde & Schwarz ZVL network analyser

Figure 5.12 shows difference of being able to couple majority of input power to the load material by using a sliding tuner compared to having no tuning of the Micro-well reactor.

After showing that the input power could be successfully coupled to the load material, initial heating using microwaves was started at 5 W and incrementally increase in 5 W steps and checked using an ETS-Lindgren EMF measurement kit, but no microwave power was detected up to an input power of 150 W for a system containing either methanol or BMA.

5.3.4 Effect of input power on reaction temperature

An investigation into the required power that is needed to successfully heat a transesterification experiment to the desired reaction temperature of 160 °C was carried out, and this can be shown in Figure 5.13.



	20 W	40 W	60 W
Time (mins)	N/A	50	5

Figure 5.13: Graph showing the heating times of different input powers. Observed that at 20 W it was not possible to achieve heat up times within the time period of the reaction

As shown by Figure 5.13, as expected, the more input power put into the reaction mixture, the quicker the reaction heats to the desired reaction temperature. However, it was noted that 20 W was not enough power to obtain the desired reaction

temperature at all, whilst 40 W obtained the target temperature after 50 minutes and 60 W achieved it in 5 minutes.

5.3.5 Synthesis of novel methacrylate monomers using micro-well reactor

To show that the Micro-well reactor was capable of synthesising novel methacrylate monomers, 4 monomers with different chemical structures were synthesised and can be shown in Figure 5.14. Each reaction was performed at 60 W and heated to 160 °C (except from methyl-2-pentyl methacrylate which was heated to 140 °C. Each reaction contained 1 % molar ratio of titanium butoxide (TNBT) and contained starting reagents of butyl methacrylate (BMA) and alcohol at a 7:5 molar ratio and each reaction was performed for 150 minutes. A typical reaction of the synthesis of cyclododecyl methacrylate contained 7.5 g of butyl methacrylate (53 mmol) and 7.0 g of cyclododecanol (38 mmol) and 0.2 g titanium butoxide (0.5 mmol).

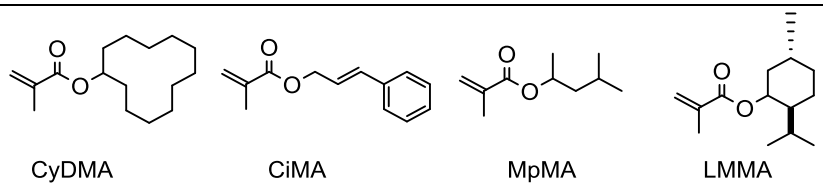


Figure 5.14: Monomers synthesised using the Micro-well reactor using 60 W input power over 150 minutes

This demonstrated the ability of the micro-well reactor to synthesise a range of monomers with cyclic, aromatic and linear-branched moieties. This was then compared to conventional and microwave heating methods to assess how the micro-well performed against other methodologies which can be shown in Table 5.2.

Table 5.2: Transesterification synthesis comparison using conventional, microwave and micro-well prototype methodologies. Materials synthesised include [a] Cyclododododecyl Methacrylate (CyDMA), [b] 3-phenyl-2-propenyl Methacrylate (CiMA), [c] 4-Methyl-2-pentyl methacrylate (MpMA) and [d] 5-methyl-2-(1-methylethyl) cyclohexyl methacrylate

	CyDMA[a]	CiMA[b]	MpMA[c]	LMMA[d]
Conventional [%]	50	41	45	22
Microwave [%]	52	15	48	38
Micro-well [%]	77	80	73	14

Table 5.2 shows how the Micro-well largely improved reaction kinetics for a range of different experiments, apart from with LMMA were the reaction kinetics were significantly reduced (NMR spectra can be found in appendices Q-BB). It was observed that a reason the reactions were only obtaining a conversion of around 80 % could be due to the increased mass transfer properties offered by the Micro-well, and this can be observed in the synthesis of CyDMA were the amount of BMA remaining compared to cyclododecanol is only 31 %, despite starting in an excess of 7:5 (BMA: cyclododecanol), and this can be shown in the NMR spectra shown in Figure 5.15.

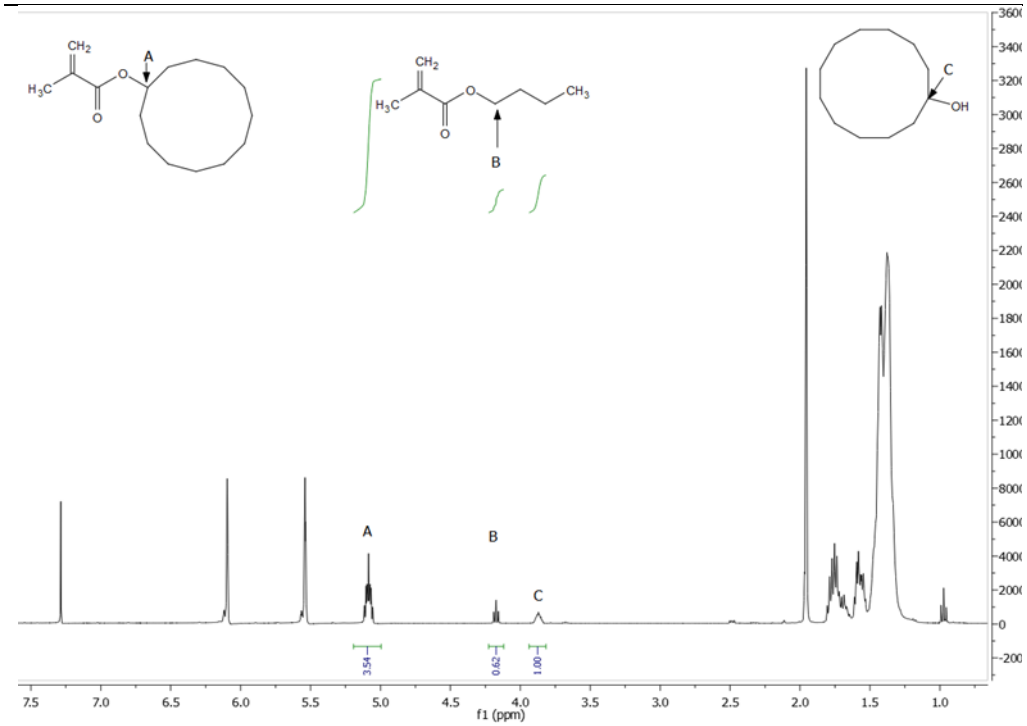


Figure 5.15: ^{1}H Spectra showing the reduction of BMA compared to cyclododecanol after 150 minutes of heating in the Micro-well reactor. NMR showed reaction mixture only containing 31 % BMA compared to the remaining cyclododecanol, with an overall conversion of 78 %

To overcome these issues, it was proposed to change the starting ratio of BMA:alcohol from 7:5 to 8:5 to allow for higher conversions to be obtained using the Micro-well reactor. The same experiment with cyclododecanol at 160 °C was performed, but with a starting ratio of 8:5 instead of 7:5 and the ^{1}H proton NMR spectra can be shown in Figure 5.16.

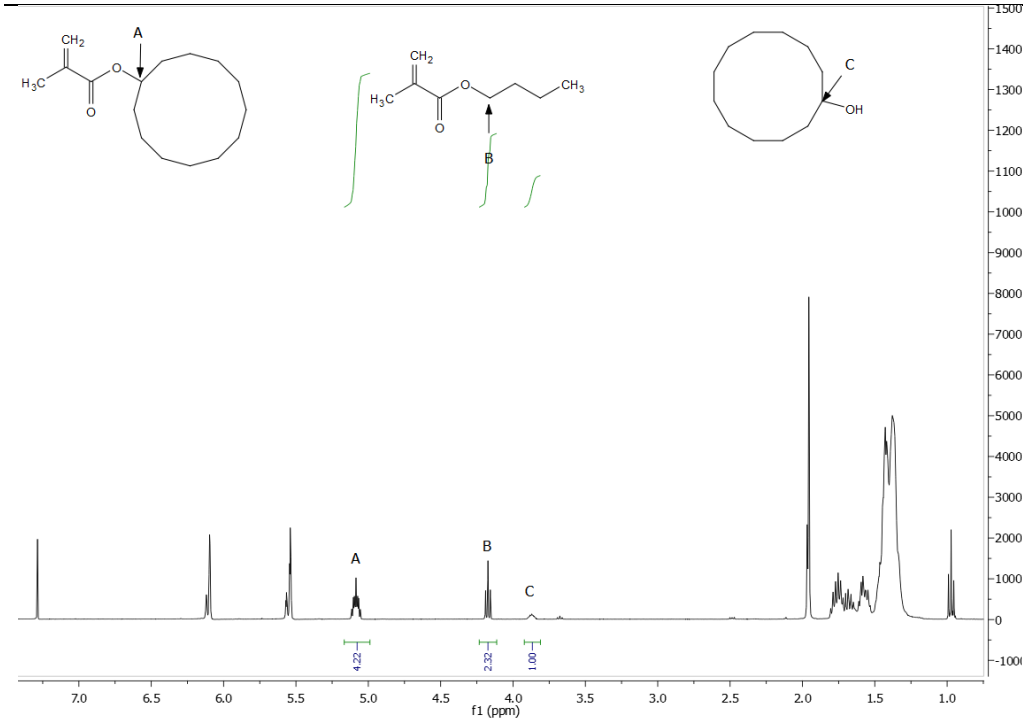


Figure 5.16: ^{1}H proton spectra showing synthesis of CyDMA in Micro-well in an 8:5 starting ratio of BMA: Cyclododecanol, showing an improved conversion of 81 % with 116% BMA leftover compared to the remaining cyclododecanol

Figure 5.16 shows that starting with a higher excess of BMA enabled the reaction to achieve a higher overall conversion of 81 % and had more leftover BMA suggesting that further conversion could be achieved with an increase in reaction time. This shows that by adding additional starting reagents, the mass-transfer properties can be manipulated to benefit the forward transesterification reaction.

5.4 Discussion

5.4.1 Effect of reactor radius on power density distribution

As part of the optimisation process, the radius of the micro-well reactor had to be optimised to achieve a design that allowed high uniform power density distribution that also produced enough material to perform numerous experiments. The sizes chosen to be investigated were 8.13, 15 and 20 mm radius reactors. As shown in Figure 5.6, as the radius of the reactor increased the overall power density decreased. For all designs the power density decreases as distance radially increases from the centre of the well and for this reason the 20 mm design was discarded due to low power density at the outer edges of the design. This can be explained by the inverse square law that the electric field decreases by a factor of r^2 as shown below.

$$E = \frac{Q}{4\pi\varepsilon_0 r^2}$$

Equation 11: Electric field inverse square law showing the decay of an electric field the further from the source as a ratio of $1/r^2$.

For the smaller reactor design, the average power density within the well is higher than the 15 mm design, however the well can only contain approximately 3 ml of reaction mixture, which is a small quantity with the large amount of characterisation tests that can be performed with the production of a novel monomer library. For that reason, the 15 mm radius well was taken forward as the reactor size, as it offers good power density distribution and can contain a larger volume of 10 ml. All designs that were tried used a reactor vessel height of 50 mm, this was to a) prevent microwave

leakage from the system b) prevent chemical leakage from the system being overfilled.

5.4.2 Effect of antenna shape on power density distribution

The next aspect of design involved changing the shape of the antenna to observe any changes in the observed power density distribution. The varied designs shown in Figure 5.7 incorporated a range of designs all formed from the extension of the inner conductor from coaxial cables. The basic design was the straight extension of the inner conductor to form a cylindrical antenna, and then changes to this geometry were made to create the other geometries. The pointed antenna was chosen due to previous reports of using a similar design to dramatically increase the power density distribution albeit, focused into a small focal point above the antenna.[101] This design has been previously used for dust-free drilling of ceramics and minerals.[99] The inverted cone design and tapered cylindrical design were produced to observe the effect of the power density distribution on antenna design.

All the designs were shown to successfully couple microwaves to couple microwaves with the methanol further into the reaction vessel, which allowed for a more uniform distribution of the microwaves with the reactor, which is important as the device was designed to work without any stirring to the reaction mixture. However, there was limited benefit to changing the cylindrical antenna geometry as shown by Figure 5.8. The tapered design was chosen to see if the power density distribution could be widened to increase the uniformity in the centre of the reaction vessel, but no change in the power density distribution was observed compared to the basic

cylindrical design and so the tapered design shown in Figure 5.7d and h was excluded. The inverted cone design was shown to slightly improve the coupling of the microwaves deeper into the methanol, but at the cost of reducing coupling to the reaction mixture in the centre of the well as shown by the XZ images in Figure 5.8g. The inverted cone design would also make it difficult to machine, and the added PTFE sheath that was used to protect the antenna would also be difficult to produce, and so the design was discarded due to insufficient advantages over the basic cylindrical design. Finally, the pointed conductor (Figure 5.8b and f) was observed to penetrate slightly less into the methanol than the cylindrical design, and as previously reported this is likely due to the high localised power density that would be observed in a small area directly above the antenna,[101] though the simulations did not directly show this large increase. In summary, the cylindrical design offered either comparable or slightly improved characteristics compared to the other antenna designs, and with the increased advantage of being simple to manufacture, the cylindrical antenna design was taken forward in the design optimisation process.

5.4.3 Effect of antenna length on observed power density distribution

The final part of the design optimisation process involved determining the optimum length of the antenna to achieve the most uniform power distribution over the entire simulated methanol. This involved observing the power density distribution over differing cylindrical antenna lengths including 0, 5, 10 and 15 mm. Figure 5.9a demonstrated the large effect that using an antenna has on the power density distribution. With no antenna, poor penetration into the reaction mixture

was observed, and Figure 5.9 showed how when the antenna is increased in length, the coupling between the microwaves and antenna allowed further penetration into the simulated methanol. This occurs due to mode conversion of the electromagnetic wave. When there is an antenna present, the geometry is the same as it is for a coaxial cable, except the PTFE dielectric is replaced with the reaction mixture and therefore the TEM mode is propagated. The higher dielectric properties of the reaction mixture compared to PTFE results in volumetric heating of the reaction. However, when there is no antenna present, the electromagnetic wave converts to the fundamental TM mode, which then fails to propagate due to operating below the cut-off frequency of the system.

Furthermore, when the antenna is extended to 15 mm, corresponding to the height of simulated methanol in the simulation (shown in Figure 5.9d), the coupling between the antenna and power source starts to spread, causing areas of low power density distribution to arise in the centre of the simulated design. The optimum height for the antenna was shown to be 2 thirds of the height of the simulated load material, (10 mm), and this design offered a compromise between power density distribution uniformity and larger penetration depth of microwaves into the load material. The design also offers practical uses, as if the reaction mixture height is not quite at 15 mm, Figure 5.9 demonstrates that a high-power density will still be delivered into the Micro-well, and hence allow for high reaction temperatures to be reached.

5.4.4 Safe design of microwave reactors to prevent exposure to microwaves

The safe design of the microwave reactor underpins the whole design process, as it is important to meet the criteria of a system that enables high power density distribution, but also a system that does not leak microwaves and can be experimentally used in a laboratory. Initial design included considering the cut-off frequency to observe if, theoretically, the proposed designs would leak microwaves. As shown by Table 5.1, all the cut-off frequencies from differing radii and load materials were larger than the operating frequency used for the system of 2.45 GHz. The cut-off frequency describes a frequency at which when operated below, microwaves will attenuate and therefore with a suitably sized headspace, would not leak microwaves into the working environment.

After an optimised reactor design was obtained with the 10-mm cylindrical antenna in a cylindrical reactor vessel of radius 15 mm, further simulations were performed to check that microwaves would not leak from the reactor. This was done to prevent any need to adjust and compromise the design of the reactor retrospectively after it had been fabricated. Figure 5.3 shows how an additional interface was added to the exterior of the reactor design to observe the coupling between the input microwaves and the exterior interface. The distance between the reactor surface and the exterior interface was 5 mm. This was to compare the results against the regulations of microwave designs that state the power density must be below 5 mW/cm^2 at 5 cm from the surface of the microwave reactor.[143] Figure 5.10 showed an increase in the microwave leakage power density around 2.6 GHz compared to the rest of

the leakage data in the range from 2 – 5 GHz although this is only measured at approximately $2x10^{-9}$ mW/cm^2, which is negligible when compared to the target set by the regulations for microwave reactors/ovens. This has shown that an effective microwave reactor has been designed which not only can reach high power densities but can also operate in a safe working environment and minimalize the exposure of operators to non-ionizing radiation. An additional benefit of having such a low leakage of microwaves come into the parallelisation of microwave reactors to produce a high throughput synthesis reactor. The combination of several reactors is still going to be negligible compared to the advised microwave dosage limit.

5.4.5 Commissioning of Micro-well reactor for safe working practice

Commissioning experiments were performed to ensure that minimal risks were taken when experimentally using the Micro-well reactor. Initial tests involved physical leak tests including room temperature and pre-heated boiling water to test the integrity of the reactor vessel. The integrity was also tested with room temperature BMA and BMA that was pre-heated to 160 °C. Small leaks were found by observing liquid residues within the coaxial section of the reactor. The design change shown in Figure 5.11 was added when these residues were detected, by added a PTFE sheath around the circumference of the reactor, which pushed against the PTFE protective cover on the base of the reactor, which largely removed physical leaks, but evidence after experiments still suggested small leaks. This could be avoided entirely by making a protective coating in a single piece of PTFE, such that there are no gaps for leaks to occur.

Swelling experiments were performed to check that no adverse effects would occur during experimentation or cleaning due to chemical incompatibilities. No effect using water, BMA or acetone was observed at ambient temperatures. However, when reaction temperatures were mimicked using conventional heating, it was observed that PTFE became more pliable. Despite being more pliable, no visible swelling was observed at elevated temperatures and so this was deemed to be a suitable inert material to improve the longevity of the Micro-well reactor.

5.4.5.1 Effective use of tuners to match microwave power source to load material

Before full microwave power could be used within the reactor, the VNA network analyser was used to observe the coupling between the microwave power source and the load material within the reactor vessel. Figure 5.12 shows the large effect of using a coaxial tuner has on the absorbed microwaves into the load material. As the Micro-well reactor was simulated with methanol to simulate a worst-case scenario of having large coupling of microwaves which could lead to microwave leakage, the coupling of microwaves to methanol without a tuner was much higher than the coupling to BMA without a tuner. However, using the tuner it was shown that comparable matching was obtained for both BMA and methanol such that over 95 % of the microwaves were absorbed by the load material. Following from this result, the Miniflow 200SS power source was attached to the Micro-well reactor and the microwave power was slowly increased and microwave leakage was measured at each increment. No microwave leakage was observed up to 150 W from any of the possible leaking sites from the reactor with both methanol and BMA, and hence was deemed safe to use for transesterification experiments.

5.4.6 Feasibility of creating multi-well microwave reactor

For creating a high throughput synthesis reactor, the power requirement for each well needed to be assessed to check if system with multiple wells would be a feasible option. Figure 5.13 showed how 20, 40 and 60 W input powers were used to observe how quickly a reaction mixture containing cyclododecanol heated up to the reaction temperature of 160 $^{\circ}$C. As expected, the more power that was put into the reactor, the quicker the reaction mixture heated up to the desired reaction temperature. However, it was shown that by using 20 W, the reaction temperature could not be obtained within the reaction period of 150 minutes. However, by using 40 W, the reaction temperature was obtained in 50 minutes and by increasing the power to 60 W the desired reaction temperature was obtained within only 5 minutes. This suggests that a 24-Well system could be feasibly made with a power source of only 960 W if each well only received 40 W. Another possibility would be to start off the reaction by using 60 W of power and then reducing the power to 40 W to maintain the reaction temperature. This would then allow the benefit of quick heat up times and low power requirements, as each individual reaction could be started 5 minutes apart to reduce power requirements of the potential system. The ability to heat a reaction with such low powers shows how efficient the micro-well system can couple microwaves to the load material and increase the reaction temperature, a property that cannot be matched by using conventional heating techniques.

5.4.7 Comparison of Micro-well, conventional and microwave heating methods on reaction conversion

To test the efficiency of the Micro-well reactor, several reactions were performed to synthesise novel methacrylate monomers with different chemical structures to test the ability of the reactor to produce a diverse range of materials. Table 5.2 showed how conventional and microwave methods were limited by the mass-transfer effect, with reactions being limited to around 50 % conversion. There was however a large difference between the conventional and microwave synthesis of CiMA, with the conventional experiment being able to achieve 41 % after 150 minutes, whilst the microwave synthesis only achieved 15 %. This however had the largest change when performed in the micro-well reactor, where a conversion of 80 % was achieved. The synthesis of CyDMA and MpMA were also improved by using the Micro-well and showed improved mass-transfer characteristics by achieving 77 and 73 % respectively. The open-vessel of the reactor allows for the evaporation of butanol from the reaction mixture which therefore aids the reaction kinetics and allow the reaction to obtain conversions more than 50 %. A major benefit of this system compared to the synthesis protocol discussed in Chapter 3.3.4 is that no nitrogen gas sparging was applied to the reactions in the micro-well reactor. This shows how comparable conversions have been able to be obtained with the novel microwave reactor, but without the need for additional processing steps to obtain high conversion materials. This is due to the open-vessel nature of the novel reactor, which allows materials with high volatility such as butanol to evaporate and allow for the reaction to be shifted towards the products as described by Le Chatelier's principle.

However, with LMMA the obtained conversion was shown to be much lower for both the microwave and conventional heating methods with conversions of 22 and 38 % respectively. This is expected due to the steric hindrance from L-menthol which slows down the reaction compared to other transesterification experiments. This then has a negative impact when synthesising in the Micro-well reactor, which a conversion of just 14 %. Due to the increased mass-transfer characteristics of the reactor, caused by a reduction in the size of the choke compared to other synthesis set-ups, this also appeared to increase the evaporation of BMA as well as butanol. Therefore, with slower reactions such as LMMA, the evaporation of BMA causes the dynamic equilibrium to be shifted back towards the starting reagents as defined by Le Chatelier's principle.[115] This property of the reactor was investigated further by adjusting the starting ratio of BMA:cyclododecanol to see if an increase in BMA would allow for larger conversions to be achieved in the same reaction period. Figure 5.15 showed how after 150 minutes with a starting ratio of 7:5, the BMA content had dropped to 31 % of the remaining alcohol, showing a vastly reduced content compared to the starting ratio. However, when this ratio was changed from 7:5 to 8:5 more than BMA, the remaining BMA content increased to 116 % of the remaining alcohol, which still shows some evaporation, but a much-reduced amount compared to the standard starting ratio of 7:5. This also led to a slight increased conversion of 81 % compared to 77 % showing the benefits of increasing the starting content of BMA compared to the alcohol.

The evaporation of chemicals from the reaction mixture has shown to affect the obtained conversion compared to conventional and microwave heating methods. However, it is important that these chemicals should be distilled to prevent unnecessary release of chemicals, which could pose a bigger problem on a larger system with multiple wells.

5.5 Conclusion

- An optimum reactor geometry was obtained using FDTD simulations, which gave a 15-mm radius reactor vessel with a cylindrical 10 mm antenna protruding from the base of the reaction vessel.
- Simulated Micro-well reactor was shown to leak a negligible power density of microwaves by observing coupled microwaves from the power source to an interface outside the reactor geometry.
- The microwave reactor was tested for both physical and electromagnetic leaks and commissioned for full experimental use to produce methacrylate monomers.
- By using a stub tuner, microwaves were successfully coupled between the source and load material, enabling maximum delivery of microwave power.
- The minimum input power required to reach desired reaction temperatures of 160 $^{\circ}$C was shown to be 40 W.
- Micro-well reactor was shown to overcome mass-transfer effects experienced by conventional and heating methods which lead to the increase of conversion for 3 out of 4 tested chemistries.

6 Conclusions

6.1 Summary

The aim of this thesis has been to develop a method for the high throughput synthesis of methacrylate monomers for the use in biological cell screening experiments. This began by outlining a suitable chemical mechanism for synthesising a diverse range of methacrylate monomers which was described in Chapter 3 using a transesterification mechanism which utilised a common monomer, butyl methacrylate, with a range of commercially available alcohols to produce novel methacrylate monomers. It was observed that an additional sparging process was required to obtain high reaction conversions which allowed for the efficient removal of the by-product of the reaction which was butanol. This allowed the reaction to progress to higher conversions. Reaction kinetics and conversions were compared for both conventional heating and microwave heating methodologies. Minor improvements were observed by using microwaves for synthesis, which was largely attributed to the volumetric heating effect allowing for reactions to reach target reaction temperatures quicker than conventional heating. Although by using nitrogen sparging both methods were able to achieve more than 80 % for a range of different reactions. Microwaves were chosen as a suitable method for high throughput synthesis methods since it offers a much higher level of control on reaction conditions in individually powering reaction vessels compared to conventional methods.

The chemical space of acrylate and methacrylate monomers outside those commercially available is vast, and therefore the need for computational models to guide material selection is essential. The *alpha* paper published by Sanni *et al* was used to decide which materials should be synthesised to reduce the attachment of *P. aeruginosa* to polymeric surfaces. Chapter 4 initially discussed how a range of materials were synthesised to give an alpha value range between -5.47 and 1.1, where cyclododecyl methacrylate (CyDMA) was predicted to resist attachment the most with an *alpha* value of -5.47 and 2-hydroxy-3-phenoxypropyl acrylate (HPhOPA) which was a commercial material had the highest *alpha* value hence predicted the highest bacterial attachment at *alpha* = 1.1. A material library comprising of 61 synthesised and commercial copolymers with diverse hydrocarbon structures were then printed onto a polymer microarray format and the adhesion of *P. aeruginosa* and *P. mirabilis* was observed. The attachment of *P. aeruginosa* was shown to have good agreement with the *alpha* parameter for the homopolymer array. The copolymer array also had very good agreement with the model, but only when restricted to the range defined by Sanni *et al* (-3 to 1.1), which suggested that as the value of *alpha* decreases, the trend may become non-linear as the bacterial adhesion reached a non-detectable limit. The attachment of *P. mirabilis* to the polymer microarrays showed to agree with the *alpha* model but to a lesser extent compared to *P. aeruginosa*, however it was still able to successfully predict that CyDMA was good at reducing attachment and HPhOPA promoted the attachment of *P. mirabilis*. However, the copolymer data showed no correlation between bacterial adhesion and the *alpha* parameter

which suggested that the mechanism of preventing biofilm adhesion between *P. aeruginosa* and *P. mirabilis* is different.

Further investigations were performed to observe how CyDMA, which was identified as a hit material for both *P. aeruginosa* and *P. mirabilis*, performs as an anti-biofilm formation coating. This was done by scaling up CyDMA and using it to coat sections of urinary catheter and then comparing bacterial culture experiments with clinically used materials and previously identified hit materials. CyDMA-coated sections of catheter were shown to reduce the attachment of *P. aeruginosa* on silicone and Bardex® I.C. Aquafil with a hydrogel and silver alloy coated catheter by 92/96 % respectively, showing a dramatic reduction in attachment to the section of urinary catheter. Again with *P. mirabilis* CyDMA was shown to reduce attachment compared Bardex® I.C. Aquafil catheter by 97 %, again showing an improvement compared to clinically used materials. CyDMA also showed to perform well compared to previously identified hit materials, proving that the *alpha* parameter was successfully used to identify a non-commercially available material which has then been proven experimentally to reduce attachment of both *P. aeruginosa* and *P. mirabilis*.

The combination of Chapter 3 and 4 showed the effectiveness of synthesising materials predicted to perform better than current standards for an application. Therefore, work in Chapter 5 included the development of a single-well microwave reactor capable of synthesising novel methacrylate monomers. Computer simulations were performed to identify a reactor which would be successful in achieving high reaction temperatures. After changing reactor size and antenna shape

and size, a 15-mm radius cylinder was chosen as the reactor with a cylindrical 1.5mm radius antenna which protruded 10 mm into the well. This enabled 10 ml of reaction mixture to be heated within the well which was determined to be enough material for characterisation and biological screening experiments. The design was then manufactured, and rigorous safety tests were performed before full experimental use. Once deemed safe, the Micro-well reactor was shown to overcome the mass-transfer barrier and be able to achieve high conversions without the need of the sparging process discussed in Chapter 3, showing a benefit of using the Micro-well system over standard microwave and conventional heating methods. The design was shown also to only require 40 W of power to achieve a reaction temperature of 160 ˚C, which meant that a 24 well system could work with a power source of total power of around 1 kW, which is feasible to be able to obtain a multi-well high throughput synthesis system. Synthesis experiments showed that the Micro-well was also capable of producing a range of different monomer structures as were produced in Chapter 2. The work in this chapter has laid foundations to produce a multi-well system capable to produce diverse monomer libraries giving unprecedented access to a range of materials for materials discovery experiments.

6.2 Recommendations for future work

The work throughout this thesis is multidisciplinary and therefore the different views on the project could take a range of different paths to build upon the work produced within this work. The main area where future work would increase the applicability of this work is to produce a multi-well synthesis

system capable of producing novel material libraries in a single batch process. This could be performed in a couple of different ways; either by using a single large (1 kW) power source and splitting the power into individual wells. Another option is to use voltage-controlled oscillators (VCO) which feed nominal power inputs into amplifiers which can produce in the range of 50 W, which can then be used to power each well individually. However, this would likely increase costs and could also be problematic if higher powers are required for a reaction as the power input to each well would be limited. Another problem would be ensuring that all the systems are successfully matching the input microwaves to the load material, and this could be solved by using automatic matching networks for each well, but this would increase the cost for each Micro-well unit.

Another aspect of this work that could be investigated further is the characterisation of the novel materials that are produced. Previous work by Kamaruddin *et al*[182] has shown it is possible to monitors reactions in situ by observing the dielectric properties of the material. Therefore, it would be of interest to perform dielectric measurement experiments to see if it is possible to determine a threshold at which after a significant change in the dielectric properties could signify when the reaction has come to completion. This could then be incorporated into the multi-well system to prevent unnecessary heating of reactions that have already gone to completion. Another improvement could be testing other reaction mechanisms to see the variety of materials that can be synthesised within the Micro-well such as attempting to synthesise new polymers.

Further work could also be performed with the bacterial work investigated during this project. For example, using the full synthesised material library to create a much larger polymer microarray where the relationship between *alpha* and bacterial attachment can be investigated with a larger sample size. Despite this project testing the model by using two different bacteria (*P. aeruginosa* and *P. mirabilis*) it could also be possible to test the materials against further bacterial species to see if the *alpha* parameter has any trends with other bacterial species. The *alpha* parameter could also be investigated further be expanding the range of materials such that lower and higher *alpha* values are tested, as it is hypothesised that this trend will not be linear at the extremities of these *alpha* values.

A final aspect that could be investigated is to test the discovered hit material, CyDMA, to observe if it shows resistance to attachment from further bacterial species. If shown to resist attachment for further bacterial species, CyDMA would have to mechanically tested to see if it would be suitable for a durable, long lasting coating.

6.3 Concluding Remarks

Throughout this thesis we have been able to show:

1. A transesterification synthesis with nitrogen sparging protocol is a suitable method for obtaining a diverse range of novel methacrylate monomers with high levels of conversion.
2. Quantitative structure-analysis relationships can be used to guide materials discovery programmes into the non-commercially available space by predicting materials

capable of resisting attachment of multiple bacterial pathogens.

3. A single mode (2.45 GHz) microwave reactor was designed and produced capable of producing novel methacrylate monomers using a transesterification mechanism without the requirement of sparging, and with powers as low as 40 W showing promise for development of a multi-well system for large batch process combinatorial chemistry reactions.

References

1. Renwick, M. J., Brogan, D. M. & Mossialos, E. A systematic review and critical assessment of incentive strategies for discovery and development of novel antibiotics. *J. Antibiot. (Tokyo).* **69,** 73–88 (2016).
2. Alanis, A. J. Resistance to antibiotics: Are we in the post-antibiotic era? *Arch. Med. Res.* **36,** 697–705 (2005).
3. Costerton, J. W., Stewart, P. S. & Greenberg, E. P. Bacterial Biofilms : A Common Cause of Persistent Infections. *Science (80-.).* **284,** (1999).
4. Bayston, R., Fisher, L. E. & Weber, K. Biomaterials An antimicrobial modified silicone peritoneal catheter with activity against both Gram positive and Gram negative bacteria. *Biomaterials* **30,** 3167–3173 (2009).
5. Hook, A. L. *et al.* Discovery of novel materials with broad resistance to bacterial attachment using combinatorial polymer microarrays. *Adv. Mater.* **25,** 2542–7 (2013).
6. Sanni, O. *et al.* Bacterial Attachment to Polymeric Materials Correlates with Molecular Flexibility and Hydrophilicity. *Adv. Healthc. Mater.* **0,** 1–7 (2014).
7. Wyss, P. C. *et al.* Novel dihydrofolate reductase inhibitors. Structure-based versus diversity-based library design and high-throughput synthesis and screening. *J. Med. Chem.* **46,** 2304–2312 (2003).
8. Thompson, L. A. & Ellman, J. A. Synthesis and Applications of Small Molecule Libraries. *Chem. Rev.* **96,** 555–600 (1996).
9. Kappe, C. O. Controlled Microwave Heating in Modern Organic Synthesis. *Angew. Chem. Int. Ed.* **43,** 6250–6284 (2004).
10. Kappe, C. O. High-speed combinatorial synthesis utilizing

microwave irradiation. *Current Opinion in Chemical Biology* **6,** 314–320 (2002).

11. Francolini, I. & Donelli, G. Prevention and control of biofilm-based medical-device-related infections. *FEMS Immunol. Med. Microbiol.* **59,** 227–238 (2010).
12. Wolcott, R. D. *et al.* Chronic wounds and the medical biofilm paradigm. *J. Wound Care* **19,** 45–46, 48–50, 52–53 (2010).
13. Kuter, D. J. Thrombotic complications of central venous catheters in cancer patients. *Oncologist* **9,** 207–16 (2004).
14. O 'neill, J. Tackling Drug-Resistant Infections Globally: Final Report and Recommendations the Review on Antimicrobial Resistance. *Comm. by UK Gov.* (2016).
15. Stone, P. W. American perspective. *Expert Rev. Pharmacoecon. Outcomes Res.* **9,** 417–422 (2010).
16. Donlan, R. M. Biofilms and device-associated infections. *Emerg. Infect. Dis.* **7,** 277–281 (2001).
17. Percival, S. L., Suleman, L., Vuotto, C. & Donelli, G. Healthcare-associated infections , medical devices and biofilms : risk , tolerance and control. *J. Med. Microbiol.* **64,** 323–334 (2015).
18. Donlan, R. M. & Costerton, J. W. Biofilms: survivalmechanisms of clinically relevant microorganisms. *Clin.Microbiol. Rev.* **15,** 167–19 (2002).
19. Flemming, H. & Wingender, J. The biofilm matrix. *Nat. Rev. Microbiol.* **8,** 623–33 (2010).
20. Garrett, T. R., Bhakoo, M. & Zhang, Z. Bacterial adhesion and biofilms on surfaces. *Prog. Nat. Sci.* **18,** 1049–1056 (2008).
21. Lorite, G. S. *et al.* The role of conditioning film formation and surface chemical changes on Xylella fastidiosa

adhesion and biofilm evolution. *J. Colloid Interface Sci.* **359,** 289–295 (2011).

22. Campoccia, D., Montanaro, L. & Arciola, C. R. The significance of infection related to orthopedic devices and issues of antibiotic resistance. *Biomaterials* **27,** 2331–2339 (2006).
23. König, C., Schwank, S. & Blaser, J. Factors Compromising Antibiotic Activity Against Biofilms of Staphylococcus epidermidis. *Eur. J. Clin. Microbiol. Infect. Dis.* **20,** 0020–0026 (2001).
24. Mah, T. F. & O'Toole, G. A. Mechanisms of biofilm resistance to antimicrobial agents. Trends Microbiol. *Trends Microbiol.* **9,** 34–39 (2001).
25. University, M. S. Biofilm Basics: Section 1. Available at: http://www.biofilm.montana.edu/biofilm-basics/what_are_biofilms.html. (Accessed: 25th February 2018)
26. Römling, U. & Balsalobre, C. Biofilm infections, their resilience to therapy and innovative treatment strategies. *J. Intern. Med.* **272,** 541–561 (2012).
27. Ding, S., Lin, F., Marshall, A. . & Gillespie, B. . Nurses' practice in preventing postoperative wound infections: an observational study. *J. Wound Care* **26,** 28–37 (2017).
28. Messing, B. Catheter-sepsis during home parenteral nutrition: use of the antibiotic-lock technique. *Nutrition* **14,** 466–468 (1998).
29. Pincock, T., Bernstein, P., Warthman, S. & Holst, E. Bundling hand hygiene interventions and measurement to decrease health care-associated infections. *Am. J. Infect. Control* **40,** S18–S27 (2012).
30. Cohen, J. *et al.* Sepsis: a roadmap for future research. *The*

Lancet Infectious Diseases Commission (2015).

31. Mermel, L. A. *et al.* Clinical Practice Guidelines for the Diagnosis and Management of Intravascular Catheter-Related Infection: 2009 Update by the Infectious Diseases Society of America. *Clin. Infect. Dis.* **49,** 466–467 (2009).
32. Messing, B., Peitra-Cohen, S., Debure, A., Beliah, M. & Bernier, J.-J. Antibiotic-Lock Technique: A New Approach to Optimal Therapy for Catheter-Related Sepsis in Home-Parenteral Nutrition Patients. *J. Parenter. Enter. Nutr.* **12,** 185–189 (1988).
33. Safdar, N. & Maki, D. G. Use of Vancomycin-Containing Lock or Flush Solutions for Prevention of Bloodstream Infection Associated with Central Venous Access Devices: A Meta-Analysis of Prospective, Randomized Trials. *Clin. Infect. Dis.* **43,** 474–484 (2006).
34. Ferreira Chacon, J. M. *et al.* Randomized study of minocycline and edetic acid as a locking solution for central line (Port-A-Cath) in children with cancer. *Chemotherapy* **57,** 285–291 (2011).
35. Heard, S. O. *et al.* Influence of Triple-Lumen Central Venous Catheters Coated with Chlorhexidine and Silver Sulfadiazine on the Incidence of Catheter-Related Bacteremia. *Arch. Intern. Med.* **158,** 81–87 (1998).
36. Weng, M., Zhu, M., Chen, W. & Miao, C. Life-threatening anaphylactic shock due to chlorhexidine on the central venous catheter: A case series. *Int. J. Clin. Exp. Med.* **7,** 5930–5936 (2014).
37. F.W., F. The side effects of silver sulfadiazine. *J. Burn Care Res.* **30,** 464–470 (2009).
38. K, S. & Tbl, L. Types of urinary catheters for management of short term voiding problems in hospitalised adults.

Cochrane Database Syst. Rev. (2010). doi:10.1002/14651858.CD004013.pub3.Copyright

39. Beattie, M. & Taylor, J. Silver alloy vs. uncoated urinary catheters: A systematic review of the literature. *J. Clin. Nurs.* **20,** 2098–2108 (2011).
40. Jahn, P. *et al.* Types of indwelling urinary catheters for long-term bladder drainage in adults. *Cochrane Database Syst. Rev.* 1–3 (2009). doi:10.1002/14651858.CD004997.pub2.Copyright
41. McFarland, E. W. & Weinberg, W. H. Combinatorial approaches to materials discovery. *Trends Biotechnol.* **17,** 107–115 (1999).
42. Kell, D. B. & Oliver, S. G. Here is the evidence, now what is the hypothesis? The complementary roles of inductive and hypothesis-driven science in the post-genomic era. *BioEssays* **26,** 99–105 (2004).
43. Kohn, J. & Road, T. New approaches to biomaterials design. *Nat. Mater.* **3,** 745–7 (2004).
44. Anderson, D. G., Putnam, D., Lavik, E. B., Mahmood, T. a & Langer, R. Biomaterial microarrays: rapid, microscale screening of polymer-cell interaction. *Biomaterials* **26,** 4892–7 (2005).
45. Hook, A. L. *et al.* Combinatorial discovery of polymers resistant to bacterial attachment. *Nat. Biotechnol.* **30,** 868–75 (2012).
46. Díaz-Mochón, J. J., Tourniaire, G. & Bradley, M. Microarray platforms for enzymatic and cell-based assays. *Chem. Soc. Rev.* **36,** 449–57 (2007).
47. Algahtani, M. S. *et al.* High throughput screening for biomaterials discovery. *J. Control. Release* **190,** 115–26 (2014).

48. Anderson, D. G., Levenberg, S. & Langer, R. Nanoliter-scale synthesis of arrayed biomaterials and application to human embryonic stem cells. *Nat. Biotechnol.* **22,** 863–6 (2004).
49. Hook, A. L. *et al.* Polymer microarrays for high throughput discovery of biomaterials. *J. Vis. Exp.* **59,** 1–9 (2012).
50. Magennis, E. P. *et al.* Engineering serendipity: High-throughput discovery of materials that resist bacterial attachment. *Acta Biomater.* **34,** 84–92 (2016).
51. Magennis, E. P., Hook, A. L., Williams, P. & Alexander, M. R. Making silicone rubber highly resistant to bacterial attachment using thiol-ene grafting. *ACS Appl. Mater. Interfaces* **8,** 30780–30787 (2016).
52. Apple, D. J. & Sims, J. Harold Ridley and the Invention of the Intraocular Lens. *Surv. Opthalmology* **40,** 279–292 (1996).
53. Ratner, B. D. & Bryant, S. J. Biomaterials : Where We Have Been and Where We Are Going. *Rev. Lit. Arts Am.* 41–75 (2004). doi:10.1146/annurev.bioeng.6.040803.140027
54. Decuzzi, P. & Ferrari, M. Modulating cellular adhesion through nanotopography. *Biomaterials* **31,** 173–179 (2010).
55. Liu, X. & Ma, P. X. Polymeric Scaffolds for Bone Tissue Engineering. *Ann. Biomed. Eng.* **32,** 477–486 (2004).
56. Boyan, B. D., Hummert, T. W., Dean, D. D. & Schwartz, Z. Role of material surfaces in regulating bone and cartilage cell response. *Biomaterials* **17,** 137–146 (1996).
57. Anselme, K. *et al.* The interaction of cells and bacteria with surfaces structured at the nanometre scale. *Acta Biomater.* **6,** 3824–3846 (2010).
58. Proft, T. & Baker, E. N. Pili in Gram-negative and Gram-

positive bacteria - Structure, assembly and their role in disease. *Cell. Mol. Life Sci.* **66,** 613–635 (2009).

59. Mitik-Dineva, N. *et al.* Escherichia coli, Pseudomonas aeruginosa, and Staphylococcus aureus Attachment Patterns on Glass Surfaces with Nanoscale Roughness. *Curr. Microbiol.* **58,** 268–273 (2009).
60. Colon, G., Ward, B. C. & Webster, T. J. Increased osteoblast and decreased staphylococcus epidermidis functions on nanophase ZnO and TiO2. *J. Biomed. Mater. Res. Part A* **78,** 595–604 (2006).
61. Ploux, L. *et al.* Opposite responses of cells and bacteria to micro/nanopatterned surfaces prepared by pulsed plasma polymerization and UV-irradiation. *Langmuir* **25,** 8161–8169 (2009).
62. Hook, A. L. *et al.* High throughput methods applied in biomaterial development and discovery. *Biomaterials* **31,** 187–98 (2010).
63. Celiz, A. D. *et al.* ToF-SIMS imaging of a polymer microarray prepared using ink-jet printing of acrylate monomers. *Surf. Interface Anal.* **45,** 202–205 (2013).
64. Epa, V. C. *et al.* Modelling and Prediction of Bacterial Attachment to Polymers. *Adv. Funct. Mater.* **24,** 2085–2093 (2014).
65. Hoque, J. *et al.* Broad spectrum antibacterial and antifungal polymeric paint materials: Synthesis, structure-activity relationship, and membrane-active mode of action. *ACS Appl. Mater. Interfaces* **7,** 1804–1815 (2015).
66. Geysen, H. M., Meloent, R. H. & Bartelingt, S. J. Use of peptide synthesis to probe viral antigens for epitopes to a resolution of a single amino acid. *Biochemistry* **81,** 3998–4002 (1984).

67. DeWitt, S. H. *et al.* 'Diversomers': an approach to nonpeptide, nonoligomeric chemical diversity. *Proc. Natl. Acad. Sci. U. S. A.* **90,** 6909–6913 (1993).
68. Meyers, H. . *et al.* Multiple simultaneous synthesis of phenolic libraries. *Mol. Divers.* **1,** 13–20 (1995).
69. Akinc, A., Lynn, D. M., Anderson, D. G. & Langer, R. Parallel synthesis and biophysical characterization of a degradable polymer library for gene delivery. *J. Am. Chem. Soc.* **125,** 5316–5323 (2003).
70. Anderson, D. G., Lynn, D. M. & Langer, R. Semi-automated synthesis and screening of a large library of degradable cationic polymers for gene delivery. *Angew. Chemie - Int. Ed.* **42,** 3153–3158 (2003).
71. Murray, J. K. & Gellman, S. H. Microwave-assisted parallel synthesis of a 14-helical beta-peptide library. *J. Comb. Chem.* **8,** 58–65 (2006).
72. Kappe, C. O. & Matloobi, M. Parallel processing of microwave-assisted organic transformations. *Comb. Chem. High Throughput Screen.* **10,** 735–750 (2007).
73. Glass, B. M. & Combs, A. P. in *High-Throughput Synthesis: Principles and Practices* 123–129 (2001).
74. Kempitiya, A., Borca-tasciuc, D. A., Mohamed, H. S. & Hella, M. M. Localized microwave heating in microwells for parallel DNA amplification applications. *Appl. Phys. Lett.* 94–96 (2009). doi:10.1063/1.3078273
75. Gedye, R. *et al.* The use of microwave ovens for rapid organic synthesis. *Tetrahedron Lett.* **27,** 279–282 (1986).
76. Giguere, R. J., Bray, T. L., Duncan, S. M. & Majetich, G. Application of commercial microwave ovens to organic synthesis. *Tetrahedron Lett.* **27,** 4945–4948 (1986).
77. Lidström, P., Tierney, J., Wathey, B. & Westman, J.

Microwave assisted organic synthesis—a review. *Tetrahedron* **57,** 9225–9283 (2001).

78. Nüchter, M., Ondruschka, B., Bonrath, W. & Gum, A. Microwave assisted synthesis–a critical technology overview. *Green Chem.* 128–141 (2004).
79. Mingos, D. M. P. & Baghurst, D. R. Synthetic Problems in Chemistry. *Chem. Soc. Rev.* **20,** 1–47 (1991).
80. Mishra, A., Vats, T. & Clark, J. H. *Microwave-Assisted Polymerization*. (The Royal Society of Chemistry, 2016). doi:10.1039/9781782623182
81. Kappe, C. O. & Dallinger, D. Controlled microwave heating in modern organic synthesis: Highlights from the 2004-2008 literature. *Mol. Divers.* **13,** 71–193 (2009).
82. Varma, R. S. Solvent-free organic syntheses using supported reagents and microwave irradiation. *Green Chem.* **1,** 43–55 (1999).
83. Strauss, C. R. & Varma, R. S. in *Microwave Methods in Organic Synthesis* (eds. Larhed, M. & Olofssonq, K.) 199–231 (Springer Berlin Heidelberg, 2006). doi:10.1007/128_060
84. Polshettiwar, V. & Varma, R. S. Aqueous microwave chemistry: a clean and green synthetic tool for rapid drug discovery. *Chem. Soc. Rev.* **37,** 1546–1557 (2008).
85. de la Hoz, A., Díaz-Ortiz, A. & Moreno, A. Microwaves in organic synthesis. Thermal and non-thermal microwave effects. *Chem. Soc. Rev.* **34,** 164–78 (2005).
86. Kappe, C. O. Microwave dielectric heating in synthetic organic chemistry. *Chem. Soc. Rev.* **37,** 1127–39 (2008).
87. Perreux, L. & Loupy, A. A tentative rationalization of microwave effects in organic synthesis according to the reaction medium, and mechanistic considerations.

Tetrahedron **57,** 9199–9223 (2001).

88. Irfan, M., Fuchs, M., Glasnov, T. N. & Kappe, C. O. Microwave-assisted cross-coupling and hydrogenation chemistry by using heterogeneous transition-metal catalysts: An evaluation of the role of selective catalyst heating. *Chem. - A Eur. J.* **15,** 11608–11618 (2009).
89. Zhang, X., Hayward, D. O., Michael, D. & Mingos, P. Apparent equilibrium shifts and hot-spot formation for catalytic reactions induced by microwave dielectric heating. *R. Soc. Chem.* **1999,** 975–6 (1999).
90. Santos, T., Valente, M. A., Monteiro, J., Sousa, J. & Costa, L. C. Electromagnetic and thermal history during microwave heating. *Appl. Therm. Eng.* **31,** 3255–3261 (2011).
91. Gabriel, C. *et al.* Dielectric parameters relevant to microwave dielectric heating. *Chem. Soc. Rev.* **27,** 213–224 (1998).
92. Binner, J. G. P., Hassine, N. A. & Cross, T. E. The possible role of the pre-exponential factor in explaining the increased reaction rates observed during the microwave synthesis of titanium carbide. *J. Mater. Sci.* **30,** 5389–5393 (1995).
93. Lewis, D. A., Summers, J. D., Ward, T. C. & McGrath, J. E. Accelerated imidization reactions using microwave radiation. *J. Polym. Sci. Part A Polym. Chem.* **30,** 1647–1653 (1992).
94. Al-Obeidi, F., Austin, R. E., Okonya, J. F. & Bond, D. R. S. Microwave-assisted solid-phase synthesis (MASS): parallel and combinatorial chemical library synthesis. *Mini Rev. Med. Chem.* **3,** 449–60 (2003).
95. Alcázar, J., Dielsb, G. & Schoentjes, B. Applications of the

combination of microwave and parallel synthesis in medicinal chemistry. *Comb. Chem. High Throughput Screen.* **10,** 918–32 (2007).

96. Metaxas, A. C. & Meredith, R. J. in *Industrial Microwave Heating* 151–207 (The Institution of Engineering and Technology, 2008).
97. Asmussen, J., Lin, H. H., Manring, B. & Fritz, R. Single-mode or controlled multimode microwave cavity applicators for precision materials processing. *Rev. Sci. Instrum.* **58,** 1477–1486 (1987).
98. Plaza-González, P., Monzó-Cabrera, J., Catalá-Civera, J. M. & Sánchez-Hernández, D. Effect of mode-stirrer configurations on dielectric heating performance in multimode microwave applicators. *IEEE Trans. Microw. Theory Tech.* **53,** 1699–1705 (2005).
99. Jerby, E., Dikhtyar, V., Aktushev, O. & Grosglick, U. The Microwave Drill. *Science (80-.).* **298,** 587–589 (2002).
100. Mcwilliams, B. T., Schnell, E. E., Curto, S., Fahrbach, T. M. & Prakash, P. A Directional Interstitial Antenna for Microwave Tissue Ablation : Theoretical and Experimental Investigation. *IEEE Trans. Biomed. Eng.* **62,** 2144–2150 (2015).
101. Jerby, E., Aktushev, O. & Dikhtyar, V. Theoretical analysis of the microwave-drill near-field localized heating effect. *J. Appl. Phys.* **97,** 1–7 (2005).
102. Jerby, E. & Dikhtyar, V. Drilling into Hard Non-Conductive Materials by Localized Microwave Radiation. *8th Ampere Proc.* 1–9 (2001).
103. Yee, K. Numerical solution of initial boundary value problems involving Maxwell's equations in isotropic media. *IEEE Trans. Antennas Propag.* **14,** 302–307 (1966).

104. Oskooi, A. F. *et al.* Meep: A flexible free-software package for electromagnetic simulations by the FDTD method. *Comput. Phys. Commun.* **181,** 687–702 (2010).
105. Pozar, D. M. in *Microwave Engineering* (eds. Zobrist, B., Kulck, P. & Aiello, G.) 117–126 (Wiley, 2005).
106. Cangellaris, A. C. & Wright, D. B. Analysis of the Numerical Error Caused by the Stair-Stepped Approximation of a Conducting Boundary in FDTD Simulations of Electromagnetic Phenomena. *IEEE Trans. Antennas Propag.* **39,** 1518–1525 (1991).
107. Hao, Y. & Railton, C. J. Analyzing electromagnetic structures with curved boundaries on cartesian FDTD Meshes. *IEEE Trans. Microw. Theory Tech.* **46,** 82–88 (1998).
108. Cavagnaro, M., Amabile, C., Bernardi, P., Pisa, S. & Tosoratti, N. A minimally invasive antenna for microwave ablation therapies: Design, performances, and experimental assessment. *IEEE Trans. Biomed. Eng.* **58,** 949–959 (2011).
109. Kim, J. & Rahmat-Samii, Y. Implanted antennas inside a human body: Simulations, designs, and characterizations. *IEEE Trans. Microw. Theory Tech.* **52,** 1934–1943 (2004).
110. Zhao, H., Crozier, S. & Liu, F. Finite difference time domain (FDTD) method for modeling the effect of switched gradients on the human body in MRI. *Magn. Reson. Med.* **48,** 1037–1042 (2002).
111. Joines, W. T., Zhang, Y., Li, C. & Jirtle, R. L. The measured electrical properties of normal and malignant human tissues from 50 to 900 MHz. *Med. Phys.* **21,** 547–550 (1994).
112. Li, X. & Hagness, S. C. A confocal microwave imaging

algorithm for breast cancer detection. *IEEE Microw. Wirel. Components Lett.* **11,** 130–132 (2001).

113. Lepage, G. & Roy, C. C. Direct transesterification of all classes of lipids in a one-step reaction. *J. Lipid Res.* **27,** 114–120 (1986).
114. Naik, S. N., Goud, V. V., Rout, P. K. & Dalai, A. K. Production of first and second generation biofuels: A comprehensive review. *Renew. Sustain. Energy Rev.* **14,** 578–597 (2010).
115. Campbell, J. A. Le Châtelier's principle, temperature effects, and entropy. *J. Chem. Educ.* **62,** 231 (1985).
116. Nosse, B., Schall, A., Jeong, W. B. & Reiser, O. Optimization of Ring-Closing Metathesis: Inert Gas Sparging and Microwave Irradiation. *Adv. Synth. Catal.* **347,** 1869–1874 (2005).
117. Dallinger, D., Irfan, M., Suljanovic, A. & Kappe, C. O. An investigation of wall effects in microwave-assisted ring-closing metathesis and cyclotrimerization reactions. *J. Org. Chem.* **75,** 5278–5288 (2010).
118. Jung, H. Y., Park, H. J., Calo, J. M. & Diebold, G. J. Comparison of ultrasonic distillation to sparging of liquid mixtures. *Anal. Chem.* **82,** 10090–10094 (2010).
119. Forsythe, C. J. Influence of inert gas sparging on fatty acid lactylate esterification kinetics. *React. Kinet. Mech. Catal.* **108,** 263–284 (2013).
120. Scott, J. Facts at your fingertips. III. *Chem. Eng.* **119,** 33 (2012).
121. Pozar, D. M. in *Microwave Engineering* (eds. Zobrist, B., Kulek, P., Kincheloe, K., Aiello, G. & Grobe, C. C.) 1–48 (Wiley & Sons, 2005).
122. David, H. & Robert, R. in *Fundamentals of Physics* (ed.

McConnin, R.) 454–534 (Wiley & Sons, 1986).

123. Kraus, J. D. in *Electromagnetics* (ed. Director, S. W.) 132–177 (McGraw-Hill International Editions, 1992).
124. Debye, P. Part 1. Dielectric Constant. Energy Absorption in Dielectrics With Polar Molecules. *Trans. Faraday Soc.* **30,** 679–684 (1934).
125. Cole, K. S. & Cole, R. H. Dispersion and Absorption in Dielectrics I. Alternating Current Characteristics. *J. Chem. Phys.* **9,** 341 (1941).
126. Metaxas, A. C. & Meredith, R. J. in *Industrial Microwave Heating* 5–25 (The Institution of Engineering and Technology, 2008).
127. Becker, E. D. A brief history of nuclear magnetic resonance. *Anal. Chem.* **65,** 295–302 (1993).
128. Bloch, F. Nuclear induction. *Phys. Rev.* **70,** 460–474 (1946).
129. Yu, Q., Zhang, Y., Wang, H., Brash, J. & Chen, H. Anti-fouling bioactive surfaces. *Acta Biomater.* **7,** 1550–1557 (2011).
130. Hwang, J., Shoji, N., Endo, A. & Daiguji, H. E ff ect of Withdrawal Speed on Film Thickness and Hexagonal Pore-Array Dimensions of SBA-15 Mesoporous Silica Thin Film. *Langmuir* **30,** 15550–15559 (2014).
131. Tourniaire, G. *et al.* Polymer microarrays for cellular adhesion. *Chem. Commun. (Camb).* 2118–20 (2006). doi:10.1039/b602009g
132. Hansen, A., Zhang, R. & Bradley, M. Fabrication of arrays of polymer gradients using inkjet printing. *Macromol. Rapid Commun.* **33,** 1114–1118 (2012).
133. Liberski, A., Zhang, R. & Bradley, M. Inkjet fabrication of polymer microarrays and grids—solving the evaporation

problem. *Chem. Commun.* 334–336 (2009). doi:10.1039/B816920A

134. Zheng, Q. *et al.* Application of inkjet printing technique for biological material delivery and antimicrobial assays. *Anal. Biochem.* **410,** 171–6 (2011).
135. Romanov, V. *et al.* A critical comparison of protein microarray fabrication technologies. *Analyst* **139,** 1303–1326 (2014).
136. Benninghoven, A. Chemical Analysis of Inorganic and Organic Surfaces and Thin Films by Static Time-of-Flight Secondary Ion Mass Spectrometry (TOF-SIMS). *Angew. Chemie Int. Ed. English* **33,** 1023–1043 (1994).
137. Mogk, D. W. Evans trift system and Camecas's IONTOF instruments. (2007). Available at: https://serc.carleton.edu/download/images/8384/evans_trift_system_and_camecas_1172767017.v2.jpg. (Accessed: 5th September 2017)
138. Keller, B. A. in *Polymer Surface Characterization* (ed. Sabbatini, L.) 39–71 (De Gruyter, 2015).
139. Sodhi, R. N. S. Time-of-flight secondary ion mass spectrometry (TOF-SIMS):- versatility in chemical and imaging surface analysis. *Analyst* **129,** 483–487 (2004).
140. Vickerman, J. C. & Briggs, D. *ToF-SIMS Surface Analysis by Mass Spectrometry*. (IM Publications, 2001).
141. Combs, C. A. Fluorescence Microscopy: A concise guide to Current Imaging Methods. *Curr. Protoc. Neurosci.* 1–19 (2010). doi:10.1002/0471142301.ns0201s50.Fluorescence
142. Elsherbeni, A. & Demir, V. in *The finite difference time domain method for electromagnetics: with MATLAB simulations* 1–32 (2016).

143. Metaxas, A. C. & Meredith, R. J. in *Industrial Microwave Heating* (eds. Johns, A. T., Ratcliff, G. & Platts, J. R.) 277–295 (IET, 2008).
144. Cleary, S. F. Microwave Radiation Effects on Humans. *Bioscience* **33,** 269–273 (1983).
145. Fukuda, H., Kondo, A. & Noda, H. Biodiesel fuel production by transesterification of oils. *J. Biosci. Bioeng.* **92,** 405–416 (2001).
146. Meher, L. C., Vidya Sagar, D. & Naik, S. N. Technical aspects of biodiesel production by transesterification - A review. *Renew. Sustain. Energy Rev.* **10,** 248–268 (2006).
147. Brady, P. A. & Sanders, J. K. M. Thermodynamically-controlled cyclisation and interconversion of oligocholates: metal ion templated 'living' macrolactonisation. *J. Chem. Soc. Perkin Trans. 1* 3237–3254 (1996). doi:10.1039/a703390g
148. De Benneville, P. L., Luskin, L. S. & Sims, H. J. Transesterification of Methyl Methacrylate with Amino Alcohols. Preparation of a Primary Aminoalkyl Methacrylate and 2-Isopropenyl-4,4-dimethyloxazoline. *J. Org. Chem.* **23,** 1355–1357 (1958).
149. International, L. Methacrylate Monomers. Available at: http://www.luciteinternational.com/monomers-emea-products-and-applications-our-products-21/. (Accessed: 24th January 2018)
150. Bao, Y., Chen, L., Gao, Z. & Chen, J. Local void fraction and bubble size distributions in cold-gassed and hot-sparged stirred reactors. *Chem. Eng. Sci.* **65,** 976–984 (2010).
151. Anderson, D. G., Akinc, A., Hossain, N. & Langer, R. Structure/property studies of polymeric gene delivery

using a library of poly(beta-amino esters). *Mol. Ther.* **11,** 426–434 (2005).

152. Chapon, P., Mignaud, C., Lizarraga, G. & Destarac, M. Automated parallel synthesis of MADIX (co)polymers. *Macromol. Rapid Commun.* **24,** 87–91 (2003).
153. Babaev, E. V. Little artifices of huge libraries: Secrets of parallel liquid-phase synthesis. *Russ. J. Gen. Chem.* **80,** 2607–2616 (2010).
154. Toolan, D. T. W. *et al.* Selective molecular annealing: in situ small angle X-ray scattering study of microwave-assisted annealing of block copolymers. *Phys. Chem. Chem. Phys.* **19,** 20412–20419 (2017).
155. Adlington, K. *et al.* Mechanistic investigation into the accelerated synthesis of methacrylate oligomers via the application of catalytic chain transfer polymerization and selective microwave heating. *Macromolecules* **46,** 3922–3930 (2013).
156. Sigma-Aldrich. *Methanol MSDS*. (2014).
157. Sigma-Aldrich. *Butyl Methacrylate MSDS*. (2014).
158. Sigma-Aldrich. *1-Butanol MSDS*. (2014).
159. Caddick, S. Microwave assisted organic reactions. *Tetrahedron* **51,** 10403–10432 (1995).
160. Loupy, A. *et al.* New Solvent--Free Organic Synthesis Using Focused Microwaves. *Synthesis (Stuttg).* **9,** 1213–1234 (1998).
161. Sigma-Aldrich. *2-Methyl-3-butyn-2-ol MSDS*. (2014).
162. Sigma-Aldrich. *4-Methyl-2-pentanol MSDS*. (2016).
163. Hansen, L. K. *et al.* In vivo model of human pathogen infection and demonstration of efficacy by an antimicrobial pouch for pacing devices. *PACE - Pacing Clin. Electrophysiol.* **32,** 898–907 (2009).

164. Patel, A. K. *et al.* High throughput screening for discovery of materials that control stem cell fate. *Curr. Opin. Solid State Mater. Sci.* **20,** 202–211 (2016).
165. Celiz, A. D. *et al.* Discovery of a Novel Polymer for Human Pluripotent Stem Cell Expansion and Multilineage Differentiation. *Adv. Mater.* **27,** 4006–4012 (2015).
166. Carr, L. R., Xue, H. & Jiang, S. Functionalizable and nonfouling zwitterionic carboxybetaine hydrogels with a carboxybetaine dimethacrylate crosslinker. *Biomaterials* **32,** 961–968 (2011).
167. Hook, A. L. & Scurr, D. J. ToF-SIMS analysis of a polymer microarray composed of poly(meth)acrylates with C6derivative pendant groups. *Surf. Interface Anal.* **48,** 226–236 (2016).
168. Vanden Eynde, X., Bertrand, P. & Penelle, J. 'Matrix' Effects in ToF-SIMS Analyses of Styrene−Methyl Methacrylate Random Copolymers †. *Macromolecules* **33,** 5624–5633 (2000).
169. Scurr, D. J. *et al.* Strategies for MCR image analysis of large hyperspectral data-sets. *Surf. Interface Anal.* **45,** 466–470 (2013).
170. Hook, A. L. *et al.* Polymers with hydro-responsive topography identified using high throughput AFM of an acrylate microarray. *Soft Matter* **7,** 7194–7197 (2011).
171. Ganesan, A. Recent developments in combinatorial organic synthesis. *Drug Discov. Today* **7,** 47–55 (2002).
172. Fergus, S., Bender, A. & Spring, D. R. Assessment of structural diversity in combinatorial synthesis. *Curr. Opin. Chem. Biol.* **9,** 304–309 (2005).
173. Bhattacharyya, S. Combinatorial approaches in anticancer drug discovery: recent advances in design and synthesis.

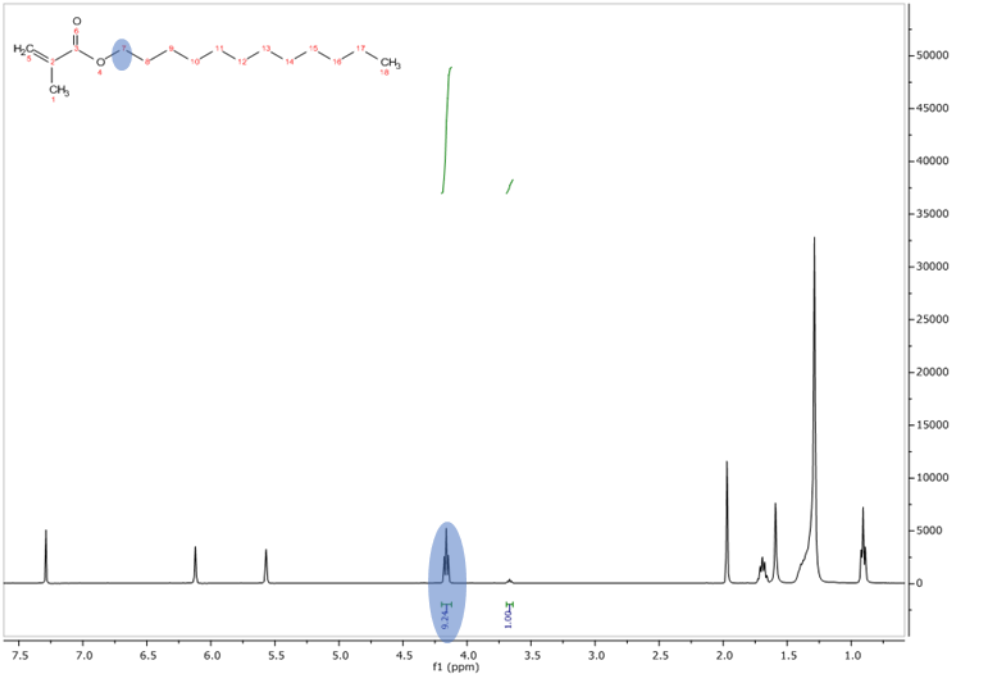
Curr. Med. Chem. **8,** 1383–1404 (2001).

174. Fagadar-Cosma, E., Cseh, L., Badea, V., Fagadar-Cosma, G. & Vlascici, D. Combinatorial synthesis and characterization of new asymmetric porphyrins as potential photosensitizers in photodynamic therapy. *Comb. Chem. High Throughput Screen.* **10,** 466–72 (2007).
175. Horton, D. A., Bourne, G. T. & Smythe, M. L. Exploring privileged structures: The combinatorial synthesis of cyclic peptides. *Mol. Divers.* **5,** 289–304 (2000).
176. Gordon, K. & Balasubramanian, S. Review Solid phase synthesis – designer linkers for combinatorial chemistry : a review. *Chem. Technol.* **851,** 835–851 (1999).
177. Goldberg, M., Mahon, K. & Anderson, D. Combinatorial and rational approaches to polymer synthesis for medicine. *Adv. Drug Deliv. Rev.* **60,** 971–978 (2008).
178. Stadler, A. *et al.* Scalability of microwave-assisted organic synthesis. From single-mode to multimode parallel batch reactors. *Org. Process Res. Dev.* **7,** 707–716 (2003).
179. Kremsner, J. M., Stadler, A. & Kappe, C. O. High-throughput microwave-assisted organic synthesis: Moving from automated sequential to parallel library-generation formats in silicon carbide microtiter plates. *J. Comb. Chem.* **9,** 285–291 (2007).
180. Chemspeed. ISYNTH SWAVE. Available at: https://www.chemspeed.com/isynth-swave/. (Accessed: 4th November 2017)
181. Ireland, D. & Abbosh, A. Modeling Human Head at Microwave Frequencies Using Optimized Debye Models and FDTD Method. *IEEE Trans. Antennas Propag.* **61,** 2352–2355 (2013).

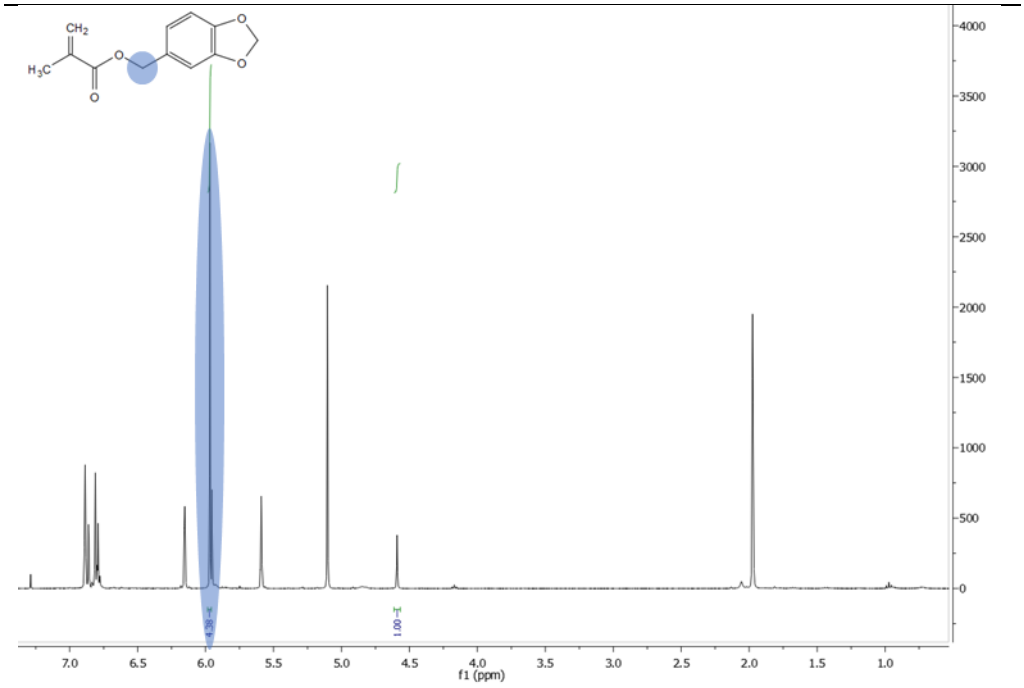
182. Kamaruddin, M. J. *et al.* Continuous and direct 'in situ' reaction monitoring of chemical reactions via dielectric property measurement: controlled polymerisation. *RSC Adv.* **4,** 5709 (2014).

Appendices

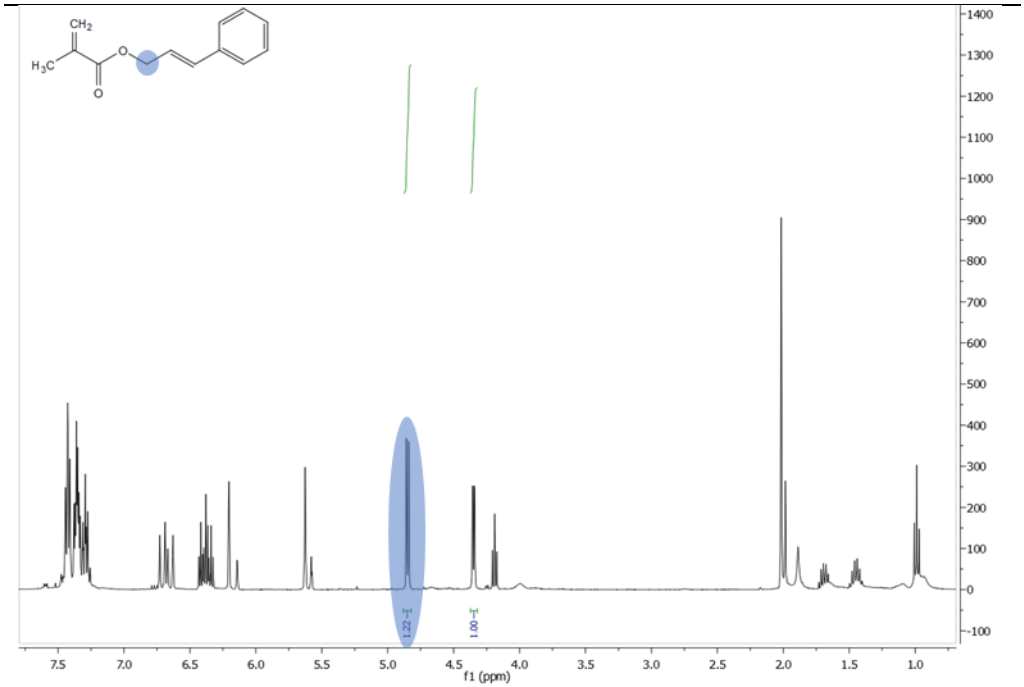
Appendices A-N relate to the conversion for the synthesised monomer library, were majority of the monomers were synthesised with an optimised sparging method described in Chapter 3



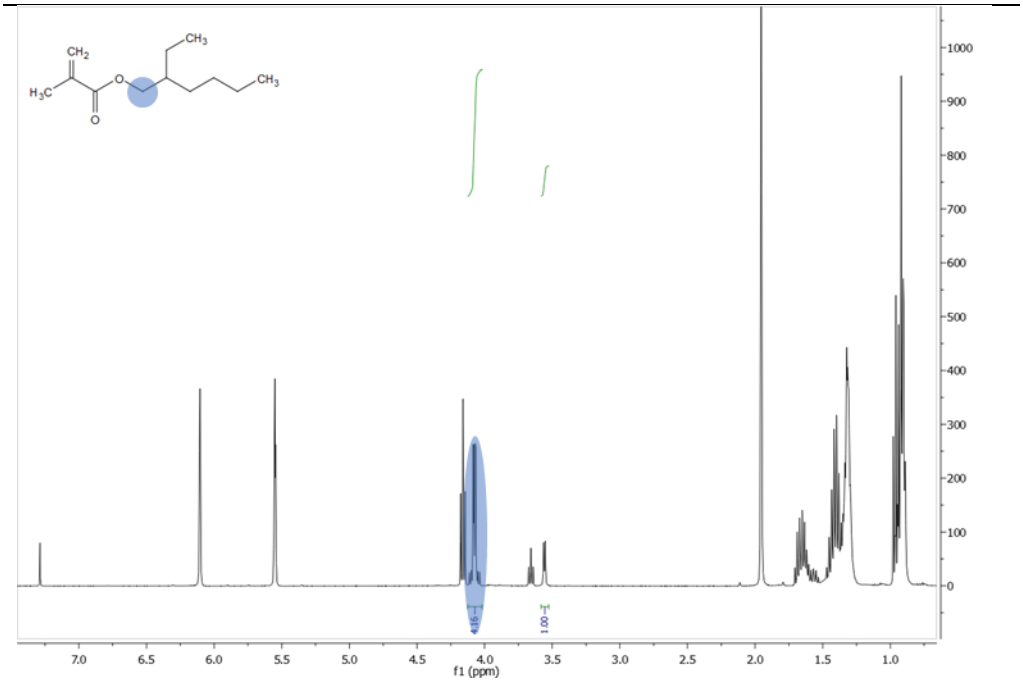
Appendix A: Conventional sparging synthesis of dodecyl methacrylate (DDMA) at 160 °C showing a conversion of 90 % after 90 minutes by comparing change of chemical environment of protons next to ester group from alcohol to methacrylate



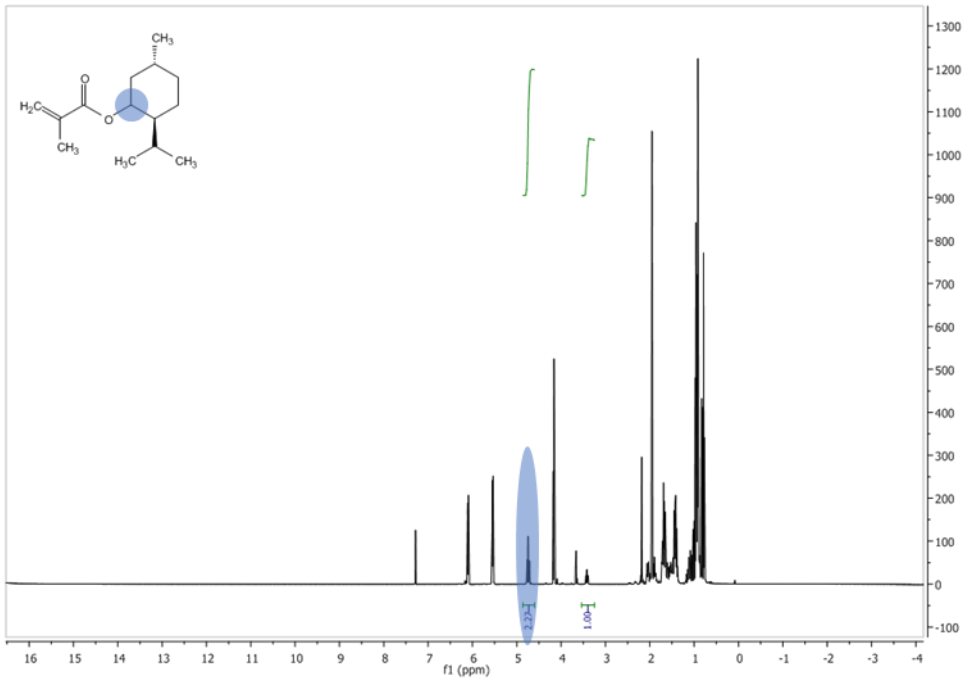
Appendix B: Conventional sparging synthesis of 3,4-(Methylenedioxy)benzyl methacrylate (PiMA) at 160 °C showing a conversion of 81 % after 90 minutes by comparing change of chemical environment of protons next to ester group from alcohol to novel methacrylate monomer



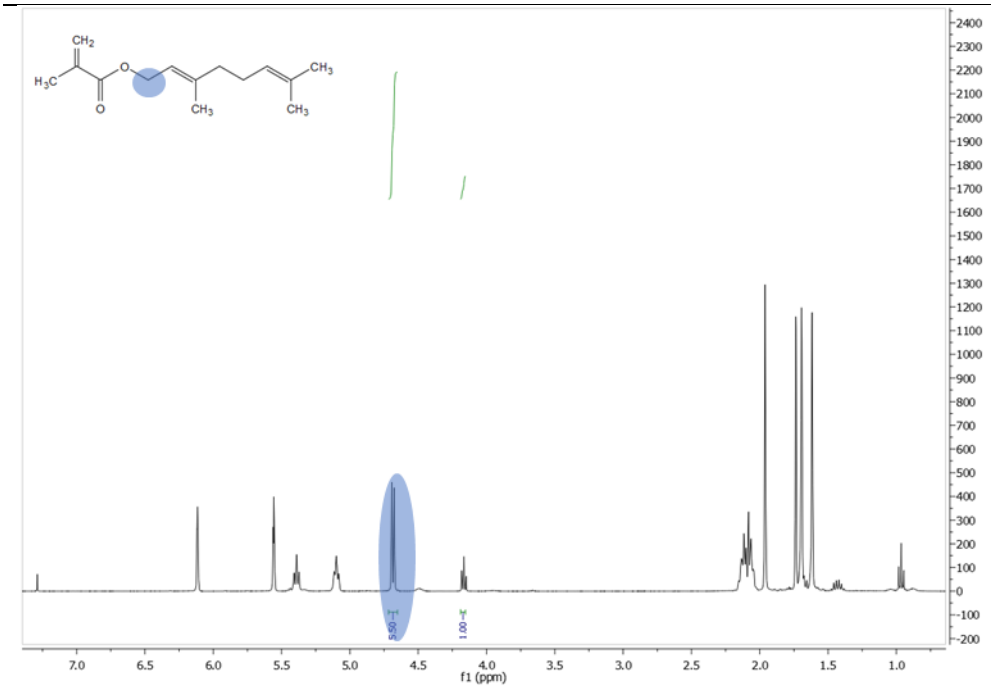
Appendix C: Conventional sparging synthesis of 3-phenyl-2-propenyl methacrylate (CiMA) at 160 °C showing a conversion of 55 % after 180 minutes by comparing change of chemical environment of protons next to ester group from alcohol to novel methacrylate monomer



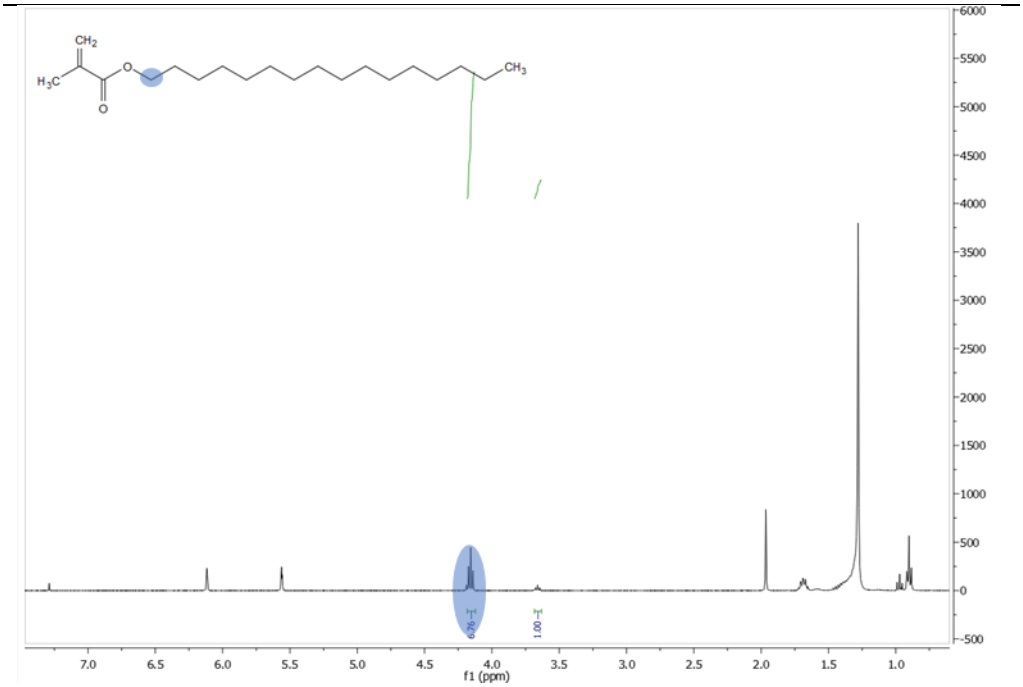
Appendix D: Conventional sparging synthesis of 2-ethylhexyl methacrylate (EhMA) at 160 °C showing a conversion of 81 % after 90 minutes by comparing change of chemical environment of protons next to ester group from alcohol to methacrylate



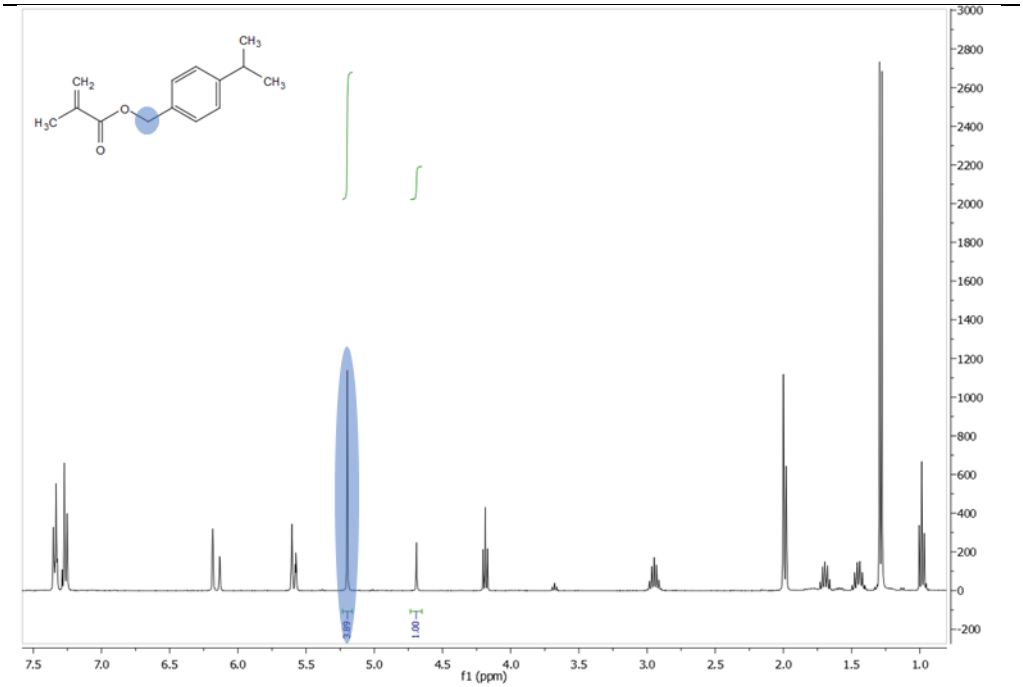
Appendix E: Conventional heating synthesis of 5-methyl-2-(1-methylethyl) cyclohexyl methacrylate (LMMA) at 160 °C showing a conversion of 69 % after 50 hours with application of vacuum pump to extract by-products. Conversion was calculated by comparing change of chemical environment of protons next to ester group from alcohol to novel methacrylate monomer



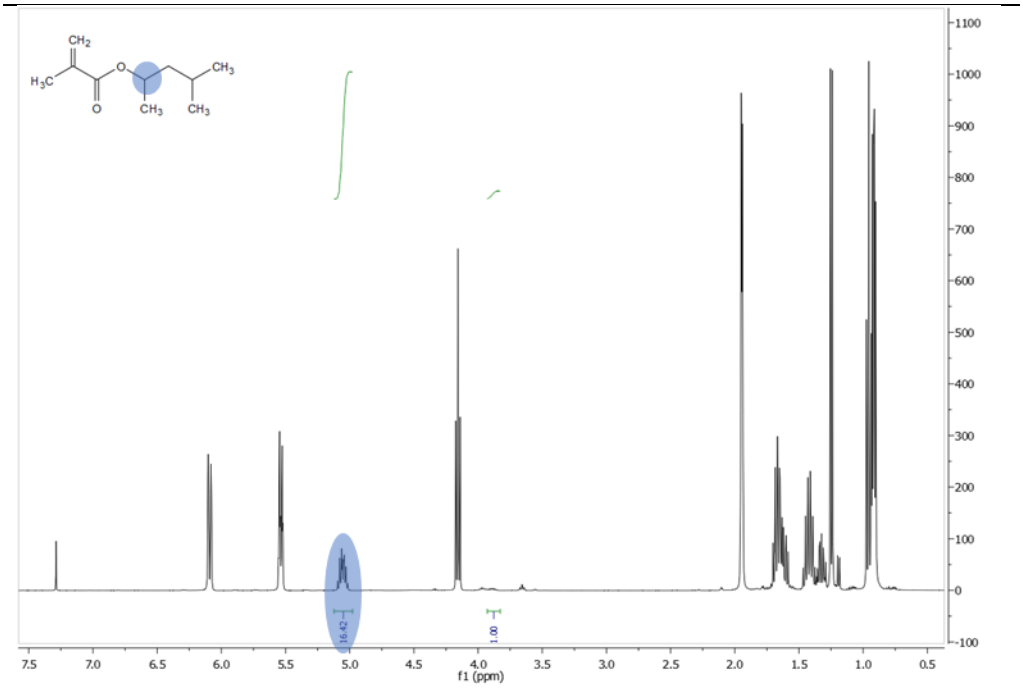
Appendix F: Conventional sparging synthesis of trans-3,7-Dimethyl-2,6-octadienyl methacrylate (GeMA) at 160 °C showing a conversion of 85 % after 105 minutes by comparing change of chemical environment of protons next to ester group from alcohol to novel methacrylate monomer. Overlap of geraniol alcohol peak would cause large source of error in this measurement



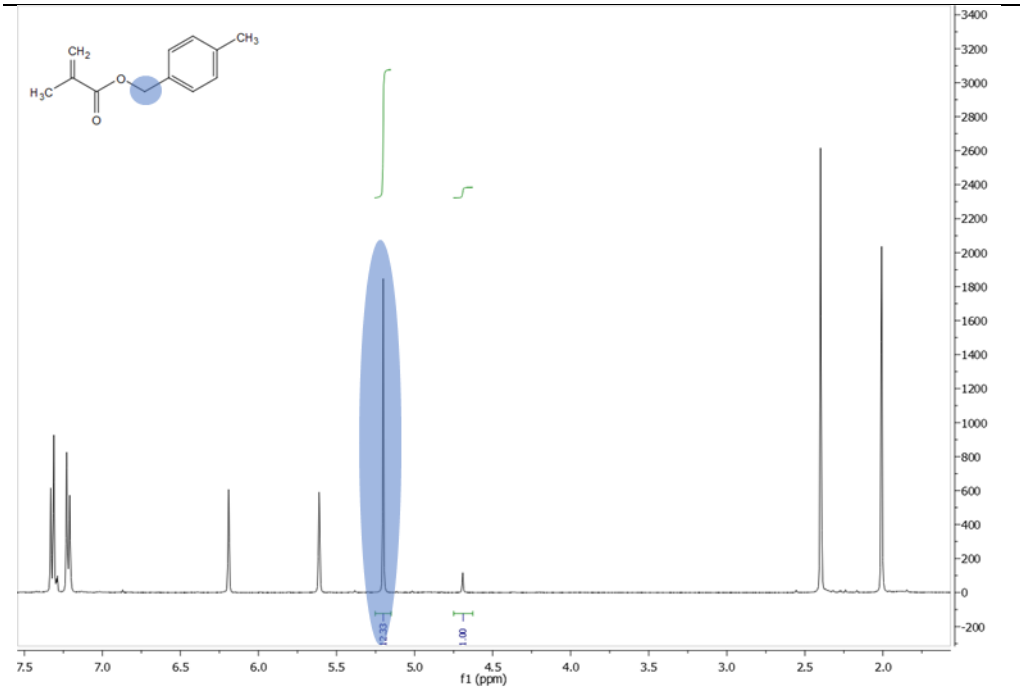
Appendix G: Conventional sparging synthesis of hexadecyl methacrylate (CMA) at 160 °C showing a conversion of 87 % after 120 minutes by comparing change of chemical environment of protons next to ester group from alcohol to novel methacrylate monomer



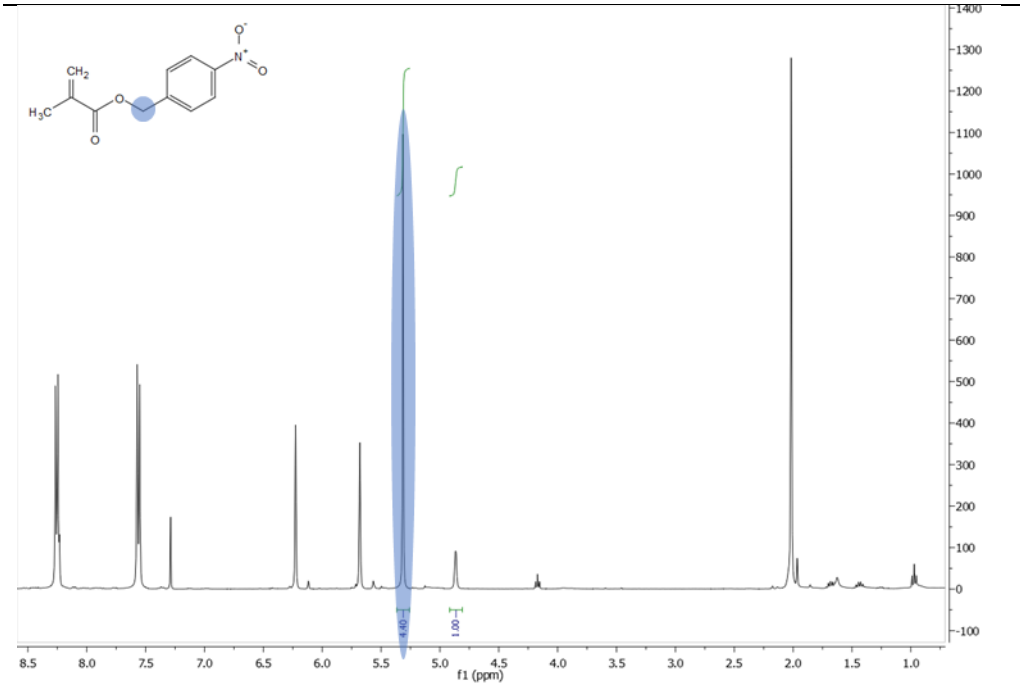
Appendix H: Conventional sparging synthesis of Isopropyl-benzyl methacrylate (IpbMA) at 160 °C showing a conversion of 80 % after 270 minutes by comparing change of chemical environment of protons next to ester group from alcohol to novel methacrylate monomer



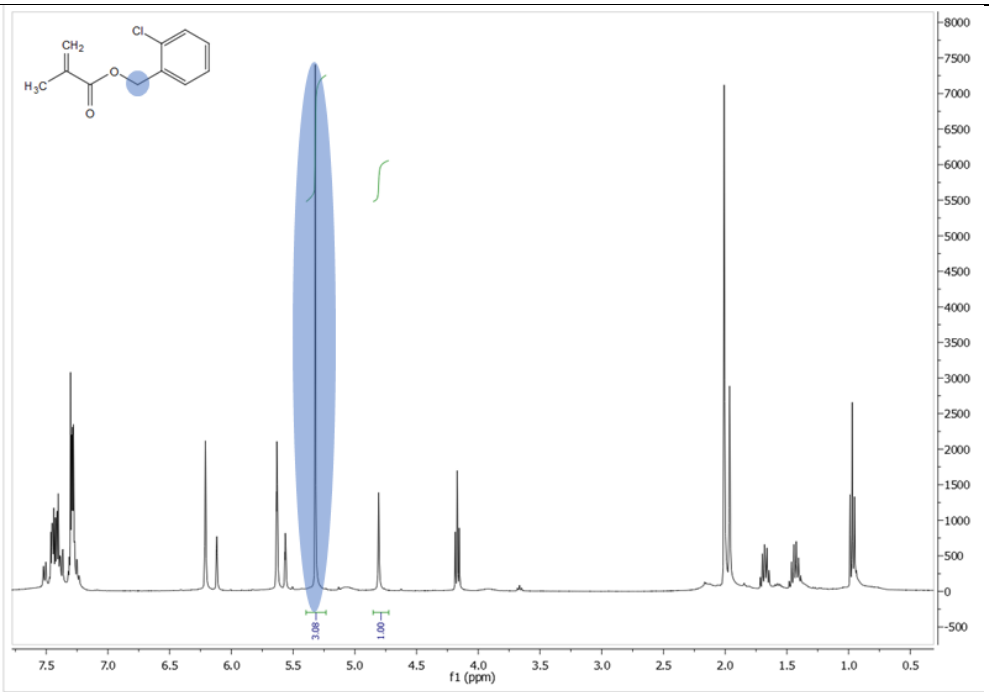
Appendix I: Conventional sparging synthesis of 4-methyl-3-pentyl methacrylate (MpMA) at 140 °C showing a conversion of 94 % after 90 minutes by comparing change of chemical environment of protons next to ester group from alcohol to novel methacrylate monomer



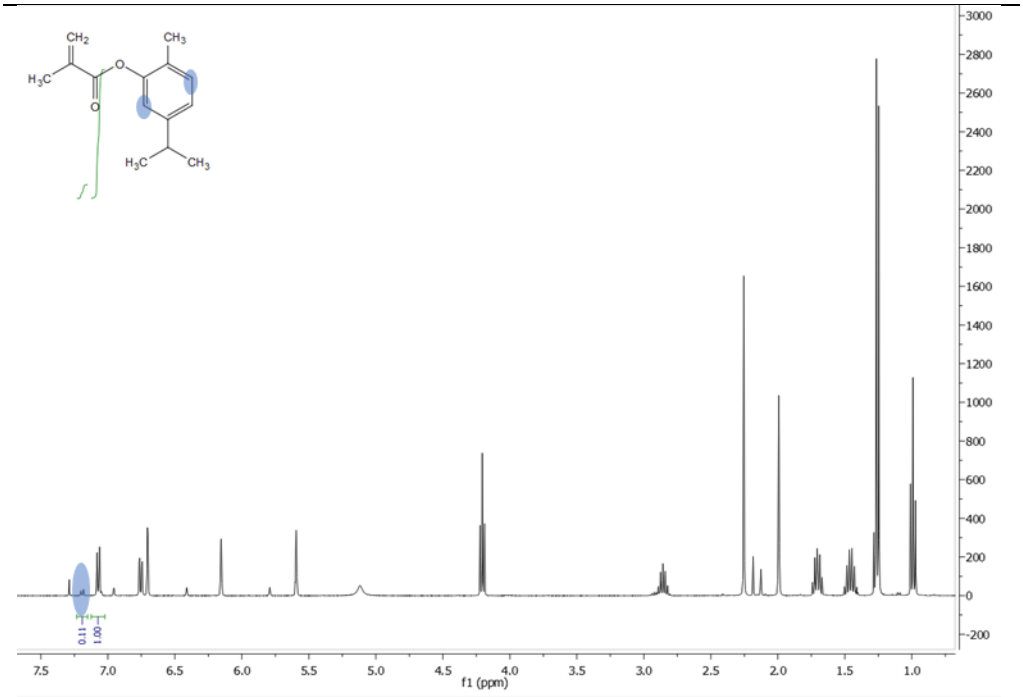
Appendix J: Conventional sparging synthesis of 4-Methylbenzyl methacrylate (MbMA) at 160 °C showing a conversion of 92 % after 120 minutes by comparing change of chemical environment of protons next to ester group from alcohol to novel methacrylate monomer



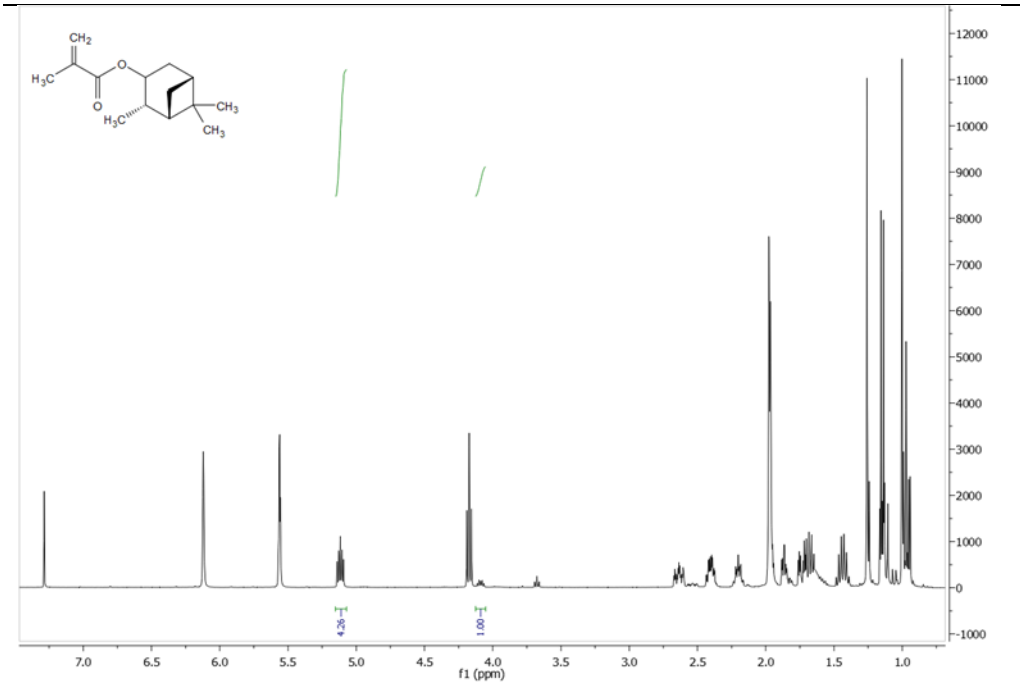
Appendix K: Conventional sparging synthesis of 4-Nitrobenzyl methacrylate(NibMA) at 160 °C showing a conversion of 81 % after 120 minutes by comparing change of chemical environment of protons next to ester group from alcohol to novel methacrylate monomer



Appendix L: Conventional sparging synthesis of 2-Chlorobenzyl methacrylate (ClbMA) at 160 °C showing a conversion of 75 % after 120 minutes by comparing change of chemical environment of protons next to ester group from alcohol to novel methacrylate monomer

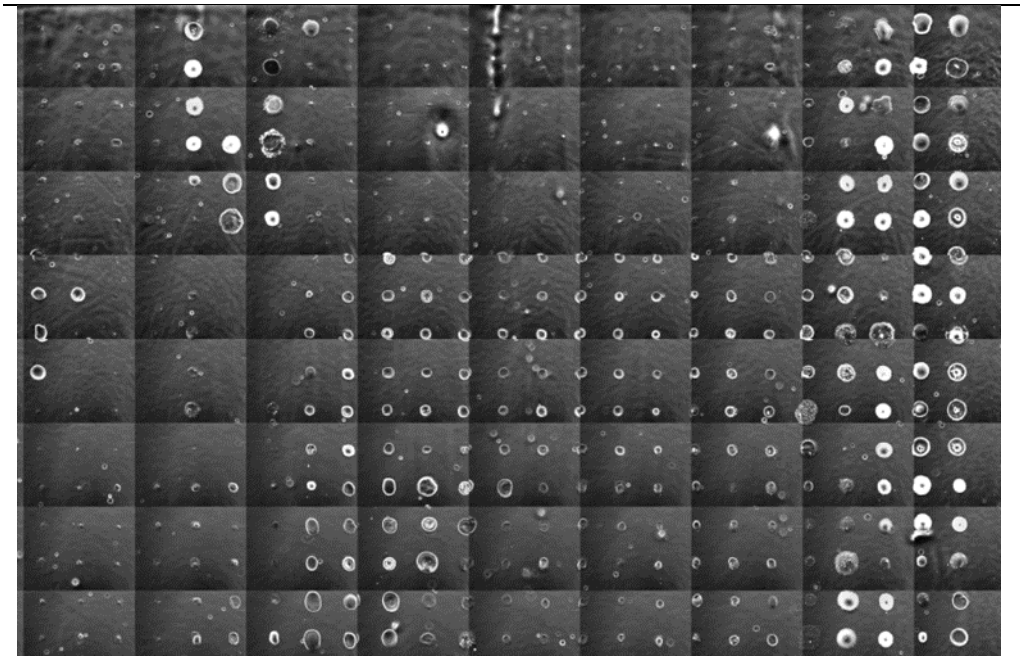


Appendix M: Conventional sparging synthesis of 5-Isopropyl-2-methylphenyl methacrylate (CaMA) at 160 °C showing a conversion of 10 % after 150 minutes by comparing change of chemical environment of protons closest to ester group from alcohol to novel methacrylate monomer

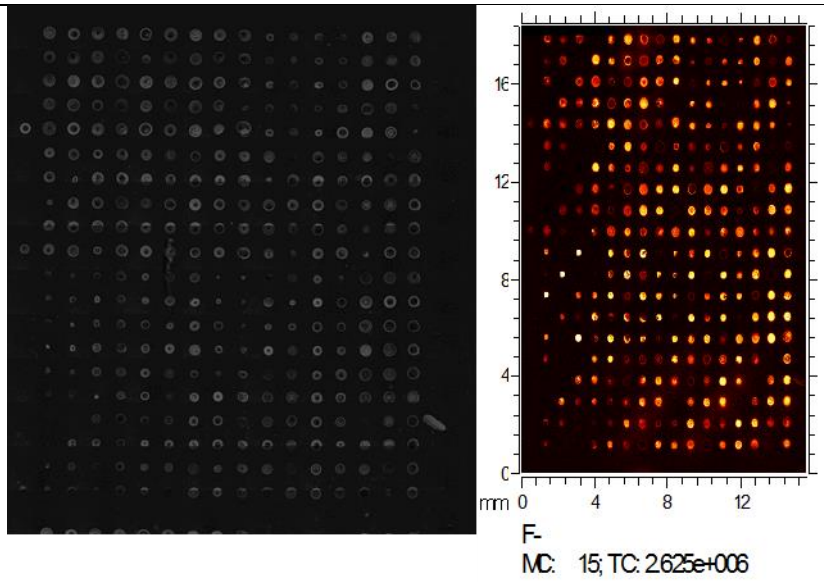


Appendix N: Conventional sparging synthesis of 2,6,6-Trimethylbicycloheptyl Methacrylate (αpMA) at 160 °C showing a conversion of 81 % after 300 minutes by comparing change of chemical environment of protons closest to ester group from alcohol to novel methacrylate monomer

Appendices O and P show the difficulty experienced when trying to produce large copolymer microarray, with misprinting of monomer material as well as contaminations identified by using ToF-SIMS.

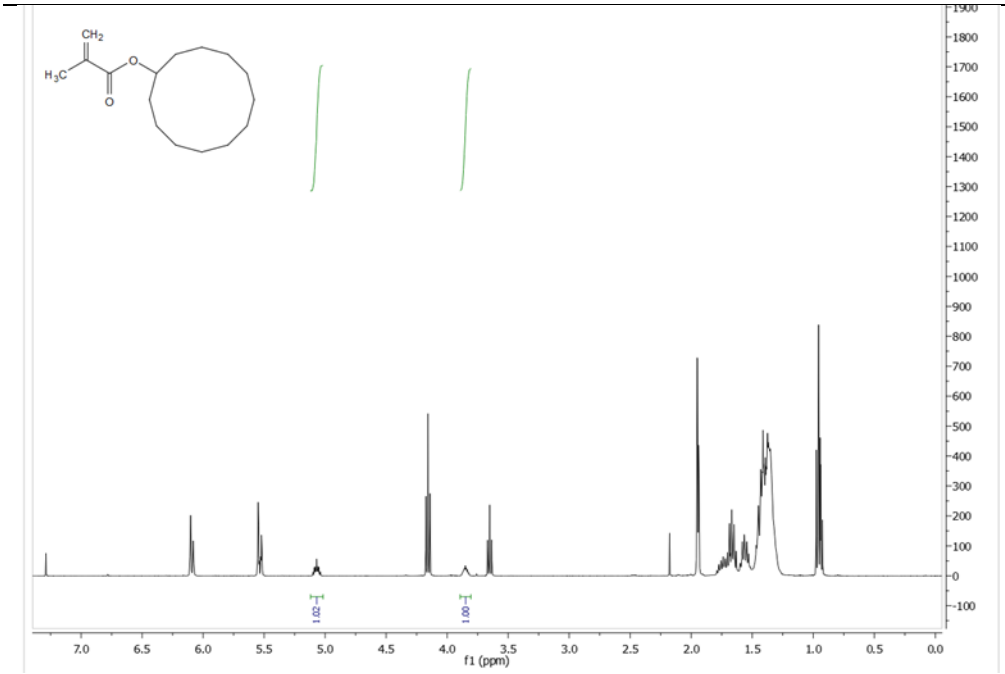


Appendix O: Phase contrast image showing problem when attempting to print large copolymer array with consistency of pin printing, where pins were shown to start off producing uniform spots, but decline over time.

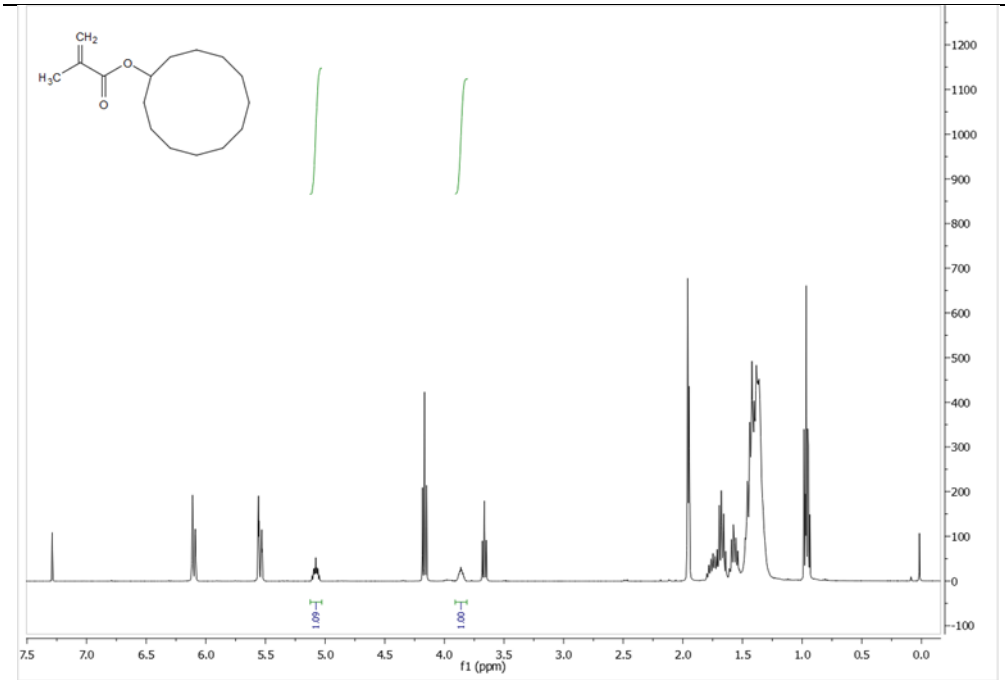


Appendix P: Phase contrast image showing successfully printed A2 polymer microarray, but then also showing the contamination of microarray with fluorine ions identified by ToF-SIMS

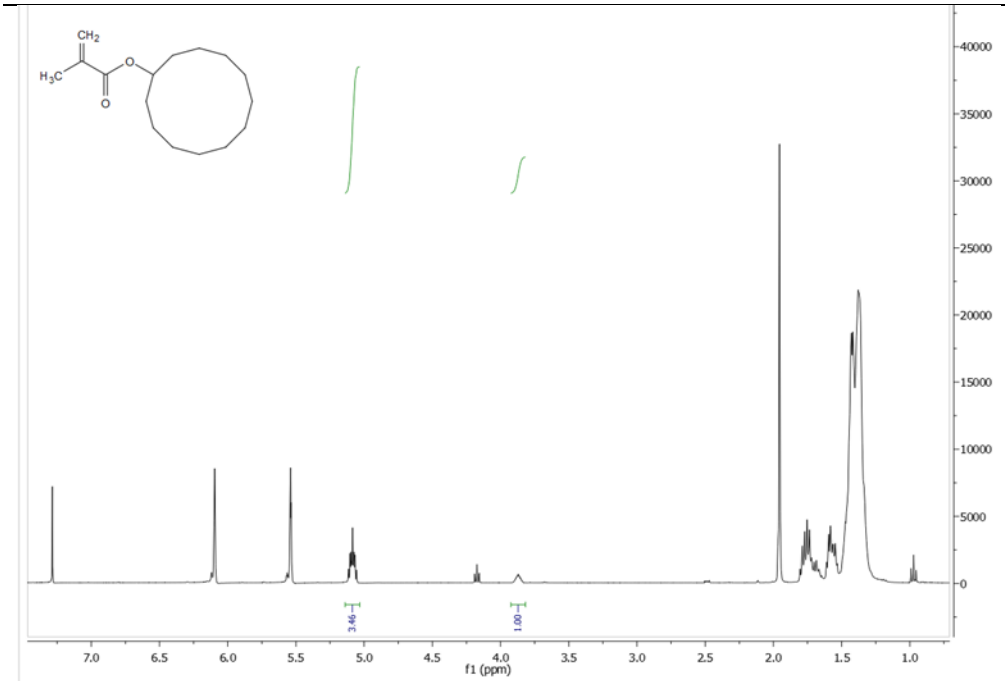
Appendices Q-BB are associated to the comparison studies of the novel micro-well reactor and corresponding standard microwave and conventional heating techniques.



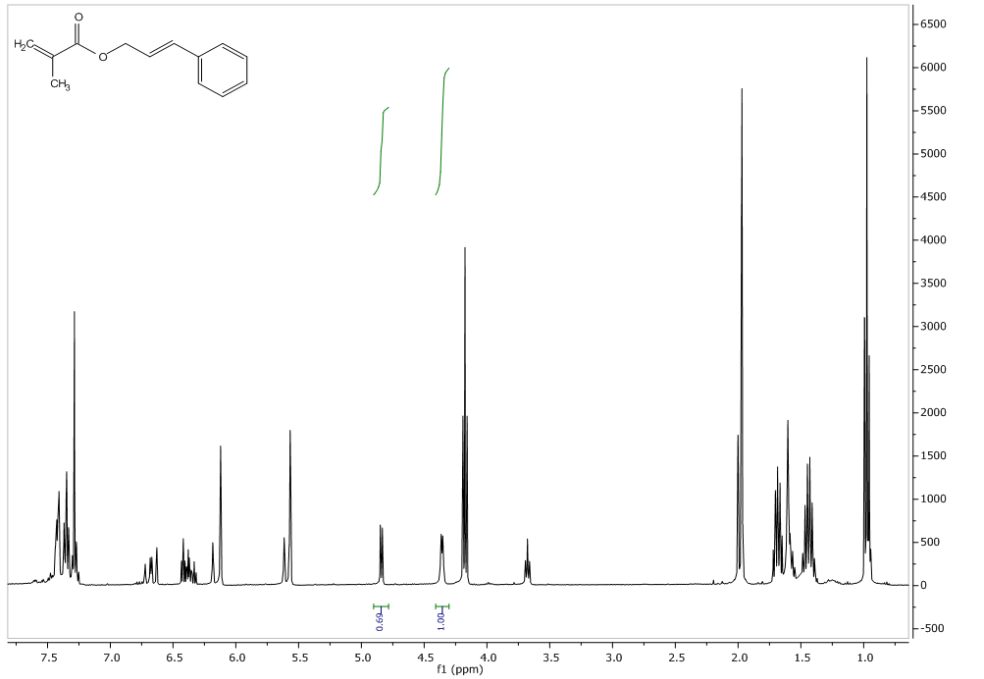
Appendix Q: Conventional synthesis of cyclododecyl methacrylate (CyDMA) at 160 °C showing a conversion of 50 % after 150 minutes by comparing change of chemical environment of protons next to ester group from alcohol to novel methacrylate monomer



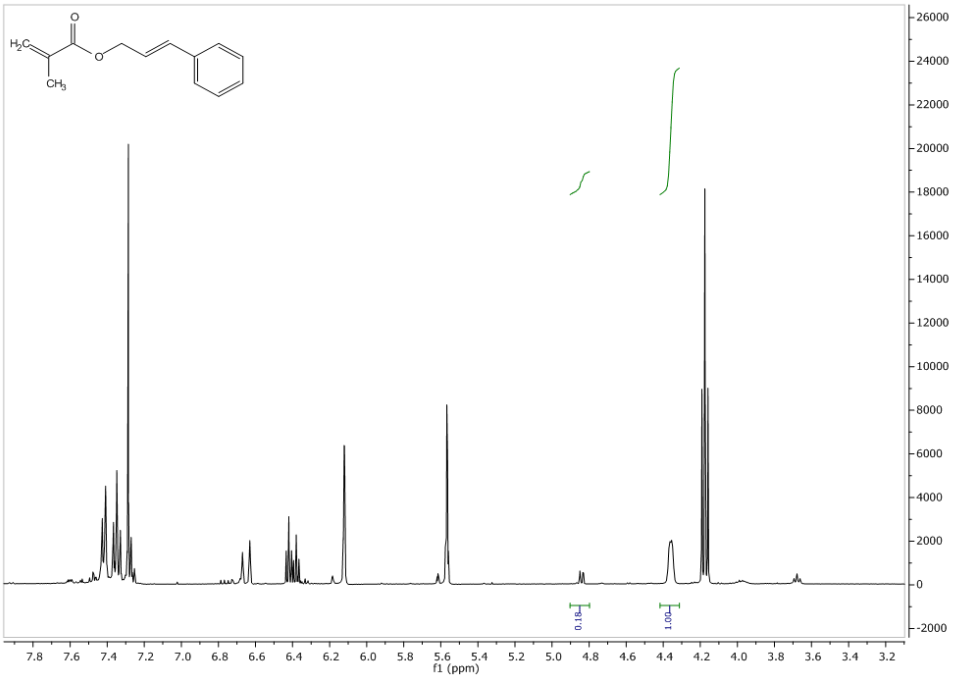
Appendix R: Microwave synthesis of cyclododecyl methacrylate (CyDMA) at 160 °C showing a conversion of 52 % after 150 minutes by comparing change of chemical environment of protons next to ester group from alcohol to novel methacrylate monomer



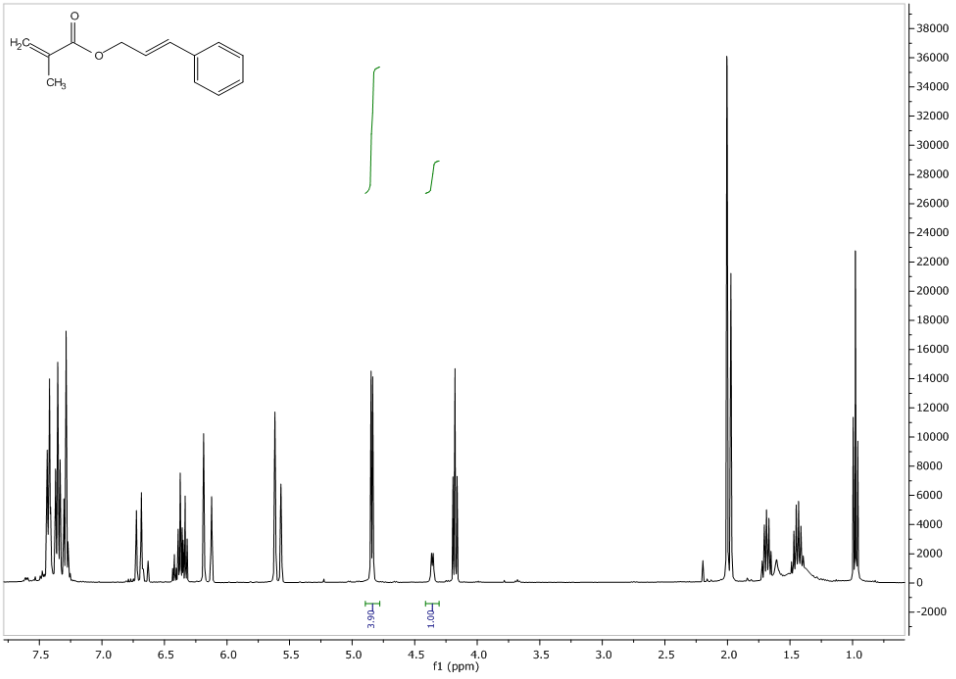
Appendix S: Microwell microwave synthesis of cyclododecyl methacrylate (CyDMA) at 160 °C showing a conversion of 78 % after 150 minutes by comparing change of chemical environment of protons next to ester group from alcohol to novel methacrylate monomer



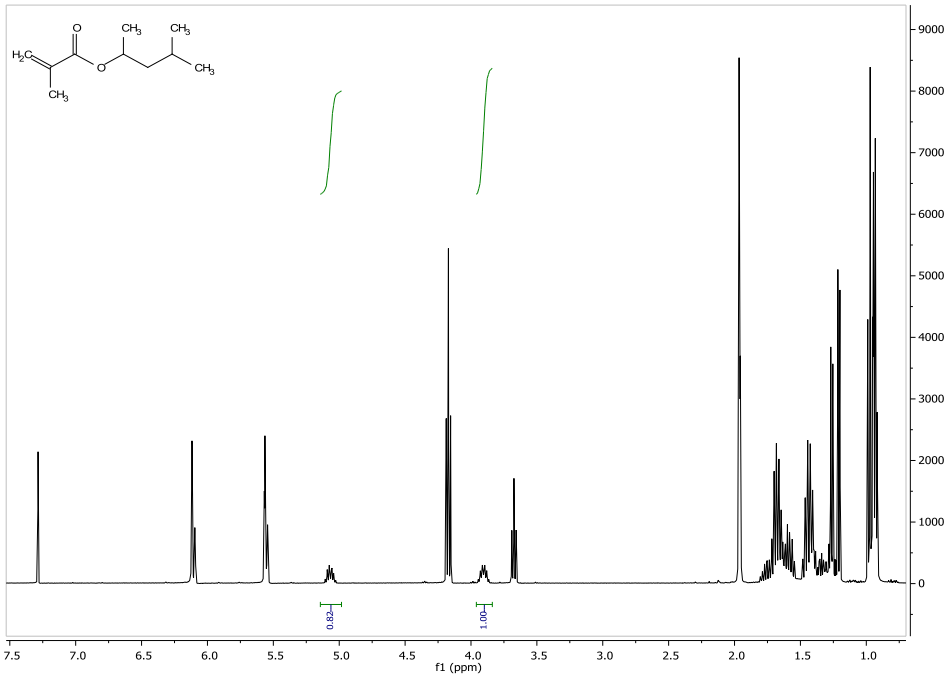
Appendix T: Conventional synthesis of 3-phenyl-2-propenyl Methacrylate (CiMA) at 160 °C showing a conversion of 41 % after 150 minutes by comparing change of chemical environment of protons next to ester group from alcohol to novel methacrylate monomer



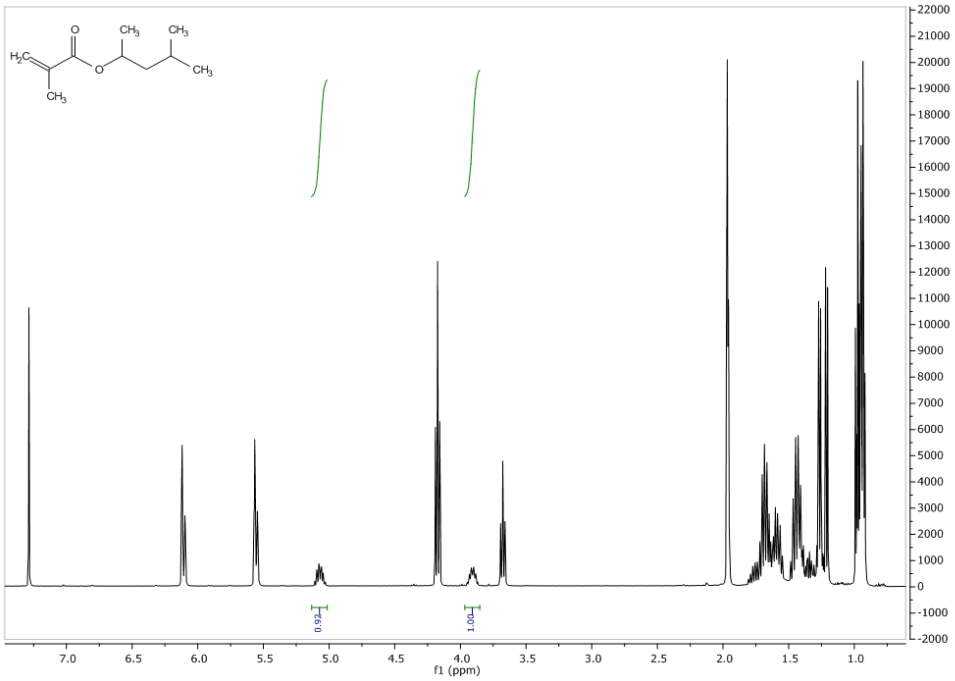
Appendix U: Microwave synthesis of 3-phenyl-2-propenyl Methacrylate (CiMA) at 160 °C showing a conversion of 15 % after 150 minutes by comparing change of chemical environment of protons next to ester group from alcohol to novel methacrylate monomer



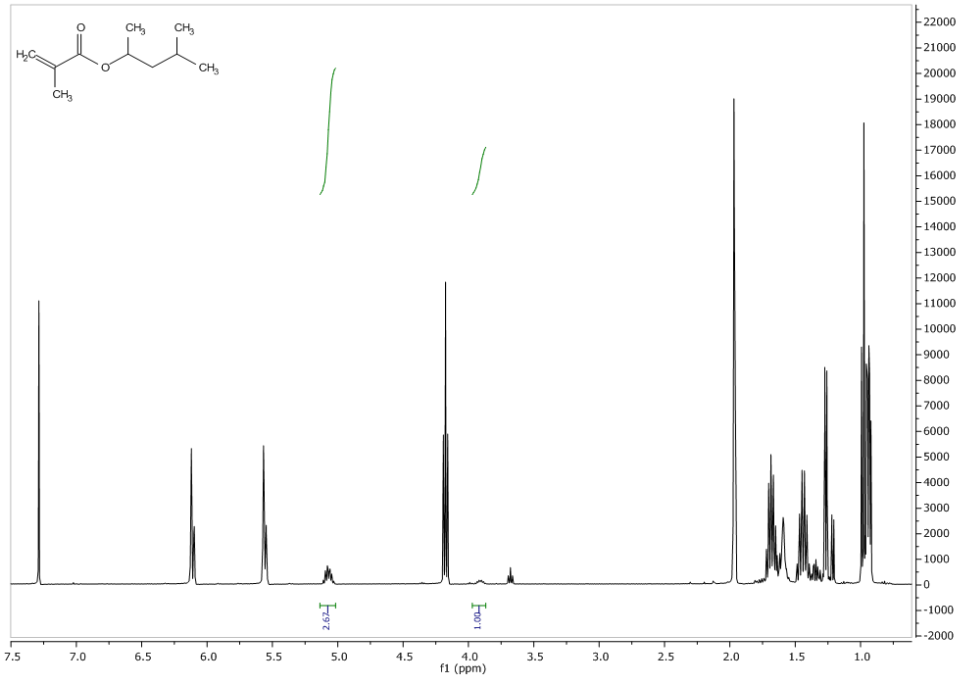
Appendix V: Microwell microwave synthesis of 3-phenyl-2-propenyl Methacrylate (CiMA) at 160 °C showing a conversion of 80 % after 150 minutes by comparing change of chemical environment of protons next to ester group from alcohol to novel methacrylate monomer



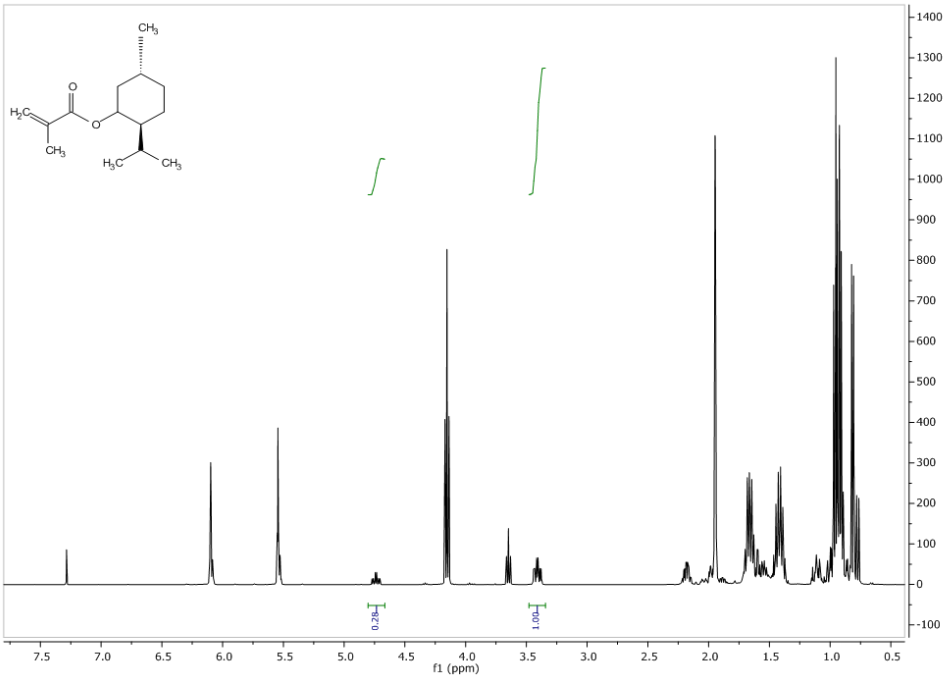
Appendix W: Conventional synthesis of 4-methylpentyl methacrylate (MpMA) at 140 °C showing a conversion of 45 % after 150 minutes by comparing change of chemical environment of protons next to ester group from alcohol to novel methacrylate monomer



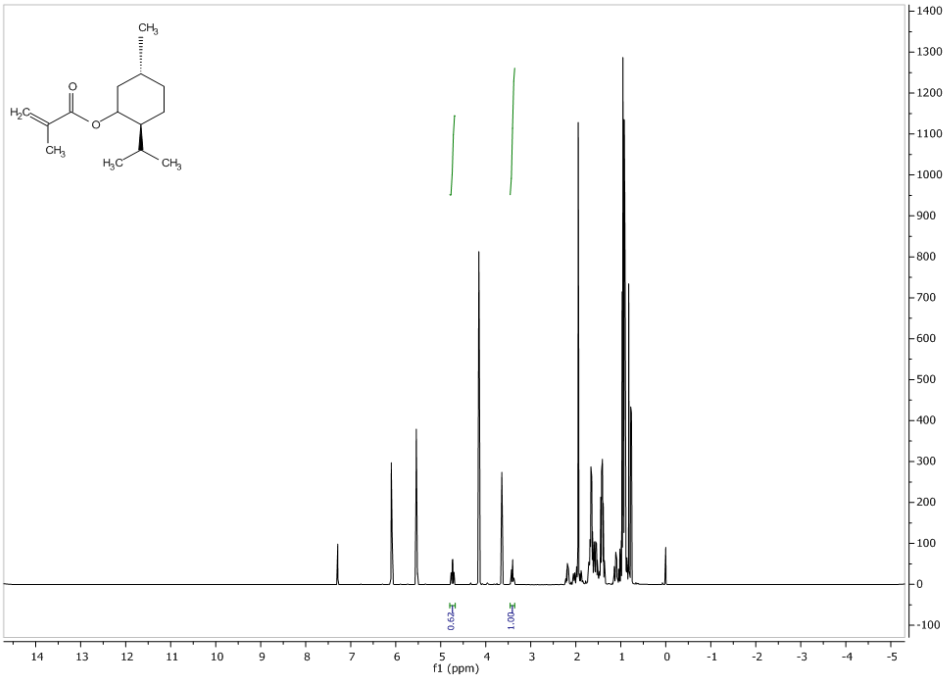
Appendix X: Microwave synthesis of 4-methylpentyl methacrylate (MpMA) at 140 °C showing a conversion of 48 % after 150 minutes by comparing change of chemical environment of protons next to ester group from alcohol to novel methacrylate monomer



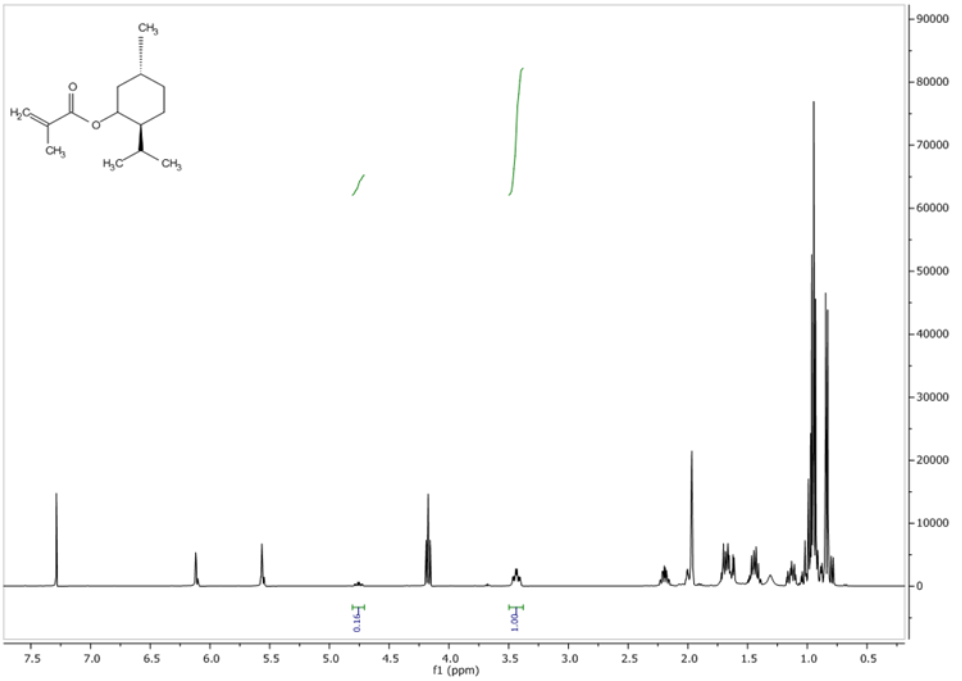
Appendix Y: Microwell microwave synthesis of 4-methylpentyl methacrylate (MpMA) at 140 °C showing a conversion of 73 % after 150 minutes by comparing change of chemical environment of protons next to ester group from alcohol to novel methacrylate monomer



Appendix Z: Conventional synthesis of 5-methyl-2-(1-methylethyl) cyclohexyl methacrylate (LMMA) at 160 °C showing a conversion of 22 % after 150 minutes by comparing change of chemical environment of protons next to ester group from alcohol to novel methacrylate monomer



Appendix AA: Microwave synthesis of 5-methyl-2-(1-methylethyl) cyclohexyl methacrylate (LMMA) at 160 °C showing a conversion of 38 % after 150 minutes by comparing change of chemical environment of protons next to ester group from alcohol to novel methacrylate monomer



Appendix BB: Microwell microwave synthesis of 5-methyl-2-(1-methylethyl) cyclohexyl methacrylate (LMMA) at 160 °C showing a conversion of 38 % after 150 minutes by comparing change of chemical environment of protons next to ester group from alcohol to novel methacrylate monomer